Aspects of Polymer Chain Dynamics in Solution Studied by Fluorescence

Mark William Ingratta

A thesis
presented to the University of Waterloo
in fulfillment of the
thesis requirement for the degree of
Doctor of Philosophy
in
Chemistry

Waterloo, Ontario, Canada, 2008

I hereby declare that I am the sole author of this thesis. This is a true copy of the thesis, including any required final revisions, as accepted by my examiners.

I understand that my thesis may be made electronically available to the public.

Abstract

Several pyrene-labeled polymers and polypeptides were synthesized and their chain dynamics were characterized using steady-state and time-resolved fluorescence techniques. Firstly, four series of pyrene-labeled polystyrenes (Py-PS) were synthesized to determine the effect that the method used for pyrene attachment, the linker connecting pyrene to the backbone, and the distribution of pyrene along the backbone all have on excimer formation. It was found that the amount of excimer formed was different in each case. The differences were described by utilizing the fluorescence blob model (FBM) analysis of the time-resolved monomer and excimer fluorescence decays. Secondly, two Py-PS series were studied in several different solvents with viscosities ranging from 0.36 to 1.19 mPa·s to demonstrate the effect of viscosity on the FBM parameters. The rate constant for excimer formation within a *blob*, k_{blob}, was found to remain constant with viscosity while the number of monomer units per *blob*, N_{blob}, increased with decreasing viscosity. Thirdly, in a technical note, the inherent analogy existing between the aggregation number of surfactant micelles, N_{agg}, and N_{blob}, is taken advantage of to establish a "model-free" procedure to determine N_{blob}. This procedure was validated through the analysis of the time-resolved fluorescence decays of five different pyrene-labeled polymers in seven different solvents. Fourthly, the side-chain dynamics of α-helical pyrene-labeled poly(glutamic acid) were investigated. A longer linker connecting pyrene to the backbone resulted in an increase in N_{blob} which agreed quantitatively with predictions made by molecular modeling. Decreasing the lifetime of the excited pyrene from 215 ns to 50 ns with a quencher increased k_{blob} significantly, while N_{blob} decreased slightly. Finally, the backbone dynamics of pyrene-labeled poly(aspartic acid) (Py-PAA) were

investigated and quantified using the FBM. It was determined that excimer formation was controlled by the very rigid polypeptide backbone and not by the solvent viscosity, contrary to previous results obtained with other pyrene-labeled vinyl polymers.

Acknowledgements

I would like to thank my supervisor Jean Duhamel for his guidance and assistance throughout this learning process; it has been a motivating and interesting experience. I would also like to thank all of my committee members: Eric Fillion and Joao Soares, with special thanks to Mario Gauthier for helpful discussions and direction regarding my work.

Thank you to all the members of the Duhamel and Gauthier lab groups who have made my time here at UW fun and memorable.

A special thanks to my parents and grandparents for their support and encouragement over the years, often reminding me that "An education is the lightest thing you can carry."

I would especially like to thank my wife Barbara for her love and support while I completed my work, the wait was definitely worth it.

Finally, I would like to thank OGSST, NSERC and the University of Waterloo for financial support.

To my loving wife, Barbara.

Table of Contents

Table of Tables

Table of Schemes

Table of Figures

List of Symbols and Acronyms

$\langle n \rangle$	average number of ground state pyrenes per blob
AFM	Atomic force microscopy
AIBN	Azobisisobutyronitrile
AP	Associative polymer
CD	Circular dichroism
CoA-PS	Poly(styrene-*co*-1-pyrenemethylacrylamide) synthesized by copolymerization
CoE-PS	Poly(styrene-*co*-4-(1-pyrene)methoxylmethylstyrene) synthesized by copolymerization
cpcl	Critical polymer chain length
DCM	Dichloromethane
DMA	*N*,*N*-Dimethylacetamide
DMF	*N*,*N*-Dimethylformamide
E_η	Activation energy of solvent viscosity
ES-PS	Polystyrene with pyrene groups evenly spaced along the backbone
FA	Fluorescence anisotropy
f_{agg}	fraction of aggregated pyrenes
FBM	Fluorescence blob model
f_D	fraction of pyrenes that form excimer improperly with a long lifetime
f_{diff}	fraction of pyrenes that form excimer via diffusion
FDQ	Fluorescence dynamic quenching
f_E	fraction of pyrenes that form excimer instantaneously
f_{Ediff}	fraction of pyrene excimers that form via diffusion
f_{Mdiff}	fraction of pyrene monomers that form excimer via diffusion
FRET	Fluorescence resonance energy transfer
GPC	Gel permeation chromatography
GrE-PS	Poly(styrene-*co*-4-(1-pyrene)methoxylmethylstyrene) synthesized using a grafting onto method
GS	Ground-state
HA	Hydrodeoxychloic acid

HASE	Hydrophobically modified water soluble polymers
HMW	High molecular weight
I_E/I_M	Intensity of the excimer peak (500 - 530 nm) divided by the monomer peak (372 - 378 nm)
k_{blob}	rate constant for excimer formation within a blob
$k_e \times [blob]$	rate constant for exchange of pyrene between blobs times blob concentration per polymer coil
LED	Light emitting diode
LRPCD	Long range polymer chain dynamics
MEK	Methyl ethyl ketone
MeOAc	Methyl acetate
MHS	Mark-Houwink-Sakurada
MMA	Methyl methacrylate
N_{agg}	Average number of surfactant molecules per micelle
N_{blob}	Number of monomer units per blob
NMR	Nuclear magnetic resonance
PAA	Poly(aspartic acid)
PBA	4-(1-Pyrene)butylamine
PBGlu	Poly(γ-benzyl–L–glutamate)
PEO	Poly(ethylene oxide)
PDMA	Poly(*N*,*N*-dimethylacrylamide)
PGA	Poly(glutamic acid)
PMA	1-Pyrenemethylamine
PMMA	Poly(methyl methacrylate)
PNAla	Poly(L-1-naphthylalanine)
PNAsp	Poly(β-naphthylmethyl–L–aspartate)
PNIPAM	Poly(N-isopropylacrylamide)
P(NAsp-co-BGlu)	Poly(β-Naphthylmethyl–L–aspartate-*co*- γ-benzyl–L–glutamate)
PPyMLGlu	Poly(L-glutamic acid) labeled with 1-pyrenemethylamine
PS	Polystyrene
P2VP	Poly(2-vinylpyridine)
PyMAAm	*N*-(1-Pyrenylmethyl)acrylamide

PyMMS	4-(1-Pyrenyl)methoxymethylstyrene
R_h	Hydrodynamic radius
T_g	Glass transition temperature
THF	Tetrahydrofuran
TY	Turro and Yekta
V_{blob}	Volume of a blob
V_h	Hydrodynamic volume
$[\theta]$	Molar ellipticity
λ_{Py}	Moles of pyrene per gram polymer

Chapter 1:
Literature Review

The aim of this chapter is to give a short review on studies of polymer chain dynamics which were conducted with pyrene labeled polymers. To this end, the basics of fluorescence and pyrene excimer formation are discussed first, followed by examples of applications that use pyrene-labeled polymers, with a focus on fluorescence dynamic quenching and how it is employed in the study of polymer chain dynamics in dilute solution. Circular dichroism analysis (CD), which is used to determine the secondary structure of polypeptides is also introduced since some conclusions of this thesis are based on the results obtained by CD. The final sections present the thesis objectives and thesis outline.

1.1 Polymer Chain Dynamics in Dilute Solution

The dynamics of polymer chains in solution play an important and determining role in the behavior of macromolecules in solution, such as the rheology of viscosity modifiers in oil and aqueous solutions or the folding of proteins. Several techniques provide information on the backbone dynamics of polymer chains, including X-ray scattering,[1] NMR,[2,3] AFM,[4,5] optical microscopy,[6] and fluorescence.[7–12] Of all these techniques, the high sensitivity of fluorescence offers the unique advantage that the measurements can be conducted on very dilute solutions, so dilute in fact that single chains can be isolated and observed.

Some of the different fluorescence techniques that can be used to study polymers are fluorescence resonance energy transfer (FRET),[11,12] fluorescence anisotropy (FA),[9] and fluorescence dynamic quenching (FDQ).[10,14–18] FRET measures the distance between a donor chromophore and its acceptor, while FA measures the tumbling rate of a chromophore in solution. Both can be used to provide information on the size of macromolecules in the range of angstroms to tens of nanometers, but FA is often applied to characterize the local dynamics undergone by a chromophore attached to a macromolecule. FDQ can also be used

to probe changes in the relative size of the polymer coil, as encountered during the transition of a pyrene-labeled poly(acrylic acid) in aqueous solution as it contracts from an expanded coil to a more collapsed conformation when the pH of the solution is decreased and the electrostatic repulsions of the carboxylate groups are eliminated.[13] More often, FDQ is used to probe the dynamics of polymer chains by attaching a chromophore and its quencher on the same chain, and monitoring the interactions between the two. The most common chromophore used in FDQ studies is pyrene and its application to the study of polymers has been discussed in numerous reviews.[14–18] Pyrene is often the chromophore of choice due to its high quantum yield, relatively long lifetime of 200-300 ns, and its ability to act as its own quencher which simplifies the labeling procedure. When an excited pyrene monomer encounters a ground-state pyrene the monomer fluorescence is quenched, and an excimer species is formed that can fluoresce within its own lifetime. Pyrene excimer formation is discussed in greater detail in Section 1.2.3.

When pyrene is covalently attached to a polymer backbone, the rate of excimer formation is controlled by the polymer chain dynamics that depend on the nature of the polymer backbone and side-chains, the polymer conformation resulting from polymer-solvent interactions and the chemical structure of the polymer, and the solvent viscosity.[17,18] Overall, excimer formation between pyrenes covalently attached to a polymer gives information on the motions of the polymer backbone in solution. Pyrene can be attached to a polymer at specific positions or randomly along the backbone. Both methods have pros and cons that are discussed in Sections 1.3.1 and 1.3.2.

In recent years, the focus of the study of polymer chain dynamics has shifted from synthetic polymers to polypeptides and proteins. Several methods have been employed to

study protein folding, such as temperature jump experiments[19–21] and photochemical initiation[22,23] where folding or unfolding of the peptide is induced by a laser in order to follow, respectively, the unfolding or folding process using time-resolved spectroscopic techniques. The end-to-end cyclization technique has been employed in several cases recently in an effort to determine the "speed limit" for protein folding. These and several other methods are presented in a recent edition of Methods in Molecular Biology entitled "Protein Folding Protocols".[24] In large part, this thesis seeks to enhance the technical knowledge base of FDQ for polypeptide chains in solution.

The following review is separated into background information on pyrene fluorescence and some techniques that can be used to study the dynamics of polymers, followed by a review of pyrene-labeled polymers studied using FDQ. The final sections focus on polypeptide chain dynamics and CD techniques used to determine polypeptide secondary structure.

1.2 Introduction to Fluorescence

1.2.1 Chromophore Lifetime

The lifetime of a chromophore is a critical parameter in the study of polymer chain dynamics because the lifetime represents the time window during which the chromophore reports on its surroundings. In cases where the chromophore is free to diffuse away, a longer lifetime implies that the chromophore explores a larger volume. In other words, controlling the lifetime of the chromophore determines the distance and the volume probed by the excited chromophore.

The fluorescence lifetime (τ) of a chromophore depends on the radiative rate constant (k_r) and the radiationless rate constant (k_{nr}) of the chromophore according to Equation 1.1.[25]

A chromophore in the excited state can return to the ground-state through several radiationless processes, including relaxation through specific interactions between the chromophore and the solvent and collisional quenching (Section 1.2.2). The larger the contribution of the radiationless processes compared to the radiative process, the shorter the lifetime of the chromophore and the smaller the quantum yield (Q). The quantum yield is the ratio of the radiative rate constant to the sum of all rate constants characterizing the relaxation of the chromophore from the excited state to the ground-state (Equation 1.2).[25]

$$\tau = \frac{1}{k_r + k_{nr}} \tag{1.1}$$

$$Q = \frac{k_r}{k_r + k_{nr}} \tag{1.2}$$

Control of the lifetime is accomplished by increasing the non-radiative rate constant through the addition of an external quencher to the solution. Common quenchers of fluorescence include nitromethane, iodide ions, 1,3-dimethylbenzophenone, and dodecylpyridinium chloride.

1.2.2 Collisional Fluorescence Quenching

Fluorescence quenching refers to any process resulting in a decrease in fluorescence intensity.[25] These processes include energy transfer, complex formation, and collisional quenching. Collisional quenching is typically described by a Stern-Volmer plot, where the ratio of the fluorescence intensity without quencher (I_o) to the fluorescence intensity upon the addition of quencher (I) is plotted as a function of quencher concentration ([Q]).[25] A linear I_o/I vs. [Q] trend demonstrates that there is only one population of fluorophore present in

solution, i.e. all chromophores are equally accessible to the quencher. The Stern-Volmer plot can then be fitted with Equation 1.3, where k_q and τ are the quenching rate constant and the natural lifetime of the chromophore, respectively. In cases where the chromophore is covalently of physically bound to a heterogeneous system like a protein, there might be several populations of chromophores experiencing a different access to the quencher species. Protective quenching results from such a situation[25] but was not encountered in this thesis.

$$I_o / I = 1 + k_q \tau \, [Q] \tag{1.3}$$

Collisional quenching is a diffusionally controlled process, where the collision frequency (Z) is equal to the product of the diffusion controlled bimolecular rate constant (k_o) and the quencher concentration (Equation 1.4).[25] k_o is proportional to the collision radius (R) and the diffusion coefficients (D) of the chromophore and quencher species (Equation 1.5). The quenching rate constant (k_q) for the chromophore-quencher pair is the product of k_o and the quenching efficiency (γ). For example, if the fluorescence is only quenched by half of that expected from the calculated k_o value, the quenching efficiency would be equal to 0.5.

$$Z = k_o[Q] \tag{1.4}$$

$$k_o = 4\pi RDN \tag{1.5}$$

$$k_q = k_o \gamma \tag{1.6}$$

1.2.3 Pyrene Excimer Formation

A ground-state pyrene can be excited by UV light around 340 nm. The excited pyrene can then either fluoresce with its natural lifetime as a monomer between 370 and 425 nm, or diffusionally encounter a ground-state pyrene with a rate constant k_1 to form an excimer species which fluoresces between 425 and 600 nm. This process is described by the Birks' scheme[26] shown in Scheme 1.1, where τ_M is the lifetime of the pyrene monomer, τ_E is the lifetime of the excimer and k_{-1} is the dissociation rate constant.

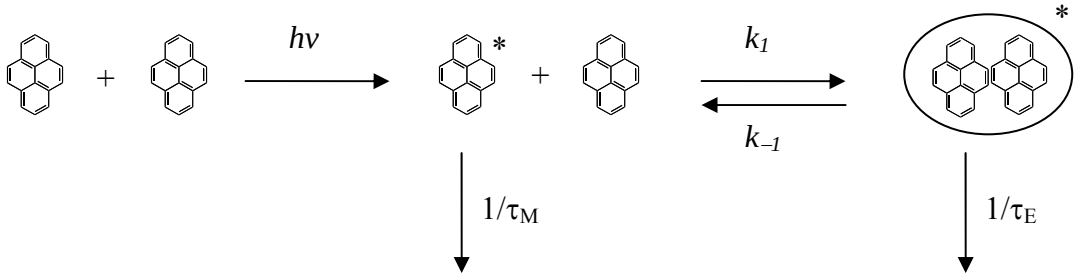

Scheme 1.1: The Birks' scheme describing pyrene excimer formation.

The steady-state fluorescence spectra shown in Figure 1.2 are typical of the pyrene emission. They show the structured monomer peaks in the 370 – 400 nm range and the structureless excimer band in the 440 – 600 nm range. Several points can be noted in Figure 1.2. First the relative amount of excimer fluorescence increases with an increase in pyrene concentration. With more pyrene present, the number of encounters increases, thus resulting in a stronger excimer peak.[26] Second, qualitative information on the rate of excimer formation is often derived from the ratio of the fluorescence intensity of the excimer to that of the monomer in the steady-state fluorescence spectrum. The monomer (I_M) and excimer

(I_E) intensities can be obtained by integrating the fluorescence spectra of the first monomer peak between 372 – 378 nm and the excimer peak between 500 – 530 nm, respectively. Third, the ratio of the fluorescence intensity of the first (I_1) to that of the third (I_3) peak of the monomer describes the polarity of the medium surrounding the pyrene.[27,28] A relatively large I_1/I_3 ratio (~1.7), indicates a more polar environment such as water, while a lower value indicates an environment of lower polarity. Both free pyrene and substituted pyrene groups attached to a polymer via a methyl group are affected by the solvent polarity, while a longer linker results in a loss of this sensitivity.[10]

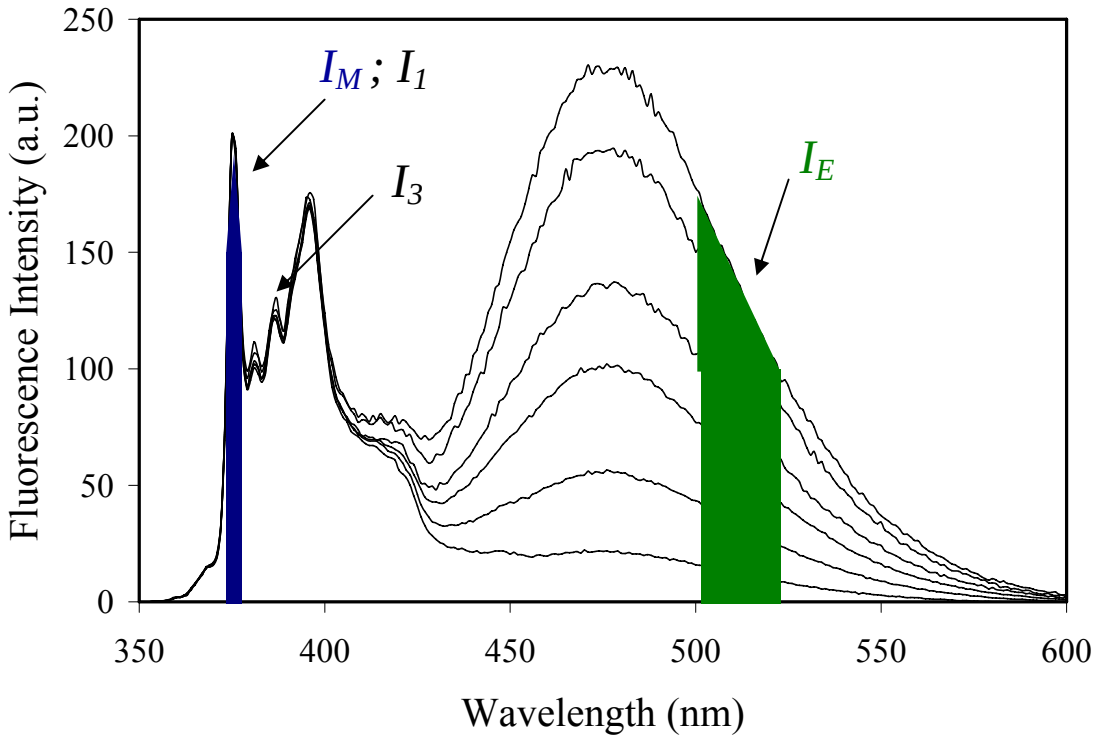

Figure 1.1: Steady-state fluorescence spectra of a series of pyrene-labeled polystyrene in tetrahydrofuran, normalized at the 0-0 peak at 375 nm. The pyrene content increases from bottom to top. The solid areas under the spectra represent the integrals used to measure I_M and I_E. [Py] = 2.5×10^{-6} M.

1.3 Pyrene Labeled Polymers

1.3.1 Labeling at Specific Positions – End-Labeling

There are several key conditions that must be met for the synthesis of polymers suitable for studies of end-to-end cyclization. The first condition is that both chain ends must have functional groups that enable pyrene attachment. Usually, the polymer synthesis must be modified to introduce a functional group at both ends of the polymer. This is the case for end-labeled polystyrenes (PS), where anionic polymerization must be initiated via electron transfer to grow the chain out from the center and terminated by reacting both propagating ends with ethylene oxide or carbon dioxide which results in hydroxyl[29] and carboxylic acid[30] end-capped PS, respectively.

The second condition that must be fulfilled to measure the end-to-end cyclization rate of fluorescently labeled polymers is that the polymer must be monodispersed in length due to the dependence of the cyclization rate constant (k_{cyc}) on the length of the polymer chain spanning the two pyrene groups.[19] Earlier work has demonstrated that k_{cyc} scales as N^{γ} where N is the number of monomer units and γ is a scaling factor dependent on solvent-polymer interactions. γ has been found to equal 1.62 for PS in cyclohexane at 34.5 ^{o}C.[31] For this reason, monodispersed polymers (PDI < 1.15) are required.

The last condition is that relatively short polymer chains are required to generate enough end-to-end cyclization events that can be monitored accurately. The longest usable polymer chain length depends on the rigidity of the backbone and the characteristics of the chosen chromophore. Using steady-state fluorescence, flexible poly(ethylene oxide) end-labeled with pyrene (Py-PEO-Py) has been studied with molecular weights up to 20 kg/mol with chain lengths of up to 1350 bonds,[32] while less flexible polystyrene has been studied up

to 27 kg/mol with chain lengths of up to 530 bonds using time-resolved fluorescence[33] and up to 100 kg/mol and chain lengths of 2000 bonds using steady-state fluorescence.[31] At higher molecular weights excimer formation becomes very infrequent and the lifetime of the pyrene monomer, which increases as the rate constant for excimer formation decreases, becomes very close to that of the unquenched pyrene preventing the determination of the rate constant for excimer formation. As a result, the type of polymers whose end-to-end cyclization can be studied by fluorescence remains limited.

While the study by time-resolved fluorescence of a polymer labeled at one end with a chromophore and at the other with a quencher remains the only procedure to yield a quantitative description of the chain end encounters, this advantage is counterbalanced by the disadvantage that the information obtained pertains only to the motions of the chain ends. In these experiments, the entire chain is invisible. To probe polymer chain dynamics by fluorescence, the chain must be labeled with chromophores. Randomly labeled polymers can be used for this purpose since they enable the study of the segmental encounters taking place along the entire polymer chain.

1.3.2 Randomly Labeled Polymers

Random labeling along the backbone of the polymer eliminates all conditions imposed by the preparation of end-labeled polymers such as the need for functional end-groups, monodispersed chains, and low molecular weights. However, the synthesis must still include the introduction of functional groups along the backbone, although this requirement is much less synthetically demanding than incorporating functional groups at specific positions of the chain.

The design of a synthetic method to incorporate pyrene along the backbone of a polymer chain can follow one of two routes. The first method is the random co-polymerization of a small amount of a pyrene labeled monomer, typically, 1 to 7 mol%, with the monomer of choice, such as styrene[34] or *N*,*N*-dimethylacrylamide.[35,36] The potential difficulty with this method is ensuring that the co-polymerization incorporates throughout the reaction a same amount of pyrene labeled monomer randomly into the backbone. Eventually the reactivity ratios of the two monomers must be determined, a usually tedious and complex experiment.

The second method for incorporating pyrene along a polymer backbone is a polymer modification reaction. In some cases, the polymer side-chains bear a functional group that can be used to react with a pyrene derivative. Alternatively, the polymer can be functionalized first, followed by a grafting onto reaction for pyrene attachment. A way of combining the two methods is to copolymerize a small amount of a functionalized monomer along with the desired monomer as a way of adding functional groups during the synthesis.[37,38] This method for incorporating pyrene onto the backbone also does so randomly throughout the chain, likely leading to a similar distribution to that of a copolymerization reaction described in the previously.

Unfortunately, although random labeling is generally a more straightforward task than labeling at specific sites of the polymer, the randomness of the pyrene groups distributed along the backbone introduces a new complication. As found for the study of end-labeled polymers, excimer formation is extremely sensitive to the length of the chain spanning the two pyrene groups.[17,18] With a randomly labeled polymer, there is an infinite number of chain lengths spanning every two chromophores, and thus creating an infinite number of rate

constants for excimer formation. This infinite number of rate constants manifests itself in a relatively *complicated* fluorescence decay, meaning that it deviates significantly from a mono-exponential function and that a multi-exponential equation is required to adequately fit the monomer and excimer decays.[17] Thus, the traditional Birks' scheme (Scheme 1.1) cannot be applied to polymers randomly labeled with pyrene and a new model is required to retrieve meaningful information about their dynamics.

1.3.3 The Fluorescence Blob Model (FBM)

The FBM was developed to study the complicated decays associated with polymers randomly labeled with pyrene.[17] The FBM is based upon the idea that an excited pyrene can probe a finite volume in solution in a given amount of time. This volume is referred to as a *blob*, V_{blob}, and is defined as the volume probed by an excited pyrene during its lifetime. The polymer coil is thus divided into a number of sub-volumes termed *blobs*, among which the pyrene pendants are randomly distributed according to a Poisson distribution (Scheme 1.2). The pyrene monomer fluorescence decays are fitted using the FBM equation (Equations 1.7-1.8) and the parameters describing excimer formation within a *blob* are retrieved. The first exponential in Equation 1.7 describes the diffusional encounters between an excited pyrene and a ground-state pyrene, $[Py^{*}_{diff}]$. The second exponential accounts for any unquenched free pyrene, $[Py^{*}_{free}]$, that fluoresces with its natural lifetime, τ_M. The parameters that describe excimer formation within a *blob* are the rate constant for excimer formation by diffusion between one excited pyrene and one ground-state pyrene located in the same *blob*, k_{blob}, the average number of ground-state pyrenes per *blob*, $<n>$, and the rate constant for the exchange of ground-state pyrenes between *blobs* times the concentration of *blobs* in the

polymer coil, k_e[*blob*]. <*n*> is also used to derive the number of monomer units within a *blob*, N_{blob}, and is calculated using Equation 1.9, where λ_{Py} is the pyrene content of the

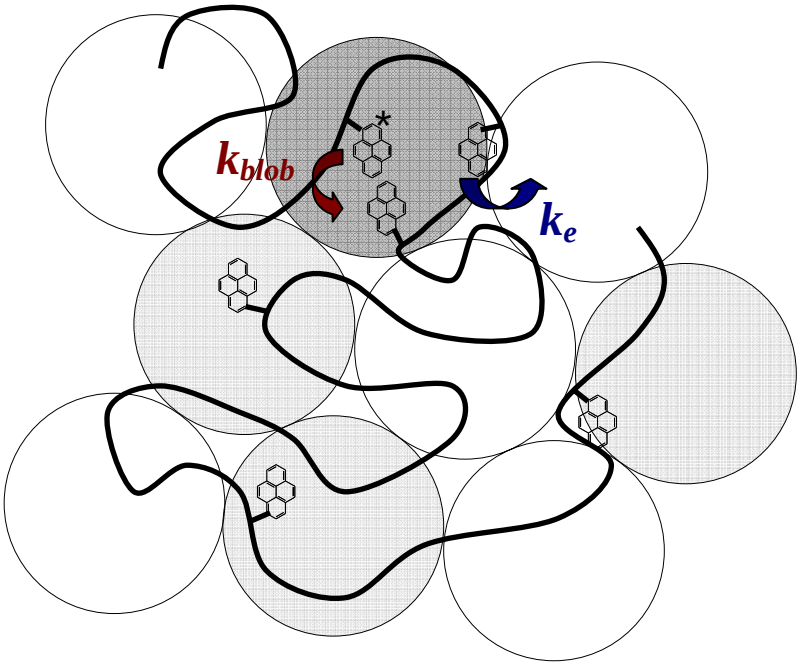

Scheme 1.2: Graphic description of a polymer arbitrarily divided into *blobs*.

polymer in moles of pyrene per gram of polymer, f_{Mdiff} is the fraction of excited pyrene monomers that can form excimer through diffusive encounters, *x* is the molar fraction of pyrene-labeled monomer, and M_{Py} and *M* are the molecular weights of the pyrene-labeled monomer and non-labeled monomer, respectively.

$$[Py^*]_{(t)} = \left[Py^*_{diff}\right]_{(t=0)} \exp\left[-\left(A_2 + \frac{1}{\tau_M}\right)t - A_3\left(1-\exp\left(-A_4 t\right)\right)\right] + \left[Py^*_{free}\right]_{(t=0)} \exp\left(-t/\tau_M\right) \quad (1.7)$$

The parameters A_2–A_4 are described in Equation 1.8.

$$A_2 = \langle n \rangle \frac{k_{blob} k_e [blob]}{k_{blob} + k_e [blob]} \quad A_3 = \langle n \rangle \frac{k_{blob}^2}{(k_{blob} + k_e [blob])^2} \quad A_4 = k_{blob} + k_e [blob] \tag{1.8}$$

$$N_{blob} = \frac{\langle n \rangle}{\lambda_{Py} / f_{Mdiff} \left[M_{Py}(x) + M(1-x) \right]} \tag{1.9}$$

In addition to the parameters that describe the diffusion controlled excimer formation obtained from the monomer decay, a global analysis[39] of both the monomer and excimer decays using, respectively, Equations 1.7 and 1.10, gives additional information on *how* excimer is formed. Three pyrene species contribute to the emission of the excimer in solution. These species result from the diffusional encounter of an excited pyrene monomer and a ground-state pyrene, and the direct excitation of well-stacked ground-state pyrene dimers ($E0^*$) that emit with a lifetime τ_{E0} on the order of 50 ns and improperly stacked ground-state pyrene dimers (D^*) that emit with a longer lifetime τ_D on the order of 140 ns.[35,36,40] Equations 1.7 and 1.10 enable one to determine the fractions of all pyrene species, Py_{diff}, Py_{free}, $E0$, and D, present in solution. The fraction of aggregated pyrenes, f_{agg}, is the ratio $([E0^*]_o + [D^*]_o)/([Py^*_{diff}]_o + [Py^*_{free}] + [E0^*]_o + [D^*]_o)$.[40]

$$[E^*] = -[Py^*_{diff}]_{(t=0)} e^{-A_3} \sum_{i=0}^{\infty} \frac{A_3^{\,i}}{i!} \frac{A_2 + i A_4}{\frac{1}{\tau_M} - \frac{1}{\tau_{E0}} + A_2 + i A_4} \exp\left(-\left(\frac{1}{\tau_M} + A_2 + i A_4 \right) t \right)$$

$$+ \left([E0^*]_{(t=0)} + [Py^*_{diff}]_{(t=0)} e^{-A_3} \sum_{i=0}^{\infty} \frac{A_3^{\,i}}{i!} \frac{A_2 + i A_4}{\frac{1}{\tau_M} - \frac{1}{\tau_{E0}} + A_2 + i A_4} \right) e^{-t/\tau_{E0}} + [D^*]_0 e^{-t/\tau_D} \tag{1.10}$$

The first example where the FBM was applied to study polymer chain dynamics was with a series of pyrene-labeled polystyrenes (Py-PS).[34] This work established that the polydispersity of the polymer does not affect the FBM parameters retrieved from the analysis of the monomer fluorescence decays. This was expected since the FBM shifts the focus of the study from the entire polymer down to a *blob*. Also, the study helped determine the existence of a critical polymer chain length (*cpcl*), below which the FBM parameters began to vary. The *cpcl* was determined to be about 6 *blobs*. This early work demonstrated that the basic idea of the FBM was sound.

1.3.4 Studies of Pyrene-Labeled Polymers

The effects that the medium hosting the polymer (gels, thin films, and solution) or polymer structure (linear vs. branched) have on the polymer chain dynamics have been studied using steady-state and time-resolved fluorescence. For instance, pyrene labeled alginate gels that are chemically cross-linked with various amounts of calcium have been studied using steady-state fluorescence.[41] The I_E/I_M ratio was said to reflect the changes in the cross-link density and led the authors to suggest that fluorescence could be used as a tool to monitor the cross-link density of these gels.

The density of arborescent polymers and dendrimers has also been studied using fluorescence.[42] In the case of the arborescent polymers, their density was assessed at the molecular level in solution by monitoring the quenching of a pyrene-labeled polystyrene (PS) arborescent polymer by a nitrobenzene-labeled PS arborescent polymer and comparing these results with those obtained with a linear pyrene-labeled PS and 1-pyrenemethanol. It was determined that the arborescent polymer allowed much less access to the pyrene pendants and thus resulted in a reduced rate of quenching relative to the linear Py-PS.

Another study of the density of a highly branched polymer involved the internal labeling of a dendrimer with pyrene, then monitoring the process of pyrene excimer formation in various solvents, and comparing this process with that of a model compound.[43] It was determined that the pyrene groups attached to the interior of the dendrimer behaved in a manner similar to the model compound, thus revealing that the interior of the dendrimer was well solvated and that the motions of the bulky pyrenes were not hindered by the chains.

A particularly interesting application for the use of fluorescence to study the chain dynamics of pyrene labeled polymers is to determine the glass transition temperature (T_g) of thin films.[44–46] As the mobility of the polymer chains increases above T_g, the value of the rate constant representing the non-radiative processes increases (k_{nr} in Equations 1.1 and 1.2) at the expense of the rate constant of the radiative process (k_r). This phenomenon enables T_g to be determined by monitoring how the fluorescence intensity changes as a function of temperature. The changes in intensity were monitored by steady-state fluorescence utilizing front-face geometry.

There has been a lot of debate in the scientific community on whether T_g at the surface of a thin film is different from that of the bulk polymer.[47] Using fluorescence, the change in T_g has been characterized as a function of film thickness. This was done by placing a thin layer of pyrene-labeled PS on or within other thin layers of unlabeled high molecular weight PS and heating the layered films to fuse the layers together. A typical film is illustrated in Figure 1.2. Measurements were conducted as a function of the thickness of the labeled layer, the under-layer thickness, and placement of the pyrene-labeled layer within the film.[44]

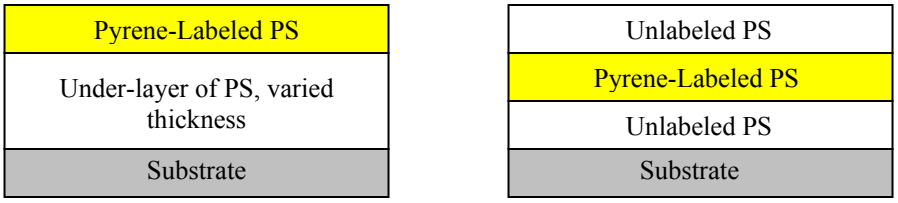

Figure 1.2: Examples of thin PS films with a single layer of Py-PS. A) A Py-PS layer at the top of the film, the under-layer thickness is varied. B) A Py-PS layer placed in several positions within the film.

The effect of molecular weight and the structure of the repeat unit on the T_g of thin films of pyrene doped PS (< 0.2 wt% of the dry polymer weight) have been studied.[45] Molecular weights between 5,000 and 3,000,000 g/mol were investigated, with no effect on T_g reported. However, a change in the structure of the styrene monomer resulted in a significant increase in the dependence of T_g on film thickness whether poly(4-methylstyrene) (PMS) or poly(*tert*-butylstyrene) (PBS) were used.

Another recent article studied the T_g of the thin films of the block copolymers polystyrene-*block*-poly(2-vinylpyridine) (PS-*b*-P2VP) and polystyrene-*block*-poly(methyl methacrylate) (PS-*b*-PMMA).[46] The copolymer compositions ensured that they would phase separate into lamellae composed of the homopolymers. The films were doped with pyrene (< 0.2 wt% of the dry polymer weight). The I_1/I_3 ratios determined from the pyrene monomer fluorescence peaks showed that the pyrene was predominantly located in the PS lamellae. Compared to the T_gs of PS films, the PMMA block did not affect the T_g of the PS lamellae. On the contrary, the P2VP block had a strong effect on the T_g of the PS lamellae, eliminating the typical decrease in T_g that accompanies a decrease in PS film thickness. Thin films of homopolymers of pyrene-labeled PS (Py-PS) and P2VP, and Py-PS and PMMA with

thicknesses similar to the lamellae generated by the block copolymers were also investigated. It was determined that the boundary between the two homopolymers had little to no effect on the T_gs of the PS layer.

1.3.5 Characterizing Polymer Chain Dynamics in Dilute Solution

Numerous theoretical treatments[48–57] have been developed to describe the kinetics of end-to-end encounters of a polymer chain since focusing on the chain ends is much simpler than dealing with the encounters between any random internal segments of the chain. The first of these was conducted by Wilemski and Fixman, who derived a model describing end-to-end cyclization using the harmonic spring[48] and the Rouse-Zimm model.[49] These initial studies triggered an intense research effort aimed at determining the rate of end-to-end cyclization of long flexible polymers.

The first end-to-end cyclization experiments carried out on pyrene-labeled polymers were conducted by Cuniberti and Perico in 1977 using a series of end-labeled poly(ethylene oxides) (Py-PEO-Py) labeled at both ends with pyrene.[32] In these experiments, a measure of the rate constant for end-to-end encounters was obtained from the I_E/I_M ratio calculated from the steady-state fluorescence spectra. Shortly afterwards, Winnik et al. used the time-resolved fluorescence decays of pyrene end-labeled PS to determine directly the end-to-end cyclization rate constant.[31,33] Following these early experiments, the chain dynamics of many polymers have been studied in dilute solution, as a function of temperature, pressure, polymer concentration, and solvent viscosity.

Quantitative end-to-end cyclization studies were first completed by using end-labeled Py-PS-Py in toluene[33] and in cyclohexane at 34.5 ^{o}C,[31] a good and a θ-solvent, respectively. Polymer chain length and solvent quality were shown to have a strong effect on excimer

formation, and hence, the end-to-end cyclization event. In more recent years, randomly labeled poly(*N*,*N*-dimethylacrylamide) (Py-PDMA) was studied in much the same manner using the FBM to extract quantitative information on the process of excimer formation in DMF and acetone, a good and a poor solvent for Py-PDMA, respectively.[35,36] This work was critical to establish the way in which k_{blob} and N_{blob} characterize the volume probed by an excited pyrene. k_{blob} was found to be independent of viscosity in DMF, a good solvent with a viscosity of 0.79 mPa.s, and acetone, a poor solvent with a viscosity of 0.31 mPa.s. By definition, k_{blob} is a pseudo-unimolecular rate constant whose expression is given in Equation 1.14, where k_{diff} is the bimolecular rate constant for excimer formation between an excited pyrene and a ground-state pyrene and V_{blob} is the volume of a *blob*. Since both k_{diff} and V_{blob} are expected to be inversely proportional to the solution viscosity, changes in the two terms due to viscosity cancel out and k_{blob} remains constant. This interpretation is similar to that used to describe changes in k_q for micelles with different interior viscosities.[58] In addition, k_{blob} was found to scale as $N_{blob}^{-3\nu}$ where ν equals 0.5 and 0.6 in poor and good solvents respectively.[36]

In concentrated PDMA solutions, the N_{blob} value of Py-PDMA was found to decrease with increasing polymer concentration, while k_{blob} remained the same.[59] As discussed previously, a constant value for k_{blob} is predicted by Equation 1.14. The increase in local viscosity experienced by the polymer chain and the covalently attached pyrene as the polymer concentration is increased was responsible for a decrease in N_{blob}. Interestingly, the reduction in excimer formation and N_{blob} was much smaller than the increase in the macroscopic viscosity of the polymer solution, indicating that the chain motions are relatively unhindered locally as the polymer concentration is increased. A similarly mild

reduction in excimer formation had been observed upon increasing the PS concentration of a solution containing pyrene labeled polystyrene.[60]

$$k_{blob} = k_{diff} \times \frac{1}{V_{blob}} \tag{1.11}$$

The first study of the effect of temperature on polymer chain dynamics was completed by Redpath and Winnik.[61] They studied the end-to-end cyclization rate of three pyrene end-labeled polystyrenes (Py-PS-Pys) with molecular weights ranging from 3900 to 9200 g/mol and at temperatures ranging from 25 to 90 ^{o}C in toluene. They determined an activation energy for excimer formation in toluene of 14.2 kJ/mol, 60% larger than the 8.7 kJ/mol activation energy of the solvent viscosity of toluene (E_{η}). They suggested that this difference was likely due to an internal energy barrier for cyclization, although it is significantly smaller than the estimated barrier for internal backbone rotation of >20.9 kJ/mol for polystyrene.[62] They also determined that the binding energy of the excimer was –29.3 kJ/mol, very close to the value of –33.5 kJ/mol determined for pyrene in cyclohexane.[63]

This work was furthered by Martinho who studied a 4500 g/mol Py-PS-Py in several solvents ranging from good to poor in quality at temperatures ranging from 22 to 95 ^{o}C.[64] More recently, Martinho et al. studied the coil-to-globule transitions of a 3280 g/mol Py-PEO-Py in toluene[65] and a 19.6 kg/mol Py-poly(ε-caprolactone)-Py in THF.[66] The more thorough study of Py-PEO-Py in toluene reported that a decrease in temperature resulted in a change from a coil conformation to a compact globule that finally aggregated and precipitated out of solution at –30 ^{o}C. By multiplying the rate constant for excimer formation, k, by η/T, the effect of viscosity on the rate of excimer formation is removed. A

plot of $\ln(k\eta/T)$ as a function of $1/T$ resulted in a fairly constant value over the temperature range studied, which led to the conclusion that the process of excimer formation was diffusion controlled.

Poly(dimethylsiloxane) end-labeled with pyrene (Py-PDMS-Py) was studied at temperatures ranging from −18 to 53 ^{o}C in ethyl acetate, a theta-solvent for PDMS.[67] The upper critical solution theta temperature for PDMS in ethyl acetate is 5 ^{o}C. An excimer binding energy of −36 kJ/mol was calculated, close to that reported previously.[61] An internal energy barrier for cyclization ($E_{a,internal} = E_{cyc} - E_{\eta}$) was reported to equal 1.7 kJ/mol in ethyl acetate, very close to the barrier for internal backbone rotation of <2.5 kJ/mol for PDMS.

Several other studies have been completed using Py-PDMS-Py as a function of added CO_2 in toluene at different pressures,[68] as well as the effect of density on the end-to-end cyclization dynamics of Py-PDMS-Py dissolved in supercritical CO_2.[69,70]

Martinho et al. have completed some very encouraging work on randomly labeled polymers in recent years, pushing the limits of the FBM's ability to characterize the volume probed by an excited pyrene. The coil to globule transition of Py-PDMA in methanol[71] and Py-PS in cyclohexane[72] were studied. In both cases, the radius of a *blob* and the radius of the polymer coil were calculated as a function of temperature. For Py-PS, the coil radius determined by fluorescence was very close to the hydrodynamic radius of the polymer coil calculated from the Mark-Houwink-Sakurada (MHS) equation.[73]

The effect of solvent viscosity on excimer formation has been discussed to some degree in every study mentioned thus far. However, at least two studies have been completed that focused on the effect that viscosity has on the excimer formation of pyrene labeled polymers specifically. The first study looked at poly(vinylacetate) randomly labeled with pyrene (Py-

PVA)[74] and used the I_M/I_E ratio to determine the change in the rate of excimer formation associated with a change in solvent viscosity (0.5 to 15.5 mPa.s) and/or quality. The product of the I_M/I_E ratio with the inverse of the viscosity ($I_M/I_E \times 1/\eta$) was found to increase linearly as a function of intrinsic viscosity. In solvents of poor quality for PVA, the I_E/I_M ratio increased linearly with increasing η^{-1}. A second study was completed using Py-PEO-Py in 12 different solvents with viscosities ranging from 0.26 to 1.3 mPa.s using both steady-state and time-resolved fluorescence.[75] Both the I_E/I_M ratios and the rate constant for cyclization were found to increase linearly as a function of η^{-1}, with the exceptions of water which is a known poor solvent for the extremely hydrophobic pyrene groups. From these results it was determined that the rate of excimer formation was viscosity controlled.

1.3.6 Water-Soluble Pyrene-Labeled Polymers

A class of pyrene-labeled polymers that has generated significant interest are the hydrophobically modified water soluble polymers (HMWSP).[16] HMWSP are used as thickeners in water-based paints due to their interesting viscoelastic properties. In aqueous solution, the hydrophobic pendants form intermolecular physical cross-links that substantially increase the viscosity of the solution. The viscosity is reduced when the solution is placed under shear, such as the shear induced by a paint brush spreading paint on a wall. By replacing the hydrophobic pendants with pyrene groups, excimer formation can be used to describe how the hydrophobic pyrene pendants associate in aqueous solution. The water-soluble polymer constituting the HMWSP can be ionic, such as poly(acrylic acid) (PAcrylA),[76–79] and polysulfonates,[80] or non-ionic, such as poly(*N*-isopropylacrylamide) (PNIPAM),[37,38,81] poly(ethylene oxide),[82,83] and cellulose.[84]

Many of these studies use the I_E/I_M (or I_M/I_E) ratio as a measure of the local conformation of the polymer, also referred to as the coiling index.[85] For example, a classic study of pyrene-labeled PAcrylA (Py-PAcrylA) by Turro and Aurora[13] showed that at low pH (3 to 6), Py-PAcrylA adopts a more collapsed conformation shielding the pyrene groups from the polar solvent, resulting in a relatively low I_M/I_E value. As the pH is raised above 6 and more of the carboxylic acid groups become ionized, the coil expands resulting in an increase of the I_M/I_E ratio due to an expanded conformation that results in less excimer formation.

Quenching studies using nitromethane were performed with pyrene-labeled hydrophobically modified PNIPAM in water to determine the relative protection afforded to the pyrene group by the collapsed polymer coil.[81] Three series of polymers were studied, one with pyrene and octadecyl groups attached randomly along the backbone, the second with the pyrene and octadecyl groups attached together at random locations along the backbone, and the third with the pyrene and octadecyl group attached together specifically at one single chain end. All three polymers exhibited protective quenching compared to free pyrene in solution, the highest protection being observed for the PNIPAM sample where the pyrene and octadecyl groups were attached together. It was concluded that the access of the quencher to pyrene was hindered due to micelle formation, with the compactness of the micelle controlling the efficiency of the quencher.

1.4 Polypeptide Chain Dynamics

In the past number of years there has been intense interest in the study of protein and polypeptide chain dynamics. Numerous methods have been developed to study the dynamics and conformation of polypeptide chains, including temperature jump,[86] photochemical

initiation,[87] isotope-edited infrared spectroscopy,[88] and a considerable number of studies using NMR spectroscopy.[89–92] Luminescence experiments have also been used extensively, either taking advantage of the intrinsic fluorescence of the tyrosine[93] and tryptophan[94,95] residues, or attaching a chromophore and using luminescence techniques such as FA,[96,97] FRET[11,12] and end-to-end cyclization experiments.[98–100]

The backbone or side-chain dynamics of pyrene-labeled polypeptides have been investigated using fluorescence.[101-104] In one study, the host capabilities of cyclodextrin was examined by labeling a short α-helix with one pyrene and one cyclodextrin at specific locations.[101] An increase in the I_E/I_M ratio was observed as the concentration of the labeled α-helix was increased up to 10 μM. The increase in excimer formation demonstrated that the modified α-helix formed an associated dimer where two pyrene groups were accommodated by two associated cyclodextrins. When a guest molecule, hyodeoxychloic acid (HA), was added to the solution up to 160 μM, the I_E/I_M ratio decreased as the HA replaced the pyrene groups in the cyclodextrin host causing the dimers to separate.

In another study of pyrene-labeled polypeptides, the I_E/I_M ratio of a pyrene end-labeled peptide was used to follow the enzymatic cleavage of the peptide as a function of time.[102] The decrease in excimer formation as a function of time was used to quantify the activity of trypsin using several short peptides ranging in length from 5 to 8 amino acids. It was proposed that this method could be used to evaluate the activity of proteases in general.

The chain dynamics of polypeptides have been investigated by using pyrene-dansyl and napthyl-dansyl donor-accetor pairs for FRET experiments, where the donor and acceptor chromophore were attached at both ends of a $(gly\text{-}ser)_{16}$ peptide.[104] The experiments were conducted in aqueous solution with guanidinium chloride present at concentrations ranging

from 0 to 8 M. It was determined that the end-to-end distance increased approximately two-fold upon denaturation, while at the same time, the end-to-end diffusion constant also increased approximately 4 fold. The increase in end-to-end cyclization accompanying the expansion of the chain was rationalized by the significant number of hydrogen-bonding interactions in water that are eliminated by the denaturant, making the chain more flexible and less compact. It was also hypothesized that hydrogen-bonding may also influence the compact structure typically encountered after the hydrophobic collapse of a folded polypeptide.

Finally, the FBM was used to study the side-chain dynamics of poly(glutamic acid) randomly labeled with 1-pyrenemethylamine in DMF. It was found that pyrene attached itself in a clustered manner, and that a Py-PGA *blob* consisted of ~ 32 amino acids, which matched the maximum possible value, as determined using *Hyperchem* modeling software. Further work conducted in Chapter 4 refined this result and expanded it to another PGA construct where pyrene was attached to the α-helix via a longer linker.[105]

1.5 Circular Dichroism

1.5.1 Introduction

Circular dichroism (CD) is used to characterize the secondary structure of proteins and polypeptides. CD utilizes the difference in the absorption of left and right handed circularly polarized light by chiral, optically active molecules, where the absorption difference is the CD spectrum of the molecule. The CD expression is given in Equation 1.12.

The difference in absorption is due to the difference in the molar extinction coefficient of the chromophore given in Equation 1.13 from a solution of the chromophore with a concentration (C) in mol.L^{-1} placed in an absorbance cell of path length L in cm. The

wavelengths between 190-250 nm are used in a standard CD experiment to study the secondary structure of proteins. CD spectra are typically displayed using the molar ellipticity ($[\theta]$) in deg.cm^2.dmol^{-1} and whose expression is given in Equation 1.14.

$$CD = \Delta A = A_L - A_R \tag{1.12}$$

$$\Delta A = (\varepsilon_L - \varepsilon_R)CL = \Delta\varepsilon CL \tag{1.13}$$

$$[\vartheta] = \frac{180 \ln 10}{4\pi}\Delta\varepsilon = 3{,}298\Delta\varepsilon \tag{1.14}$$

Characteristic minima and maxima for the CD spectra of the three typical secondary structures found in proteins, namely α-helicies, β-sheets, and random coils, are shown in Figure 1.3. In this thesis, *N*,*N*-dimethylformamide (DMF) was used as a solvent for the polypeptides. This prevents the use of the 190 to 250 nm region employed to study the conformation of the polypeptide backbone, since it overlaps with the absorption wall of DMF which covers all wavelengths smaller than 270 nm when using a 0.1 cm cell typical of CD experiments. Despite this complication, the structure of a polypeptide can still be inferred from the orientation of the side-chains if a CD signal characteristic of the side-chains can be detected above 250 nm. This methodology has been applied in a number of instances described in the following section.

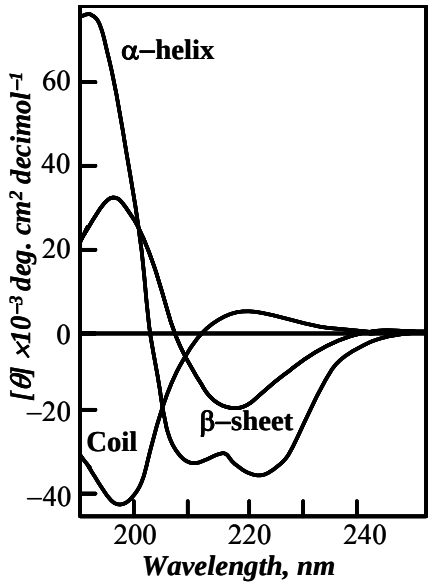

Figure 1.3: Examples of molar ellipticity curves corresponding to the three major secondary structures present in polypeptides and proteins. Poly(L-lysine) is shown in this diagram at various pH values; α-helix in basic, β-sheet in neutral, and random coil in acidic solutions.[106]

1.5.2 Circular Dichroism of Peptides Labeled with Chromophores

In addition to the CD spectra acquired between 190 and 250 nm resulting from the absorption of the peptide backbone, structural characteristics can also be determined from the side-chains of peptides bearing aromatic groups. Several polypeptides with side-chains labeled with pyrene or naphthalene have been studied using CD. [107–112] The example of two naphthalene-labeled polypeptides, namely poly(β-naphthylmethyl–L–aspartate) (PNAsp) and poly(L-1-naphthylalanine) (PNAla) is presented hereafter.

In the first study, PNAsp was shown to form a left-handed α-helix both in the solid state and in a mixture of dichloroethane and hexafluoroisopropanol.[107] The study also reported the CD spectra of copolymers of β-naphthylmethyl–L–aspartate and γ-benzyl–L–glutamate [P(NAsp-co-BGlu)] containing from 11 to 82 mol% NAsp residues. Poly(γ-benzyl–L–glutamate) (PBGlu) is known to form a right-handed helix in solution.[113] CD

spectra of PNAsp showed a positive peak centered at 280 nm, while the P(NAsp-co-BGlu) copolymers containing less than 82% NAsp residues had a negative peak, indicating that the PNAsp formed a left-handed helix of chirality opposite to that of PBGlu.

The second study using PNAla in trimethylphosphate solution presented six sets of theoretically calculated CD spectra representative of the structures potentially adopted by PNAla such as left and right handed α-helices, a 3_{10}-helix, and a δ-helix.[108,109] Comparison of the theoretically determined and experimentally acquired CD spectra led to the conclusion that the most likely structure was that of a left-handed 3_{10}-helix or a right handed δ-helix.

More recently, Nakahira et al. completed a study of poly(L-glutamic acid) labeled with 1-pyrenemethylamine (PPyMLGlu) in *N*,*N*-dimethylacetamide (DMA) solution and thin films as a function of pyrene content ranging from 25 to 45 mol% with degrees of polymerization ranging from 70 to 700.[110] Comparison of the CD spectra obtained experimentally and from molecular mechanics calculations indicated that for the highest molecular weight, the side-chains and main-chain were oriented differently whether the PPyMLGlu was in solution or in the film, this effect being likely due to intermolecular interactions in the film.

A second study of PPyMLGlu using chiral R- and S-(1-pyrenyl)ethyl-L-glutamic acids as the chromophore was completed as a function of temperature from 0 to 50 ^{o}C in DMA solution.[111] Higher excimer formation was found for the S configuration at all temperatures studied. Also, a lower activation energy for excimer formation was determined for the S configuration, 18 kJ/mol compared to 21.8 kJ/mol for the R configuration. Both observations indicate that the side-chains are more disordered when in the S configuration. Theoretical CD calculations were also conducted to determine possible side-chain orientations for each

structure, and indicated that a substantial amount of hydrogen bonding was present between the side chain amide groups and the backbone for both configurations.

Finally, a series of α-helical polypeptides containing L-1-pyrenylalanine and L-*p*-nitrophenylalanine separated by 0-8 amino acids was studied by CD and by measuring the electron transfer rates between the excited pyrene and nitrophenylalanine.[112] The CD intensity was determined at 278 nm for each sample in DMF and trimethylphosphate and confirmed the formation of an α-helix. The CD intensity was found to depend strongly on the number of amino acids separating the pyrene from the nitro group. Further experiments were conducted to measure the electron transfer rates as a function of the distance between the donor pyrene and acceptor nitro groups.

1.6 Project Objectives

For three decades, polymer chain dynamics have been studied using fluorescence and pyrene labeled polymers.[14-18] The original studies focused on synthetic polymers such as Py-PEO-Py and Py-PS-Py.[32,33] However, more recent investigations have focused on the time scale of protein folding.[98-100] The objective of this thesis is to use FDQ and the FBM analysis to study the backbone and side-chain dynamics of polymers and polypeptides randomly labeled with pyrene. In this respect, this thesis reports on two major accomplishments. The first one is to have contributed to a better understanding of the meaning of the FBM parameters. This was done by first exploring how the method of pyrene labeling affects excimer formation, and thus the FBM parameters that are retrieved from the analysis of the monomer and excimer fluorescence decays. This knowledge is essential since every polymer requires a unique synthetic strategy for pyrene labeling. A companion study was completed to determine how the FBM parameters respond to a change of excimer formation due to a

change in solvent viscosity. Finally, the similarities between the N_{blob} value determined from the FBM analysis and N_{agg}, the aggregation number of a surfactant micelle is discussed.

The second major accomplishment of this thesis is to have further established that polypeptides randomly labeled with pyrene can be studied with the FBM. A significant volume of work has been completed on the study of side-chain and backbone dynamics of polypeptides using NMR techniques and end-to-end cyclization techniques. However, considering the large body of work devoted to characterizing the chain dynamics of pyrene-labeled synthetic polymers such as Py-PS-Py, there is a glaring lack of studies where this knowledge has been applied to characterize the chain dynamics of polypeptides randomly labeled with pyrene. To address this deficiency, two studies of polypeptide chain dynamics were completed. The first study focuses on the side-chain dynamics of an α-helical polypeptide which were investigated for two different linker lengths connecting pyrene to the polypeptide backbone. The volume probed by the excited pyrene and the rate of excimer formation were determined and compared for both linker lengths. The second study focuses on the backbone dynamics of pyrene labeled poly(aspartic acid), an industrially important polypeptide that has generated significant interest as a biocompatible polymer.[114,115,116]

1.7 Thesis Outline

This thesis is organized in the following manner: Chapter 1 is a literature review of the use of fluorescence to study the chain dynamics of polymers and polypeptides. Chapter 2 is an in depth study of how the method of pyrene attachment onto a polymer backbone affects excimer formation and the FBM parameters used to describe them. In Chapter 3, the long range polymer chain dynamics of two pyrene-labeled polymers are studied as a function of solvent viscosity. A correlation between the N_{blob} value determined using an analogy with micellar quenching and the FBM is presented in Chapter 4. Chapter 5 explores the side-chain dynamics of an α-helical polypeptide as a function of probing time and side-chain length. Chapter 6 studies the chain dynamics of pyrene-labeled poly(aspartic acid). Finally, Chapter 7 offers several conclusions and some recommendations for future work.

1.8 References

1. Wouters, M. E. L.; Litvinov, V. M.; Binsbergen, F. L.; Goossens, J. P. G.; van Duin, M.; Dikland, H. G. *Macromolecules* **2003**, *36*, 1147-1156.

2. Spiess, H. W. *Macromol. Chem. Phys*. **2003**, *204*, 340-346.

3. Kimmich, R.; Fatkullin, N. *Adv. Polym. Sci*. **2004**, *170*, 1-113.

4. Mitsui, K.; Hara, M.; Ikai, A. *FEBS Lett*. **1996**, *385*, 29-33.

5. Kawakami, M.; Byrne, K.; Brockwell, D. J.; Radford, S. E.; Smith, D. A. *Biophys. J. Biophys. Lett*. **2006**, *91*, L16-L18.

6. Qian, H.; Elson, E. L. *Biophys. J*. **1999**, *76*, 1598-1605.

7. Perkins, T. T.; Quake, S. R.; Smith, D. E.; Chu, S. *Science* **1994**, *264*, 822-826.

8. Perkins, T. T.; Quake, S. R.; Smith, D. E.; Larson, R. G.; Chu, S. *Science* **1995**, *268*, 83-87.

9. a) Ono, K.; Ueda, K.; Sasaki, T.; Murase, S.; Yamamoto, M. *Macromolecules* **1996**, *29*, 1584-1588. b) Horinaka, J.; Amano, S.; Funada, H.; Ito, S.; Yamamoto, M. *Macromolecules* **1998**, *31*, 1197-1201.

10. Duhamel, J. in *Molecular Interfacial Phenomena of Polymers and Biopolymers* Editor: P. Chen, Woodhead Publishing Limited, Cambridge, **2005**, p 214-248.

11. Ha, T.; Ting, A. Y.; Liang, J.; Caldwell, W. B.; Deniz, A. A.; Chemla, D. S.; Schultz, P. G.; Weiss, S. *Proc. Natl. Acad. Sci. USA* **1999**, *96*, 893-898.

12. Nienhaus, G. U. *Macromol. Biosci*. **2006**, *6*, 907-922.

13. Turro, N. J.; Arora, K. S. *Polymer* **1986**, *27*, 783-796.

14. Cuniberti, C.; Perico, A. *Prog. Polym. Sci*. **1984**, *10*, 271-316.

15. Morewetz, H *J. Lumin*. **1989**, *43*, 59-71.

16. Winnik, F. M. *Chem. Rev*. **1993**, *93*, 587-614.

17. Duhamel, J. *Acc. Chem. Res.* **2006**, *39*, 953-960.

18. Winnik, M. A. *Acc. Chem. Res.* **1985**, *18*, 73-79.

19. Williams, S.; Causgrove, T. P.; Gilmanshin, R.; Fang, K. S.; Callender, R. H.; Woodruff, W. H.; Dyer, R. B. *Biochemistry* **1996**, *35*, 691-697.

20. Lednev, I. K.; Karnoup, A. S.; Sparrow, M. C.; Asher, S. A. *J. Am. Chem. Soc*. **1999**, *121*, 8074-8086.

21. Thompson, P. A.; Munoz, V.; Jas, G. S.; Henry, E. R.; Eaton, W. A.; Hofrichter, J. *J. Phys. Chem. B* **2000**, *104*, 378-389.

22. Hagen, S. J.; Hofrichter, J.; Szabo, A.; Eaton, W. A. *Proc. Natl. Acad. Sci. USA* **1996**, *93*, 11615-11617.

23. Abel, C. J.; Goldbeck R. A.; Latypov, R. F.; Roder, H.; Kliger, D. S. *Biochemistry* **2007**, *46*, 4090-4099.

24. Bai, Y.; Nussinov, R. Eds. *Protein Folding Protocols; Methods in Molecular Biology 350*, 2007, p 1-327.

25. Lakowicz, J. R. *Principles of Fluorescence Spectroscopy, 2nd Ed*. Kluwer Academic/Plenum Publishers: New York, 1999.

26. Birks, J. B. *Photophysics of Aromatic Molecules*. Wiley: New York, 1970, p 301.

27. Kalyanasundaran, K.; Thomas, J. K. *J. Am. Chem. Soc.* **1977**, *99*, 2039-2044.

28. Dong, D. C.; Winnik, M. A. *Can. J. Chem*. **1984**, *62*, 2560-2565.

29. Winnik, M. A.; Paton, K.; Danhelka, J.; Redpath, A. E. C. *J. Chrom*. **1982**, *242*, 97-102.

30. Mansson, P. *J. Polym. Sci,. Polym. Chem. Ed*. **1980**, *18*, 1945-1956.

31. Redpath, A. E. C.; Winnik, M. A. *J. Am. Chem. Soc*. **1980**, *102*, 6869-6871.

32. Cuniberti, C.; Perico, A. *Eur. Polym. J*. **1977**, *13*, 369-374.

33. Winnik, M. A.; Redpath, T.; Richards, D. H. *Macromolecules* **1980**, *13*, 328-335.

34. Mathew, H.; Siu, H.; Duhamel, J. *Macromolecules* **1999**, *32*, 7100-7108.

35. Kanagalingam, S.; Ngan, C. F.; Duhamel, J. *Macromolecules* **2002**, *35*, 8560-8570.

36. Kanagalingam, S.; Spartalis, J.; Cao, T.-C.; Duhamel, J. *Macromolecules* **2002**, *35*, 8571-8577.

37. Winnik, F. M. *Polymer* **1990**, *31*, 2125-2134.

38. Winnik, F. M. *Macromolecules* **1990**, *23*, 233-242.

39. Siu, H.; Duhamel, J. *Macromolecules* **2004**, *37*, 9287-9289.

40. Prazeres, T. J. V.; Beingessner, R.; Duhamel, J.; Olesen, K.; Shay, G.; Bassett, D. R. *Macromolecules*, **2001**, *34*, 7876-7884.

41. Kong H. J.; Lee, K. Y.; Mooney, D. J. *Macromolecules* **2003**, *36*, 7887-7890.

42. Frank, R. S.; Merkle, G.; Gauthier, M. *Macromolecules* **1997,** *30*, 5397-5402.

43. Brauge, L.; Caminade, A.-M.; Majoral, J.-P.; Slomkowski, S.; Wolszczak, M. *Macromolecules* **2001**, *34*, 5599-5606.

44. Ellison, C. J.; Torkelson, J. M. *Nat. Mater*. **2003**, *2*, 695-700.

45. Ellison, C. J.; Mundra, M. K.; Torkelson, J. M. *Macromolecules* **2005**, *38*, 1767-1778.

46. Roth, C. B.; Torkelson, J. M. *Macromolecules* **2007**, *40*, 3328-3336.

47. a) Forrest, J. A.; Dalnoki-Veress, K.; Stevens, J. R.; Dutcher, J. R. *Phys. Rev. Lett*. **1996**, *77*, 2002-2005. b) Tsui, O. K. C.; Wang, X. P.; Ho, J. Y. L.; Ng, T. K.; Xiao, X. *Macromolecules* **2000**, *33*, 4198-4204. c) Kim, S. D.; Torkelson, J. M. *Macromolecules* **2002**, *35*, 5943-5952.

48. Wilemski, G.; Fixman, M. *J. Chem. Phys*. **1974**, *60*, 866-877.

49. Wilemski, G.; Fixman, M. *J. Chem. Phys*. **1974**, *60*, 878-890.

50. Doi, M. *Chem. Phys*. **1975**, *9*, 455-466.

51. Szabo, A.; Schulten, K.; Schulten, Z. *J. Chem. Phys*. **1980**, *72*, 4350-4357.

52. Perico, A.; Bisio, S.; Cuniberti, C. *Macromolecules* **1984**, *17*, 2686-2689.

53. Camacho, C. J.; Thirumalai, D. *Proc. Natl. Acad. Sci. USA* **1995**, *92*, 1277-1281.

54. Ortiz-Repiso, M.; Freire, J. J.; Rey, A. *Macromolecules* **1998**, *31*, 8356-8362.

55. Rubio, A. M.; Pita, M.; Freire, J. J. *Macromolecules* **2002**, *35*, 5681-5687.

56. Doucet, D.; Roitberg, A.; Hagen, S. J. *Biophys. J*. **2007**, *92*, 2281-2289.

57. Hyeon, C.; Thirumalai, D. *J. Chem. Phys*. **2006**, *124*, 104905-104919.

58. Almgren, M.; Lofroth, J.-E. *J. Coll. Inter. Sci*. **1980**, *81*, 486-499.

59. Irondi, K.; Zhang, M.; Duhamel, J. *J. Phys. Chem. B* **2006**, *110*, 2628-2637.

60. Winnik, M. A.; Li, X.-B.; Guillet, J. E. *Macromolecules* **1984**, *17*, 699-702.

61. Redpath, A. E. C.; Winnik, M. A. *J. Am. Chem. Soc*. **1982**, *104*, 5604-5607.

62. Friedrich, C.; Lauprete, F.; Noel, C.; Monnerie, L. *Macromolecules* **1981**, *14*, 1119-1125.

63. Birks, J. B.; Lumb, M. D.; Munro, I. H. *Proc. R. Soc. London, Ser. A* **1964**, *280*, 289.

64. Martinho, J. M. G.; Resi e Sousa, A. T. *Macromolecules* **1993**, *26*, 4484-4488.

65. Farinha, J. P. S.; Picarra, S.; Miesel, K.; Martinho, J. M. G *J. Phys. Chem. B* **2001**, *105*, 10536-10545.

66. Picarra, S.; Gomes, P. T.; Martinho, J. M. G. *Macromolecules* **2000**, *33*, 3947-3950.

67. Gardinier, W. E.; Bright, F. V. *J. Phys. Chem. B* **2005**, *109*, 14824-14829.

68. Kane, M. A.; Baker, G. A.; Pandey, S.; Maziarz, E. P.; Hoth, D. C.; Bright, F. V. *J. Phys. Chem. B* **2000**, *104*, 8585-8591.

69. Kane, M. A.; Pandey, S.; Baker, G. A.; Perez, S. A.; Bukowski, E. J.; Hoth, D. C.; Bright, F. V. *Macromolecules* **2001**, *34*, 6831-6838.

70. Gardinier, W. E.; Kane, M. A.; Bright, F. V. *J. Phys. Chem. B* **2004**, *108*, 18520-18529.

71. Picarra, S.; Relogio, P.; Afonso, C. A. M.; Martinho, J. M. G.; Farhina, J. P. S. *Macromolecules* **2003**, *36*, 8119-8129.

72. Picarra, S.; Duhamel, J.; Fedorov, A.; Martinho, J. M. G. *J. Phys. Chem. B* **2004**, *108*, 12009-12015.

73. Bandrup, J.; Immergut, E. H.; Grulke, E. A. *Polymer Handbook*, 4th ed.; John Wiley & Sons: New York, 1999; p VII 675-683.

74. Cuniberti, C.; Perico, A. *Eur. Polym. J.* **1980**, *16*, 887-893.

75. Cheung, S.-T.; Winnik, M. A.; Redpath, A. E. C. *Makromol. Chem.* **1982**, *183*, 1815-1824.

76. Anghel, D. F.; Toca-Herrera, J. L.; Winnik, F. M.; Rettig, W.; Klitzing, R. *Langmuir* **2002**, *18*, 5600-5606.

77. Pokhrel, M. R.; Bossman, S. H. *J. Phys. Chem. B* **2000**, *104*, 2215-2223.

78. Deo, P.; Deo, N.; Somasundaran, P.; Jockusch, S.; Turro, N. J. *J. Phys. Chem. B*, **2005**, *109*, 20714-20718.

79. Seixas de Melo, J.; Costa, T.; da G. Miguel, M.; Lindman, B.; Schillen, K. *J. Phys. Chem. B* **2003**, *107*, 12605-12621.

80. Morishima, Y.; Tominaga, Y.; Kamachi, M.; Okada, T.; Hirata, Y.; Mataga, N. *J. Phys. Chem.* **1991**, *95*, 6027-6034.

81. Barros, T. C.; Adronov, A.; Winnik, F. M.; Bohne, C. *Langmuir* **1997**, *13*, 6089-6094.

82. Char, K.; Frank, C. W.; Gast, A. P. *Macromolecules* **1989**, *22*, 3177-3180.

83. Duhamel, J.; Yekta, A.; Hu, Y.-Z.; Winnik, M. A. *Macromolecules* **1992**, *25*, 7024-7030.

84. Winnik, F. M.; Winnik M. A.; Tazuke, S.; Ober, C. K. *Macromolecules* **1987**, *20*, 38-44.

85. Kramer, G.; Somasundaran, P. *Langmuir* **2002**, *18*, 9357-9361.

86. a) Williams, S.; Causgrove, T. P.; Gilmanshin, R.; Fang, K. S.; Callender, R. H.; Woodruff, W. H.; Dyer, R. B. *Biochemistry* **1996**, *35*, 691-697. b) Lednev, I. K., Karnoup, A. S., Sparrow, M. C., Asher, S. A. *J. Am. Chem. Soc*. **1999**, *121*, 8074-8086. c) Thompson, P. A.; Munoz, V.; Jas, G. S.; Henry, E. R.; Eaton, W. A.; Hofrichter, J. *J. Phys. Chem. B* **2000**, *104*, 378-389.

87. a) Hagen, S. J.; Hofrichter, J.; Szabo, A.; Eaton, W. A. *Proc. Natl. Acad. Sci. USA* **1996**, *93*, 11615-11617. b) Abel, C. J.; Goldbeck R. A.; Latypov, R. F.; Roder, H.; Kliger, D. S. *Biochemistry* **2007**, *46*, 4090-4099.

88. Decatur, S. M. *Acc. Chem. Res*. **2006**, *39*, 169-175.

89. Palmer, A. G. *Annu. Rev. Biophys. Biomol. Struc*. **2001**, *30*, 129-155.

90. Kay, L. E. *Biochem. Cell Biol*. **1998**, *76*, 145-152.

91. Jarymowycz, V. A.; Stone, M. J. *Chem. Rev*. **2006**, *106*, 1624-1671.

92. Igumenova, T. I.; Frederick, K. K.; Wand, A. J. *Chem. Rev*. **2006**, *106*, 1672-1699.

93. Unruh, J. R.; Liyange, M. R., Johnson, C. K. *J. Phys. Chem. B* **2007**, *111*, 5494-5502.

94. Gonelli, M.; Strombini, G. B. *Biochemistry* **1995**, *34*, 13847-13857.

95. Clayton, A. H. A.; Sawyer, W. A. *Eur. Biophys. J*. **2002**, *31*, 9-13.

96. Ha, T. H.; Laurence, T. A.; Chemla, D. S.; Weiss, S. *J. Phys. Chem. B* **1999**, *103*, 6839-6850.

97. Sharma, J.; Tleugabulova, D.; Czardybon, W.; Brennan, J. D. *J. Am. Chem. Soc*. **2006**, *128*, 5496-5505.

98. a) Bieri, O.; Wirz, J.; Hellrung, B.; Schutkowski, M.; Drewello, M.; Kiefhaber, T. *Proc. Natl. Acad. Sci. USA* **1999**, *96*, 9597-9601. b) Satzger, H.; Schmidt, B.; Root, C.; Zinth, W.; Fierz, B.; Krieger, F.; Kiefhaber, T.; Gilch, P. *J. Phys. Chem. A* **2004**, *108*, 10072-10079. c) Krieger, F.; Fierz, B.; Bieri, O.; Drewello, M.; Kiefhaber, T. *J. Mol. Biol*. **2003**, *332*, 265-274. d) Kriger, F.; Fierz B.; Axthelm, F.; Joder, K.; Meyer, D.;

Kiefhaber, T. *Chem. Phys.* **2004**, *307*, 209-215. e) Moglich, A.; Krieger, F.; Kiefhaber, T. *J. Mol. Biol*. **2005**, *345*, 153-162.

99. a) Hudgins, R. R.; Huang, F.; Gramlich, G.; Nau, W. M. *J. Am. Chem. Soc*. **2002**, *124*, 556-564. b) Huang, F.; Hudgins, R. R.; Nau, W. M. *J. Am. Chem. Soc*. **2004**, *126*, 16665-16675. c) Roccatano, D.; Sahoo, H.; Zacharias, M.; Nau, W. M. *J. Phys. Chem. B* **2007**, *111*, 2639-2646.

100. a) Neuweiler, H.; Schulz, A.; Bohmer, M.; Enderlein, J.; Sauer, M. *J. Am. Chem. Soc*. **2003**, *125*, 5324-5330. b) Neuweiler, H.; Lollmann, M.; Doose, S.; Sauer, M. *J. Mol. Biol*. **2007**, *365*, 856-869.

101. Hossain, M. A.; Hamasaki, K.; Mihara, H.; Ueno, A. *Chem. Lett*. **2000**, *3*, 252-253.

102. Ahn, T.; Kim, J.-S.; Choi, H.-I.; Yun, C.-H. *Anal. Biochem*. **2002**, *306*, 247-251.

103. Jones II, G.; Zhou, X.; Vullev, V. I. *Photochem. Photobiol. Sci*., **2003**, *2*, 1080-1087.

104. Moglich, A.; Joder, K.; Kiefhaber, T. *Proc. Natl. Acad. Sci*. **2006**, *103*, 12394-12399.

105. Duhamel, J.; Kanagalingam, S.; O'Brien, T.; Ingratta, M. *J. Am. Chem. Soc.* **2003**, *125*, 12810-12822.

106. Greenfield, N.; Fasman, G. D. *Biochemistry* **1969**, *8*, 4108-4116.

107. Ueno, A.; Ishiguro, T.; Toda, F.; Uno, K.; Iwakura, Y. *Biopolymers* **1975**, *14*, 353-362.

108. Sisido, M.; Egusa, S.; Imanshi, Y. *J. Am. Chem. Soc*. **1983**, *105*, 1041-1049.

109. Sisido, M.; Egusa, S.; Imanshi, Y. *J. Am. Chem. Soc*. **1983**, *105*, 4077-4082.

110. Shoji, O.; Ohkawa, M.; Kuwata, H.; Sumida, T.; Kato, R.; Annaka, M.; Yoshikuni, M.; Nakahira, T. *Macromolecules* **2001**, *34*, 4270-4276.

111. Shoji, O.; Nakajima, D.; Ohkawa, M.; Fujiwara, Y.; Annaka, M.; Yoshikuni, M.; Nakahira, T. *Macromolecules* **2003**, *36*, 4557-4566.

112. Sisido, M.; Hoshino, S.; Kusano, H.; Kuragaki, M.; Makino, M.; Sasaki, H.; Smith, T.; Ghiggino, K. P. *J. Phys. Chem. B* **2001**, *105*, 10407-10415.

113. a) Doty, P.; Wada, A.; Yang, J. T.; Blout, E. R. *J. Polym. Sci*. **1957**, *23*, 851-861. b) Idelson, M.; Blout, E. R. *J. Am. Chem. Soc*. **1958**, *80*, 4631-4634. c) Yamaoka, K.; Ueda, K. *J. Phys. Chem*. **1982**, *86*, 406-413.

114. Caldwell, G.; Neuse, N. W.; Perlwitz, A. G. *J. Appl. Polym. Sci*. **1997**, *66*, 911-919.

115. Shinoda, H.; Asou, Y.; Suetsugu, A.; Tanaka, K. *Macromol. Biosci*. **2003**, *3*, 34-43.

116. Kang, H. S.; Yang, R. R.; Kim, J.-D.; Han, S.-H.; Chang, I.-S. *Langmuir* **2001**, *17*, 7501-7506.

Chapter 2:
Correlating Pyrene Excimer Formation with Polymer Chain Dynamics in Solution: Possibilities and Limitations

2.1 Abstract

Four types of pyrene-labeled polystyrene samples (Py-PS) were prepared and the process of excimer formation between the pyrene labels was characterized by steady-state and time-resolved fluorescence to assess the effect the mode of pyrene incorporation into a polymer has on the kinetics of excimer formation. The pyrene label was incorporated into the PS backbone by either 1) reacting sodium 1-pyrenemethoxide with a chloromethylated polystyrene backbone to yield the GrE-PS series, 2) copolymerizing styrene with 4-(1-pyrenyl)methoxymethyl styrene to yield the CoE-PS series, 3) copolymerizing styrene with *N*-(1-pyrenylmethyl)acrylamide to yield the CoA-PS series, or 4) polymerizing α,ω-dicarboxyl end-capped polystyrenes with *L*-lysine-1-pyrenemethylamide dihydrochloride to yield the ES-PS series. Steady-state and time-resolved fluorescence experiments demonstrated that the long and flexible linker of GrE-PS and CoE-PS enabled more efficient excimer formation than the short and rigid linker of CoA-PS, and that spacing the pyrene pendants in ES-PS led to a strong reduction in excimer formation. The fluorescence blob model (FBM) was applied to analyse quantitatively the monomer and excimer fluorescence decays of the four Py-PSs. The FBM analysis confirmed that the longer ether linker of GrE-PS and CoE-PS enabled the excited pyrene label to probe a larger volume inside the polymer coil. The level of clustering of the pyrene pendants was found to be minimal for ES-PS, as expected from its structural design. Interestingly, the pyrene pendants were twice more clustered for GrE-PS than for CoE-PS, despite both polymers having an identical chemical structure. The results for the GrE-PS and CoE-PS series suggest that reacting groups distribute themselves differently in a copolymer whether they are incorporated by a *grafting onto* reaction or copolymerization.

2.2 Introduction

Ever since Cuniberti and Perico[1,2] and Winnik[3] demonstrated 30 years ago that information on end-to-end chain cyclization could be obtained by labeling both ends of a chain with a pyrene moiety and monitoring excimer formation from the diffusive encounters between the two pyrene moieties, the process of pyrene excimer formation has been used to gain information about polymer chain dynamics. Since then, the use of fluorescence to monitor the encounters between two pyrene chromophores attached onto a polymer has yielded a wealth of information on long range dynamics,[4,5] conformation,[6-8] and aggregation[9,10] of polymers in solution. These fluorescence experiments are conducted by exciting a pyrene moiety with UV light and monitoring its emission at around 375 nm. An encounter between an excited pyrene and a ground-state pyrene results in the formation of an excimer whose emission is red-shifted with respect to that of the monomer, to about 480 nm.[11] Since the pyrene moieties are attached onto the polymer, excimer formation indicates that two units of the polymer have encountered. By analyzing the process of excimer formation, information on the behaviour of the polymer in solution is retrieved.[1,5]

In the majority of cases, the rule of thumb for incorporating pyrene into a polymer depends to a large extent on the labeling strategy being as easy as possible and the linker connecting pyrene to the polymer being as stable as possible in the given solvent. Once labeled, the behaviour of the polymer is investigated by following the kinetics of excimer formation.[1-10] Amoung the numerous studies conducted using pyrene-labeled polymers, only a few have noted a difference in excimer formation when changes are made to the method of pyrene incorporation,[12] or to the length[13] or type[14] of the linker used to connect the pyrene probe to the polymer backbone. In view of the large body of studies where pyrene-labeled

polymers are used,[4,5,9,10] there is a glaring lack of knowledge on the effect that the mode of pyrene incorporation into a polymer has on the very excimer formation used to draw conclusions on the polymer behaviour. This study addresses this issue by investigating the effect that the three following parameters have on the process of excimer formation between pyrenes attached along a polymer chain: 1) the method of pyrene incorporation, 2) the nature of the linker connecting pyrene to the backbone, and 3) the pyrene distribution along the polymer backbone. The study focuses on pyrene-labeled polymers where pyrene is incorporated along the backbone since the preparation of such polymers is usually much less demanding[5,9,10,15-17] than that of polymers where pyrene is introduced at specific positions, typically the chain ends.[1-4]

To determine the effect of the method of pyrene incorporation, two series of pyrene labeled polystyrene (Py-PS) with identical structure were synthesized in two different ways. The first was prepared by synthesizing PS, chloromethylating a small portion of the aromatic rings, and subsequently reacting the chloromethylated backbone with sodium 1-pyrenemethoxide. This process yields PS where pyrene was grafted onto the PS backbone via an ether linkage (GrE-PS).[18] The second was prepared by synthesizing a 4-(1-pyrenyl)methoxymethyl styrene monomer and copolymerizing it with styrene (CoE-PS). Both of these syntheses produce PS samples randomly labeled with pyrene groups which have identical chemical structure, but potentially different distributions of pyrene pendants along the chain.

To determine the effect that the linker connecting pyrene to the backbone has on excimer formation, a second copolymer was prepared using N-(1-pyrenylmethyl)acrylamide as the pyrenyl monomer (CoA-PS). CoE-PS and CoA-PS are expected to display a similar

distribution of pyrene pendants along the backbone with the stiffer amide linker of CoA-PS keeping the pyrene much closer to the backbone than the ether linker used for the CoE-PS series.

Finally, the effect of pyrene distribution was determined by condensation of *L*-lysine-1-pyrenemethylamide dihydrochloride containing two free amines with short monodispersed PS chains terminated with carboxylic acid functions at both ends. This route yields PS with pyrene evenly-spaced throughout the backbone (ES-PS). The side-chain structure is the same as that of the N-(1-pyrenylmethyl)acrylamide used for the CoA-PS series which allows the comparison of a PS sample where pyrene has been incorporated in a well-defined manner (ES-PS) with a PS sample randomly labeled with pyrene (CoA-PS).

To the best of our knowledge, this study represents the first example where the effect of the mode of pyrene incorporation into a polymer on the kinetics of excimer formation is systematically investigated. The quantitative analysis of the fluorescence data presented in this work is enabled by the recently developed fluorescence blob model (FBM).[18] Currently, this is the only analytical tool available capable of differentiating the contributions made by the chain dynamics and local pyrene concentration which both affect the formation of excimer between pyrenes attached randomly onto a polymer.[5] The body of results generated in the study is expected to become a reference point used to compare trends obtained from the kinetics of excimer formation between pyrene pendants attached onto a polymer via different methods. It is expected to facilitate the comparison between the numerous trends resulting from the vast number of studies that have been and continue to be conducted with pyrene-labeled polymers.[4,5,9,10]

2.3 Experimental

Materials: Chemicals were purchased from Sigma-Aldrich (Milwaukee, WI) and used as received unless otherwise stated. Distilled in glass DMF and THF were purchased from Caledon Laboratories (Georgetown, ON) and used as received. Three α,ω-dicarboxyl end-capped polystyrenes: i) M_n = 3000, PDI = 1.10, Func. = 1.90; ii) M_n = 4500, PDI = 1.12, Func. = 1.95; and iii) M_n = 8000, PDI = 1.09, Func. = 1.95; were purchased from Polymer Source (Montréal, QC).

Pyrene-labeled polystyrene obtained by grafting pyrene onto the chain (GrE-PS): The synthesis and characterization of the GrE-PS has been described elsewhere.[18] Molecular weights and polydispersities can be found in Table A2.1 in the Appendix. The chemical structure of GrE-Ps and all other polymers can be found in Scheme 2.1.

CoE-PS and GrE-PS	CoA-PS	ES-PS
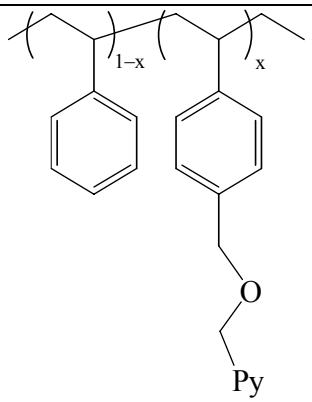	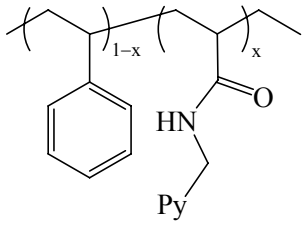	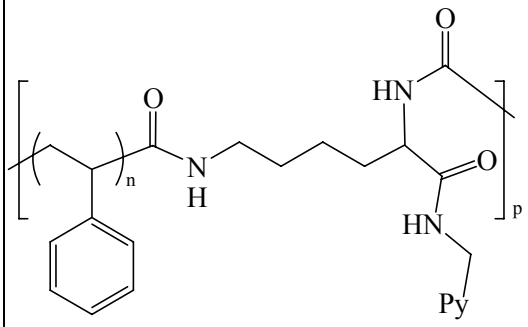

Scheme 2.1: Chemical structures of CoA-PS, CoE-PS, GrE-PS, and ES-PS.

Synthesis of N-(1-pyrenylmethyl)acrylamide: The synthesis and purification of N-(1-pyrenylmethyl)acrylamide (PyMAAm) has been described elsewhere.[19]

Synthesis of 4-(1-pyrenyl)methoxymethyl styrene (PyMMS): In a dry 50 mL round bottom flask, 5.4 mg (2.16 mmol) of sodium hydride was added to 6 mL of DMF and stirred for 5 minutes at room temperature. 1-Pyrenemethanol (0.575 g, 2.48 mmol) was added and stirred for 30 minutes at room temperature. *p*-Chloromethylstyrene (0.343 g, 2.25 mmol) was added and the solution was heated to 60 ^{o}C and stirred for 4 hours. The solution was removed from heat and precipitated in water, followed by centrifugation to isolate the solid product. The crude product was dissolved in methylene chloride ($MeCl_2$) and washed with 1 N HCl, 5 wt% sodium carbonate solution, and water. The methylene chloride was dried with Na_2SO_4 filtered and removed by rotary evaporation. A silica gel column using 1:1 hexane and methylene chloride was used to further purify the product. The solid was then re-crystallized in cyclohexane to obtain a white-yellow solid in a 41% yield. 300 MHz ^{1}H NMR ($CDCl_3$) PyMMS: δ 4.6 (s, 2H, Ar-CH_2-O), δ 5.2 (dd, 1H, alkene trans-H), δ 5.2 (s, 2H, Py-CH_2-O), δ 5.7 (dd, 1H, alkene cis-H), δ 6.7 (q, 1H, alkene gem-H), δ 7.4 (m, 4H, ArH), δ 7.9-8.4 (several peaks, 9H, pyrenyl H's).

Random copolymerization: The copolymers were prepared by radical polymerization of styrene and PyMAAm or PyMMS. Styrene was purified by three successive washes with 4 M NaOH to remove inhibitor, followed by two distillations under reduced pressure. The pyrene content was varied by adding increasing amounts of the pyrenyl monomer. The final pyrene content was determined post-synthesis using UV-Vis analysis.

The general synthesis using PyMAAm as an example is described in detail. A Schlenk tube was flame dried and purged with N_2, followed by the addition of 0.4 g (3.84 mmol)

styrene, 90 mg (0.31 mmol) PyMAAm, and 2 mL of 0.2 mg/mL AIBN solution in DMF. The solution was deaerated by bubbling N_2 for 15 mins. The reaction was conducted at 65 ^oC to a conversion of approximately 0.2 to minimize composition drift. Conversion was determined through ^1H NMR analysis (vide infra). The polymer was precipitated in methanol, re-dissolved in THF and precipitated in methanol 5-7 times to remove unreacted pyrenyl monomer. The final yield was approximately 10% in each case.

300 MHz ^1H NMR ($CDCl_3$): Poly(styrene-*co*-PyMMS): δ 1.2 (broad, ~ 2H, CH_2), δ 1.8 (broad, ~1H, CH), δ 4.5 (broad, seen in polymers with pyrene contents > 5 mol %, Ar-CH_2-O), δ 5.4 (broad, seen in polymers with pyrene contents > 5 mol %, Py-CH_2-O), δ 5.7, δ 6.5 and δ 7.0 (broad, 4H, ArH), δ 7.9-8.4 (multiple peaks, pyrenyl H's). UV-vis (THF): peaks at 314, 328, 344 nm.

300 MHz ^1H NMR ($CDCl_3$): Poly(styrene-*co*-PyMAAm): δ 1.2 (broad, ~ 2H, CH_2), δ 1.8 (broad, ~1H, CH), δ 5.2 (broad, seen in polymers with pyrene contents > 5 mol %, Py-CH_2), δ 6.5 and δ 7.0 (broad, 4H, ArH), δ 7.9-8.4 (broad, pyrenyl H's). UV-vis (THF): peaks at 314, 328, 344 nm.

Molecular weight determination: Apparent molecular weights were determined by Gel Permeation Chromatography (GPC) with a Waters 501 HPLC pump and a Waters 410 DRI, using THF as an eluent and a 500 mm Jordi linear DVB mixed-bed column with a 10 mm inner diameter. All measurements were conducted at room temperature. The column was calibrated using known molecular weight polystyrene standards. These experiments were carried out at room temperature. Many of the M_n values were in the ~30 K range with a polydispersity index (PDI) around 1.8 - 2.0 (Table A2.1).

An earlier study on pyrene-labeled GrE-PS demonstrated that the fluorescence signal of the randomly labeled polymers does not depend on polymer chain length as long as the polymer chain length is longer than a *critical polymer chain length* (*cpcl*) whose value was estimated to lay between 6 and 40 K.[18] Consequently, a 30 K PS sample with a PDI of 2.0 might contain a substantial fraction of chains whose chain length is smaller than the *cpcl*. As a result, GPC was used to fractionate the PS samples. Due to the high sensitivity of fluorescence measurements and the small amounts of sample required, a standard GPC column was adequate for the fractionation instead of a preparatory column. The fluorescence experiments were run with the whole Py-PS samples, as well as their fractions containing a polymer molecular weight larger than 40 K (Table A2.2). Within experimental error, no discrepancy could be found between the results whether the fluorescence experiments were conducted with the whole Py-PS sample or the Py-PS fraction having a larger molecular weight. (See Figures A2.1 and A2.2 and Tables A2.3 – A2.10). Nevertheless, the Results and Discussion sections present the results obtained from the steady-state and time-resolved fluorescence experiments conducted on the high molecular weight fractions to ensure that all conclusions are drawn from data acquired with polymers whose chain length is larger than the *cpcl*.

Composition drift during polymerization: The reactivity ratios for styrene and *p*-chloromethylstyrene in benzene are 0.62 and 1.12, respectively.[20] The reactivity ratios for styrene and *N*-methylacrylamide in dioxane are 2.10 and 0.64, respectively.[21] The different reactivity ratios imply that some composition drift might occur during the copolymerization. To minimize this eventuality, the copolymerizations were conducted up to a low conversion. Changes in monomer incorporation into the copolymer were monitored as a function of

conversion for both copolymerizations. Samples were removed periodically during the reaction. ^{1}H NMR was used to determine the conversion and GPC coupled with a fluorescence detector was employed to determine the ratio of the fluorescence intensity of the excimer over that of the monomer, the I_E/I_M ratio, as a function of conversion to detect eventual deviations from a random incorporation of the pyrene labeled monomers. The I_E/I_M ratio is sensitive to the pyrene content of the polymer and is expected to respond to an eventual composition drift during the copolymerization.

The conversion of the reaction was determined by integrating the vinyl monomer peaks in the ^{1}H NMR spectrum relative to the signal of trifluoroacetic acid (TFA) which was placed in a small insert at the center of the NMR tube containing a measured aliquot of the reaction solution in $CDCl_3$. For the copolymerization between styrene and PyMAAm, the monomer peaks used were 5.7 ppm and 6.1 ppm, respectively. For the copolymerization of styrene and PyMMS, the peaks overlapped at 5.7 ppm and were integrated together. The same insert was used for the acquisition of each NMR spectrum and the signal of the TFA standard was taken as a reference. Thus, as the monomers were consumed, the vinyl peaks at 5.7 and 6.1 ppm decreased, and the monomer conversion was calculated. The samples were also injected into a GPC instrument equipped with an online Agilent 1100 series fluorescence detector. The GPC column enabled the separation of the labeled polymer from the unreacted pyrene-labeled monomer. The I_E/I_M ratios were obtained for the peak corresponding to the polymer in the GPC trace (I_E = 490 nm; I_M = 390 nm). Within experimental error, the I_E/I_M ratios remained constant over the low conversion (~0.2) used for these copolymerizations. Two examples are shown in Table A2.11.

Synthesis of L-lysine-1-pyrenemethylamide dihydrochloride: In a round bottom flask, 0.500 g (1.07 mmol) N_α,N_ε-di-Boc-*L*-lysine paranitrophenol ester (Bachem Chemicals), 0.258 g (0.963 mmol) 1-pyrenemethylamine hydrochloride, 0.2 g (1.98 mmol) triethylamine, and 20 mL $MeCl_2$ were added. The reaction was stirred overnight at room temperature. The reaction mixture was extracted 2 × with 1 M HCl, 2 × with 5 wt% sodium bicarbonate solution, and 2 × with water. The $MeCl_2$ solution was dried over $MgSO_4$, filtered, and the $MeCl_2$ was removed by rotary evaporation. The remaining solid was washed in a 1:1 benzene:hexane mixture and N_α,N_ε-di-Boc-*L*-lysine-1-pyrenemethylamide was recovered in a 85% yield.

300MHz ^{1}H NMR (DMSO-*d6*): N_α,N_ε-di-Boc-*L*-lysine-1-pyrenemethylamide: δ 1.3 (broad, 18H t-boc and 4H, 2 × CH_2), δ 1.5 (m, 2H, CH_2), δ 2.8 (m, 2H, CH_2), δ 3.9 (broad, 1H, CH), δ 5.0 (m, 2H, Py-CH_2), δ 6.7 (t, 1H, NH), δ 6.9 (d, 1H, NH), δ 7.9-8.4 (many sharp pyrene peaks, broad amine peaks), δ 8.5 (t, 1H, amide NH).

In a round bottom flask, 0.4 g (0.714 mmol) N_α,N_ε-di-Boc-*L*-lysine-1-pyrenemethylamide and 10 mL of 4 M HCl in dioxane were added and stirred for 1 hr. Dioxane was removed by rotary evaporation, and the *L*-lysine-1-pyrenemethylamide dihydrochloride was precipitated as a solid product in ether in a 90% yield.

300MHz ^{1}H NMR (DMSO-*d6*) *L*-lysine-1-pyrenemethylamide dihydrochloride: δ 1.3 (m, 2H CH_2), δ 1.4 (m, 2H, CH_2), δ 1.7 (m, 2H, CH_2), δ 2.6 (m, 2H, CH_2), δ 3.8 (m, 1H, CH), δ 5.1 (d, 2H, Py-CH_2), δ 7.9-8.4 (many sharp pyrene peaks, broad amine peaks), δ 9.3 (t, 1H, amide NH).

Synthesis of evenly-spaced polystyrene (ES-PS): The ES-PS samples were prepared by copolymerizing α,ω-dicarboxyl end-capped polystyrene having M_n equal to 3000, 4500, and

8000 g/mol with *L*-lysine-1-pyrenemethylamide dihydrochloride. An example synthesis is described for the polymer having an M_n of 4500 g/mol.

In a 7 mL vial, 0.1 g (0.022 mmol) 4500 g/mol α,ω-dicarboxyl end-capped polystyrene, 9.6 mg (0.022 mmol) *L*-lysine-1-pyrenemethylamide dihydrochloride, 42 mg (0.22 mmol) EDC, 30 mg (0.22 mmol) HOBt, 0.50 g (0.05 mmol) triethylamine, and 1 mL DMF were added. The reaction was stirred at room temperature for 20 hrs. The polymer was precipitated in methanol, re-dissolved in THF and precipitated in methanol 5-7 times to remove unreacted pyrenyl monomer. A very broad molecular weight distribution was obtained. The ES-PS sample contained a substantial amount of the PS starting material which could not be separated from the longer polymer chains using precipitation. To circumvent this problem, the polymer was fractionated using GPC to obtain a high molecular weight (HMW) fraction used for the fluorescence experiments. Molecular weights of the HMW fractions were determined using a fluorescence detector where the column was calibrated by using the fluorescence of polystyrene standards and are found in Table A2.2. Only the HMW fractions of the ES-PS samples were investigated.

Pyrene content: A Hewlett Packard 8452A diode array spectrophotometer was used for the absorption measurements. The copolymer composition was determined from its pyrene content.

The pyrene content of the polymer (λ_{Py}) was obtained by dissolving a known mass of pyrene labeled polymer (m) in a known volume of THF (V). The concentration of pyrene, [Py], was then determined by applying Beer-Lambert's Law to the peak absorption at 344 nm and using the extinction coefficient of the model compound 1-pyrenemethanol in THF (ε_{py}) found

to equal 43,000 $M^{-1}.cm^{-1}$. The pyrene content, λ_{Py}, whose expression is given in Equation 2.1, is expressed in μmole of pyrene per gram of polymer ($\mu mol.g^{-1}$).

$$\lambda_{Py} = \frac{[Py]}{m/V} \tag{2.1}$$

Steady-state fluorescence measurements: All fluorescence spectra were acquired on a PTI fluorometer. The spectra were obtained with the usual right angle geometry. Polymer solutions had a pyrene concentration below 3×10^{-6} M to avoid intermolecular interactions and were degassed with N_2 for 20 minutes to remove oxygen. The solution OD was ~ 0.1 at 344 nm in each case. The solutions were excited at 344 nm and the fluorescence intensity of the monomer (I_M) and excimer (I_E) were obtained by integrating the fluorescence intensity between 372-378 nm for the monomer and 500-530 nm for the excimer, respectively.

Time-resolved fluorescence measurements: Monomer and excimer decays were obtained by exciting the solutions at 340 nm with an IBH 340 nm LED and monitoring the fluorescence emission at 375 and 510 nm, respectively. All decays were collected over 1024 channels with up to 20,000 counts at the peak maximum for the lamp and decay curves. The instrument response function was determined by applying the MIMIC method[22] to the lamp reference decays obtained with PPO [2,5-diphenyloxazole] in cyclohexanol (τ = 1.42 ns) and BBOT [2,5-bis(tert-butyl-2-benzoxazolyl)thiopene] in ethanol (τ =1.47 ns) for the monomer and excimer decays, respectively. The polymer solutions were prepared in the same manner as for the steady-state fluorescence experiments.

Analysis of the fluorescence decays: The fluorescence decays of the monomer and excimer were fit with a sum of exponentials (Equation 2.2) or by using a global analysis based on the

FBM to fit the monomer (Equation 2.3) and excimer (Equation 2.5) simultaneously.[23] In the FBM framework, a *blob* represents the volume probed by an excited pyrene during its lifetime. Equation 2.3 was originally developed by applying the same mathematical derivation used to describe the formation of excimer between pyrene molecules distributed in surfactant micelles,[24] but has since been used in several recent publications to study polymer dynamics in solution.[5,18,19,23,25,26]

$$i(t) = \sum_{i=1}^{n_{\exp}} a_i \exp(-t/\tau_i) \text{ with } n_{exp} = 2\text{-}4 \tag{2.2}$$

$$[Py^*]_{(t)} = \left[Py^*_{diff}\right]_{(t=0)} \exp\left[-\left(A_2 + \frac{1}{\tau_M}\right)t - A_3\left(1-\exp\left(-A_4 t\right)\right)\right] + \left[Py^*_{free}\right]_{(t=0)} \exp\left(-t/\tau_M\right) \tag{2.3}$$

The parameters A_2, A_3, and A_4 used in Equation 2.3 are described in Equation 2.4.

$$A_2 = \langle n \rangle \frac{k_{blob} k_e [blob]}{k_{blob} + k_e [blob]} \quad A_3 = \langle n \rangle \frac{k^2_{blob}}{\left(k_{blob} + k_e [blob]\right)^2} \quad A_4 = k_{blob} + k_e [blob] \tag{2.4}$$

The first exponential of Equation 2.3, which is used to fit the monomer decays, assumes that excimer formation occurs via diffusion between pyrene monomers, $[Py^*_{diff}]$. In the first exponential of Equation 2.3, three parameters are retrieved that describe the kinetics of excimer formation for a given pyrene labeled polymer. They are the rate constant for excimer formation by diffusion between one excited pyrene and one ground–state pyrene located in the same *blob*, k_{blob}, the average number of ground–state pyrenes per *blob*, <*n*>, and the rate constant for the exchange of ground–state pyrenes between blobs times the

concentration of blobs in the polymer coil, $k_e[blob]$. The second exponential accounts for the fluorescence of any unquenched pyrene monomer, $[Py^*_{free}]$, that fluoresces with its natural lifetime, τ_M. These long-lived species do not form excimer and thus are not described by the FBM. For each Py-PS series, a low pyrene content polymer (< 0.2 mol%) was synthesized. With the low pyrene content, very little excimer is formed and fitting the monomer decays with a sum of exponentials (Equation 2.2) resulted in a strong contribution (> 80%) from pyrenes emitting with their natural lifetime, τ_M. The τ_M values retrieved from this analysis were in the 253-259 ns range for all Py-PS samples in THF (Table A2.12). All analyses presented in this work were conducted with a τ_M value set to equal 260 ns.

$$[E^*] = -[Py^*_{diff}]_{(t=0)}\, e^{-A_3} \sum_{i=0}^{\infty} \frac{A_3^{\,i}}{i!} \frac{A_2 + i\,A_4}{\frac{1}{\tau_M} - \frac{1}{\tau_{E0}} + A_2 + i\,A_4} \exp\left(-\left(\frac{1}{\tau_M} + A_2 + i\,A_4 \right) t \right)$$

$$+ \left([E0^*]_{(t=0)} + [Py^*_{diff}]_{(t=0)}\, e^{-A_3} \sum_{i=0}^{\infty} \frac{A_3^{\,i}}{i!} \frac{A_2 + i\,A_4}{\frac{1}{\tau_M} - \frac{1}{\tau_{E0}} + A_2 + i\,A_4} \right) e^{-t/\tau_{E0}} + [D^*]_0 e^{-t/\tau_D} \quad (2.5)$$

The excimer decays were fit using Equation 2.5, where τ_{E0} is the excimer lifetime. Equation 2.5 which was derived and applied in earlier studies[19,26-29] assumes that the excimer is formed and emits as one of three species in solution. These species result from the diffusional encounter of an excited pyrene monomer and a ground-state pyrene, and the direct excitation of ground-state dimers, ($E0^*$), and long-lived ground-state dimers, (D^*). The fits of the monomer and excimer decays with Equations 2.3 and 2.5 enables one to

determine the fractions of all pyrene species, Py_{diff}, Py_{free}, $E0$, and D, in solution. The fraction of aggregated pyrenes, f_{agg}, is the sum of $f_{E0} + f_D$. A more detailed explanation on the determination of the fractions is found in previous works.[19,26-29]

Optimization of the parameters used in Equations 2.2, 2.3, and 2.5 to fit the fluorescence decays was performed with the Marquardt-Levenberg algorithm.[30] The IBH 340 LED used to acquire the fluorescence decays was found to generate a higher noise level than the IBH hydrogen lamp used previously.[23,28] Consequently, a background correction was applied to fit the fluorescence decays.[31] As done in earlier publications, a light scattering correction was also applied to account for those pyrene pairs which are in close contact and form excimer on a time-scale which is too fast to be detected accurately by our instrument.[31] The fits of the monomer and excimer decays were considered good if the χ^2 was below 1.4 and the residuals were randomly distributed around zero (see Figures A2.3 and A2.4 for sample decays).

2.4 Results

The steady-state fluorescence spectra were obtained in THF for all polystyrene samples. The spectra of the Py-PS samples containing ~3.5 mol% pyrene are shown in Figure 2.1. The largest amount of excimer is obtained with the GrE-PS and CoE-PS samples. The ES-PS sample forms the least excimer, and the CoA-PS sample generates an intermediate amount of excimer. Qualitatively, this result demonstrates that the process of excimer formation depends strongly on the method of pyrene incorporation. The ratios of the fluorescence intensity of the monomer over that of the excimer, the I_E/I_M ratios, are plotted as a function of pyrene content for the four Py-PS series in Figure 2.2. For each series, I_E/I_M increases exponentially with pyrene content, as found in previous studies of polymers

randomly labeled with pyrene.[18,19,26] The same differences in excimer formation observed for the samples containing ~ 3.5 mol% of pyrene in Figure 2.1 are found over the entire range of pyrene contents. The series with major structural differences (side-chain type and pyrene distribution) generate very different amounts of excimer over the entire range of pyrene contents, while the two series with identical chemical structures, namely CoE-PS and GrE-PS, follow a similar trend.

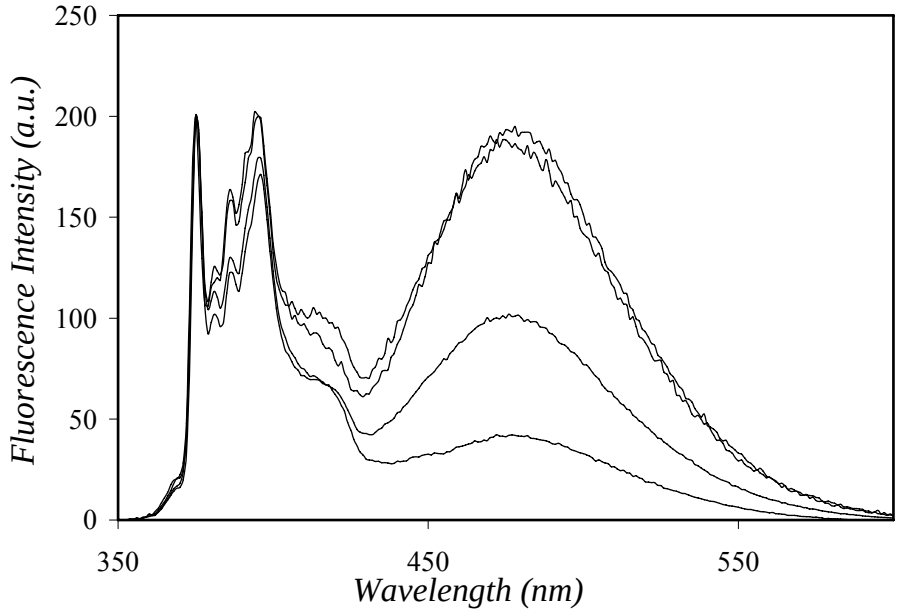

Figure 2.1: Steady-state fluorescence spectra of polystyrene labeled with ~ 3.5 mol% pyrene in THF. From top to bottom: CoE-PS, GrE-PS, CoA-PS, and ES-PS; [Py] = 3×10^{-6} M, λ_{ex} = 344 nm. Note: The slit widths were kept constant for each measurement. Therefore, as more excimer is formed, the overall fluorescence intensity decreases. This leads to an increase in the noise in the excimer portion of the spectra.

The monomer and excimer decays were acquired and analyzed using a multi-exponential fit usually resulting in χ^2 smaller than 1.3. The decay times and pre-exponential factors are reported in Tables A2.3 and A2.4 in the Appendix. The monomer decays were analyzed using up to four exponentials with the longest decay time fixed to τ_M, the lifetime of

the pyrene label in THF (260 ns). The fluorescence decays of the pyrene monomer for the Py-PS samples containing ~3.5 mol% of pyrene are shown in Figure 2.3. The pyrene monomer decays more quickly according to the sequence ES-PS < CoA-PS < CoE-PS ≅ GrE-PS. Since a steeper monomer decay reflects an increased excimer production, the trend obtained in Figure 2.3 by time-resolved fluorescence is similar to that obtained in Figure 2.1 by steady-state fluorescence. The results obtained from the analysis of the monomer decays with a sum of exponentials can be used to estimate the pseudo–unimolecular rate constant of excimer formation, k_{exci}, according to Equation 2.6 which has been applied earlier.[32]

$$k_{exci} = \frac{1}{<\tau>} - \frac{1}{\tau_M} \tag{2.6}$$

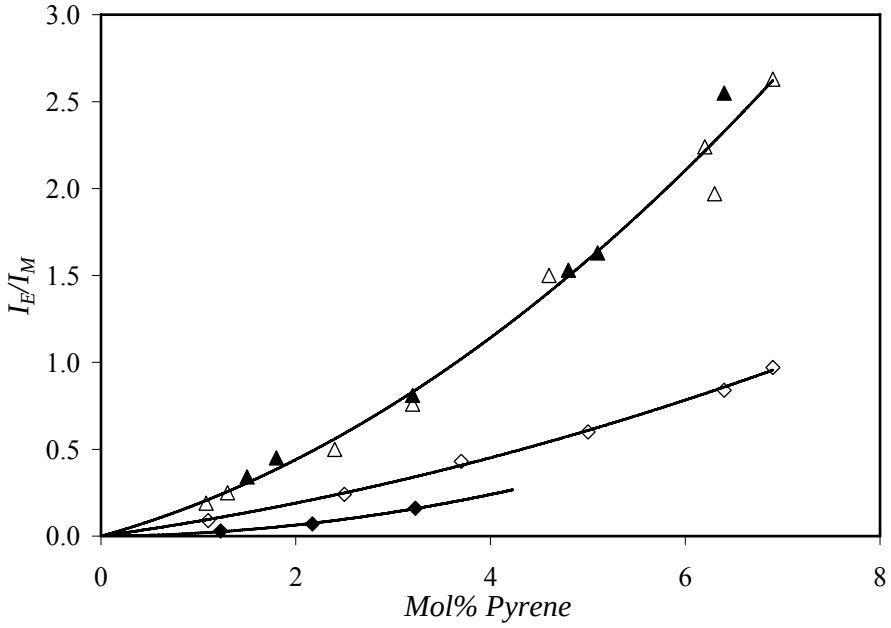

Figure 2.2: I_E/I_M ratios as a function of pyrene content; GrE-PS (△), CoE-PS (▲), CoA-PS (◇), ES-PS (◆); [Py] = 3×10^{-6} M, λ_{ex} = 344 nm. Error analysis on some of the I_E/I_M ratios is provided in Table A2.14.

In Equation 2.6, $<\tau>$ represents the number-average decay time of the pyrene monomer, while τ_M represents the unquenched lifetime of the monomer. Figure 2.4 gives the trends obtained by plotting k_{exci} as a function of the pyrene content of the four PS samples. According to Equation 2.6, a larger k_{exci} implies a more efficient excimer formation.

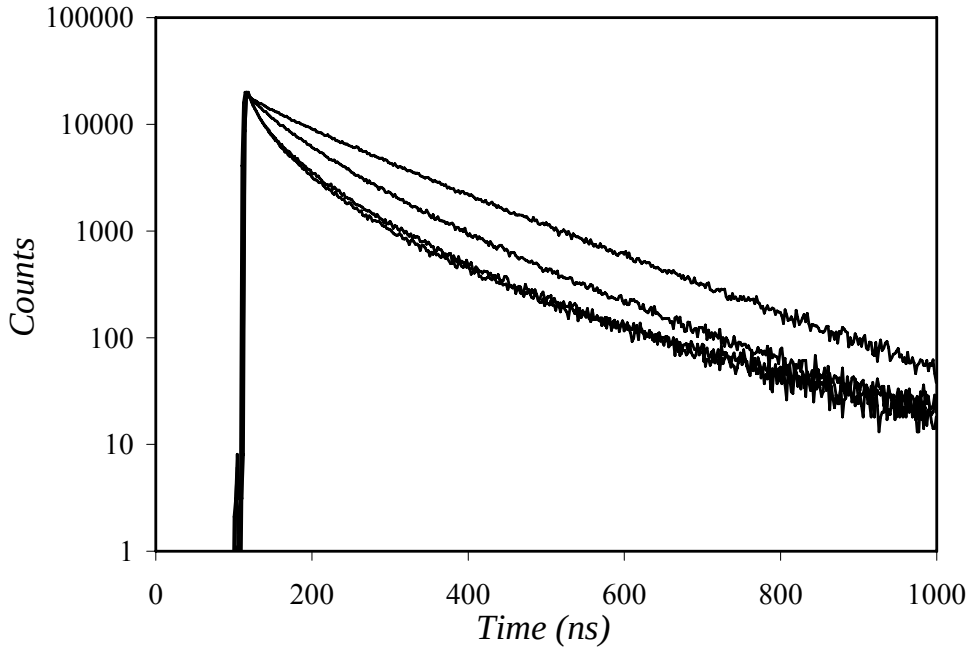

Figure 2.3: Monomer fluorescence decays of polystyrene labeled with ~ 3.5 mol% pyrene in THF. From top to bottom: ES-PS, CoA-PS, CoE-PS, and GrE-PS; [Py] = 3×10^{-6} M, λ_{ex} = 340 nm, λ_{em} = 375 nm.

The trends shown in Figure 2.4 indicate that the efficiency of excimer formation increases according to the sequence: ES-PS < CoA-PS < CoE-PS ≤ GrE-PS. The rate of excimer formation can usually be compared to the I_E/I_M ratio since a larger k_{exci} results in a larger I_E/I_M ratio. The I_E/I_M ratios and k_{exci} values shown in Figures 2.2 and 2.4 for ES-PS, CoA-PS, and CoE-PS yield the expected trends. However, although the I_E/I_M ratios of CoE-PS and GrE-PS yield identical trends in Figure 2.2, k_{exci} of GrE-PS appears to be substantially

larger than k_{exci} of CoE-PS in Figure 2.4. Since the chemical structures of GrE-PS and CoE-PS are identical, an increase of the rate of excimer formation suggests that the pyrene pendants are incorporated closer to one another in GrE-PS.

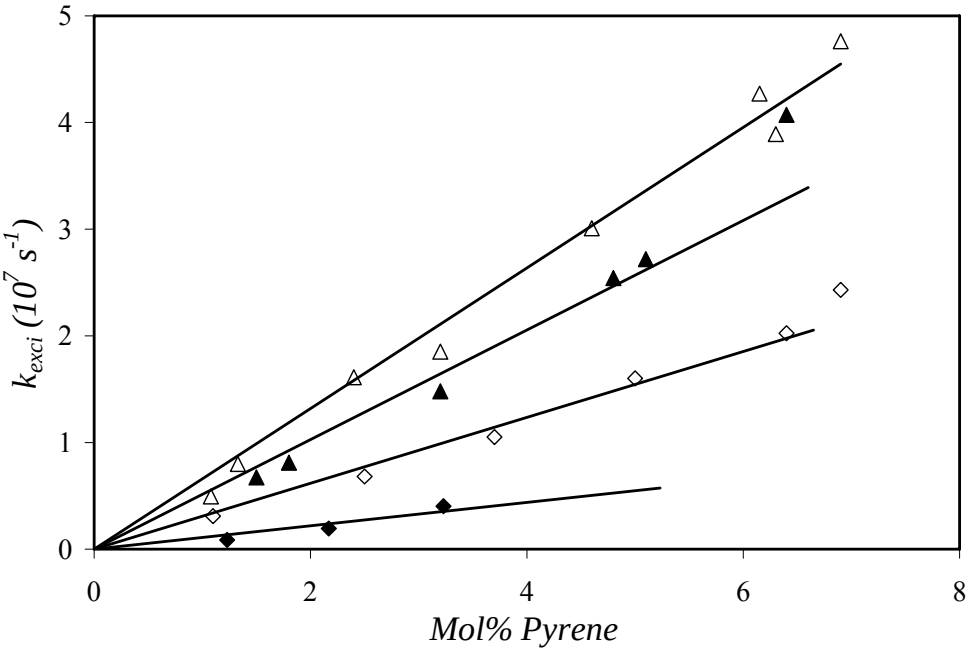

Figure 2.4: k_{exci} as a function of pyrene content; GrE-PS (△), CoE-PS (▲), CoA-PS (◇), ES-PS (◆); [Py] = 3×10^{-6} M. Error analysis on some of the k_{exci} values is provided in Table A2.15.

An indication that this might be the case is obtained from the close inspection of the P_A and a_{E-}/a_{E+} ratios. The peak-to-valley ratio or P_A ratio has been shown to take a lower value than 3.0 when pyrene aggregates are present in solution.[9] Similarly, the a_{E-}/a_{E+} ratio obtained from the ratio of the sum of the negative pre-exponential factors of the excimer decay over the sum of the positive ones takes values more positive than −1.0 in the presence of pyrene aggregates.[19,27] The P_A values for GrE-PS and CoE-PS were 2.83 ± 0.06 and 3.02 ± 0.03, respectively, while the a_{E-}/a_{E+} ratios were −0.74 ± 0.04 and −0.85 ± 0.04, respectively. Both ratios indicate that the GrE-PS series bears pyrene pendants which are

more aggregated than in the CoE-PS series. The clustering of the pyrene pendants implies that some pyrenes are attached on neighboring styrene units. This geometric arrangement restricts the number of conformations available to two pyrene neighbors preventing them from adopting the ideal stacking required for excimer formation. As a result, excimers formed by clustered pyrenes have a lower quantum yield than excimers formed from the diffusive encounter between two pyrenes.[13,33-35]

The influence of aggregation is most likely the reason for the discrepancy between the steady-state (Figure 2.2) and time-resolved (Figure 2.4) fluorescence data. The clustering of the pyrenes leads to faster excimer formation since the pyrene pendants are close to one another, but also a lower excimer fluorescence emission due to poor stacking.[13,33-35] The two effects seem to cancel each other out resulting in a similar trend for the I_E/I_M ratios obtained for CoE-PS and GrE-PS in Figure 2.2. This example highlights the need for caution when determining rates of excimer formation qualitatively using I_E/I_M ratios alone.

Although pronounced differences are observed in the process of excimer formation depending on the method of incorporation of pyrene into the polymer, little can be inferred about the reasons causing the differences observed by steady-state (Figures 2.1 and 2.2) and time-resolved (Figures 2.3 and 2.4) fluorescence. A more comprehensive picture about the process of excimer formation can only be achieved through the quantitative analysis of the pyrene monomer and excimer fluorescence decays of the pyrene labeled polymers using the FBM.[5]

FBM Results:

Over the last number of years, numerous polymers randomly labeled with pyrene have been studied with an analysis based on the FBM.[5,18,19,25-29] Equations 2.3 and 2.5 are used to

fit the monomer and excimer decays, respectively, to retrieve the parameters k_{blob}, $k_e[blob]$, and $<n>$. These parameters were obtained from fitting the decays acquired with all Py-PS samples. They are listed in Tables A2.5–10. Plots of k_{blob}, $<n>$, and $k_e[blob]$ as a function of pyrene content are found in Figures 2.5–2.7. The corrected pyrene content, λ_{Py}/f_{Mdiff}, is introduced in Figures 2.5–2.7 to account for those domains of the polymer that are pyrene poor and do not form any excimer. The fraction f_{Mdiff} is equal to $[Py^*_{diff}]_{(t=0)}$ / ($[Py^*_{diff}]_{(t=0)}$ + $[Py^*_{free}]_{(t=0)}$) and is obtained from Equation 2.3. It is usually close to 1.0 for pyrene contents greater than 2.5 mol% so that this correction is not too important. For all Py-PS series, k_{blob} increases gently with pyrene content, $k_e[blob]$ exhibits a slightly more pronounced increase with increasing pyrene content, and $<n>$ increases with increasing pyrene content over the range studied. The trends shown in Figures 2.5–2.7 are consistent with those obtained with a series of poly(*N*,*N*-dimethylacrylamides) (Py-PDMA) in acetone and DMF.[19]

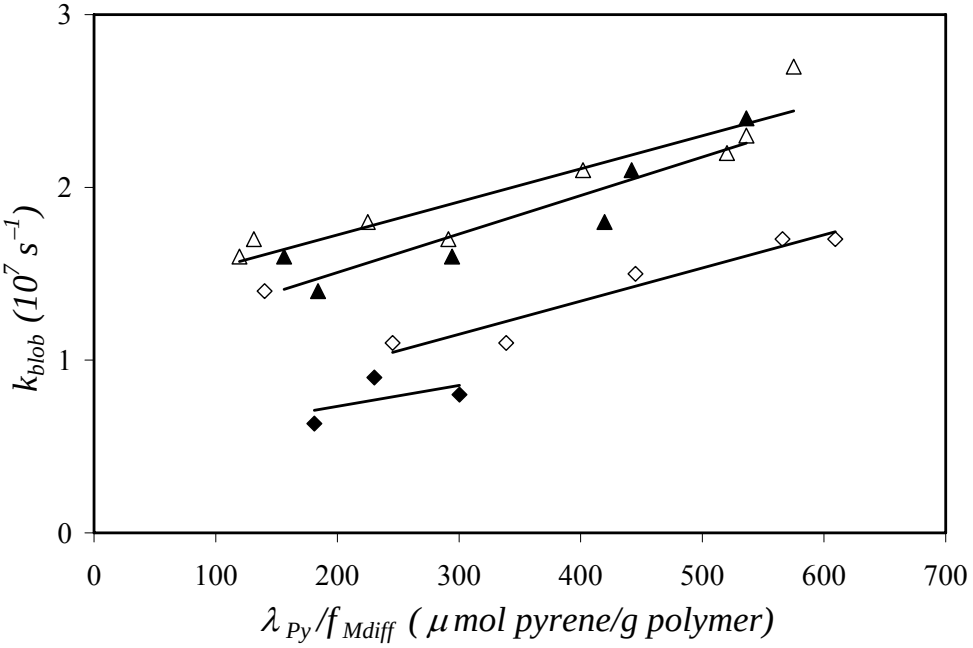

Figure 2.5: k_{blob} as a function of pyrene content; GrE-PS (△), CoE-PS (▲), CoA-PS (◇), ES-PS (◆); [Py] = 3×10^{-6} M.

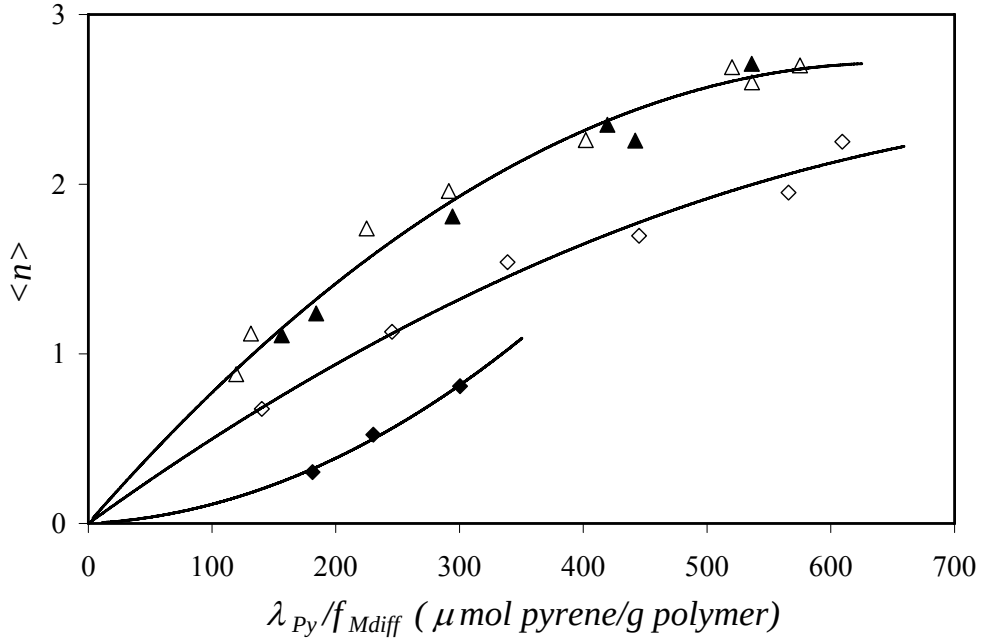

Figure 2.6: <*n*> as a function of pyrene content; GrE-PS (△), CoE-PS (▲), CoA-PS (◇), ES-PS (◆); [Py] = 3×10^{-6} M.

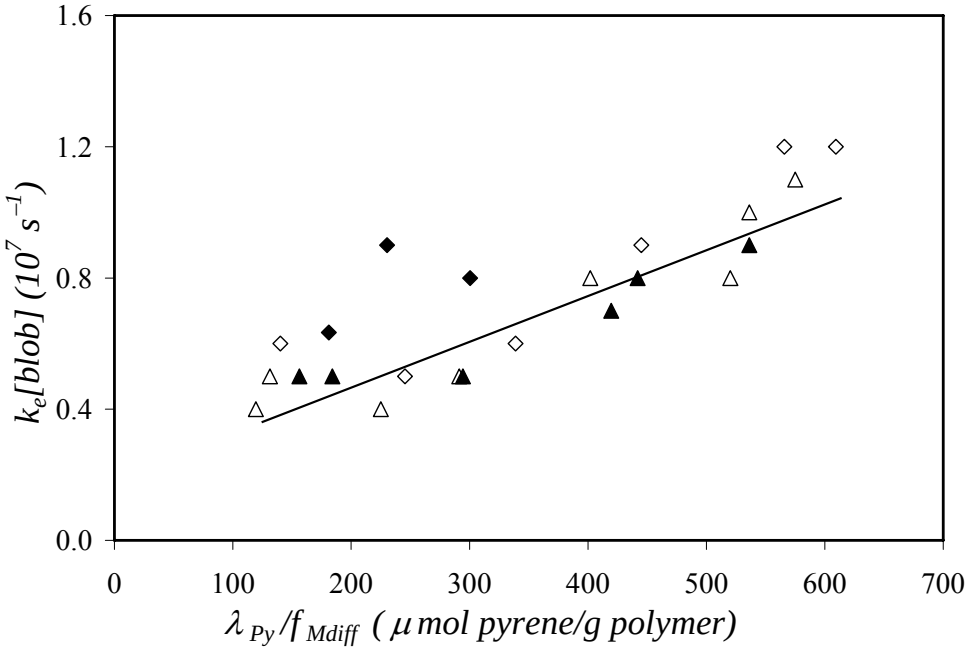

Figure 2.7: $k_e[blob]$ as a function of pyrene content; GrE-PS (△), CoE-PS (▲), CoA-PS (◇), ES-PS (◆); [Py] = 3×10^{-6} M.

Extensive studies have been completed on Py-PDMA using the FBM.[19,25] One of the important conclusions drawn from these studies was that k_{blob} is a pseudo-unimolecular rate constant that is the product of the rate constant for diffusive encounter between an excited pyrene and a ground–state pyrene, k_{diff}, and the inverse of the blob volume, $1/V_{blob}$ (Equation 2.7).[19,25] Equation 2.7 implies that multiplying k_{blob} by $<n>$ yields a measure of the *local pyrene concentration*, $[Py]_{loc}$, equal to $<n>/V_{blob}$. A plot of $k_{blob}\times<n>$ vs. pyrene content is shown in Figure 2.8. As expected, a linear increase in $k_{blob}\times<n>$ is observed with increasing pyrene content for all four polymer series, reflecting the linear dependence of $[Py]_{loc}$ with pyrene content.

$$k_{blob} = k_{diff} \times \frac{1}{V_{blob}} \qquad (2.7)$$

The $k_{blob}\times<n>$ values shown in Figure 2.8 suggest that $[Py]_{loc}$ decreases according to the sequence GrE-PS ≥ CoE-PS > CoA-PS > ES-PS. Since excimer formation depends on $[Py]_{loc}$, k_{exci} should also be a measure of $[Py]_{loc}$. The $k_{blob}\times<n>$ trends obtained in Figure 2.8 are in agreement with the k_{exci} trends shown in Figure 2.4. At a given pyrene content, the k_{exci} values for GrE-PS are 1.3 ± 0.1 times larger than those for CoE-PS, which are themselves 1.6 ± 0.2 times larger than those obtained for CoA-PS, themselves 2.8 ± 0.7 times larger than for ES-PS. Similarly, the $k_{blob}\times<n>$ products at a given pyrene content reported in Figure 2.8 for GrE-PS are 1.2 ± 0.2 times larger than those for CoE-PS, which are themselves 1.8 ± 0.2 times larger than those obtained for CoA-PS, themselves being 2.9 ± 0.6 times larger than for ES-PS. The actual slopes and errors on the slope of the trends shown in Figures 2.4 and 2.8

can be found in Table A2.13. The agreement obtained between the trends of k_{exci} and $k_{blob}\times\langle n\rangle$ vs. pyrene content further supports the assertion made earlier[19,25] that the product $k_{blob}\times\langle n\rangle$ is a measure of $[Py]_{loc}$.

If the product $k_{blob}\times\langle n\rangle$ is a measure of $[Py]_{loc}$, one might ask why all $k_{blob}\times\langle n\rangle$ values do not merge on a single master curve in Figure 2.8. The reason why this is not the case lays in the excimer formation depending not only on $[Py]_{loc}$, but also on the flexibility of the chain and linker connecting the pyrene probe to the chain. As will be discussed later on, faster chain and linker dynamics result in more efficient excimer formation for polymers having a same $[Py]_{loc}$. The inherent ability of the FBM to differentiate between the contributions to excimer formation due to polymer chain dynamics and $[Py]_{loc}$ by using, respectively, k_{blob} and $\langle n\rangle$ is what constitute the main advantage of the FBM over more traditional analyses of excimer formation with pyrene-labeled polymers that rely only on the I_E/I_M ratio and k_{exci}.

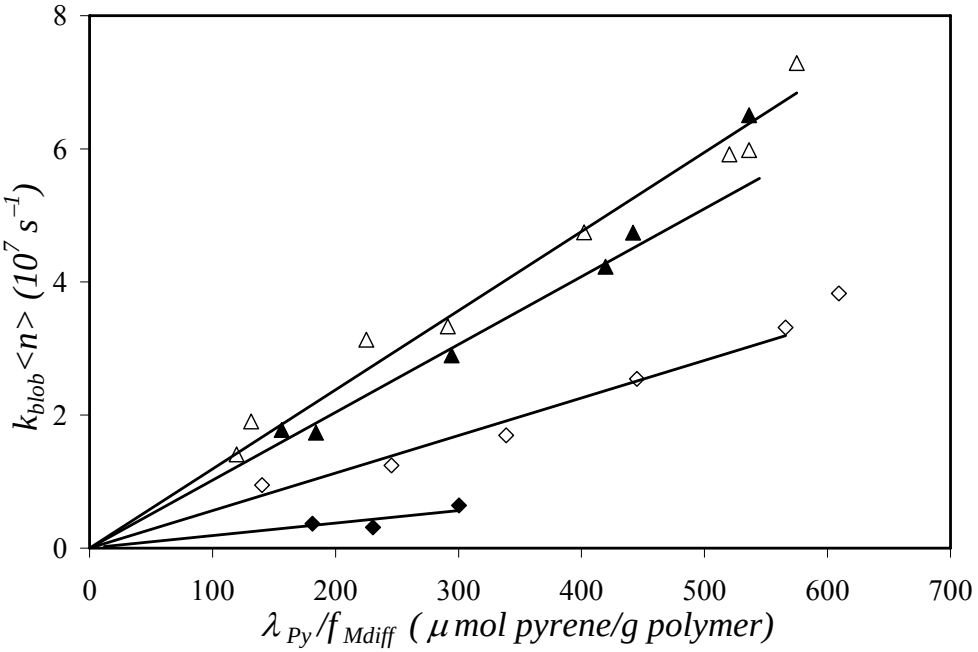

Figure 2.8: $k_{blob} \times \langle n\rangle$ as a function of pyrene content; GrE-PS (△), CoE-PS (▲), CoA-PS (◇), ES-PS (◆); [Py] = 3×10^{-6} M.

Besides k_{blob} which is inversely proportional to V_{blob} (Equation 2.7), a second general measure of the volume probed by an excited pyrene, V_{blob}, is obtained from N_{blob}, which is the number of styrene monomers constituting a *blob*.[5] N_{blob} is calculated with Equation 2.8, where $<n>$ is the average number of pyrenes per *blob*, retrieved from the FBM analysis of the monomer decays, M_{Py} is the molecular weight of the pyrene labeled monomer, M_{Sty} is the molecular weight of the styrene monomer, x is the mole fraction of the pyrene labeled monomer, λ_{Py} is the pyrene content in moles of pyrene per gram of polymer, and f_{Mdiff} is the fraction of pyrenes that form excimer by diffusion.

$$N_{blob} = \frac{\langle n \rangle}{\lambda_{Py} / f_{Mdiff} \left[M_{Py}(x) + M_{Sty}(1-x) \right]} \tag{2.8}$$

Regardless of pyrene content, N_{blob} is found to increase according to the sequence ES-PS < CoA-PS < CoE-PS ≅ GrE-PS (Figure 2.9). For each PS series except that of ES-PS, N_{blob} increases with decreasing pyrene content. The value of N_{blob} for a pyrene labeled polymer is found by extrapolating the trends shown in Figure 2.9 to zero pyrene content, where potential distortions of the polymer conformation induced by the pyrene labels are expected to be minimized.[18,26] N_{blob} was found to equal 85 ± 4, 74 ± 4, 51 ± 3, and 20 ± 3 styrene units for GrE-PS, CoE-PS, CoA-PS, and ES-PS, respectively. Since a *blob* is the volume probed by an excited pyrene, the differences in N_{blob} shown in Figure 2.9 imply that the mode of pyrene incorporation into a polymer does affect its mobility.

Comparison of the N_{blob} values for the CoA-PS and CoE-PS series indicates that V_{blob} increases with increasing length of the linker connecting pyrene to the backbone. Yet,

Equation 2.7 predicts that this increase in V_{blob} should be accompanied by a decrease in k_{blob}. Interestingly, the opposite is observed in Figure 2.5. The parallel increase of k_{blob} and V_{blob} with increasing linker length implies that k_{diff} in Equation 2.7 must increase substantially to offset the change in V_{blob}. This interesting development is probed in more detail in the Discussion section.

The FBM parameters account for those pyrenes that form excimer by diffusion. However, an excimer can also be produced by the direct excitation of a pyrene cluster.[9] As discussed earlier, pyrene aggregation affects excimer formation and thus, the I_E/I_M ratios in Figure 2.2. The fraction of aggregated pyrene pendants, f_{agg}, is retrieved from the analysis of the monomer and excimer fluorescence decays and has been used extensively to study the associative strength of associative polymers (AP) where the associating moiety is either pyrene or labeled with pyrene.[19,23,26-29]

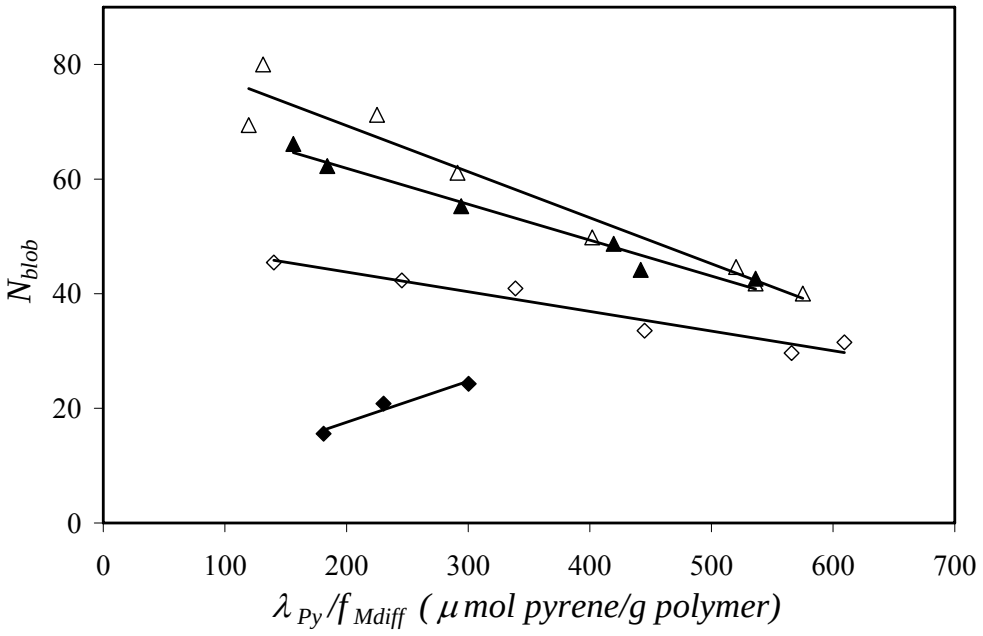

Figure 2.9: N_{blob} as a function of pyrene content; GrE-PS (△), CoE-PS (▲), CoA-PS (◇), ES-PS (◆); [Py] = 3×10^{-6} M

The plot of f_{agg} vs. pyrene content in Figure 2.10 indicates that the pyrenyl pendants are much less aggregated in the ES-PS series than in any of the other Py-PSs. This is reasonable since the synthetic route followed to generate the ES-PS series forces the pyrenes apart along the backbone preventing them from being located adjacent to one another. The other three Py-PSs however, show a quite remarkable result. The two polymers obtained by copolymerizing styrene with a pyrene labeled monomer (CoA-PS and CoE-PS) have a similar level of aggregation, but the GrE-PS series yields a significantly higher f_{agg} at almost all pyrene contents. This result suggests that the pyrene groups are **not** incorporated in the same manner depending on the synthetic method being used.

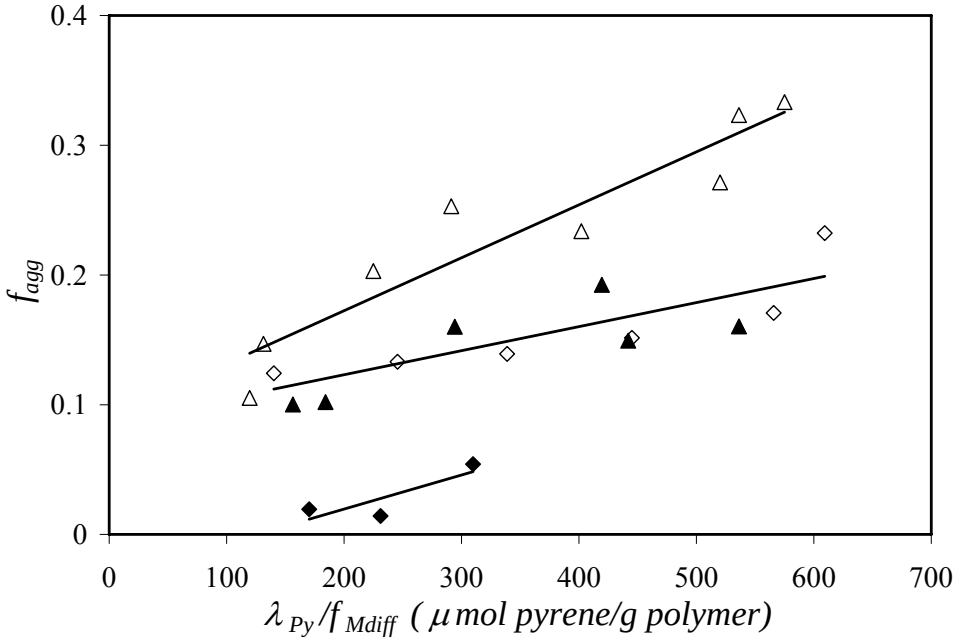

Figure 2.10: f_{agg} as a function of pyrene content; GrE-PS (△), CoE-PS (▲), CoA-PS (◇), ES-PS (◆); [Py] = 3×10^{-6} M.

2.5 Discussion

1) *Effect of the method of pyrene incorporation*

The CoE-PS and GrE-PS series were synthesized to determine if the synthetic route taken to build a pyrene labeled polymer would play any role in the formation of excimers. These two series should both produce randomly labeled copolymers with identical chemical composition, and thus should form excimer in a similar manner. However, it was found that although their I_E/I_M ratios were similar, the k_{exci} and f_{agg} values shown in Figures 2.4 and 2.10 indicate that the pyrenyl pendants are more clustered in GrE-PS than in CoE-PS.

The higher level of aggregation is also reflected in the slightly increased local pyrene concentration in the GrE-PS series given by $k_{blob}\times\langle n\rangle$ as seen in Figure 2.8. The larger f_{agg} values and higher $[Py]_{loc}$ obtained for GrE-PS might also explain why, although the N_{blob} vs. pyrene content (λ_{Py}/f_{Mdiff}) trends shown in Figure 2.9 are similar for GrE-PS and CoE-PS, extrapolating the trends to $\lambda_{Py}/f_{Mdiff} = 0$ yields a slightly lower N_{blob} value for CoE-PS (74 ± 4) than for GrE-PS (85 ± 4). Indeed, a higher $[Py]_{loc}$ results in a higher $\langle n\rangle$ value, which according to Equation 2.8, yields a larger N_{blob} value.

The higher clustering of the pyrene pendants observed with GrE-PS could be caused by two different effects, or a combination of both. The first possibility is that the graft-onto modification reaction occurs in a clustered manner. Since a polymer coil is expected to be denser at its center according to Flory,[36] the chloromethylation reaction used in the preparation of GrE-PS[18] could be favored towards the center of the polymer coils resulting in an increased local pyrene concentration towards the center of the polymer coil and thus an increased clustering of the pyrene groups in GrE-PS. Copolymerization, which depends only on the reactive end of the growing chain, ensures that the pyrene labeled co-monomers are

incorporated throughout the chain, minimizing the probability of forming pyrene clusters. The second reason for observing an increased level of pyrene clustering in the GrE-PS series could be an undesired side effect of the polymer modification. The chloromethylation reaction is known to induce cross-linking.[37] Precautions were taken to prevent cross-linking during the chloromethylation reaction by using relatively low polymer concentrations and no evidence of intermolecular cross-linking was found in the GPC traces of the chloromethylated polystyrenes.[18] Nevertheless, the occurrence of intramolecular cross-linking cannot be ignored. Since its effect on excimer formation of a pyrene labeled polymer has not been previously explored, it remains a possible explanation for the discrepancy. In any case, the data obtained by time-resolved fluorescence demonstrate that the two synthetic methods used to prepare CoE-PS and GrE-PS yield similar polymers but with different levels of clustering of the pyrene pendants that affect excimer formation.

2) *Effect of linker length on excimer formation*

The copolymers CoE-PS and CoA-PS were prepared to assess the effect that the length of the linker connecting the pyrene probe to the PS backbone has on excimer formation. The main differences for the two copolymer series are observed for the parameters k_{blob} (Figure 2.5), $<n>$ (Figure 2.6), and N_{blob} (Figure 2.9). The value of each of these parameters is always smaller for the CoA-PS series than for the CoE-PS series. These differences are certainly due to the longer reach and the increased flexibility enabled by the ether linker of the CoE-PS series (Scheme 2.1).

According to the definition of a *blob*, N_{blob} represents the number of monomer units constituting a *blob*. Since N_{blob} for CoE-PS (74 ± 4) is larger than for CoA-PS (51 ± 3), V_{blob} for CoE-PS must be larger than for CoA-PS. An estimate of V_{blob} can be obtained by using

the Mark-Houwink-Sakurada equation to determine the hydrodynamic volume V_h of a PS chain made of N_{blob} units. Using the K = 0.011 mL/g and a = 0.725 values for PS in THF,[38] one finds that the hydrodynamic radius of a *blob*, R_h, equals 1.7 nm and 2.1 nm for CoA-PS and CoE-PS, respectively. The increase in R_h results in a 1.9 fold increase in V_h. Using V_h as a measure of V_{blob} suggests that V_{blob} for CoE-PS is 1.9 times larger than for CoA-PS.[39] The difference in R_h is 3.8 Å, very close to the longest carbon-to-carbon distance found for toluene to equal 4.3 Å by using the molecular modeling software package HyperChem™ 7.02. This 4.3 Å distance represents the extra length separating pyrene from the CoE-PS backbone with respect to CoA-PS (Scheme 1). Consequently, these results suggest that the larger N_{blob} value obtained for CoE-PS is due in part to the longer linker between pyrene and the main chain, enabling pyrene to probe a larger V_{blob} in solution.

According to the definition of k_{blob} given in Equation 2.7, the trends obtained for k_{blob} (Figure 2.5) and N_{blob} (Figure 2.9) are somewhat contradictory. Indeed, the above discussion indicates that a larger N_{blob} for the CoE-PS series implies a larger V_{blob}, which should result in a smaller k_{blob} for CoE-PS than for CoA-PS according to Equation 2.7. Instead, the opposite effect is observed in Figure 2.5 with k_{blob}^{CoE-PS} being 1.4 times larger than k_{blob}^{CoA-PS} over the entire range of pyrene content. The reason for this discrepancy lays in the erroneous assumption being implicitly made that k_{diff} in Equation 2.7 is not affected by the linker connecting pyrene to the backbone. Indeed, combining Equation 2.7 with the fact that $k_{blob}^{CoE-PS} = 1.4 \times k_{blob}^{CoA-PS}$ and $V_{blob}^{CoE-PS} = 1.9 \times V_{blob}^{CoA-PS}$ implies that $k_{diff}^{CoE-PS} = 2.7 \times k_{diff}^{CoA-PS}$. In other words, the longer and more flexible ether linker of CoE-PS results in faster dynamics for excimer formation.

The differences in k_{diff} values can be rationalized by considering that the diffusional encounters between two pyrenes attached onto a polymer occur in a sequence of two steps as shown in Scheme 2.2. In the first step, the two polymer units bearing the pyrenes diffuse slowly towards each other with a forward (k_1) and backward (k_{-1}) reaction rate constant. In the second step, the pyrenes probe their nearby environment to form the excimer with a forward (k_2) and backward (k_{-2}) reaction rate constant. For the formation of pyrene excimer, the dissociation rate constant k_{-2} is usually negligible[4,5,11] so that k_{diff} can be approximated by Equation 2.9.

$$k_{diff} = \frac{k_1 \times k_2}{k_{-1} + k_2} \qquad (2.9)$$

In Equation 2.9, k_1 and k_{-1} depend solely on the polymer backbone whereas k_2 depends on the linker. According to Equation 2.9, the largest value taken by k_{diff} is k_1 which is observed only if $k_{-1} \ll k_2$, i.e. when the pyrenyl pendants rearrange themselves much more rapidly than two polymer units have time to diffuse away from one another. These conditions might be fulfilled for the CoE-PS samples where the longer and more flexible linker provides enough freedom of motion to the pyrenyl pendants. They are certainly much less likely to be fulfilled for the CoA-PS series where the short and rigid amide linker reduces the mobility of the pyrenyl pendant, resulting in a k_{diff} value smaller than k_1. Switching from the rigid amide linker of CoA-PS to the flexible ether linker of CoE-PS seems to result in a 2.7 fold reduction of k_{diff}, a substantial slow down of pyrene mobility and decrease in excimer formation as observed in Figures 2.2 and 2.4.

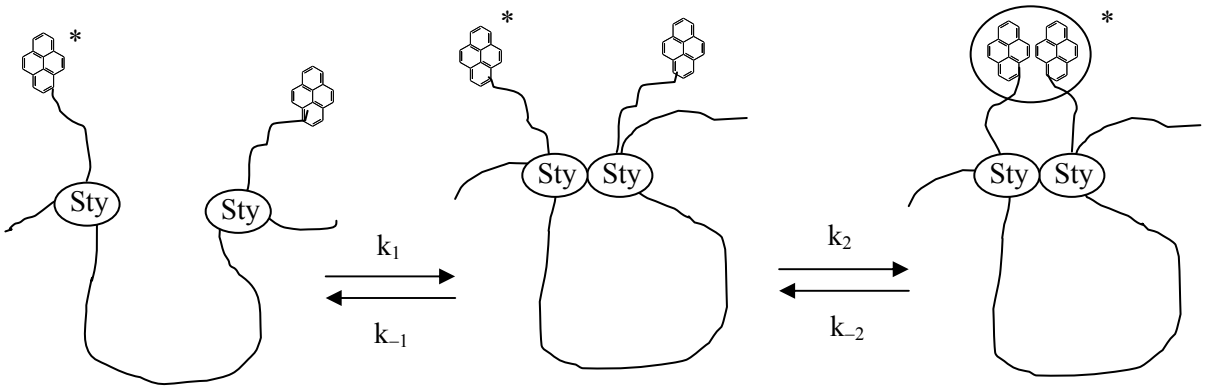

Scheme 2.2: Effect of backbone and side-chain motion on the kinetics of excimer formation.

3) *Effect of the distribution of pyrene pendants*

Interestingly, the monomer fluorescence decays of ES-PS where the pyrenes are spaced evenly along the backbone are very different from those of the randomly labeled polymer, CoA-PS (Figure 3). Instead of the complicated, multi-exponential decays obtained for CoA-PS, the ES-PS decays are bi-exponential and nearly mono-exponential in the 1.2 and 2.2 mol% labeling cases. Although the pyrenes of ES-PS are evenly-spaced in 1-dimension, the random coil conformation of the polymer in solution is expected to produce a distribution of distances between pyrene labels resulting in a fluorescence decay more complicated and similar to that of a randomly labeled polymer. Such an example has been reported by Winnik et al. using an evenly-spaced pyrene labeled polystyrene.[6]

In this work, the ES-PS monomer decays become slightly more complicated – less mono-exponential – as the pyrene content increased from 1.2 up to 3.2 mol%. This is illustrated in the polydispersity (PDI) of the decays found in Table A2.3. Similarly to the PDI used for describing the molecular weight distribution of polymers, a PDI can be defined

for the fluorescence decays by taking the ratio τ_W/τ_N, where τ_N and τ_W are the number-average and weight-average lifetimes, respectively. The PDI of the decays increases from 1.05-1.16 for ES-PS and 1.27-1.40 for CoA-PS in the same pyrene content range of ~1.1-3.5 mol%. Much larger PDI values were obtained for CoE-PS and GrE-PS. The more pronounced mono-exponential character of the ES-PS decays suggests that excimer formation occurs via a single rate constant, i.e. that the pyrenes distribute themselves much more evenly in the ES-PS coil than in the polymer coil of any of the other Py-PS samples.

The even distribution of pyrene along the ES-PS chain has an interesting effect on the *blob* model parameters k_{blob} and $k_e[blob]$. To date, k_{blob} has always been greater than $k_e[blob]$ for all polymers randomly labeled with pyrene that have been studied using the FBM. This was the case with GrE-PS, CoE-PS, and CoA-PS, as well as with Py-PDMA[19,25] and pyrene labeled poly(*L*−glutamic acid).[26] k_{blob} being greater than $k_e[blob]$ implies that a ground−state pyrene located inside a *blob* is more likely to quench an excited pyrene than to diffuse out of the *blob*. However, the ES-PS series has k_{blob} and $k_e[blob]$ values that are almost identical, indicating that ground−state pyrenes are just as likely to diffuse away as they are to remain inside a *blob* and quench the excited pyrene. This observation suggests that the pyrene labels are not only evenly-spaced in one dimension but also evenly distributed in three dimensions inside the polymer coil. This conclusion is in agreement with the absence of curvature found in the monomer decays (Figure 2.3) which suggests that excimer formation can be described by a single rate constant. This unusual distribution also has an effect on $<n>$, resulting in a much lower value than that of CoA-PS (Figure 2.6). Since pyrene appears to not distribute itself in the polymer coil of the ES-PS series according to the Poisson distribution usually

encountered with randomly labeled polymers,[5] further comparisons of the FBM parameters between the CoA-PS and ES-PS series should be made with caution.

2.6 Conclusions

1) *Using the FBM to describe excimer formation for pyrene-labeled polymers*

The experiments conducted in this study have demonstrated 1) how sensitive excimer formation is to the method of pyrene attachment and 2) that a rational for the trends shown in Figures 2.2 and 2.4 can only be obtained through a quantitative analysis of the pyrene monomer and excimer fluorescence decays. Presently, the FBM is the best suited tool to carry out this task.

Despite the resemblance in chemical structure and pyrene content of those four Py-PS series (Scheme 2.1), all Py-PS showed major differences in excimer formation. Qualitative analysis of the fluorescence data using the ratio I_E/I_M (Figure 2.2) and the excimer formation rate constant k_{exci} (Figure 2.4) indicates that the long and flexible ether linker of GrE-PS and CoE-PS favors excimer formation. Excimer formation is reduced first when the linker is made shorter and stiffer (CoA-PS) and second, when the pyrene pendants are kept apart from one another (ES-PS). Quantitative analysis of the fluorescence decays using the FBM demonstrates that the long and flexible ether linker of GrE-PS and CoE-PS enables pyrene to probe a larger volume inside the polymer coil (Figure 2.9). The difference in volume probed by a pyrene between CoE-PS and CoA-PS is compatible with the length difference between the amide and ether linkers found by molecular modeling.

2) *Distribution of modifications*

The physical properties of homopolymers are often modified by covalently incorporating a molecule B into a homopolymer (polyA).[41,42] Most modifications use a

molecule B whose properties are very different from those of polyA. For example, the covalent attachment of a hydrophobic B molecule onto a water-soluble polyA results in a water-soluble associative thickener.[42] Interestingly, not only does the nature of the modification affect the behaviour of the modified polymer, but so does the distribution of these modifications along the chain.[43,44] The inherent sensitivity limits set by most analytical techniques make it very difficult to gain more information about these modifications beyond the typical modification content of a modified polymer. The experiments conducted in this study demonstrate that by selectively labeling the modifications made to a polymer with pyrene (cf. ES-PS and CoA-PS which share a same linker to connect pyrene to the PS backbone), information on the fraction of aggregated pyrene labels and, consequently, the level of clustering of the modifications is obtained through the parameter f_{agg}. As expected from the design of ES-PS, f_{agg} was found to be much smaller for ES-PS than for CoA-PS (Figure 2.10). These results validate the use of f_{agg} to determine the level of clustering of the modifications made to a polymer, as has been done earlier to determine the clustering of succinic anhydride pendants along maleated ethylene-propylene random copolymers[29,44] as well as the level of association of water-soluble associative thickeners.[19,23,28]

Analysis of the fluorescence decays acquired for the two Py-PSs obtained by copolymerization (CoA-PS and CoE-PS) resulted in similar f_{agg} values. Interestingly, GrE-PS and CoE-PS which have identical chemical structure do not yield similar f_{agg} values. The pyrene pendants appear to be more clustered in GrE-PS. It remains to be seen whether this observation can be generalized to other polymeric backbones.

3) *Protein folding*

Proteins are polypeptides where the distribution of pendants along the backbone is defined exactly by the 1-dimensional sequence of their gene. The early stages of protein folding are believed to involve the random diffusion-controlled encounters of the amino acids (aa) constituting the protein.[45] These encounters lead to the intramolecular associations of some aa into nuclei from which the nascent secondary structures of the folded protein originate. If the polypeptide is initially in a random coil conformation, the perfectly aligned aa in the 1-dimensional sequence of the protein are expected to distribute themselves randomly in the 3-dimensional polypeptide coil. The random positioning of the aa inside the polymer coil would be expected to result in random encounters between aa which are no longer influenced by the specific location of the aa along the chain. However this expectation is not supported by a comparison of the trends obtained in Figures 2.2 and 2.4 between ES-PS where the pyrenes are located at specific positions along the chain and CoA-PS where the pyrenes are randomly incorporated into the chain. For a same pyrene content, much fewer encounters were observed for ES-PS than for CoA-PS. This observation confirms that the exact positioning of the aa along the polymer chain also controls the rate at which aa encounter in the polypeptide coil, information which might have some relevance for the study of the early stages of protein folding.

2.7 References and Notes

1. Cuniberti, C.; Perico, A. *Eur. Polym. J.* **1977**, *13*, 369-374.

2. Perico, A.; Cuniverti, C. *J. Polym. Sci,.Polym. Phys. Ed.* **1977**, *15*, 1435-1450.

3. Winnik, M. A.; Redpath, T.; Richards, D. H. *Macromolecules* **1980**, *13*, 328-335.

4. Winnik, M. A. *Acc. Chem. Res.* **1985**, *18*, 73-79.

5. Duhamel, J. *Acc. Chem. Res.* **2006**, *39*, 953-960.

6. Winnik, M. A.; Li, X.-B.; Guillet, J. E. *Macromolecules* **1984**, *17*, 699-702.

7. Martinho, J. M. G.; Winnik, M. A. *Macromolecules* **1986**, *19*, 2281-2284.

8. Picarra, S.; Duhamel, J.; Fedorov, A.; Martinho, J. M. G. *J. Phys. Chem. B* **2004**, *108*, 12009-12015.

9. Winnik, F. M. *Chem. Rev.* **1993**, *93*, 587-614.

10. Duhamel, J. in *Molecular Interfacial Phenomena of Polymers and Biopolymers*. Chen, P. Editor, Woodhead Publishing Company, **2005**, p 214-248.

11. Birks, J. B. in *Photophysics of Aromatic Molecules*. Wiley: New York, 1970; p 301.

12. Ezzell, S. A.; Hoyle, C. E.; Creed, C. E.; McCormick, C. L. *Macromolecules* **1992**, *25*, 1887-1895.

13. Anghel, D. A.; Alderson, V.; Winnik, F. M.; Mizusaki, M.; Morishima, Y. *Polymer* **1998**, *39*, 3035-3044.

14. Farinha, J. P. S.; Martinho, J. M. G.; Xu, H.; Winnik, M. A. Quirk, R. P. *J. Polym. Sci,. Part B*: *Polym. Phys.* **1994**, *32*, 1635-1642.

15. Cuniberti, C.; Perico, A. *Eur. Polym. J.* **1980**, *16*, 887-893.

16. Wang, F. W.; Lowry, R. E.; Cavanagh, R. R. *Polymer* **1985**, *26*, 1657-1660.

17. Seixas de Melo, J.; Costa, T.; Miguel, M. da. G.; Lindman, B.; Schillen, K. *J. Phys. Chem. B* **2003**, *107*, 12605-12621.

18. Mathew, A. K.; Siu, H.; Duhamel, J. *Macromolecules* **1999**, *32*, 7100-7108.

19. Kanagalingam, S.; Ngan, C. F.; Duhamel, J. *Macromolecules* **2002**, *35*, 8560-8570.

20. Braun, D.; Czerwinski, W.; Disselhoff, G.; Tudos, F.; Kelen, T.; Turcanyi, B. *Makromol. Chem.* **1984**, *125*, 161-205.

21. Leoni, A.; Franco, S.; Saini, G. *Makromol. Chem.* **1973**, *165*, 97-104.

22. James, D. R.; Demmer, D. R. M.; Verrall, R. E.; Steer, R. P. *Rev. Sci. Instrum.* **1983**, *54*, 1121-1130.

23. Siu, H.; Duhamel, J. *Macromolecules*, **2004**, *37*, 9287-9289.

24. Tachiya, M. *Chem. Phys. Lett.* **1975**, *33*, 289-292.

25. Kanagalingam, S.; Spartalis, J.; Cao, T.-M.; Duhamel, J. *Macromolecules* **2002**, *35*, 8571-8577.

26. Duhamel, J.; Kanagalingam, S.; O'Brien, T.; Ingratta, M. *J. Am. Chem. Soc.* **2003**, *125*, 12810-12822.

27. Prazeres, T. J. V.; Beingessner, R.; Duhamel, J.; Olesen, K.; Shay, G.; Bassett, D. R. *Macromolecules* **2001**, *34*, 7876-7884.

28. Siu, H.; Duhamel, J. *Macromolecules* **2006**, *39* 1144-1155.

29. Zhang, M.; Duhamel, J. *Macromolecules* **2005**, *38*, 4438-4446

30. Press, W. H.; Flannery, B. P.; Teukolsky, S. A.; Vetterling, W. T. *Numerical Recipes. The Art of Scientific Computing (Fortran Version)*; Cambridge University Press: Cambridge, 1992, p 523 – 528.

31. Demas, J. N. *Excited-State Lifetime Measurements*; Academic Press: New York, 1983, p 134, 147.

32. Winnik, M. A.; Egan, L. S.; Tencer, M.; Croucher, M. D. *Polymer* **1987**, *28*, 1553-1560.

33. Siu, H.; Duhamel, J. *Macromolecules* **2005**, *38*, 7184-7186.

34. Anghel, D. F.; Toca-Herrera, J. L.; Winnik, F. M.; Rettig, W.; v. Kliting, R. *Langmuir* **2002**, *18*, 5600-5606.

35. Winnik, F. M.; Regismond, S. T. A.; Goddard, E. D. *Langmuir* **1997**, *13*, 111-114.

36. Flory, P. J. *Principles of Polymer Chemistry*, Cornell University Press, Ithaca, 1953, p 598.

37. Gauthier, M.; Möller, M. *Macromolecules* **1991**, *24*, 4548-4553.

38. Bandrup, J.; Immergut, E. H.; Grulke, E. A. *Polymer Handbook*, 4th ed.; John Wiley & Sons: New York, 1999; p VII 675-683.

39. A similar conclusion can be reached by using scaling arguments[40] and noting that $V_{blob} \propto N_{blob}^{3\nu}$ where ν is the Flory exponent equal to 0.6 for PS in THF.

40. de Gennes, P.-G. *Scaling Concepts in Polymer Physics*; Cornell University Press: Ithaca, NY, 1979.

41. Jao, T. C.; Passut, C. A. *Handbook of Detergents*, *Part D: Formulation*, Showell, M. S. Ed., CRC Press, Taylor and Francis Group, Boca Raton, FL, 2006, p 437-471.

42. Winnik, M. A.; Yekta, A. *Curr. Opin. Colloid Interface Sci.* **1997**, *2*, 424-436.

43. Volpert, E.; Selb, J.; Candau, F. *Macromolecules* **1996**, *29*, 1452-1463.

44. Zhang, M.; Duhamel, J.; van Duin, M.; Meessen, P. *Macromolecules* **2004**, *37*, 1877-1890.

45. Karplus, M.; Weaver, D. L. *Nature* **1976**, *260*, 404-406.

2.8 Appendix

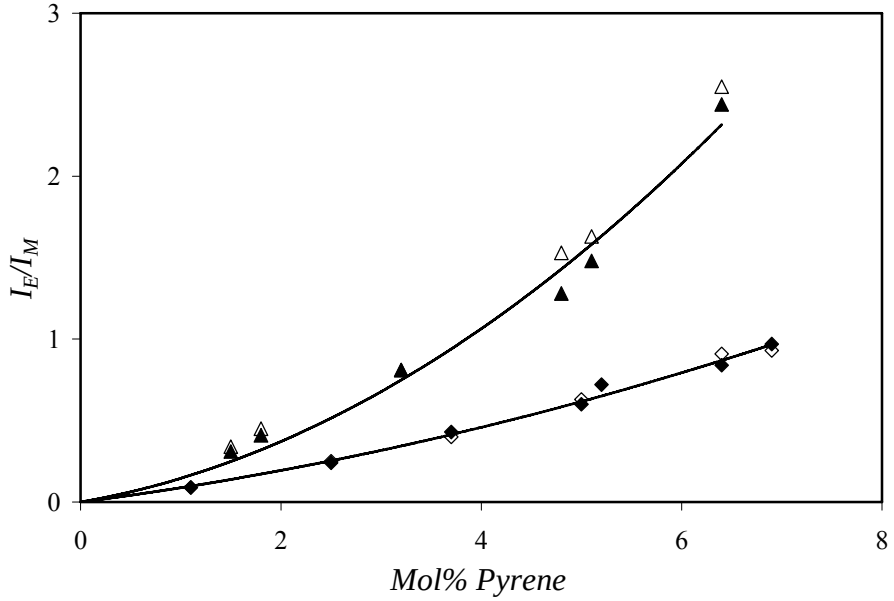

Figure A 2.1: I_E/I_M ratios as a function of pyrene content; CoE-PS (▲), CoE-PS HMW (△), CoA-PS (◆), CoA-PS HMW (◇); [Py] = 3×10^{-6} M, λ_{ex} = 344 nm.

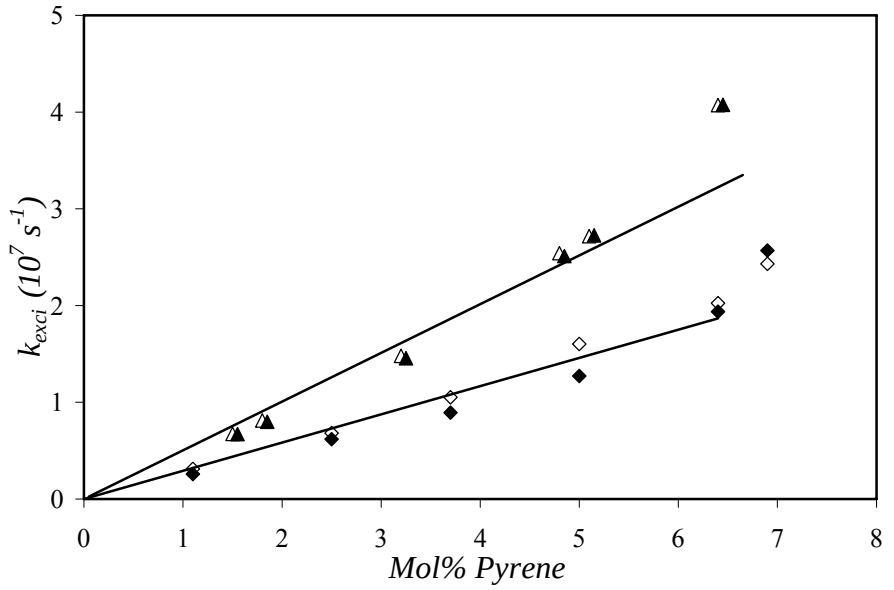

Figure A2.2: k_{exci} as a function of pyrene content; CoE-PS (▲), (the mol% was shifted by 0.2 units for clarity), CoE-PS HMW (△), CoA-PS (◆), CoA-PS HMW (◇); [Py] = 3×10^{-6} M.

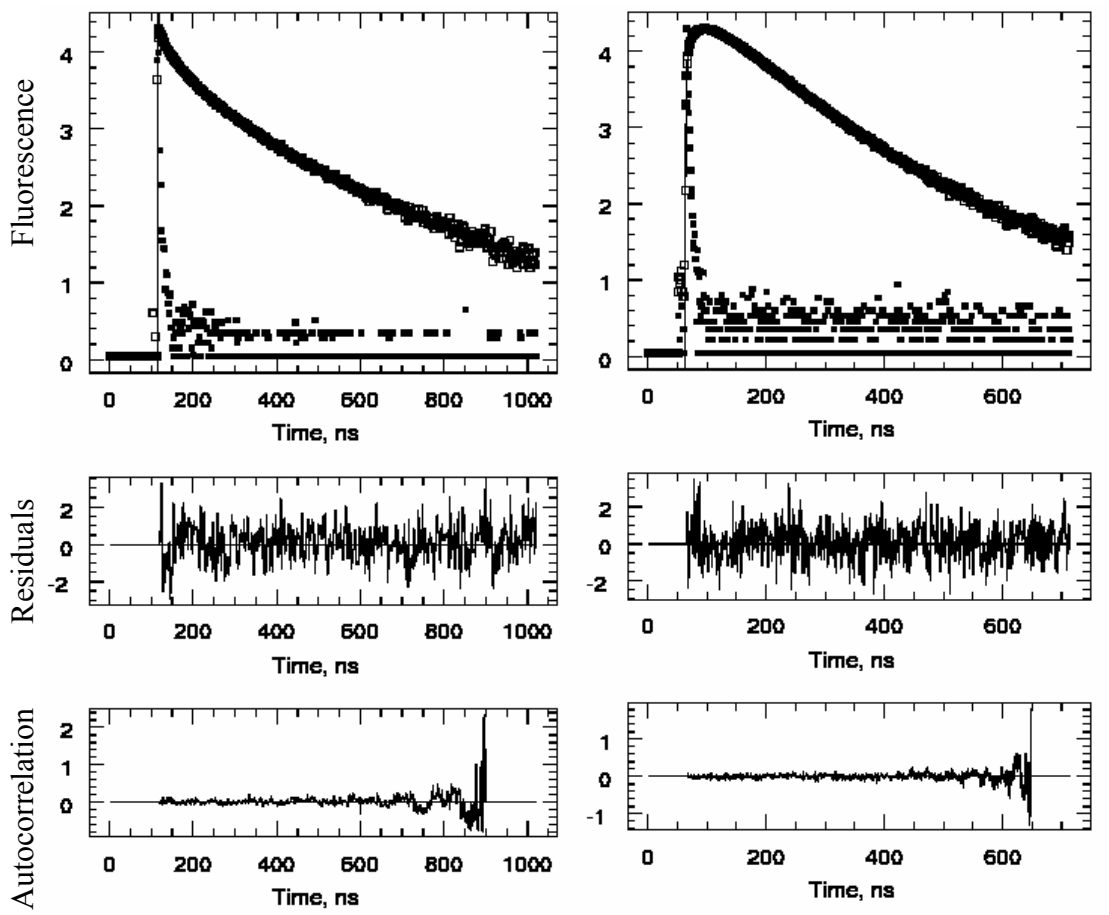

Figure A2.3: Monomer (left) and excimer (right) fluorescence decays CoE-PS labeled with 3.2 mol% pyrene. The monomer and excimer decays are analyzed simultaneously with Equations 2.3 and 2.4, respectively. [Py] = 3×10^{-6} M, λ_{ex} = 344 nm, λ_{em}(mono) = 375 nm, λ_{em}(exci)= 510 nm; $\chi^2 = 1.01$.

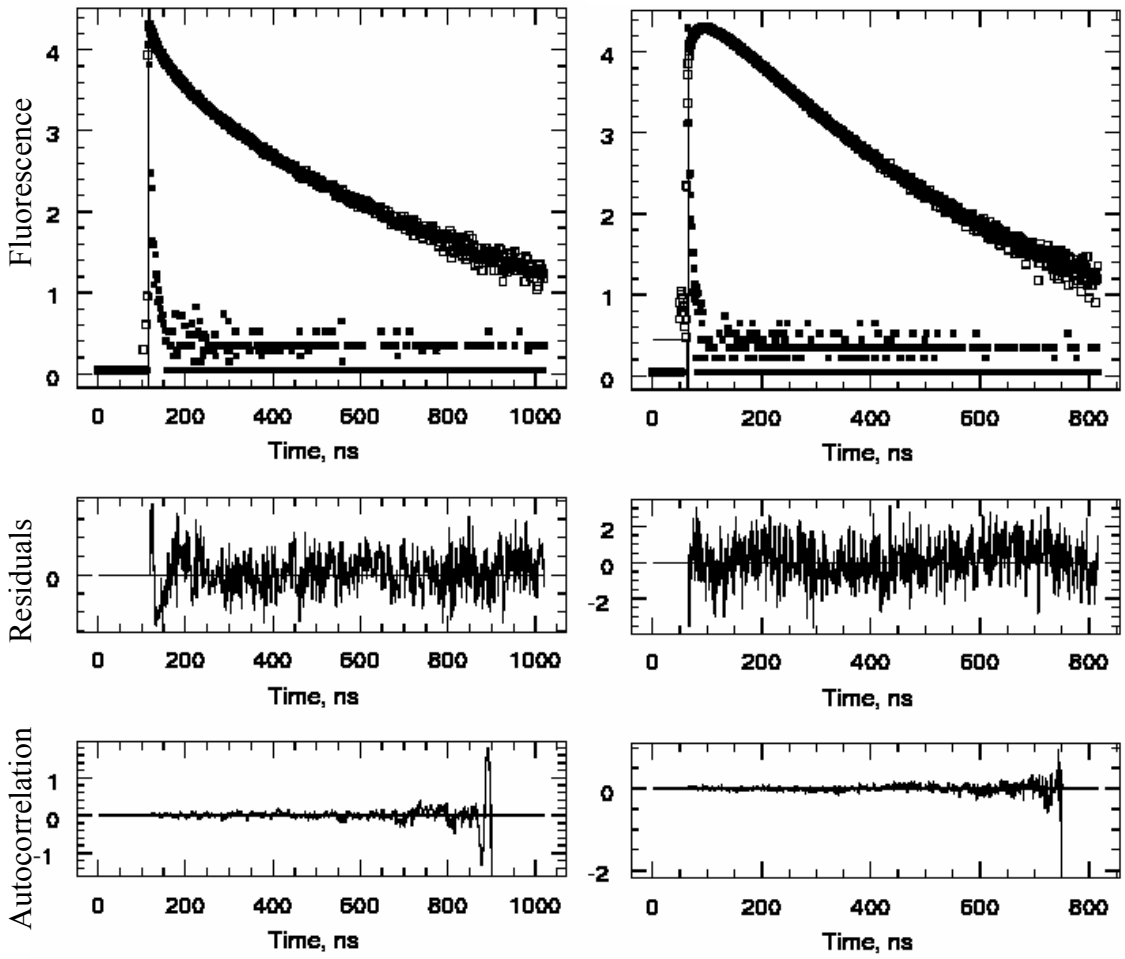

Figure A2.4: Monomer (left) and excimer (right) fluorescence decays CoE-PS (High MW) labelled with 3.2 mol% pyrene. The monomer and excimer decays are analyzed simultaneously with Equations 2.3 and 2.4, respectively. [Py] = 3×10^{-6} M, λ_{ex} = 344 nm, λ_{em}(mono) = 375 nm, λ_{em}(exci)= 510 nm; $\chi^2 = 1.34$.

Table A2.1: Molecular weights of the GrE-PS, CoA-PS, CoE-PS, and ES-PS series found using a GPC with a DRI detector and a calibration curve based on polystyrene standards.

Sample	mol % pyrene	M_n (kg/mol)	M_w (kg/mol)	PDI
GrE-PS[a]	1.1	113	116	1.03
	1.3	113	116	1.03
	2.4	110	163	1.48
	3.2	110	163	1.48
	4.6	113	116	1.03
	6.2	110	163	1.48
	6.3	110	163	1.48
	6.9	110	163	1.48
CoE-PS	1.5	35	63	1.81
	1.8	45	84	1.87
	3.2	32	63	1.99
	4.8	16	30	1.85
	5.1	34	62	1.80
	6.4	46	75	1.65
CoA-PS	1.1	43	80	1.88
	2.5	39	80	2.04
	3.7	55	102	1.90
	5.0	28	53	1.88
	6.4	39	74	1.91
	6.9	36	84	2.30
ES-PS	1.1	23	80	3.5
	2.2	11	25	2.2
	3.2	17	59	3.5

[a] The preparation of these samples was reported in reference number 18.

Table A2.2: Molecular weights of the High Molecular Weight (HMW) fractions of the CoA-PS, CoE-PS, and ES-PS series found using GPC with an online fluorescence detector and a calibration curve based on polystyrene standards. The fluorescence detector was set up with excitation and emission wavelengths at, respectively, 260 nm and 400 nm to monitor the PS emission of the PS standards and, respectively, 344 nm and 375 nm to monitor the more intense pyrene emission of the pyrene labeled samples.

HMW fraction	mol % pyrene	M_n (kg/mol)	M_w (kg/mol)	PDI
CoE-PS	1.5	78	110	1.41
	1.8	135	171	1.26
	3.2	87	135	1.56
	4.8	42	61	1.45
	5.1	58	88	1.50
	6.4	107	133	1.25
CoA-PS	1.1	169	217	1.28
	2.5	113	166	1.46
	3.7	134	187	1.39
	5.0	84	114	1.36
	6.4	64	97	1.51
	6.9	99	153	1.54
ES-PS	1.1	225	289	1.28
	2.2	204	239	1.17
	3.2	85	98	1.15

Table A2.3: Parameters retrieved from the multi-exponential fits of the monomer decays of Py–PSs in THF with Equation 2.2.

Sample	mol%	τ_1 (ns)	τ_2 (ns)	τ_3 (ns)	τ_4 (ns)	a_1	a_2	a_3	a_4	χ^2	PDI (τ_w/τ_n)
GrE-PS	1.1	13	57	150	260	0.20	0.25	0.39	0.16	1.09	1.51
	1.3	14	63	147	260	0.29	0.34	0.31	0.06	1.04	1.62
	2.4	11	40	109	260	0.40	0.34	0.23	0.03	1.04	2.05
	3.2	11	40	100	260	0.39	0.39	0.19	0.02	1.02	2.05
	4.6	6	25	67	260	0.29	0.50	0.20	0.01	1.19	1.94
	6.2	4	18	51	260	0.31	0.50	0.19	0.01	1.13	2.25
	6.3	4	16	46	260	0.28	0.49	0.22	0.02	1.37	3.11
	6.9	5	17	47	260	0.35	0.47	0.16	0.01	1.06	2.93
CoE-PS	1.5	10	52	147	260	0.22	0.34	0.35	0.09	1.11	1.64
	1.8	11	50	135	260	0.24	0.34	0.35	0.07	1.03	1.66
	3.2	9	37	100	260	0.28	0.41	0.29	0.03	1.03	1.90
	4.8	8	33	89	260	0.44	0.40	0.14	0.02	1.01	2.49
	5.1	7	28	76	260	0.36	0.45	0.19	0.01	1.07	2.12
	6.4	6	22	57	260	0.37	0.47	0.15	0.01	1.11	2.28
CoE-PS High Molecular Weight	1.5	9	52	147	260	0.23	0.33	0.35	0.09	1.11	1.64
	1.8	11	48	132	260	0.22	0.33	0.39	0.05	1.04	1.60
	3.2	8	35	96	260	0.27	0.40	0.30	0.03	0.95	1.94
	4.8	8	32	88	260	0.44	0.40	0.14	0.02	1.01	2.51
	5.1	8	30	81	260	0.38	0.45	0.16	0.01	1.06	2.04
	6.4	6	22	57	260	0.37	0.47	0.15	0.01	1.11	2.27
CoA-PS	1.1	7	61	167	260	0.09	0.20	0.47	0.24	1.07	1.27
	2.5	15	64	148	260	0.14	0.40	0.40	0.05	0.97	1.39
	3.7	12	52	117	260	0.14	0.43	0.40	0.03	1.01	1.40
	5.0	21	62	129	260	0.31	0.53	0.14	0.01	1.08	1.45
	6.4	7	33	75	260	0.20	0.49	0.30	0.01	1.23	1.64
	6.9	6	27	62	260	0.24	0.47	0.28	0.00	1.10	1.55
CoA-PS High Molecular Weight	1.1	8	57	161	260	0.13	0.18	0.47	0.22	0.96	1.33
	2.5	7	56	143	260	0.15	0.39	0.43	0.04	0.97	1.43
	3.7	9	49	114	260	0.15	0.47	0.37	0.01	1.16	1.40
	5.0	7	32	81	260	0.17	0.41	0.40	0.01	0.99	1.56
	6.4	8	30	65	260	0.21	0.44	0.32	0.02	1.05	1.92
	6.9	5	21	53	260	0.21	0.41	0.36	0.03	1.03	2.37
ES-PS High Molecular Weight	1.2	85	222		260	0.10	0.72		0.18	0.95	1.05
	2.2	82	189		260	0.15	0.83		0.02	1.03	1.05
	3.2	39	137		260	0.17	0.76		0.07	1.08	1.16

Table A2.4: Parameters retrieved from the multi-exponential fits of the excimer decays of Py–PSs in THF with Equation 2.2.

Sample	mol%	τ_1 (ns)	τ_2 (ns)	τ_3 (ns)	a_1	a_2	a_3	χ^2	a_{E-}/a_{E+}
GrE-PS	1.1	26	80	177	-0.79	0.86	0.14	1.10	-0.79
	1.3	25	72	150	-0.77	0.86	0.14	1.11	-0.77
	2.4	22	69	161	-0.74	0.96	0.04	1.18	-0.74
	3.2	20	66	237	-0.70	0.99	0.01	1.09	-0.70
	4.6	11	22	59	-0.32	-0.45	1.00	1.10	-0.77
	6.2	6	19	55	-0.17	-0.59	1.00	1.25	-0.76
	6.3	8	20	55	-0.19	-0.51	1.00	1.04	-0.70
	6.9	7	19	54	-0.23	-0.46	1.00	1.11	-0.69
CoE-PS	1.5	23	84	224	-0.83	0.95	0.05	1.15	-0.83
	1.8	23	81	181	-0.85	0.95	0.05	1.11	-0.85
	3.2	21	67	104	-0.81	0.87	0.13	1.13	-0.81
	4.8	4	19	61	-0.14	-0.75	1.00	1.27	-0.89
	5.1	4	19	62	-0.09	-0.73	1.00	1.33	-0.82
	6.4	9	23	56	-0.28	-0.52	1.00	1.12	-0.81
CoE-PS High Molecular Weight	1.5	24	84	166	-0.82	0.92	0.08	1.13	-0.82
	1.8	25	78	172	-0.83	0.93	0.07	1.25	-0.83
	3.2	15	24	74	-0.20	-0.59	1.00	1.38	-0.79
	4.8	5	21	61	-0.15	-0.71	1.00	1.20	-0.86
	5.1	5	21	61	-0.16	-0.74	1.00	1.03	-0.91
	6.4	5	19	56	-0.21	-0.67	1.00	1.09	-0.89
CoA-PS	1.1	32	106	205	-0.73	0.81	0.19	0.94	-0.73
	2.5	28	97	206	-0.78	0.93	0.07	1.14	-0.78
	3.7	27	89	220	-0.81	0.99	0.01	1.14	-0.81
	5.0	5	26	79	-0.11	-0.78	1.00	1.18	-0.89
	6.4	7	24	72	-0.08	-0.73	1.00	1.27	-0.82
	6.9	8	25	66	-0.16	-0.65	1.00	1.03	-0.81
CoA-PS High Molecular Weight	1.1	31	105	206	-0.67	0.84	0.16	1.04	-0.67
	2.5	28	95	182	-0.75	0.91	0.09	1.06	-0.75
	3.7	24	36	90	-0.70	-0.13	1.00	1.18	-0.83
	5.0	12	30	77	-0.18	-0.66	1.00	1.16	-0.84
	6.4	6	25	70	-0.11	-0.73	1.00	1.06	-0.83
	6.9	4	22	67	-0.07	-0.71	1.00	1.12	-0.78
ES-PS High Molecular Weight	1.1	41	141	229	-0.84	0.20	0.80	1.03	-0.84
	2.2	49	64	184	-0.95	0.44	0.56	1.00	-0.95
	3.2	39	44	137	-14.90	8.93	6.99	0.97	-0.94

Table A2.5: Parameters retrieved from the global FBM analysis of the monomer decays of GrE-PS, CoE-PS and CoA-PS in THF with Equation 2.3.

Sample	mol%	f_{Mdiff}	f_{Mfree}	k_{blob} (10^7 s^{-1})	$k_e[blob]$ (10^7 s^{-1})	$\langle n \rangle$	χ^2
GrE-PS	1.1	0.82	0.18	1.6	0.5	0.9	1.15
	1.3	0.91	0.09	1.7	0.5	1.1	1.16
	2.4	0.97	0.03	1.8	0.4	1.7	1.27
	3.2	0.97	0.03	1.7	0.5	2.0	1.18
	4.6	0.99	0.01	2.1	0.8	2.3	1.21
	6.2	0.99	0.01	2.2	0.8	2.7	1.28
	6.3	0.98	0.02	2.3	1.0	2.6	1.23
	6.9	0.99	0.01	2.7	1.1	2.7	1.17
CoE-PS	1.5	0.88	0.12	1.4	0.4	1.1	1.21
	1.8	0.91	0.09	1.5	0.5	1.2	1.23
	3.2	0.96	0.04	1.6	0.6	1.7	1.01
	4.8	0.97	0.03	1.8	0.5	2.3	1.33
	5.1	0.98	0.02	1.8	0.7	2.3	1.25
	6.4	0.99	0.01	2.4	1.0	2.5	1.24
CoE-PS High Molecular Weight	1.5	0.90	0.10	1.6	0.5	1.1	1.29
	1.8	0.92	0.08	1.4	0.5	1.2	1.33
	3.2	0.97	0.03	1.6	0.5	1.8	1.34
	4.8	0.98	0.02	1.8	0.7	2.4	1.28
	5.1	0.99	0.01	2.1	0.8	2.3	1.25
	6.4	0.99	0.01	2.4	0.9	2.7	1.35
CoA-PS	1.1	0.71	0.29	1.1	0.6	0.7	1.07
	2.5	0.91	0.09	1.0	0.6	1.2	1.14
	3.7	0.96	0.04	1.0	0.6	1.5	1.16
	5.0	0.97	0.03	1.4	0.9	1.6	1.25
	6.4	0.98	0.02	1.3	0.9	2.2	1.29
	6.9	0.99	0.01	1.8	1.2	2.1	1.13
CoA-PS High Molecular Weight	1.1	0.75	0.25	1.4	0.6	0.7	1.06
	2.5	0.94	0.06	1.1	0.5	1.1	1.16
	3.7	0.98	0.02	1.1	0.6	1.5	1.26
	5.0	0.98	0.02	1.5	0.9	1.7	1.18
	6.4	0.97	0.03	1.7	1.2	2.0	1.12
	6.9	0.97	0.03	1.7	1.2	2.3	1.06

Table A2.6: Parameters retrieved from the global FBM analysis of the excimer decays of GrE-PS, CoE-PS and CoA-PS in THF with Equation 2.5.

Sample	mol%	τ_{EE0} (ns)	τ_{ED} (ns)	f_{Ediff}	f_{EE0}	f_{ED}	χ^2
GrE-PS	1.1	62	383	0.88	0.12	0.00	1.15
	1.3	58	973	0.84	0.16	0.00	1.16
	2.4	58		0.79	0.21		1.27
	3.2	54		0.74	0.26		1.18
	4.6	50		0.76	0.24		1.21
	6.2	50		0.72	0.27		1.28
	6.3	50		0.67	0.33		1.23
	6.9	50		0.66	0.34		1.17
CoE-PS	1.5	57		0.90	0.10		1.21
	1.8	56		0.90	0.10		1.23
	3.2	52		0.85	0.15		1.01
	4.8	53		0.81	0.19		1.33
	5.1	51		0.80	0.20		1.25
	6.4	51		0.80	0.20		1.24
CoE-PS High Molecular Weight	1.5	59		0.89	0.11		1.29
	1.8	54		0.89	0.11		1.33
	3.2	56		0.84	0.16		1.34
	4.8	51		0.80	0.20		1.28
	5.1	52		0.85	0.15		1.25
	6.4	51		0.84	0.16		1.35
CoA-PS	1.1	67	292	0.88	0.11	0.01	1.07
	2.5	60	289	0.88	0.12	0.01	1.14
	3.7	55	161	0.88	0.12	0.00	1.16
	5.0	54	89	0.88	0.08	0.04	1.25
	6.4	52	99	0.81	0.12	0.07	1.29
	6.9	53	95	0.78	0.15	0.07	1.13
CoA-PS High Molecular Weight	1.1	74	417	0.84	0.15	0.01	1.06
	2.5	62	259	0.86	0.14	0.00	1.16
	3.7	58	306	0.86	0.14	0.00	1.26
	5.0	58	63	0.85	0.15	0.01	1.18
	6.4	54	98	0.82	0.11	0.07	1.12
	6.9	54	121	0.76	0.21	0.03	1.06

Table A2.7: Fractions of all pyrene species for GrE-PS, CoE-PS and CoA-PS, calculated from f_{Mdiff}, f_{Mfree}, f_{Ediff}, f_{EE0}, and f_{ED}.[21]

Sample	mol%	f_{diff}	f_{free}	f_{E0}	f_{D}	f_{agg}	χ^2
GrE-PS	1.1	0.74	0.17	0.10	0.00	0.10	1.15
	1.3	0.78	0.07	0.14	0.00	0.15	1.16
	2.4	0.77	0.02	0.20		0.20	1.27
	3.2	0.73	0.02	0.25		0.25	1.18
	4.6	0.76	0.01	0.23		0.23	1.21
	6.2	0.72	0.01	0.27		0.27	1.28
	6.3	0.66	0.01	0.32		0.32	1.23
	6.9	0.66	0.01	0.33		0.33	1.17
CoE-PS	1.5	0.80	0.11	0.09		0.09	1.21
	1.8	0.83	0.08	0.10		0.10	1.23
	3.2	0.82	0.04	0.15		0.15	1.01
	4.8	0.79	0.02	0.19		0.19	1.33
	5.1	0.79	0.01	0.20		0.20	1.25
	6.4	0.79	0.01	0.20		0.20	1.24
CoE-PS High Molecular Weight	1.5	0.81	0.09	0.10		0.10	1.29
	1.8	0.82	0.07	0.10		0.10	1.33
	3.2	0.81	0.03	0.16		0.16	1.34
	4.8	0.79	0.01	0.19		0.19	1.28
	5.1	0.84	0.01	0.15		0.15	1.25
	6.4	0.83	0.00	0.16		0.16	1.35
CoA-PS	1.1	0.65	0.27	0.08	0.01	0.08	1.07
	2.5	0.81	0.08	0.11	0.01	0.11	1.14
	3.7	0.85	0.03	0.12	0.00	0.12	1.16
	5.0	0.85	0.03	0.08	0.04	0.12	1.25
	6.4	0.80	0.01	0.11	0.07	0.19	1.29
	6.9	0.78	0.01	0.15	0.07	0.21	1.13
CoA-PS High Molecular Weight	1.1	0.66	0.22	0.12	0.00	0.12	1.06
	2.5	0.81	0.05	0.13	0.00	0.13	1.16
	3.7	0.84	0.02	0.14	0.00	0.14	1.26
	5.0	0.83	0.01	0.14	0.01	0.15	1.18
	6.4	0.81	0.02	0.10	0.07	0.17	1.12
	6.9	0.74	0.02	0.20	0.03	0.23	1.06

Table A2.8: Parameters retrieved from the global FBM analysis of the monomer decays of ES-PSs in THF with Equation 2.3. Note: Because of the small amount of curvature in the decays, more than one good fit could be obtained. Therefore, the possible fits were averaged to find the parameters.

Sample	mol%	f_{Mdiff}	f_{Mfree}	k_{blob} (10^7 s^{-1})	$k_e[blob]$ (10^7 s^{-1})	<n>	χ^2
ES-PS	1.1	0.66	0.34	0.8	0.7	0.3	1.04
High Molecular	1.1	0.65	0.36	1.1	0.6	0.3	1.00
Weight	1.1	0.53	0.47	1.6	0.6	0.4	1.16
AVERAGE		0.61	0.39	1.2	0.6	0.3	
	2.2	0.90	0.10	0.5	0.8	0.6	1.01
	2.2	0.89	0.11	0.6	0.9	0.5	1.01
	2.2	0.92	0.08	0.4	0.8	0.7	1.01
	2.2	0.88	0.12	0.7	1.0	0.5	1.01
AVERAGE		0.90	0.10	0.6	0.9	0.6	
	3.2	0.94	0.06	0.9	1.0	0.7	1.09
	3.2	1.00	0.00	0.7	0.6	0.87	1.18
AVERAGE		0.97	0.03	0.80	0.80	0.81	

Table A2.9: Parameters retrieved from the global FBM analysis of the excimer decays of ES-PSs in THF with Equation 2.5.

Sample	mol%	τ_{EE0} (ns)	τ_{ED} (ns)	f_{Ediff}	f_{EE0}	f_{ED}	χ^2
ES-PS	1.1	73	284	0.97	0	0.03	1.04
High Molecular	1.1	88	285	0.97	0	0.03	1.00
Weight	1.1	108	313	0.96	0	0.04	1.16
AVERAGE		90	294	0.97	0	0.03	
	2.2	65	244	0.98	0	0.02	1.01
	2.2	66	249	0.98	0	0.02	1.01
	2.2	62	238	0.98	0	0.02	1.01
	2.2	66	253	0.98	0	0.02	1.01
AVERAGE		65	246	0.98	0	0.02	
	3.2	58	173	0.94	0	0.06	1.09
	3.2	67	50	0.94	0	0.06	1.18
AVERAGE		63	112	0.94	0.000	0.059	

Table A2.10: Fractions of all pyrene species for ES-PS, calculated from f_{Mdiff}, f_{Mfree}, f_{Ediff}, f_{EE0}, and f_{ED}.[21]

Sample	mol%	f_{diff}	f_{free}	f_{E0}	f_D	f_{agg}	χ^2
ES-PS	1.1	0.65	0.33		0.02	0.017	1.04
High Molecular	1.1	0.63	0.35		0.02	0.019	1.00
Weight	1.1	0.52	0.46		0.02	0.024	1.16
AVERAGE		0.60	0.38		0.02	0.020	
	2.2	0.89	0.09		0.02	0.015	1.01
	2.2	0.87	0.11		0.01	0.014	1.01
	2.2	0.91	0.08		0.02	0.016	1.01
	2.2	0.87	0.12		0.01	0.014	1.01
AVERAGE		0.88	0.10		0.01	0.015	
	3.2	0.89	0.06		0.05	0.054	1.09
	3.2	0.94	0.00		0.06	0.06	1.18
AVERAGE		0.91	0.03		0.06	0.06	

Table A2.11: Monomer conversions from ^{1}H NMR and I_E/I_M ratios measured with the GPC on-line fluorometer of aliquots taken over time from the reaction mixture.

CoA-PS		CoE-PS	
Conversion (^{1}H NMR)	I_E/I_M (GPC fluorometer)	Conversion (^{1}H NMR)	I_E/I_M (GPC fluorometer)
0.03	0.71	0.06	1.09
0.06	0.73	0.08	1.02
0.15	0.73	0.35	1.02
		0.55	0.99

Table A2.12: Lifetime (τ_M) retrieved from low labeled polymers (≤ 0.2% Pyrene) and monomer compounds in THF.

Polymer	a_1	a_2	τ_1 (ns)	τ_2 (ns)	χ^2	Monomer	τ_M (ns)	χ^2
GrE-PS	0.23	0.76	59	253	1.00	PyMMS	259	1.16
CoE-PS	0.12	0.87	80	258	0.99	PyMAM	255	1.19
ES-PS[a]	0.11	0.89	90	257	1.03			

[a] Synthesis with ~9:1 aniline:pyrene labeled derivative of lysine monomer

Table A2.13: Slopes and errors for trend lines in Figures 2.4 and 2.8.

Series	$k_{blob} \times \langle n \rangle$		k_{exci}	
	Slope (10^9 s^{-1} g/mol)	Error (±)	Slope (10^7 s^{-1} /mol%)	Error (±)
GrE-PS	119	6	0.66	0.02
CoE-PS	103	5	0.51	0.04
CoA-PS	56	2	0.31	0.02
ES-PS	19	3	0.11	0.02

Table A2.14: Reproducibility of the I_E/I_M ratios and effect of the excitation wavelength (λ_{ex} = 340 or 344 nm). Each entry represents a freshly prepared solution which was degassed and run on the steady-state fluorometer.

Sample	mol %	λ_{ex} (nm)	Experiment #			average	error
			A	B	C		
CoA-PS	1.1	340	0.09	0.09	0.09	0.09	0.00
	2.5		0.26	0.26	0.24	0.25	0.01
	3.7		0.47	0.47	0.47	0.47	0.00
	3.7	344	0.47				
CoE-PS	3.2	340	0.84	0.85	-	0.84	0.01
	3.2	344	0.84	0.84	0.85	0.85	0.01
GrE-PS	3.2	340	0.86	0.73	0.78	0.82	0.03
	3.2	344	0.85	0.80	0.80	0.79	0.07

Table A2.15: Reproducibility of the average monomer lifetime $<\tau>$ used to determine k_{exci} according to Equation 2.6. λ_{ex} = 340 nm. Each entry represents a freshly prepared solution which was degassed and run on the time-resolved fluorometer.

Sample	mol %	τ_1 (ns)	τ_2 (ns)	τ_3 (ns)	τ_4 (ns)	a_1	a_2	a_3	a_4	χ^2	$<\tau>$ (ns)
GrE-PS	3.2	11	40	100	260	0.363	0.416	0.209	0.012	0.88	44
		11	40	100	260	0.390	0.396	0.190	0.024	1.12	46
		11	41	105	260	0.358	0.441	0.191	0.010	1.02	45
CoE-PS	3.2	8	34	99	260	0.243	0.415	0.309	0.033	1.14	55
		11	39	102	260	0.280	0.407	0.284	0.029	0.92	55
		9	35	97	260	0.265	0.398	0.302	0.035	1.05	54
CoA-PS	3.7	17	61	135	260	0.198	0.522	0.274	0.006	1.01	74
		12	51	118	260	0.128	0.440	0.411	0.021	0.95	78
		11	54	124	260	0.146	0.486	0.353	0.014	1.17	75
ES-PS	3.2	-	35	135	260	-	0.159	0.764	0.076	1.08	129
		-	33	136	260	-	0.138	0.747	0.115	1.05	136
		-	59	151	260	-	0.216	0.753	0.031	1.09	134

Chapter 3:
Effect of Viscosity on Long Range Polymer Chain Dynamics in Solution Studied with a Fluorescence Blob Model

3.1 Abstract

The process of excimer formation for two pyrene labeled polystyrenes was studied in seven different solvents. The solvent viscosities ranged from 0.36 to 1.18 mPa·s, while the solvent quality ranged from good to theta-solvents for polystyrene, as determined by intrinsic viscosity measurements. Steady-state fluorescence spectra of the pyrene-labeled polymers were acquired and the excimer to monomer intensity ratios showed that excimer formation increased strongly with a decrease in solvent viscosity. Time-resolved fluorescence decays were also acquired and the fluorescence blob model (FBM) was applied to fit globally the monomer and excimer decays. Among the parameters that were retrieved from the FBM analysis of the fluorescence decays, the rate constant of excimer formation between two pyrenes located inside a blob, k_{blob}, was found to remain constant over the entire range of viscosities for a given pyrene labeled polymer, whereas the number of monomers making up a blob, N_{blob}, changed noticeably with solvent viscosity. Since N_{blob} is a measure of the volume probed by an excited pyrene during is lifetime, V_{blob}, and since V_{blob} is affected by solvent viscosity, solvent quality, and the lifetime of the pyrene chromophore, N_{blob} is also affected by these parameters. On the other hand, the product $k_{blob} \times N_{blob}$ was shown to depend uniquely on the product of the inverse of the solvent viscosity and the polymer intrinsic viscosity. This study demonstrates that the FBM properly describes how the process of excimer formation between pyrenes randomly attached onto polystyrene is affected by changes in solvent viscosity and solvent quality toward the polymer.

3.2 Introduction

Over the past few decades, pyrene labeled polymers have provided a means to probe how intramolecular long range polymer chain dynamics (LRPCD) are affected by changes in solvent quality,[1–6] solution temperature,[7–9] and polymer concentration,[10–12] to name but a few, and these studies have led to a number of reviews.[13–15] A majority of this work has employed polymers end-labeled with a chromophore and quencher, namely pyrene. In these experiments a cyclization event is observed as an excited pyrene located at one end of the chain diffusionally encounters a ground–state pyrene at the other end of the chain to form an excimer. This approach benefits from the unexpected simplicity of the mathematical treatment of the kinetics describing the end-to-end cyclization event, which is well represented by a single apparent rate constant for a polymer of a given chain length.[16] Although this route has provided a wealth of information on polymer chain dynamics in solution, it is limited in the sense that only relatively short polymers can generate enough cyclization events for accurate quantification of the kinetic parameters.

This shortcoming is avoided with randomly labeled polymers where the average distance between two labels can be adjusted by increasing the labeling level. Also, the synthesis of monodispersed, end-labeled polymers is generally more demanding than that of polydisperse, randomly labeled polymers.[15,17] Unfortunately, the obvious advantages associated with the use of polymers randomly labeled with pyrene are counterbalanced by an increased complexity of the kinetics describing the process of excimer formation. As a matter of fact, analysis of the fluorescence decays obtained with polymers randomly labeled with pyrene is inherently *complicated* by the distribution of rate constants associated with the varied chain lengths separating every two pyrenes. This complication is overcome by

analyzing the fluorescence decays with the fluorescence blob model (FBM).[18] The FBM has been used to study polymer chain dynamics in organic solvents,[3,18,19] polymer solutions in the semi-dilute regime,[12] and hydrophobically modified water-soluble polymers, also called associative polymers.[20,21]

Recently, it was found that the rate of excimer formation for pyrene-labeled polystyrene (Py-PS) was very sensitive to the manner that pyrene was attached to the PS backbone.[22] The FBM was used to differentiate the changes in excimer formation exhibited by Py-PS when pyrene was attached to the backbone via four different methods. This study emphasized the ability of the FBM to differentiate between the effects due to polymer chain dynamics and those resulting from the nature of the linker connecting pyrene to the polymer backbone.

The demonstrated ability of the FBM to describe the diffusive encounters between pyrene pendants randomly attached onto a polymer[15] demands that the FBM be used to investigate how those encounters are affected by the parameter having the most obvious effect on LRPCD, namely solvent viscosity. Interestingly, there have been rather few reports that use the process of excimer formation to probe the effect that viscosity has on LRPCD. Previous studies of pyrene end-labeled poly(ethylene oxide) (Py-PEO-Py)[23] and poly(vinyl acetate) randomly labeled with pyrene (Py-PVA)[17] have monitored the changes in excimer formation as a function of viscosity. Both studies concluded that excimer formation is largely controlled by viscosity, with the Py-PVA study also focusing on solvent quality which was reflected by the intrinsic viscosity of the polymer solutions. The effects of pressure and associated viscosity increase on the kinetics of excimer formation have also been monitored for pyrene end-labeled polystyrene[24,25] and polydimethylsiloxane.[26] Other

work on pyrene labeled poly(*N*,*N*-dimethylacrylamide) (Py-PDMA)[19] utilized the FBM to describe the differences in the LRPCD experienced by PDMA when dissolved in either a good solvent (*N*,*N*-dimethylformamide) or a lower viscosity theta-solvent (acetone). However, a broad study of the ability of the FBM to probe the effect of solvent viscosity on LRPCD has yet to be completed.

In order to achieve this objective, the present work investigates how the process of excimer formation between pyrene pendants is affected by solvent quality and viscosity for two series of Py-PS. The difference between the two Py-PS series resides in the linker joining the pyrene to the PS backbone, with each linker having different lengths and flexibilities. The effect of viscosity on excimer formation was investigated quantitatively by monitoring the trends obtained with the FBM parameters. This study further extends the working knowledge of the FBM and its ability to describe LRPCD.

3.3 Experimental

Materials: Distilled in glass *N*,*N*-dimethylformamide (DMF), tetrahydrofuran (THF), and dioxane were purchased from Caledon Laboratories (Georgetown, ON). Certified A. C. S. methyl ethyl ketone (MEK), benzene, and HPLC grade ethyl acetate were purchased from Fischer Scientific (Fair Lawn, NJ). HPLC grade dichloromethane (DCM), chloroform, and toluene were purchased from EMD Science (Gibbstown, NJ). HPLC grade *N*,*N*-dimethylacetamide, methyl acetate, and spectroscopy grade *N*-methyl-2-pyrolidinone were purchased from Sigma-Aldrich (Oakville, ON). All solvents were used as received.

Synthesis of pyrene-labeled polystyrene: The synthesis and characterization of poly(styrene-*co*-1-pyrenemethylacrylamide) (CoA-PS) and poly(styrene-*co*-4-(1-pyrenyl)methoxymethyl styrene) (CoE-PS) have been described in Chapter 2 and reference 22 The pyrene content

expressed in mol% of pyrene labeled monomer (x) or μmol of pyrene per gram of polymer (λ_{Py}), the number-average molecular weights, and the polydispersity indices of the Py-PS samples are listed in Table 3.1. The number-average molecular weights of the Py-PSs was typically ~40 kg/mol with a PDI of ~1.9. The structures of CoA-PS and CoE-PS are shown in Scheme 3.1.

Intrinsic viscosity measurements: A narrow molecular weight polystyrene (PS-40K, M_n = 40 kg/mol; M_w = 42 kg/mol) was used as a model for the CoA-PS and CoE-PS series. The pyrene labeled polymers were not used themselves due to the very small amount of pyrene-labeled polymer synthesized (typically ~ 40 mg). Four-to-five concentrations ranging from 3 – 10 g/L were used to find the intrinsic viscosities for PS in each solvent. The viscosity measurements were conducted with an Übbelohde viscometer placed in an ethylene glycol bath maintained at a temperature of 25 ^{o}C (± 0.1). Plots of the reduced viscosity as a function of the polymer concentration are shown in Figure A3.1 in the Appendix. The intrinsic viscosity ([η]) of PS-40K in different solvents was obtained by extrapolating the plots shown in Figure A3.1 to zero polymer concentration. The [η] values are reported in Table 3.2.

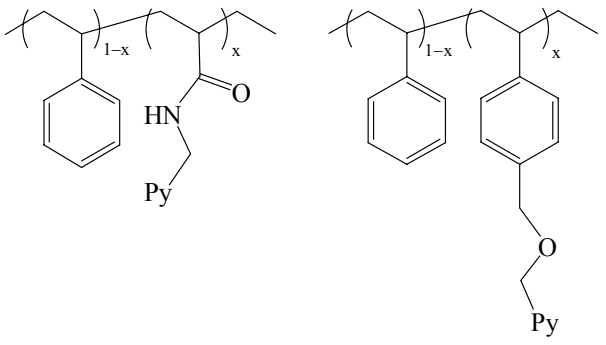

CoA-PS CoE-PS

Scheme 3.1: Chemical structures of CoA-PS and CoE-PS.

Table 3.1: Pyrene contents x in mol% (see Scheme 3.1) and λ_{Py} in μmol.g^{-1}, molecular weights and PDI of the CoA-PS and CoE-PS samples.

Sample	x, mol %	λ_{Py}, μmol·g^{-1}	M_n, kg·mol^{-1}	PDI
CoE-PS	1.5	141	35	1.81
	1.8	169	45	1.87
	3.2	284	32	1.99
	4.8	412	16	1.85
	5.1	436	34	1.80
	6.4	533	46	1.65
CoA-PS	1.1	105	43	1.88
	2.5	230	39	2.04
	3.7	331	55	1.90
	5.0	437	28	1.88
	5.2	459	34	1.96
	6.4	550	39	1.91

Steady-state fluorescence measurements: All fluorescence spectra were obtained on a PTI fluorometer using the right angle geometry. All solutions had an optical density of 0.1 and were degassed for 30 minutes under a gentle flow of N_2 to remove oxygen. The degassed solutions were excited at 344 nm and the emission spectrum was collected from 350 to 600 nm. The fluorescence intensity of the monomer (I_M) and excimer (I_E) was integrated between 372 and 378 nm and between 500 and 530 nm, respectively.

Time-resolved fluorescence measurements: Fluorescence decays were obtained by exciting the solutions at 340 nm with an IBH 340 nm LED and collecting the emission at 375 nm and 510 nm for the monomer and excimer, respectively. All decays were acquired using 1024 channels to a peak maximum of 20,000 counts for the lamp and decay curves. The instrument response function was determined by applying the MIMIC method[27] to the reference decays obtained with PPO [2,5-diphenyloxazole] in cyclohexanol (τ = 1.42 ns) and BBOT [2,5-

bis(*tert*-butyl-2-benzoxazolyl)thiopene] in ethanol (τ =1.47 ns) for the monomer and excimer decays, respectively. The polymer solutions were prepared in the same manner as for the steady-state fluorescence experiments.

Table 3.2: Solvent viscosities and intrinsic viscosities for PS-40K at T = 25 ^{o}C.

Solvent	η, mPa·s	[η], L/g	± [η], L/g
Methyl Acetate	0.36	0.0159	0.0001
MEK	0.41	0.0178	0.0002
DCM	0.41	0.0248	0.0004
THF	0.46	0.0246	0.0014
Toluene	0.56	0.0259	0.0003
DMF	0.79	0.0192	0.0003
Dioxane	1.18	0.0241	0.0001

Analysis of the fluorescence decays: The monomer and excimer decays were analyzed using a global analysis whereby the monomer and excimer decays were simultaneously fitted with Equations 3.1 and 3.2, respectively.[28]

$$\left[Py^{*}\right]_{(t)} = \left[Py^{*}_{diff}\right]_{(t=0)} \exp\left[-\left(A_2 + \frac{1}{\tau_M}\right)t - A_3\left(1-\exp\left(-A_4 t\right)\right)\right] + \left[Py^{*}_{free}\right]_{(t=0)} \exp\left(-t/\tau_M\right) \qquad (3.1)$$

$$[E^{*}] = -[Py^{*}_{diff}]_{(t=0)}\, e^{-A_3} \sum_{i=0}^{\infty} \frac{A_3{}^{i}}{i!} \frac{A_2 + i\,A_4}{\frac{1}{\tau_M} - \frac{1}{\tau_{E0}} + A_2 + i\,A_4} \exp\left(-\left(\frac{1}{\tau_M} + A_2 + i\,A_4\right)t\right)$$

$$+ \left([E0^{*}]_{(t=0)} + [Py^{*}_{diff}]_{(t=0)}\, e^{-A_3} \sum_{i=0}^{\infty} \frac{A_3{}^{i}}{i!} \frac{A_2 + i\,A_4}{\frac{1}{\tau_M} - \frac{1}{\tau_{E0}} + A_2 + i\,A_4} \right) e^{-t/\tau_{E0}} + \left[D^{*}\right]_0 e^{-t/\tau_D} \qquad (3.2)$$

The parameters A_2, A_3, and A_4 used in Equations 3.1 and 3.2 are described in Equation 3.3. Equations 3.1 to 3.3 have been used extensively over the past decade to study polymer dynamics in solution.[15]

$$A_2 = \langle n \rangle \frac{k_{blob} k_e [blob]}{k_{blob} + k_e [blob]} \qquad A_3 = \langle n \rangle \frac{k_{blob}^2}{(k_{blob} + k_e [blob])^2} \qquad A_4 = k_{blob} + k_e [blob] \tag{3.3}$$

Equations 3.1-3.3 assume that some of the excimer is formed through diffusive encounters between an excited pyrene, Py^*_{diff}, and a ground–state pyrene. In the monomer decay, the Py^*_{diff} monomers are described by the first exponential in Equation 3.1. The fraction of pyrene groups that are isolated and cannot form excimer, Py^*_{free}, are accounted for by the second exponential in Equation 3.1. The lifetime of the unquenched pyrene monomer, τ_M, was estimated through the biexponential analysis of the fluorescence decays of a low pyrene content CoE-PS and CoA-PS sample (< 0.2 mol% pyrene) where the exponential with the longest decay time contributed more than 80% of the total pre-exponential weight of the decay. The lifetimes were found to be in the 144 - 258 ns range depending on the solvent as shown in Table 3.3.

The FBM parameters retrieved from the analysis of the monomer decay and used in Equation 3.3 are defined as the rate constant of encounter between one excited pyrene and one ground–state pyrene located in the same *blob*, k_{blob}, the average number of ground–state pyrenes per *blob*, $\langle n \rangle$, and the rate constant describing the exchange of ground–state pyrenes between *blobs* times the *blob* concentration in the polymer coil, $k_e \times [blob]$.

Table 3.3: Pyrene monomer lifetimes, τ_M, retrieved from Py-PS samples with λ_{Py} < 20 μmol/g.

Solvent	CoE-PS τ_M (ns)	CoA-PS τ_M (ns)
Methyl Acetate	248	251
MEK	172	170
DCM	144	152
THF	257	258
Toluene	230	241
DMF	220	220
Dioxane	242	243

Equation 3.2 fits the excimer decays assuming three pathways toward excimer formation. The excimers, *E0**, formed through the diffusive encounter of an excited pyrene, Py^*_{diff}, and a ground-state pyrene emit with a lifetime τ_{E0}. They can also be generated through direct excitation of a pre-associated dimer, *E0*. The long-lived species, *D**, fluoresces with a long lifetime τ_D. Usually, *D** is attributed to the presence of improperly stacked pyrene dimers that emit with a long lifetime τ_D. Their contribution increases with increasing pyrene content. In the present case, however, their contribution was found to increase slightly with decreasing pyrene contents and was much stronger for the CoA-PS series than for the CoE-PS series. This observation leads us to two other possibilities for the presence of a long-lived excimer species in the excimer decay. The first possibility is that instead of dealing with ground-state pyrene dimers, some residual exciplex formation occurs between an excited pyrene and a styrene unit. This process is favored at low pyrene contents and when pyrene is held closer to the backbone, as with CoA-PS. The second possibility is that the shorter linker of CoA-PS hinders excimer formation to such an extent that some excimers formed via diffusional encounters require a longer time to re-arrange and form

excimer, and thus appear later in the excimer decay. The relative fraction of excimers formed this way would decrease as more pyrene is added to the backbone, where excimer formation is enhanced. In any case, the fraction of pyrenes that form excimer with a lifetime τ_D is very small for all Py-PS above 2 mol% pyrene. Using the two CoA-PS samples having the lowest λ_{Py} values, τ_D values around 180 ns were obtained, regardless of the solvent. Since the τ_D contribution is negligible at higher pyrene content, a τ_D value of 180 ns was fixed in the analysis of all Py-PS samples. The simultaneous analysis of the monomer and excimer decays enables the determination of the fractions f_{diff}, f_{free}, f_{E0}, and f_D of the species Py^*_{diff}, Py^*_{free}, $E0^*$, and D^* and the sum of the fractions f_{E0} + f_D gives the fraction of aggregated pyrene groups, f_{agg}. Determination of these species is described in more detail in a previous publication.[29]

Optimization of the parameters used in Equations 3.1-3.3 to fit globally the monomer and excimer fluorescence decays was performed with the Marquardt-Levenberg algorithm.[30] The IBH 340 LED used to acquire the fluorescence decays was found to generate a higher background noise level than the hydrogen lamp used previously. Therefore a background correction was applied to fit the fluorescence decays.[22,31] As done in earlier publications, a light scattering correction was also applied to account for those pyrene pairs which are in close contact and form excimer on a time-scale which is too fast to be detected accurately by our instrument.[31] The fits of the monomer and excimer decays were considered good if the χ^2 was below 1.3 and the residuals were randomly distributed around zero.

3.4 Results

The solvents were chosen to provide a broad range of viscosities (0.36 – 1.18 mPa·s). The quality of the solvents toward PS was assessed from intrinsic viscosity measurements. Intrinsic viscosity measurements were conducted at a temperature of 25 ^{o}C for each of the solvents using the PS-40K sample, a monodispersed PS with M_n of 40 kg/mol and M_w of 42 kg/mol. The plots relating the specific viscosity of the polymer solutions to the polymer concentration are shown in Figure A3.1. THF, toluene, dioxane, and DCM being known good solvents for PS at 25 ^{o}C[32] yield large and similar [η] values for PS-40K confirming that the quality of these solvents toward PS is good, whereas MEK, DMF, and methyl acetate yielding lower [η] values are poorer solvents. The intrinsic viscosities obtained for PS-40K in THF, toluene, and MEK are in good agreement with the intrinsic viscosities of a PS sample having an M_w of 42 kg/mol calculated with the published Mark-Houwink-Sakurada (MHS) constants in their respective solvents.[32] The intrinsic viscosity obtained in methyl acetate is similar to that calculated with the MHS parameters for a PS sample under theta-conditions for PS, as PS is in cyclohexane at 34.5 ^{o}C.[32] Thus at 25 ^{o}C, the PS-methyl acetate system is near a theta-solvent condition, consistent with literature indicating that theta-temperature for the PS-methyl acetate system is 43 ^{o}C.[33]

Steady-state fluorescence spectra were acquired for six CoA-PS and six CoE-PS samples in methyl acetate, MEK, DCM, THF, toluene, DMF, and dioxane. The fluorescence spectra for the CoA-PS sample containing 3.7 mol% pyrene are shown in Figure 3.1. The spectra for a CoE-PS sample containing 3.2 mol% pyrene are shown in Figure A3.2 in the Appendix. The spectra are normalized at the 0-0 peak located at either 375 or 376 nm,

depending on the solvent. Excimer formation appears to be strongly affected by the nature of the solvent. It is also more efficient for the CoE-PS than for the CoA-PS series.

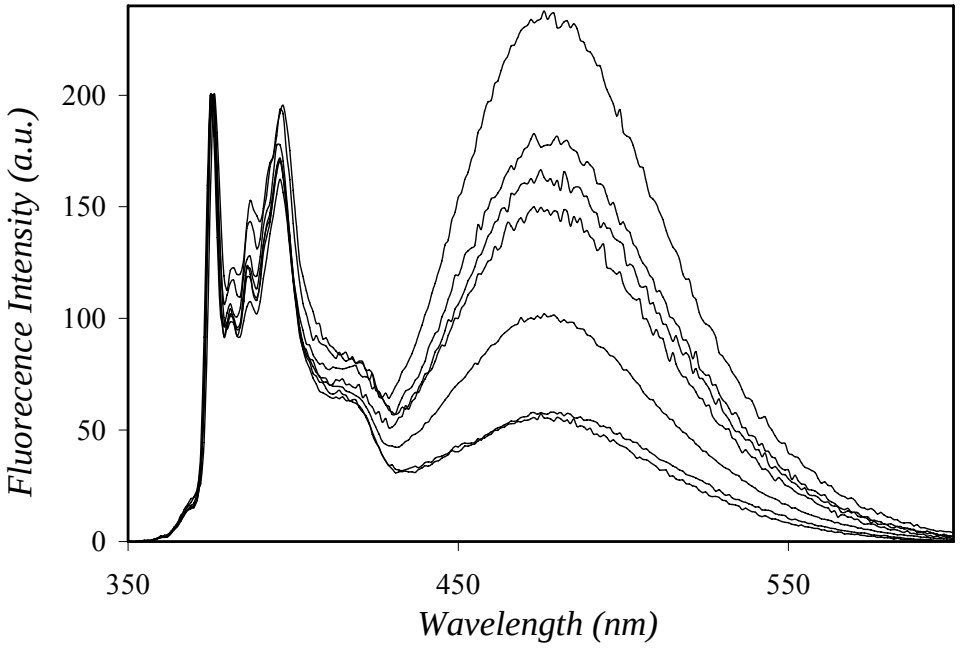

Figure 3.1: Steady-state fluorescence spectra of CoA-PS. From top to bottom, the polymers are dissolved in methyl acetate, MEK, DCM, THF, toluene, DMF, and dioxane, respectively. [Py] = 3×10^{-6} M, λ_{ex} = 344 nm, λ_{Py} = 331 μmol/g.

The steady-state fluorescence spectra were also acquired in five additional solvents, namely *N,N*-dimethylacetamide (DMA), *N*-methyl-2-pyrrolidinone (NMP), benzene, chloroform, and ethyl acetate for the CoA-PS sample with a pyrene content of 3.7 mol% and the CoE-PS sample with a pyrene content of 3.2 mol%. The I_E/I_M ratios were calculated for the 3.7 mol% CoA-PS and 3.2 mol% CoE-PS in all solvents and are shown in Figure 3.2 and Figure A3.3, respectively. Although there is some scatter, I_E/I_M increases somewhat linearly with the inverse of the viscosity. This trend is very similar to that obtained by Winnik et al. for an 8 kg/mol PEO sample labeled at both ends with pyrene (Py-PEO-Py) in several

solvents,[23] and to that obtained by Cuniberti and Perico with a PVAc sample randomly labeled with pyrene in mixtures of methanol–ethylene glycol and ethyl acetate–glycerol triacetate.[17] Figures 3.3 and A3.4 shows the I_E/I_M values of the CoA-PS and CoE-PS samples in the seven solvents used over the entire range of pyrene contents, respectively. The trends in Figures 3.1 to 3.3 and A3.2 to A3.4 are very similar; however, the CoE-PS series generates much more excimer than the CoA-PS series. This is due to the longer more flexible linker connecting pyrene to the backbone that enhances the rate of excimer formation.[22] Nevertheless, the nature of the linker connecting pyrene to the PS backbone does not seem to affect much the order of the solvents having an increasingly favorable effect on excimer formation. The efficiency of excimer formation seems to follow the sequence dioxane ≈ DMF < THF < toluene < DCM ≈ MEK < methyl acetate.

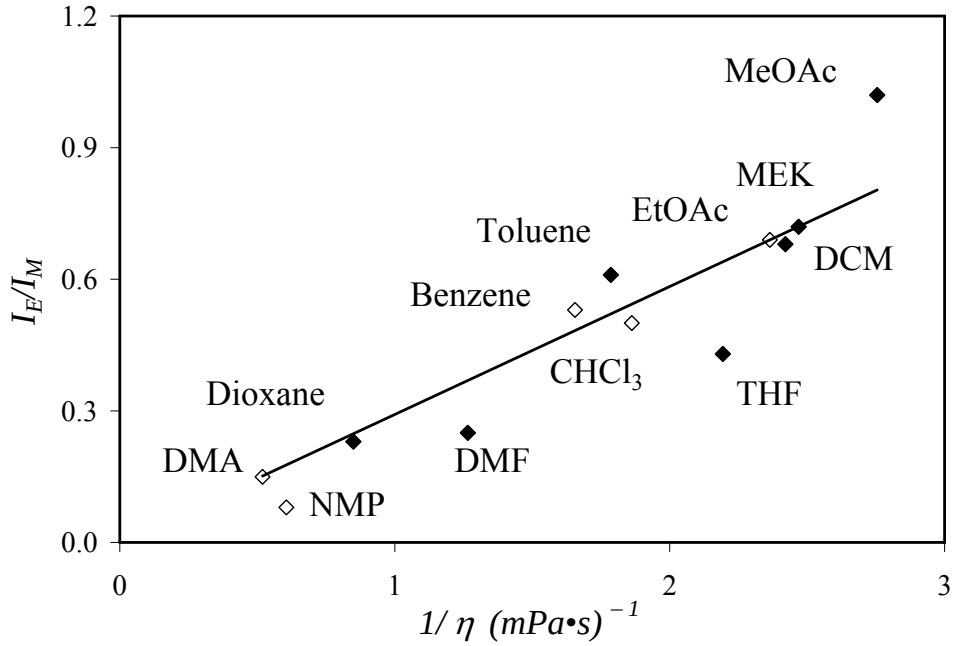

Figure 3.2: I_E/I_M ratios of a 3.7 mol% CoA-PS; [Py] = 3×10^{-6} M, λ_{ex} = 344 nm.

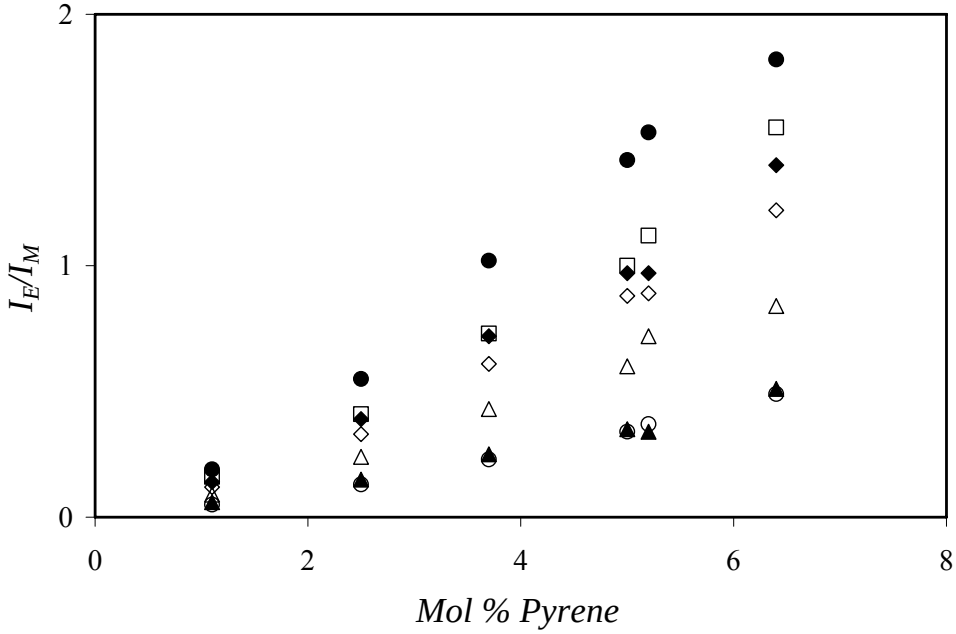

Figure 3.3: I_E/I_M ratios as a function of pyrene content. CoA-PS in methyl acetate (●), MEK (◆), DCM (□), toluene (◇), THF (△), DMF (▲), and dioxane (○); [Py] = 3×10^{-6} M, λ_{ex} = 344 nm.

Time-resolved fluorescence decays were also acquired for the CoA-PS and CoE-PS series in methyl acetate, MEK, DCM, THF, toluene, DMF, and dioxane. The FBM parameters were recovered by fitting globally the monomer and excimer decays with Equations 3.1 and 3.2, respectively. High viscosity reduces diffusive excimer formation, dampens the curvature in the monomer decays, and results in large variations in the FBM parameters retrieved from the fits making them less informative. Consequently, solvents with viscosity higher than that of dioxane (η = 1.18 mPa·s) were not investigated using lifetime measurements due to the decrease in excimer formation associated with a larger viscosity.

All monomer and excimer decays were analyzed with Equations 3.1 to 3.3 yielding the parameters k_{blob}, $\langle n \rangle$, and $k_e \times [blob]$, and the fractions f_{diff}, f_{free}, f_{E0}, and f_D, whose values are

listed in Tables A3.1-6. Examples of fits of the monomer and excimer decays of a CoE-PS and CoA-PS sample in DMF are shown in Figures A3.5 and A3.6, respectively. In Figure 3.4, k_{blob} is plotted as a function of the corrected pyrene content. The corrected pyrene content is given by λ_{Py}/f_{Mdiff}, the pyrene content divided by the fraction of pyrene monomers that form excimer by diffusion ($f_{Mdiff} = [Py^*_{diff}]_o/([Py^*_{diff}]_o + [Py^*_{free}]_o)$. In most cases, f_{Mdiff} is very close to 1.0 and the correction is small.[18,22] k_{blob} values are larger for CoE-PS than for CoA-PS due to the larger and more flexible linker connecting pyrene to the PS backbone.[22] Yet all k_{blob} trends in Figure 3.4 seem to converge to a same value when extrapolated to zero pyrene content. k_{blob} increases with increasing pyrene content for both polymers in all solvents. Since k_{blob} is inversely proportional to the volume of a blob, V_{blob},[19] which is the volume probed by an excited pyrene during its lifetime, the increase in k_{blob} observed for a given polymer series in a given solvent indicates that a smaller volume is being probed by the excited pyrene as the pyrene content is increased. This is believed to be a consequence of a reduced mobility experienced by the excited pyrene as the backbone is labeled with increasingly large numbers of bulky pyrenes.[18] Since k_{blob} changes with pyrene content, k^o_{blob} for a particular polymer and solvent system is found by extrapolating the trends shown in Figure 3.4 to zero pyrene content. k^o_{blob} is shown as a function of the inverse of viscosity in Figure 3.5. Interestingly, all k^o_{blob} values cluster around 1.0×10^7 s^{-1}, with the k^o_{blob} values of CoE-PS being slightly higher than those of CoA-PS in general. Also of note is that the trends obtained for k^o_{blob} do not show any significant difference between the good (DCM, THF, toluene, dioxane) and poor (methyl acetate, MEK, DMF) solvents.

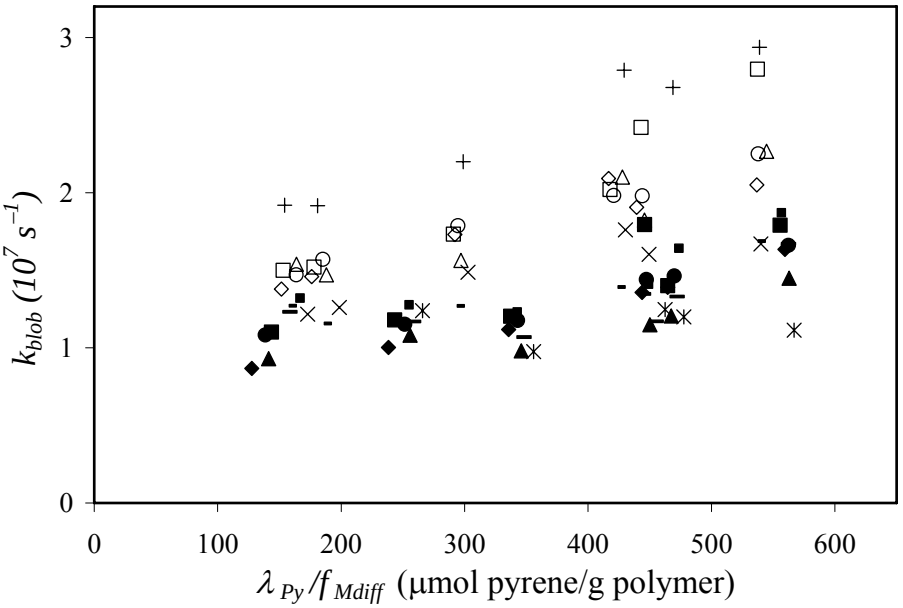

Figure 3.4: k_{blob} as a function of pyrene content. Methyl acetate (CoA-PS, ◆; CoE-PS, ◇), MEK (CoA-PS, ■; CoE-PS, □), DCM (CoA-PS, ▪; CoE-PS, +), THF (CoA-PS, ▲; CoE-PS, △), toluene (CoA-PS, ●; CoE-PS, ○), DMF (CoA-PS, —; CoE-PS, –), dioxane (CoA-PS, ∗; CoE-PS, ×); [Py] = 3×10^{-6} M.

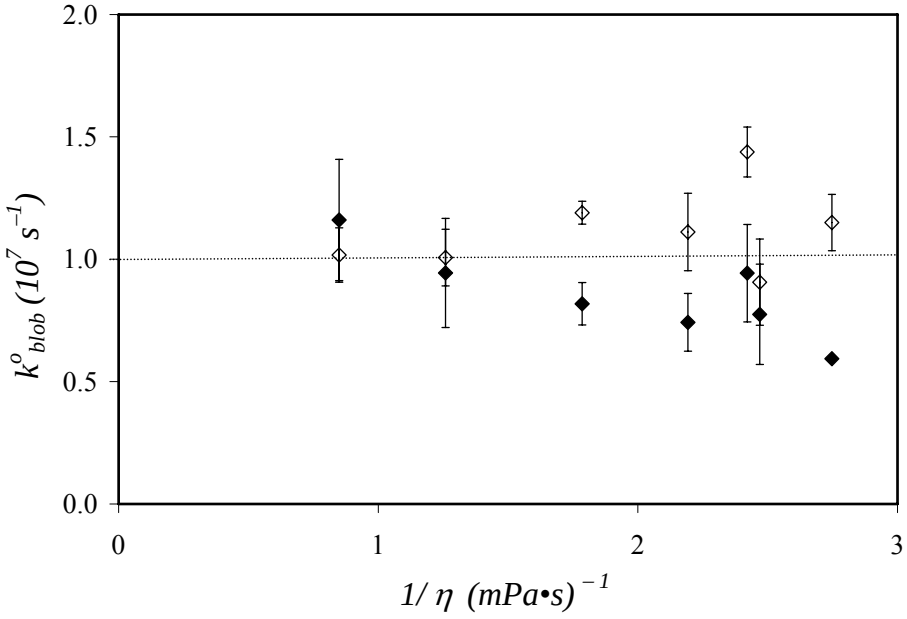

Figure 3.5: k^o_{blob} as a function of the inverse solvent viscosity. CoA-PS (◆), CoE-PS (◇); [Py] = 3×10^{-6} M.

The change in V_{blob} resulting from a change in viscosity has little effect on k_{blob}^{o}, but has a strong effect on <*n*> and in turn N_{blob}. N_{blob} represents the number of monomers found in V_{blob}. N_{blob} is calculated from <*n*> according to Equation 3.4, where λ_{Py}/f_{Mdiff} is the corrected pyrene content, M_{Py} and M_{Sty} are the molecular weights of the two monomer species, and *x* is the pyrene content of the polymer expressed in mol%.

$$N_{blob} = \frac{\langle n \rangle}{\lambda_{Py} / f_{Mdiff} \left[M_{Py}(x) + M_{Sty}(1-x) \right]} \qquad (3.4)$$

A plot of N_{blob} as a function of the corrected pyrene content is shown in Figures 3.6 and A3.7 for CoA-PS and CoE-PS, respectively. N_{blob} is found to decrease with increasing pyrene content, as observed for other pyrene-labeled polymers. This result is internally consistent with the increase of k_{blob} with pyrene content shown in Figure 3.4. As done for k_{blob}^{o}, N_{blob}^{o} for a particular polymer and solvent system is found by extrapolating to zero pyrene content and is shown in Figure 3.7 as a function of the inverse of viscosity, η^{-1}.[18,22,34] With significant scatter, N_{blob}^{o} increases with increasing η^{-1} values.

The scatter observed in Figure 3.7 might have several roots. N_{blob}^{o} reflects the changes in the volume probed by an excited pyrene that, are due to changes in coil density, solvent viscosity, and chromophore lifetime. All these factors are expected to affect excimer formation since the ability of an excited pyrene to probe a larger V_{blob} increases its probability to encounter a ground-state (GS) pyrene and form excimer. Thus, the

relationship between N_{blob}^{o} and viscosity alone is difficult to isolate. Nevertheless, the data shown in Figure 3.7 indicate a general trend where N_{blob}^{o} increases with decreasing viscosity.

Beside the N_{blob} and k_{blob} parameters respectively reported in Figures 3.4, 3.6 and A3.7, analysis of the monomer and excimer fluorescence decays with Equations 3.1 and 3.2 also retrieves the excimer lifetime, τ_{E0}, and the fraction of aggregated GS pyrenes, f_{agg}. τ_{E0} takes values ranging between 50 and 60 ns in Tables A3.2 and A3.5, as expected for a pyrene excimer formed in organic solvents. Long-lived pyrene dimers, *D**, could hardly be detected with CoE-PS, whereas the fits were not good if the long-lived dimers were not accounted for with the CoA-PS series. This might be a result of the more flexible ether linker used with CoE-PS which enables proper stacking of the pyrene moieties resulting in efficient excimer formation or that pyrene is held away from the PS backbone minimizing the probability of forming an exciplex between an excited pyrene and a styrene moiety.[22] The stiffer and shorter amide linker connecting pyrene to the CoA-PS backbone might restrict the freedom of motion of the pyrenyl moieties which might hinder their proper stacking into an excimer or promote the formation of an exciplex which is probed by our experiments.

Information on the fraction of aggregated pyrenes, f_{agg}, is obtained from the global analysis of the monomer and excimer decays. f_{agg} is shown in Figure A3.8 as a function of the corrected pyrene content. For both CoA-PS and CoE-PS, f_{agg} increases with increasing pyrene content. This is expected since increased λ_{Py} values cause an increased number of successive incorporations of pyrene labeled monomers which form excimer on a time scale too fast to be resolved by our time-resolved fluorometer. These types of excimers are accounted for as GS pyrene dimers in the FBM analysis and their contribution increases with increasing pyrene content. CoE-PS yields similar values for all solvents examined, except

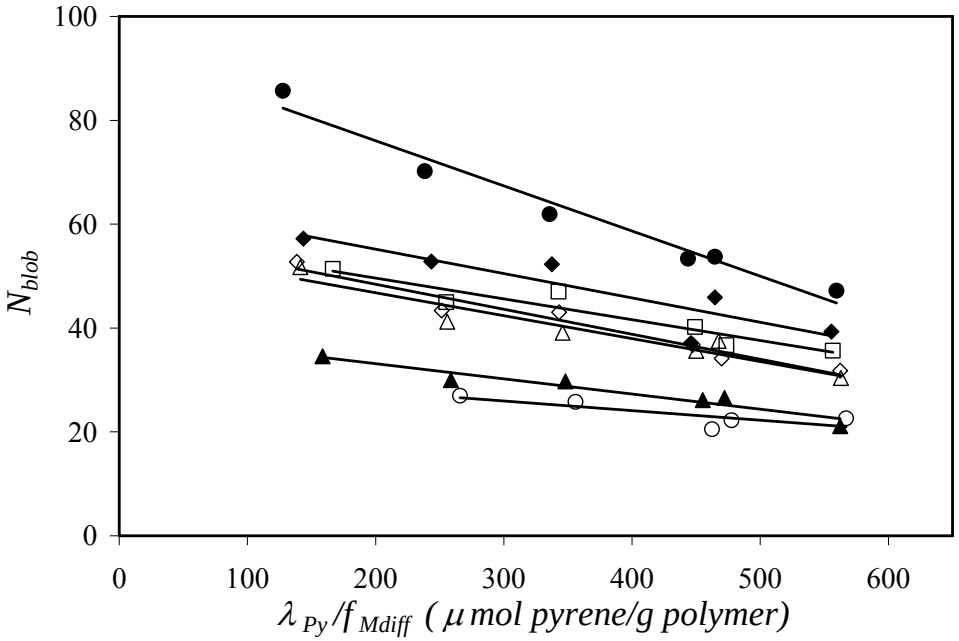

Figure 3.6: N_{blob} as a function of pyrene content. CoA-PS in methyl acetate (●), MEK (◆), DCM (□), THF (△), toluene (◇), DMF (▲), dioxane (○); [Py] = 3×10^{-6} M.

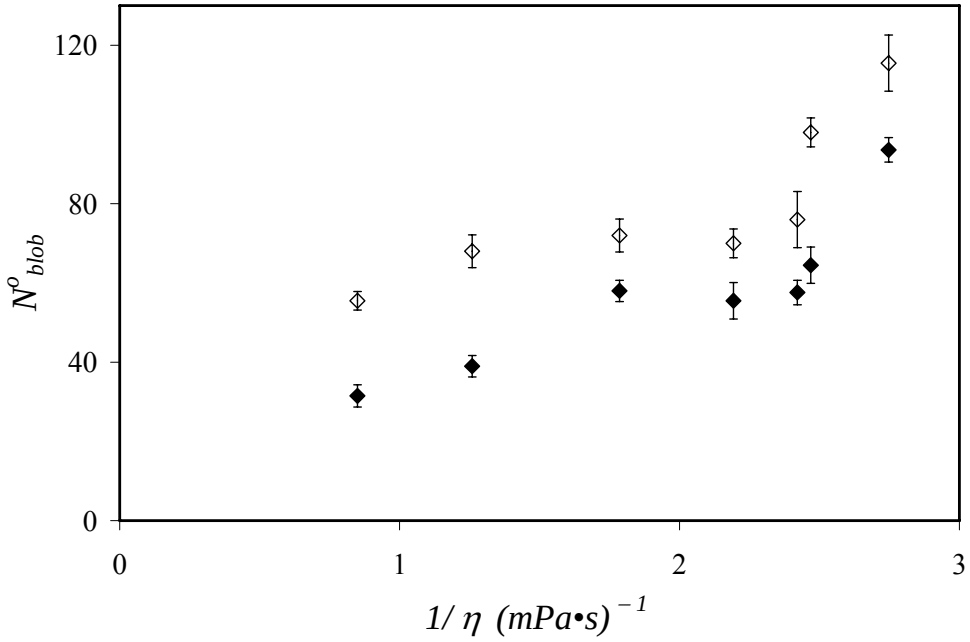

Figure 3.7: N^o_{blob} as a function of inverse viscosity. CoA-PS (◆), CoE-PS (◇); [Py] = 3×10^{-6} M.

for methyl acetate which has slightly larger f_{agg} values. CoA-PS yields lower f_{agg} values in DMF and dioxane whereas higher f_{agg} values are observed with methyl acetate. In the majority of solvent/polymer systems tested, the f_{agg} values are smaller than 0.25, implying that excimer formation occurs mostly by diffusive encounters between two pyrene moieties.

3.5 Discussion

The meaning of the parameters retrieved from a FBM analysis rests on the definition of a *blob*, which represents the volume, V_{blob}, inside the polymer coil that is probed by a pyrene while it remains excited. Based on this definition, V_{blob} is affected by several parameters, some of which depend uniquely on the chromophore such as the pyrene lifetime which ranges from 144 ns in DCM to 258 ns in THF (Table 3.3), uniquely on the solvent such as the solvent viscosity which ranges from 0.36 mPa.s for methyl acetate to 1.18 mPa.s for dioxane (Table 3.2), uniquely on the polymer structure where a bulky side-chain slows down polymer chain dynamics, and also on polymer-solvent interactions which were found to be good in DCM, THF, toluene, and dioxane and poor in methyl acetate, MEK, and DMF (Figure A3.1 and Table 3.2). Of those parameters, the two later ones are more relevant to the study of a given polymer since they pertain to the polymer itself. The Discussion section describes how the FBM parameters k_{blob} and N_{blob} are related to the chain dynamics of and solvent quality toward a given polymer.

It is somewhat of a paradox that, although V_{blob} is the basic element from which the FBM originates, V_{blob} can not be determined directly in most instances. In fact, information on V_{blob} can only be inferred from two FBM parameters which are determined quantitatively, namely k_{blob} and N_{blob}. N_{blob} is the number of monomers found in V_{blob}. V_{blob} is expected to scale as $N_{blob}^{3\nu}$ where ν is the Flory exponent that equals 0.5 and 0.6 in θ– and good solvents,

respectively.[35] k_{blob} is a pseudo-unimolecular rate constant that describes excimer formation between one excited pyrene and one ground-state pyrene located in a same *blob*. Based on this definition, k_{blob} can be represented by Equation 3.5 as the product of a rate constant, k_{diff}^{b}, that describes the diffusive encounters between one excited pyrene and one ground-state pyrene located in the same *blob*, and the concentration equivalent to a ground-state pyrene located inside the *blob* given by $1/V_{blob}$.[19,22]

$$k_{blob} = k_{diff}^{b} \times \frac{1}{V_{blob}} \tag{3.5}$$

A chromophore can probe a larger V_{blob} if it remains excited for a longer time. Except for MEK and DCM, the pyrene lifetimes were between 220 and 258 ns, a rather narrow range. The lifetimes of pyrene in MEK and DCM were 171±1 and 148±4 ns, respectively. Based on this observation, V_{blob} is not expected to be affected by the pyrene lifetime in most solvents studied except in DCM and MEK, where k_{blob} and N_{blob} might take, respectively, larger and smaller values than expected.

Within the framework of the FBM, k_{blob} is expected to remain constant with increasing pyrene content. In practice however, some polymers studied using the FBM exhibit an increase in k_{blob} with increasing pyrene content,[18,22,34] as is the case in Figure 3.4. According to Equation 3.5, an increase in k_{blob} for a given solvent/polymer system suggests a decrease in V_{blob}. This prediction is verified since the increase in k_{blob} is matched by a decrease in N_{blob} with increasing pyrene content (Figures 3.6 and A3.7). k_{blob}^{o} obtained from the extrapolation of k_{blob} shown in Figure 3.4 to zero pyrene content appears to be little affected by viscosity

for the CoA-PS and CoE-PS series (Figure 3.5), although CoE-PS yields generally slightly higher k_{blob}^{o} values than CoA-PS. The constancy of k_{blob}^{o} with viscosity has been rationalized in previous articles by introducing Equation 3.5.[3,12,19] In Equation 3.5, both k_{diff}^{b} and V_{blob} are expected to be inversely proportional to viscosity, so that the effect of viscosity on k_{blob} cancels out.[19] The data shown in Figure 3.5 and obtained with two Py-PSs in seven solvents support this contention.

A constant k_{blob}^{o} with viscosity is interesting not only because this behavior is predicted by the FBM framework, but also because this behavior is quite different from that expected for k_{cycl}, the rate constant for end-to-end cyclization. In a study of end-labeled Py-PEO-Py,[23] both the I_E/I_M ratio and k_{cycl} were found to increase linearly with η^{-1}. In the current work using the FBM to study two randomly labeled Py-PSs, the I_E/I_M ratio for CoA-PS and CoE-PS increased linearly with increasing η^{-1} (Figures 3.2 and A3.3) as observed for Py-PEO-Py, but k_{blob}^{o} remained fairly constant with viscosity (Figure 3.5). On the surface, these two results might seem at odd with each other, but can be reconciled by comparing the expression of k_{blob} given in Equation 3.5 with that of k_{cycl} given in Equation 3.6.[36]

$$k_{cycl} = k_{diff}^{c} \times \frac{1}{V_{coil}} \tag{3.6}$$

As for k_{blob}, k_{cycl} is a pseudo-unimolecular rate constant which is the product of the rate constant k_{diff}^{c} that describes the diffusional encounters between the two pyrene labels located at the chain ends of Py-PEO-Py and the concentration equivalent to one ground-state pyrene

inside the polymer coil given by $1/V_{coil}$. The index "*c*" of k_{diff}^{c} emphasizes that diffusion must occur more quickly when pyrene is attached at the chain ends rather than in the interior of the polymer chain so that k_{diff}^{c} in Equation 3.6 is expected to be larger than k_{diff}^{b} in Equation 3.5.

The different behaviors observed between k_{blob}^{o} with Py-PS in Figure 3.5 and k_{cycl} with Py-PEO-Py in ref. 23 is certainly a result of V_{coil} of Py-PEO-Py being smaller than the volume probed by an excited pyrene attached at the end of the short and highly flexible PEO chain (M_n = 8 kg/mol). In the case of Py-PEO-Py, the excited pyrene probes the entire polymer coil and can not "escape" beyond the coil boundary. V_{coil} being a constant in Equation 3.6, k_{cycl} behaves as k_{diff}^{c}, namely it increases with decreasing solvent viscosity as found in ref. 23. The situation is different for k_{blob}^{o} since within the FBM framework, V_{blob} is free to increase as the excited pyrene probes a larger volume following a decrease in viscosity. Both k_{diff}^{b} and V_{blob} increase with decreasing solvent viscosity. According to Equation 3.5, both effects cancel each other and k_{blob}^{o} does not change much with viscosity (Figure 3.5).

The second interesting paradox that must be dealt with is why both k_{cycl} and the I_E/I_M ratio increase with η^{-1} for Py-PEO-Py as expected theoretically and experimentally, and why k_{blob}^{o} remains constant with viscosity in Figure 3.5 whereas the I_E/I_M ratio increases with η^{-1} in Figure 3.2. This apparent contradiction is a consequence of the I_E/I_M ratio being proportional to the product of k_{diff}^{c} by the local concentration of ground-state (GS) pyrenes inside the polymer coil ($[Py]_{loc}$).[37] According to the expression of k_{cycl} given in Equation 3.6,

k_{cycl} is indeed equal to $k_{diff}^{c} \times [\text{Py}]_{\text{loc}} = k_{diff}^{c} \times (1/V_{coil})$. As a result, k_{cycl} is expected to behave in a manner similar to the I_E/I_M ratio, as found experimentally for Py-PEO-Py in ref. 23. k_{blob}^{o} on the other hand is not proportional to $[\text{Py}]_{\text{loc}}$ but rather to the concentration equivalent to one GS pyrene inside a *blob*, namely $1/V_{blob}$. In the case of a polymer randomly labeled with pyrene, $[\text{Py}]_{\text{loc}}$ is given by $\langle n \rangle / V_{blob}$, so that, according to Equation 3.5, the product $k_{blob} \times \langle n \rangle = k_{diff}^{b} \times (\langle n \rangle / V_{blob})$ is expected to behave as the I_E/I_M ratio. This is indeed observed in Figure 3.8 where $k_{blob} \times \langle n \rangle$ for the CoA-PS sample containing 3.7 mol% pyrene and the CoE-PS sample containing 3.2 mol% pyrene increases with η^{-1} as found for the I_E/I_M ratio in Figure 3.2. The one point off the line in Figure 8 corresponds to the solutions in THF. Interestingly the I_E/I_M ratio obtained for Py-PEO-Py in THF was also off the main trend in ref. 23.

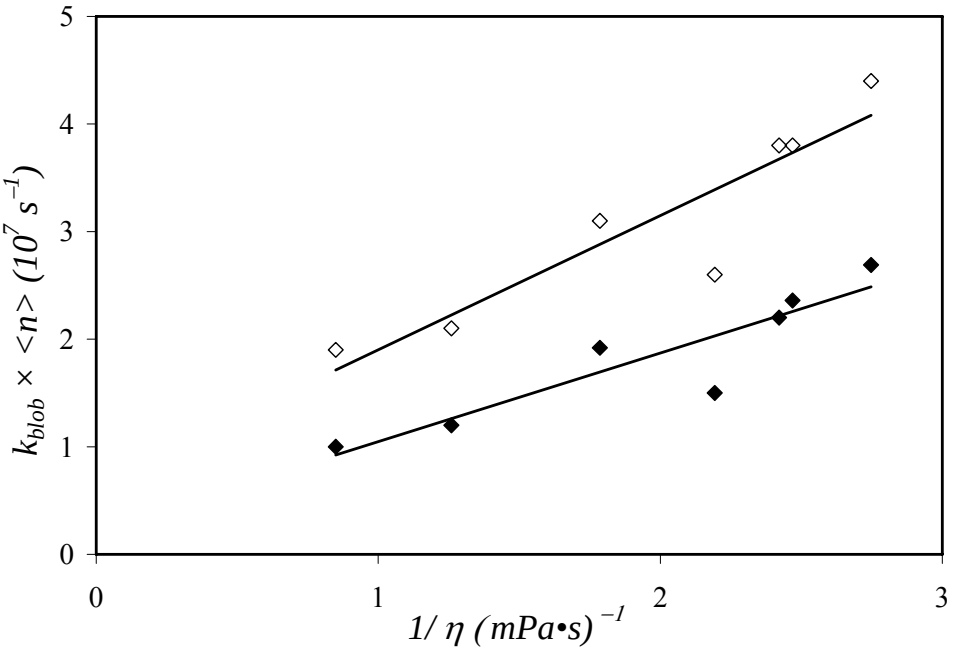

Figure 3.8: $k_{blob} \times \langle n \rangle$ as a function of inverse viscosity. CoA-PS sample containing 3.7 mol% pyrene (◆), CoE-PS sample containing 3.2 mol% pyrene (◇); [Py] = 3×10^{-6} M.

Although k^o_{blob} does not change much with solvent viscosity, N^o_{blob} in Figure 3.7 is found to depend strongly on solvent viscosity. N^o_{blob} increases more than two folds for either CoA-PS or CoE-PS as the solvent viscosity changes from 0.36 mPa·s for methyl acetate to 1.18 mPa·s for dioxane. These results are reasonable since N_{blob} reflects the size of a *blob* and since an excited pyrene probes a larger volume when the solvent viscosity is lower. Nevertheless, N_{blob} and V_{blob} are also expected to depend on the chromophore lifetime and the solvent quality toward the polymer. A longer-lived chromophore probes a larger *blob* and a collapsed polymer coil results in a larger N_{blob}.[19] The scatter in the plot of N^o_{blob} shown in Figure 3.7 reflects the combined effects that chromophore lifetime, solvent viscosity, and solvent quality have on N_{blob}.

Interestingly, all these factors can be accounted for by considering the product $k_{blob}\times N_{blob}$. According to Equation 3.5, the product $k_{blob}\times N_{blob}$ can be rewritten as in Equation 3.7.

$$k_{blob} \times N_{blob} = k^b_{diff} \times \frac{N_{blob}}{V_{blob}} \tag{3.7}$$

In Equation 3.7, the ratio N_{blob}/V_{blob} represents the density of the polymer coil which is only affected by the solvent quality whereas k^b_{diff} is only affected by viscosity. Consequently, the chromophore lifetime does not affect the product $k_{blob}\times N_{blob}$ in Equation 3.7. The increase in k_{blob} with increasing pyrene content shown in Figure 3.4 was associated with a decrease of N_{blob} with increasing pyrene content shown in Figure 3.6. These two effects cancel out when considering the product $k_{blob}\times N_{blob}$ which is shown to remain more or

less constant with pyrene content in Figures 3.9 and A3.9 for CoA-PS and CoE-PS, respectively. Averaging each trend in Figures 3.9 and A3.9 yields the $k_{blob} \times N_{blob}$ product for a given Py-PS/solvent system.

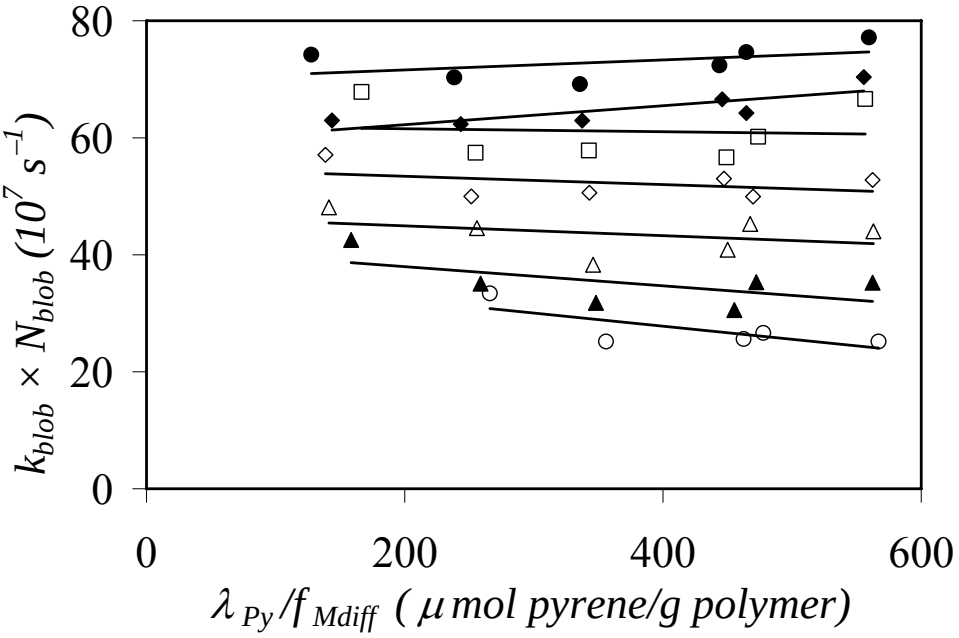

Figure 3.9: $k_{blob} \times N_{blob}$ as a function of pyrene content. CoA-PS in methyl acetate (●), MEK (◆), DCM (□), THF (△), toluene (◇), DMF (▲), dioxane (○); [Py] = 3×10^{-6} M.

The coil density of a polymer given by the ratio N_{blob}/V_{blob} can be approximated by the inverse of the intrinsic viscosity, $[\eta]^{-1}$, which was measured for the PS-40K sample in Table 3.2. Taking into account that a measure of N_{blob}/V_{blob} is given by $[\eta]^{-1}$ and that k_{diff}^{b} depends on η^{-1}, the product $k_{blob} \times N_{blob}$ was plotted as a function of $[\eta]^{-1} \times \eta^{-1}$ in Figure 3.10 for the CoA-PS and CoE-PS series which have M_n values close to that of PS-40K. With noticeably less scatter than in Figure 3.7, all data points appear to converge along two straight lines, one for each Py-PS series, regardless of solvent quality or chromophore lifetime, as expected from Equation 3.7. The different trends obtained for CoA-PS and CoE-PS result from k_{diff}^{b}

being larger for CoE-PS than for CoA-PS due to the longer and more flexible ether linker connecting pyrene to the PS backbone of CoE-PS.[22] The linear trends obtained in Figure 3.10 were expected from Equation 3.7 and they suggest that the parameters retrieved from the FBM provide an accurate description of the kinetics of excimer formation inside the polymer coil of a Py-PS sample and reflect the LRPCD of these polymers.

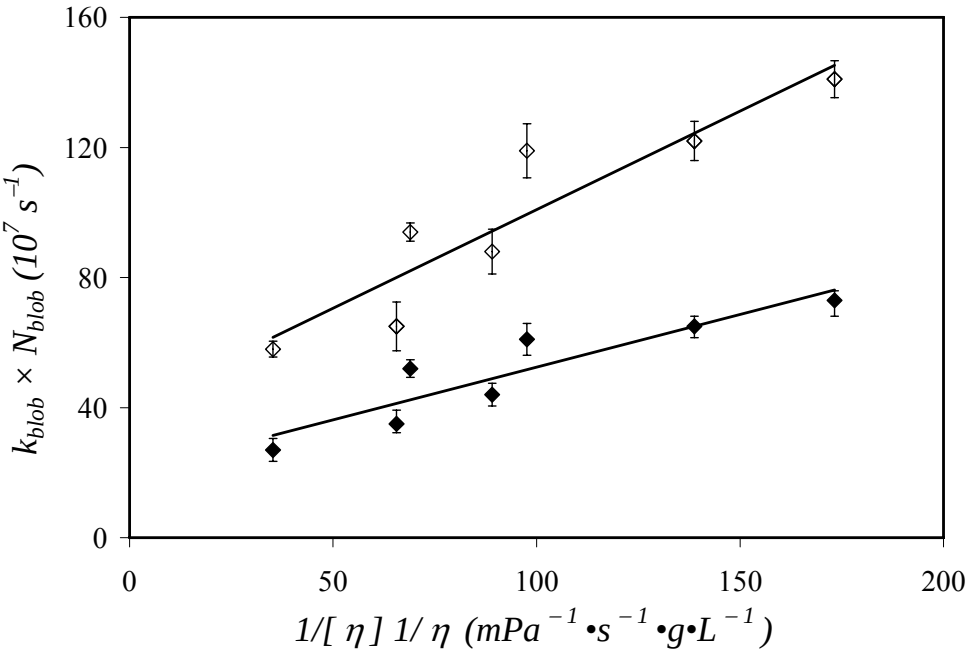

Figure 3.10: $k_{blob} \times N_{blob}$ as a function of the inverse of the product of viscosity by the intrinsic viscosity. CoA-PS (◆), CoE-PS (◇); [Py] = 3×10^{-6} M.

One important feature of Equation 3.7 is that it separates the effects due to the excluded volume quantified by $[\eta]$ from those due to solvent viscosity accounted for by η. Similarly, the ratio I_E/I_M for a randomly labeled polymer has been shown to depend on the product $[\eta]^{-1} \times \eta^{-1}$.[17] This conclusion can be reached by noticing that the ratio I_E/I_M for a randomly labeled polymer should be proportional to the product $k_{diff}^{b} \times [\mathrm{Py}]_{\mathrm{loc}}$ where k_{diff}^{b} and $[\mathrm{Py}]_{\mathrm{loc}}$ are

proportional to η^{-1} and $[\eta]^{-1}$, respectively. With some scatter, this is indeed observed in Figure 3.11 for the CoA-PS and CoE-PS samples containing 3.7 and 3.2 mol% of pyrene, respectively. Actually the ratio I_E/I_M in Figure 3.11 parallels very closely the product $k_{blob} \times N_{blob}$ plotted as a function of $[\eta]^{-1} \times \eta^{-1}$ in Figure 3.10, another indication that the I_E/I_M ratio and the $k_{blob} \times N_{blob}$ product represent similar quantities.

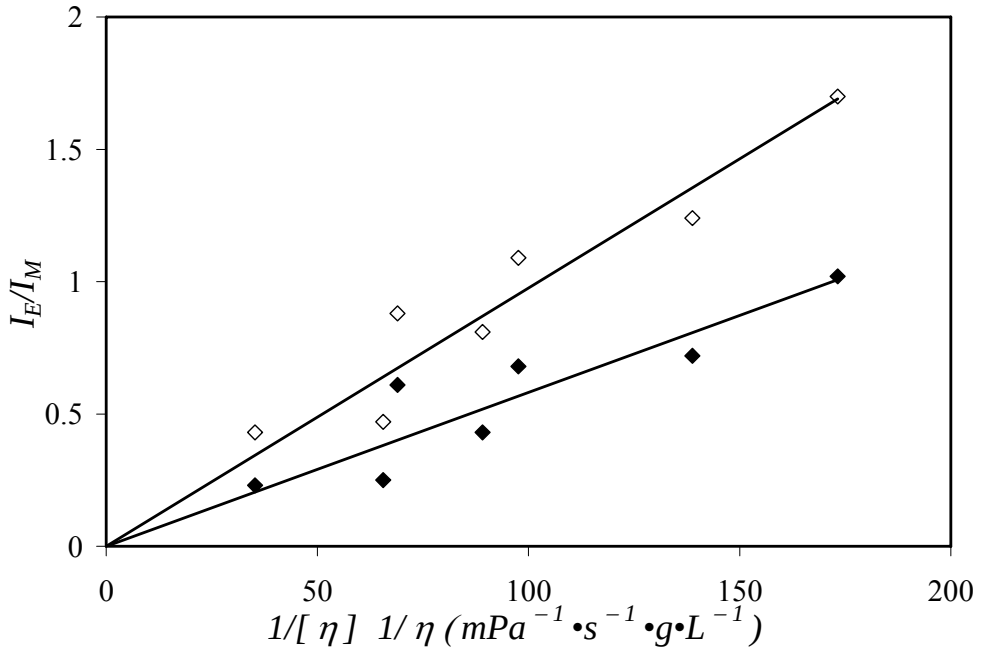

Figure 3.11: I_E/I_M as a function of the inverse of the product of viscosity by the intrinsic viscosity. CoA-PS sample containing 3.7 mol% pyrene (◆) and CoE-PS sample containing 3.2 mol% pyrene (◇); [Py] = 3×10^{-6} M.

Although the product $k_{blob} \times N_{blob}$ and the I_E/I_M ratio appear to represent similar quantities, they differ in one main aspect. On the one hand, the I_E/I_M ratio represents an average of all excimer formation events taking place inside the polymer coil and does not provide any detailed information on LRPCD. On the other hand, the product $k_{blob} \times N_{blob}$ is obtained through a precise description of the processes leading to excimer formation inside the polymer coil made via the FBM. Through the FBM, a measure of the volume probed by

the excited chromophore inside the polymer coil is obtained with N_{blob} which, when combined with the knowledge of k_{blob}, provides information on LRPCD. The good agreement observed between both quantities comes as an additional support towards establishing the validity of the FBM.

3.6 Conclusions

The LRPCD of two series of pyrene labeled PSs were studied in seven different solvents using the FBM. The two different series of Py-PSs had pyrene groups attached via a short amide linker or a longer ether linker (Scheme 3.1). The longer ether linker facilitated excimer formation compared to the amide linker over the entire range of solvents and pyrene contents studied. The trends of the parameters describing excimer formation were similar between the two series of Py-PSs as a function of solvent viscosity (Figures 3.2, 3.7, and 3.8).

The I_E/I_M ratios calculated from the steady-state fluorescence spectra indicated that excimer formation increased with decreasing viscosity. However, quantitative information on the dynamics of the Py-PS backbone could only be retrieved by applying the FBM analysis to the time-resolved fluorescence decays. This analysis provided a measure of the changes in the volume probed by the excited pyrene as a function of viscosity. Using the FBM, k^o_{blob} was found to remain constant with solvent viscosity, averaging around 1×10^7 s^{-1}, with CoE-PS generally yielding k^o_{blob} values being a little larger than those obtained with CoA-PS (Figure 3.5). The significance of the 1×10^7 s^{-1} value for k^o_{blob} is not clear at this point in time, but appears to be consistent for both polymers in a large range of solvents and

certainly must have a physical meaning in terms of excimer formation and polymer chain dynamics.

The change in V_{blob} is represented by the change in the number of monomer units within a *blob*, N_{blob}. The N_{blob} value extrapolated to zero pyrene content, N^{o}_{blob}, was found to increase with decreasing solvent viscosity (Figure 3.7). Since V_{blob} is affected by many factors, including solvent viscosity, polymer chain dynamics, polymer-solvent interactions, and pyrene lifetime, the product $k_{blob}\times N_{blob}$ was used. This product is expected to depend only on solvent viscosity and solvent quality toward the polymer (Equation 3.7). $k_{blob}\times N_{blob}$ was found to increase with decreasing solvent quality and viscosity for both Py-PSs (Figure 3.10) with trends very similar to those obtained with the I_E/I_M ratios (Figure 3.11). The product $k_{blob}\times N_{blob}$ is more descriptive however, since it is obtained from the parameters N_{blob} and k_{blob} which represent physical quantities pertaining directly to the polymer chains themselves, whereas the I_E/I_M ratios are averages of the overall excimer formation for a given polymer-solvent system.

In summary, this study provides the first quantitative description of how the diffusional encounters between the pyrene pendants randomly attached onto polystyrene are affected by solvent viscosity and solvent quality towards the polymer via the k_{blob} and N_{blob} parameters retrieved from the FBM analysis of the fluorescence decays. It is expected to constitute an important benchmark against which the LRPCD of other pyrene labeled polymers can be compared as a function of polymer chemical composition, backbone flexibility, or architecture.

3.7 References

1. Cuniberti, C.; Perico, A. *Eur. Polym. J.* **1977**, *13*, 369-374.

2. Martinho, J. M. G.; Winnik, M. A. *Macromolecules* **1986**, *19*, 2281-2284.

3. Kanagalingam, S.; Ngan, C. F.; Duhamel, J. *Macromolecules* **2002**, *35*, 8560-8570.

4. Zhang. M.; Duhamel, J. *Macromolecules* **2006**, *38*, 4438-4446.

5. Gardinier, W. E.; Kane, M. A.; Bright, F. V. *J. Phys. Chem. B* **2004**, *108*, 18520-18529.

6. Kane, M. A.; Pandey, S.; Baker, G. A.; Perez, S. A.; Bukowski, E. J.; Hoth, D. C.; Bright, F. V. *Macromolecules* **2001**, *34*, 6831-6838.

7. Redpath, A. E. C.; Winnik, M. A. *J. Am. Chem. Soc.* **1982**, *104*, 5604-5607.

8. Farinha, J. P. S.; Piçarra, S.; Miesel, K.; Martinho, J. M. G. *J. Phys. Chem. B* **2001**, *105*, 10536-10545.

9. Picarra, S.; Duhamel, J.; Fedorov, A.; Martinho, J. M. G. *J. Phys. Chem. B* **2004**, *108*, 12009-12015.

10. Winnik, M. A.; Li, X.-B.; Guillet, J. E. *Macromolecules* **1984**, *17*, 699-702.

11. Redpath, A. E. C.; Winnik, M. A. *Polymer* **1983**, *24*, 1286-1290.

12. Irondi, K.; Zhang, M.; Duhamel, J. *J. Phys. Chem. B* **2006**, *110*, 2628-2637.

13. Cuniberti, C.; Perico, A. *Prog. Polym. Sci.* **1984**, *10*, 271-316.

14. Winnik, M. A. *Acc. Chem. Res.* **1985**, *18*, 73-79.

15. Duhamel, J. *Acc. Chem. Res.* **2006**, *39*, 953-960.

16. Winnik, M. A.; Redpath, T.; Richards, D. H. *Macromolecules* **1980**, *13*, 328-335.

17. Cuniberti, C.; Perico, A. *Eur. Polym. J.* **1980**, *16*, 887-893.

18. Mathew, H.; Siu, H.; Duhamel, J. *Macromolecules* **1999**, *32*, 7100-7108.

19. Kanagalingam, S.; Spartalis, J.; Cao, T.-C.; Duhamel, J. *Macromolecules* **2002**, *35*, 8571-8577.

20. Prazeres, T. J. V.; Duhamel, J.; Olesen, K.; Shay, G. *J. Phys. Chem. B* **2005**, *109*, 17406-17416.

21. Siu, H.; Duhamel, J. *Macromolecules* **2006**, *39*, 1144-1155.

22. Ingratta, M.; Duhamel, J. *Macromolecules* **2007**, *40*, 6647-6657.

23. Cheung, S.-T.; Winnik, M. A.; Redpath, A. E. C. *Makromol. Chem.* **1982**, *183*, 1815-1824.

24. Reis e Sousa, A. T.; Castanheira, E. M. S.; Martinho, J. M. G.; Saghbini, S.; Baros, F.; André, J. C.; Winnik, M. A. *Chem. Phys. Lett.* **1993**, *213*, 333-337.

25. Martinho, J. M. G.; Castanheira, E. M. S.; Reis e Sousa, A. T. Saghbini, S.; André, J. C.; Winnik, M. A. *Macromolecules* **1995**, *28*, 1167-1171.

26. Kane, M. A.; Pandey, S.; Baker, G. A.; Perez, S. A.; Bukowski, E. J.; Hoth, D. C.; Bright, F. *Macromolecules* **2001**, *34*, 6831-6838.

27. James, D. R.; Demmer, D. R.; Verall, R. E.; Steer, R. P. *Rev. Sci. Instrum.* **1983**, *54*, 1121-1130.

28. Siu, H.; Duhamel, J. *Macromolecules* **2004**, *37*, 9287-9289.

29. Prazeres, T. J. V.; Beingessner, R.; Duhamel, J.; Olesen, K.; Shay, G.; Bassett, D. R. *Macromolecules* **2001**, *34*, 7876-7884.

30. Press, W. H.; Flannery, B. P.; Teukolsky, S. A.; Vetterling, W. T. *Numerical Recipes. The Art of Scientific Computing (Fortran Version)*; Cambridge University Press: Cambridge, 1992, p 523 – 528.

31. Demas, J. N. *Excited-State Lifetime Measurements*; Academic Press: New York, 1983, p 134, 147.

32. Bandrup, J.; Immergut, E. H. ; Grulke, E. A. *Polymer Handbook*, 4th ed.; John Wiley & Sons: NY, 1999, p VII 675-683.

33. Saeki, S.; Konno, S.; Kuwahara, N.; Nakata, M.; Kaneko, M. *Macromolecules* **1974**, *7*, 521-526.

34. Duhamel, J.; Kanagalingam, S.; O'Brien, T.; Ingratta, M. *J. Am. Chem. Soc.* **2003**, *125*, 12810-12822.

35. de Gennes, P-G. *Scaling Concepts in Polymer Physics*. Cornell University Press: New York, 1979.

36. Lee, S.; Duhamel, J. *Macromolecules* **1998**, 9293-9200.

37. Birks, J. B. Photophysics of Aromatic Molecules. Wiley: New York, 1970; p 301.

3.8 Appendix

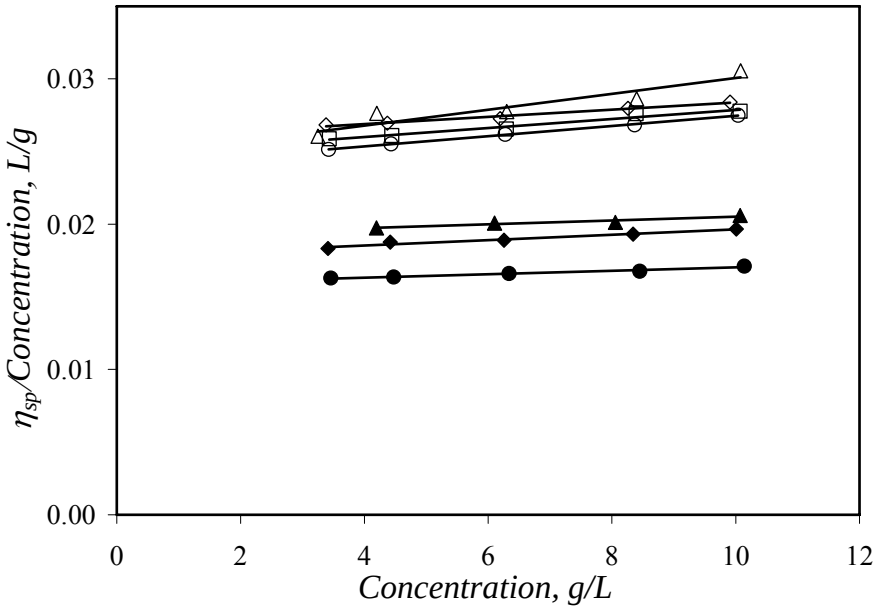

Figure A3.1: Reduced viscosity of PS-40K at T = 25 °C in methyl acetate (●), MEK, (◆) DCM (□), THF (△), toluene (◇), DMF (▲), dioxane (○).

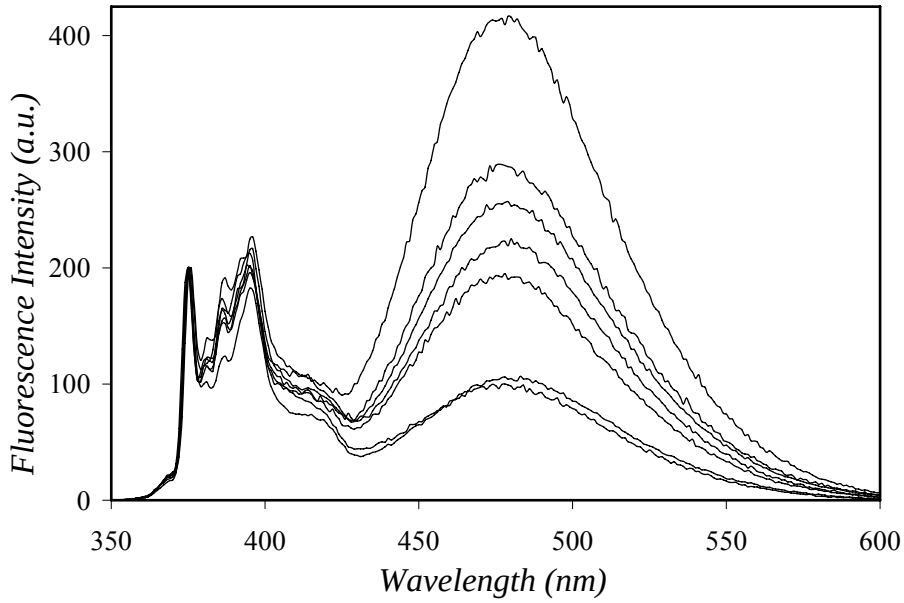

Figure A3.2: Steady-state fluorescence spectra of CoE-PS. From top to bottom, the polymer is dissolved in methyl acetate, MEK, DCM, THF, toluene, DMF, and dioxane, respectively. [Py] = 3×10^{-6} M, λ_{ex} = 344 nm, λ_{Py} = 284 μmol/g.

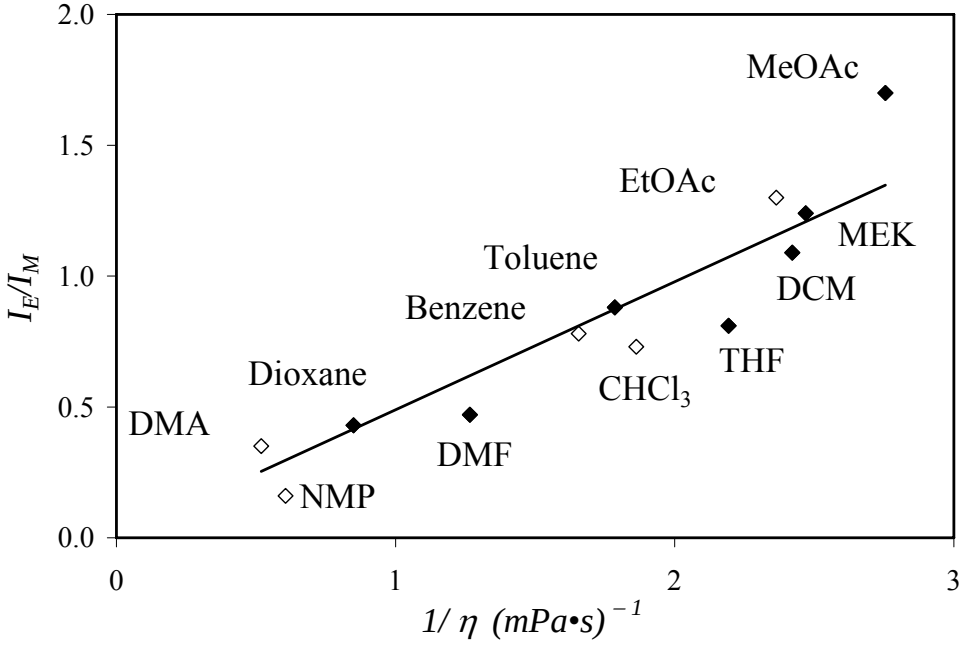

Figure A3.3: I_E/I_M ratios of 3.2 mol% CoE-PS; [Py] = 3×10^{-6} M, λ_{ex} = 344 nm.

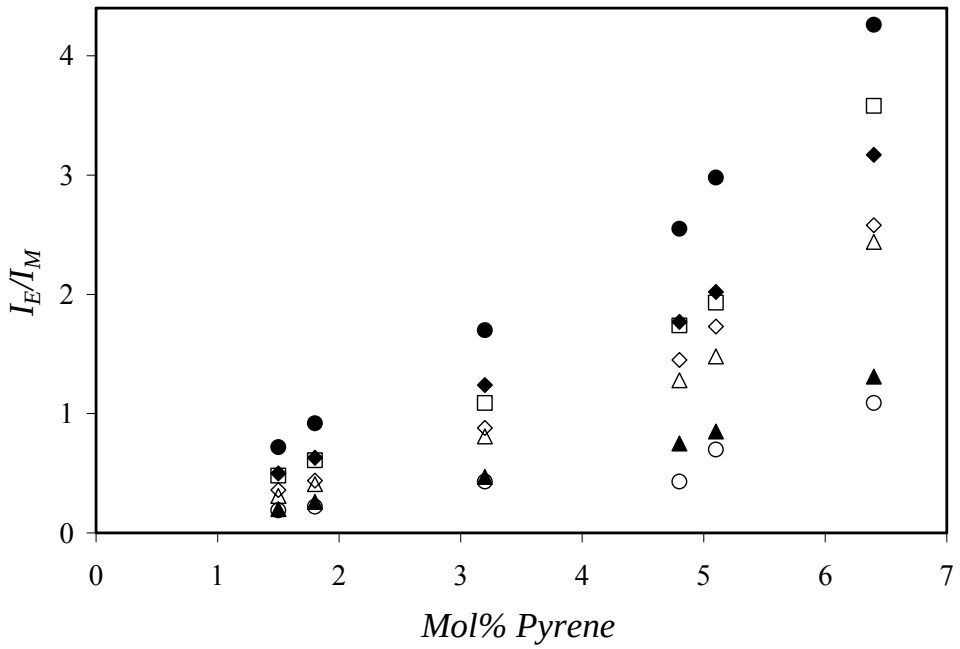

Figure A3.4: I_E/I_M ratios as a function of pyrene content for CoE-PS in methyl acetate (●), MEK (◆) DCM (□), toluene (◇), THF (△), DMF (▲), and dioxane (○); [Py] = 3×10^{-6} M, λ_{ex} = 344 nm.

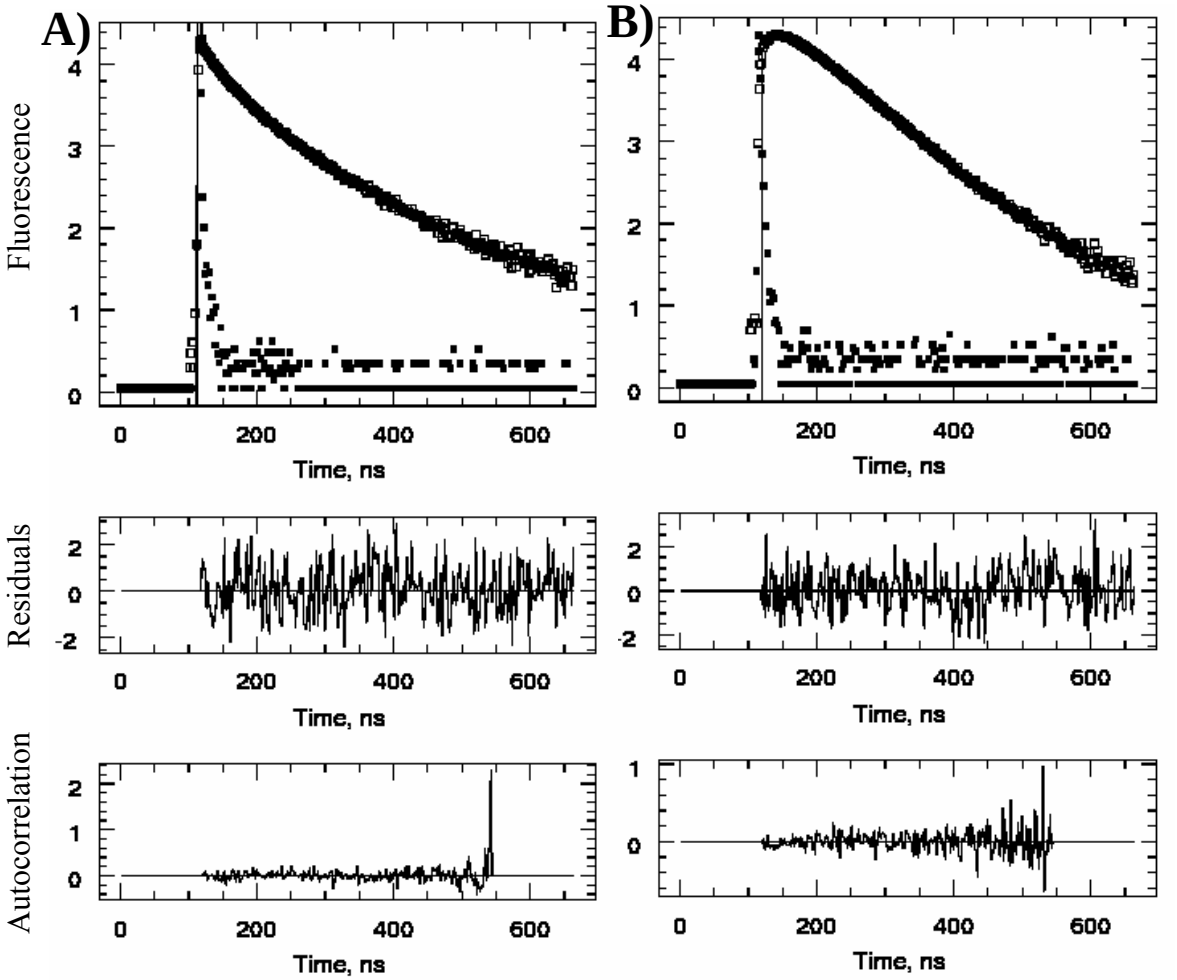

Figure A3.5: Monomer (A) and excimer (B) decays acquired for the CoE-PS sample labeled with 5.1 mol% pyrene in DMF, χ^2 =1.08. λ_{ex} = 340 nm, λ_{em} = 375 nm (monomer), λ_{em} = 510 nm (excimer). [Py] = 3×10^{-6} M.

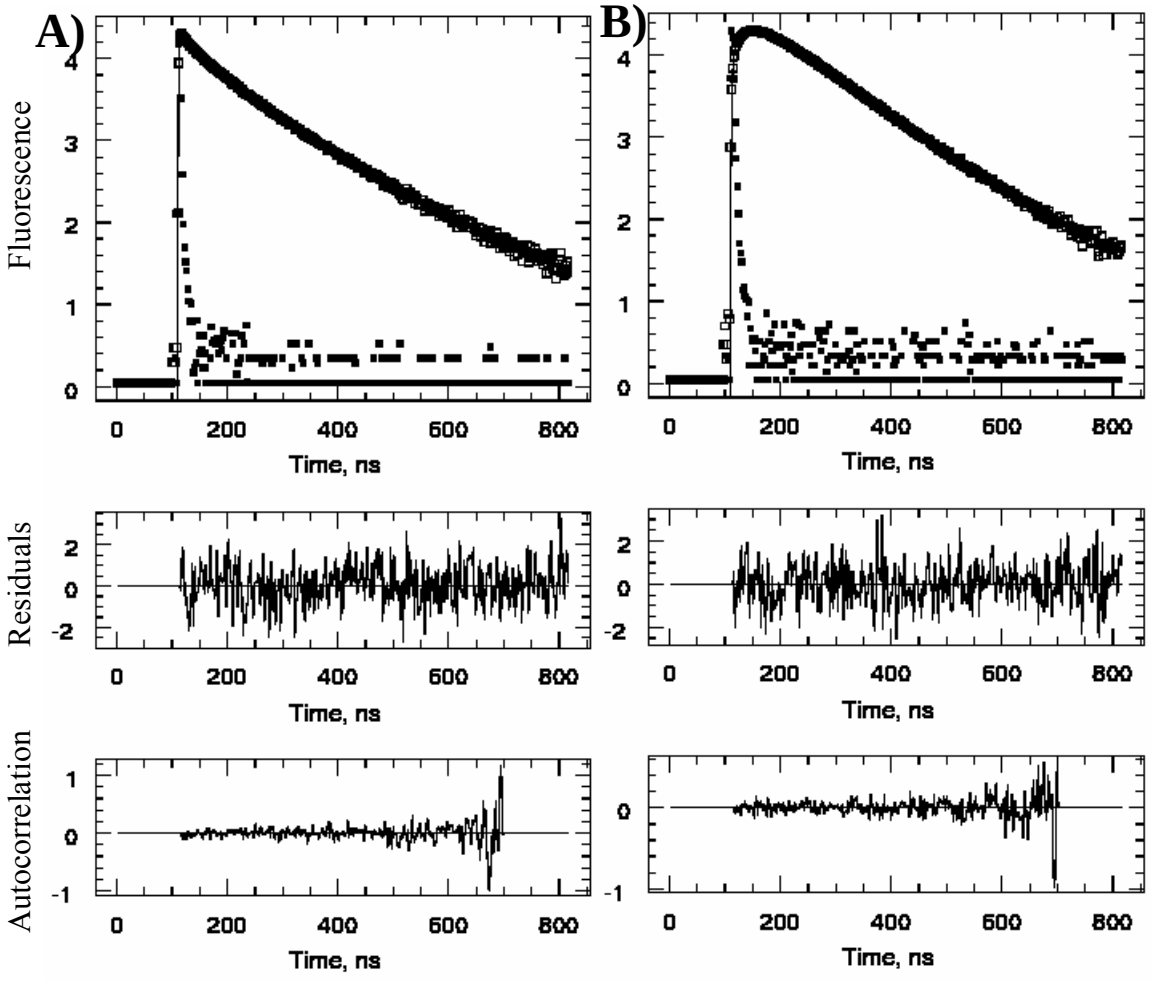

Figure A3.6: Monomer (A) and excimer (B) decays acquired for a CoA-PS sample labeled with 5.0 mol% pyrene in DMF, χ^2 =1.02. λ_{ex} = 340 nm, λ_{em} = 375 nm (monomer), λ_{em} = 510 nm (excimer). [Py] = 3×10^{-6} M.

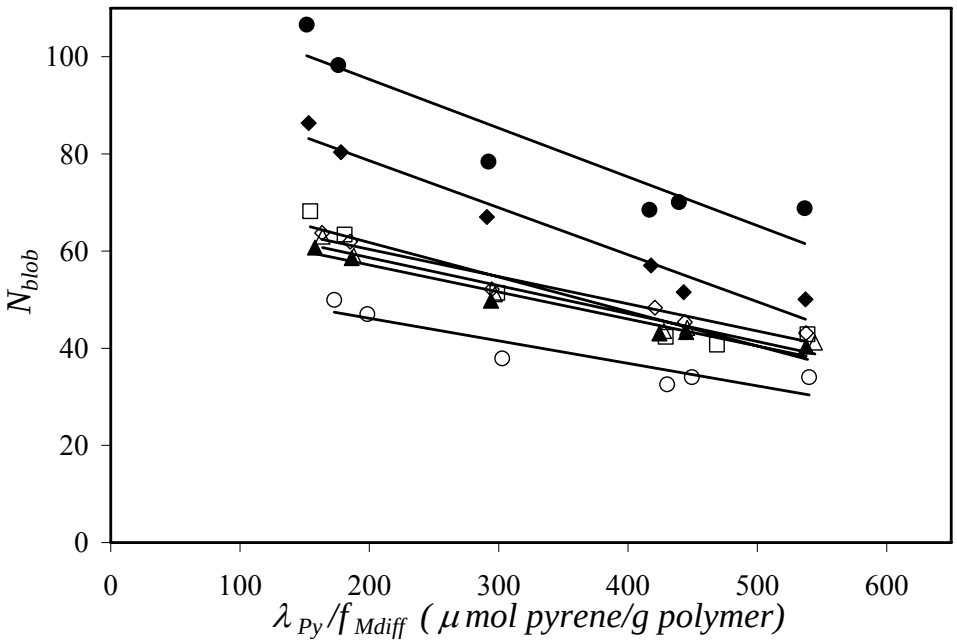

Figure A3.7*:* N_{blob} as a function of pyrene content for CoE-PS in methyl acetate (●), MEK (◆), DCM (□), THF (△), toluene (◇), DMF (▲), dioxane (○); [Py] = 3×10^{-6} M.

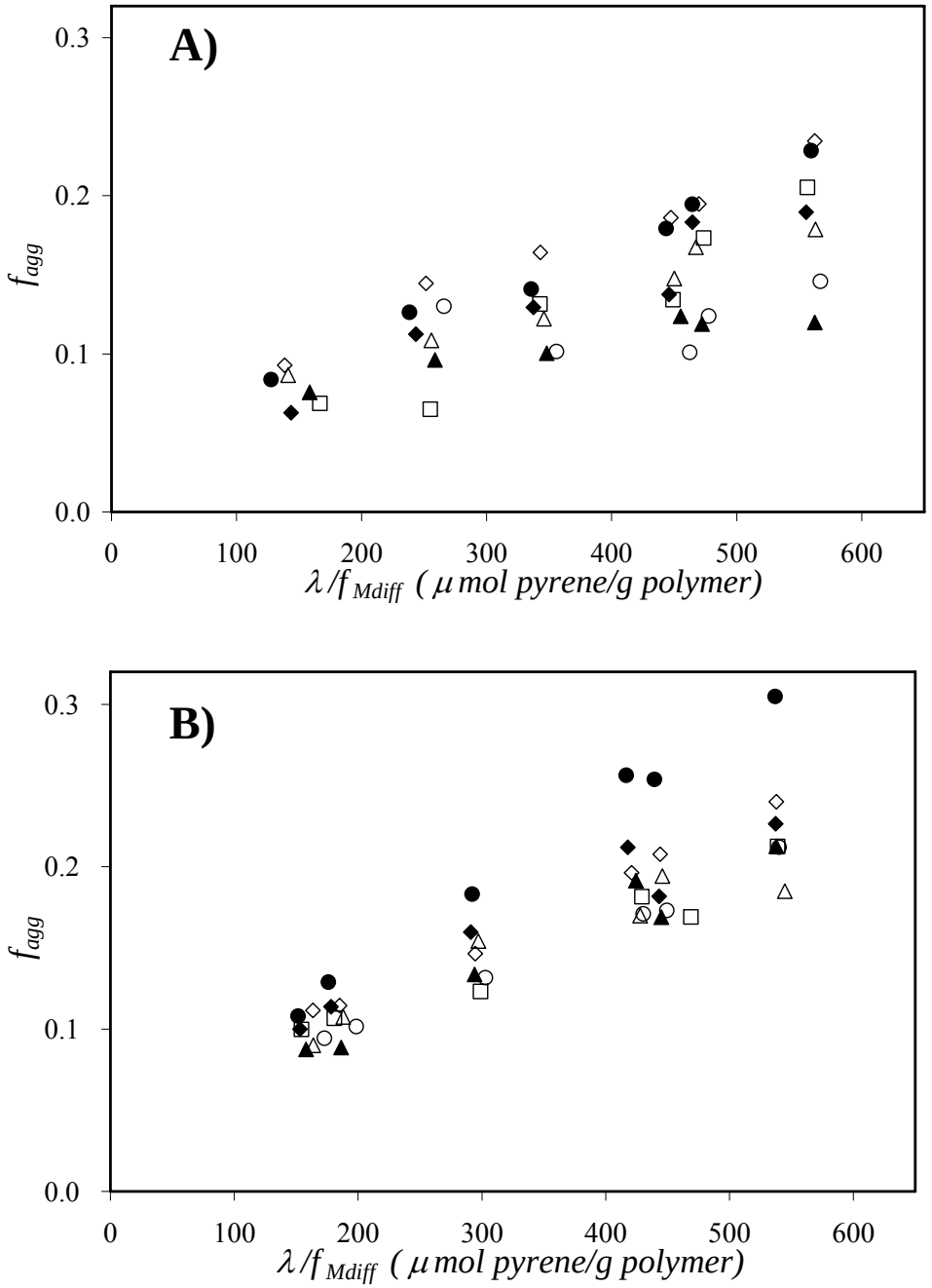

Figure A3.8: f_{agg} as a function of pyrene content. A) CoA-PS and B) CoE-PS in methyl acetate (●), MEK (◆) DCM (□), THF (△), toluene (◇), DMF (▲), dioxane (○); [Py] = 3×10^{-6} M.

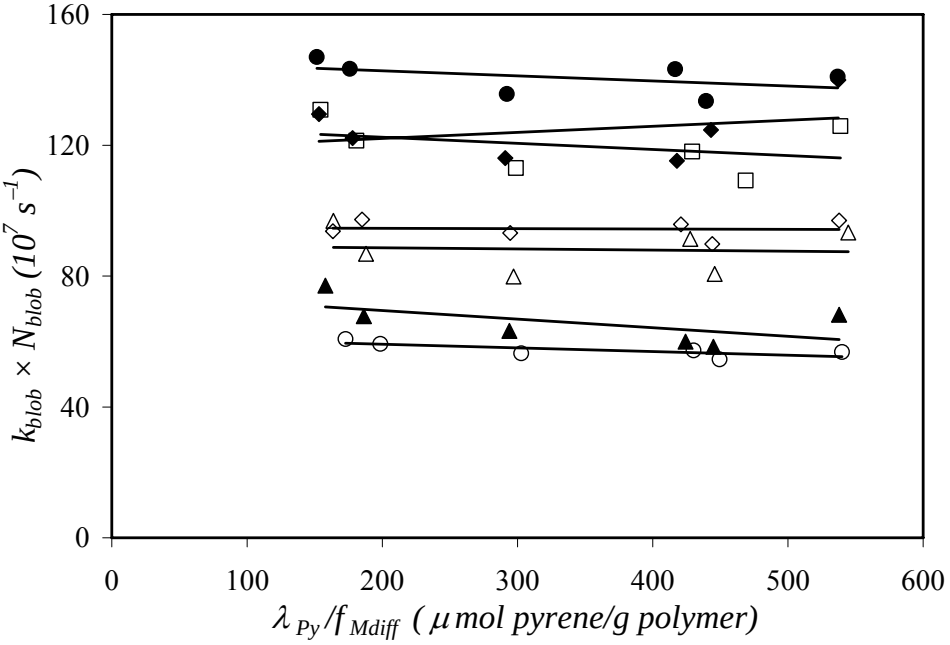

Figure A3.9: $k_{blob} \times N_{blob}$ as a function of pyrene content for CoE-PS in methyl acetate (●), MEK (◆), DCM (□), THF (△), toluene (◇), DMF (▲), dioxane (○); [Py] = 3×10^{-6} M.

Table A3.1: Parameters retrieved from the global FBM analysis of the monomer decays of CoE-PS in various solvents with Equation 3.1.

Solvent	mol%	f_{Mdiff}	f_{Mfree}	k_{blob} (10^7 s^{-1})	$k_e[blob]$ (10^7 s^{-1})	<n>	χ^2
Methyl Acetate	1.5	0.93	0.07	1.4	0.6	1.7	1.09
	1.8	0.96	0.04	1.5	0.6	1.9	1.18
	3.2	0.97	0.03	1.7	0.7	2.6	1.09
	4.8	0.99	0.01	2.1	0.5	3.3	1.13
	5.1	0.99	0.01	1.9	0.5	3.6	1.15
	6.4	0.99	0.01	2.0	0.5	4.4	1.08
Methyl Ethyl Ketone (MEK)	1.5	0.92	0.08	1.5	0.7	1.4	1.17
	1.8	0.95	0.05	1.5	0.7	1.5	1.08
	3.2	0.98	0.02	1.7	0.8	2.2	1.07
	4.8	0.99	0.01	2.0	0.6	2.7	1.21
	5.1	0.98	0.02	2.4	1.1	2.6	1.20
	6.4	0.99	0.01	2.8	1.3	3.2	1.18
Dichloromethane (DCM)	1.5	0.91	0.09	1.9	0.7	1.1	1.17
	1.8	0.93	0.07	1.9	0.7	1.2	1.13
	3.2	0.95	0.05	2.2	1.0	1.7	1.21
	4.8	0.96	0.04	2.8	1.2	2.1	1.23
	5.1	0.93	0.03	2.7	1.2	2.2	1.18
	6.4	0.99	0.01	2.9	1.2	2.7	1.18
Tetrahydrofuran (THF)	1.5	0.86	0.14	1.5	0.5	1.1	1.12
	1.8	0.90	0.10	1.5	0.5	1.2	1.07
	3.2	0.96	0.04	1.6	0.6	1.7	1.00
	4.8	0.96	0.04	2.1	0.7	2.1	1.19
	5.1	0.98	0.02	1.8	0.8	2.3	1.20
	6.4	0.98	0.02	2.3	0.8	2.6	1.14
Toluene	1.5	0.86	0.14	1.5	0.5	1.1	1.18
	1.8	0.91	0.09	1.6	0.5	1.2	1.12
	3.2	0.96	0.04	1.8	0.6	1.7	1.17
	4.8	0.98	0.02	2.0	0.5	2.3	1.24
	5.1	0.98	0.02	2.0	0.6	2.3	1.12
	6.4	0.99	0.01	2.3	0.9	2.8	1.17
Dimethylformamide (DMF)	1.5	0.89	0.11	1.3	0.6	1.0	1.09
	1.8	0.91	0.09	1.2	0.7	1.2	1.22
	3.2	0.97	0.03	1.3	0.6	1.6	1.18
	4.8	0.97	0.03	1.4	0.7	2.1	1.11
	5.1	0.98	0.02	1.3	0.8	2.2	1.08
	6.4	0.99	0.01	1.7	0.9	2.6	1.08
Dioxane	1.5	0.82	0.18	1.2	0.5	0.9	1.17
	1.8	0.85	0.15	1.3	0.6	1.0	1.14
	3.2	0.94	0.06	1.5	0.6	1.3	1.16
	4.8	0.96	0.04	1.8	0.7	1.6	1.24
	5.1	0.97	0.03	1.6	0.6	1.8	1.19
	6.4	0.99	0.01	1.7	0.7	2.2	1.14

Table A3.2: Parameters retrieved from the global FBM analysis of the excimer decays of CoE-PS in various solvents with Equation 3.2.

Solvent	mol%	τ_{EE0} (ns)	τ_{ED} (ns)	f_{Ediff}	f_{EE0}	f_{ED}	χ^2
Methyl Acetate	1.5	53	180	0.88	0.12	0.01	1.09
	1.8	54		0.87	0.13		1.18
	3.2	51		0.81	0.19		1.09
	4.8	51		0.75	0.26		1.13
	5.1	52		0.75	0.26		1.15
	6.4	50		0.69	0.30		1.08
Methyl Ethyl Ketone (MEK)	1.5	49		0.89	0.11		1.17
	1.8	49		0.88	0.12		1.08
	3.2	48		0.84	0.16		1.07
	4.8	47		0.79	0.21		1.21
	5.1	47		0.82	0.18		1.20
	6.4	46	180	0.77	0.22	0.01	1.18
Dichloromethane (DCM)	1.5	47		0.90	0.11		1.17
	1.8	47		0.89	0.11		1.13
	3.2	46		0.87	0.13		1.21
	4.8	47		0.81	0.19		1.23
	5.1	46		0.82	0.17		1.18
	6.4	46		0.79	0.21		1.18
Tetrahydrofuran (THF)	1.5	57		0.90	0.10		1.12
	1.8	56		0.89	0.12		1.07
	3.2	52		0.84	0.16		1.00
	4.8	53		0.82	0.18		1.19
	5.1	50	180	0.80	0.19	0.01	1.20
	6.4	50		0.81	0.19		1.14
Toluene	1.5	52		0.87	0.13		1.18
	1.8	53		0.88	0.12		1.12
	3.2	50		0.85	0.15		1.17
	4.8	50		0.80	0.20		1.24
	5.1	48		0.79	0.21		1.12
	6.4	48		0.73	0.23		1.17
Dimethylformamide (DMF)	1.5	54		0.91	0.10		1.09
	1.8	51		0.90	0.09		1.22
	3.2	50		0.87	0.13		1.18
	4.8	48		0.80	0.19		1.11
	5.1	47		0.83	0.17		1.08
	6.4	47		0.79	0.21		1.08
Dioxane	1.5	61	180	0.89	0.09	0.02	1.17
	1.8	61		0.88	0.12		1.14
	3.2	57		0.87	0.14		1.16
	4.8	55		0.82	0.18		1.24
	5.1	55		0.82	0.18		1.19
	6.4	53		0.79	0.21		1.14

Table A3.3: Fractions of all pyrene species for CoE-PS, calculated from f_{Mdiff}, f_{Mfree}, f_{Ediff}, f_{EE0}, and f_{ED}.[26]

Solvent	mol%	f_{diff}	f_{free}	f_{E0}	f_{D}	f_{agg}	χ^2
Methyl Acetate	1.5	0.82	0.06	0.11	0.00	0.11	1.09
	1.8	0.84	0.03	0.13		0.13	1.18
	3.2	0.79	0.02	0.18		0.18	1.09
	4.8	0.74	0.01	0.26		0.26	1.13
	5.1	0.74	0.01	0.25		0.25	1.15
	6.4	0.69	0.00	0.30		0.30	1.08
Methyl Ethyl Ketone (MEK)	1.5	0.83	0.07	0.10		0.10	1.17
	1.8	0.84	0.04	0.11		0.11	1.08
	3.2	0.82	0.02	0.16		0.16	1.07
	4.8	0.78	0.01	0.21		0.21	1.21
	5.1	0.81	0.01	0.18		0.18	1.20
	6.4	0.77	0.01	0.22	0.00	0.22	1.18
Dichloromethane (DCM)	1.5	0.83	0.08	0.10		0.10	1.17
	1.8	0.84	0.06	0.11		0.11	1.13
	3.2	0.83	0.04	0.12		0.12	1.21
	4.8	0.79	0.03	0.18		0.18	1.23
	5.1	0.81	0.02	0.17		0.17	1.18
	6.4	0.78	0.01	0.21		0.21	1.18
Tetrahydrofuran (THF)	1.5	0.79	0.13	0.09		0.09	1.12
	1.8	0.81	0.09	0.11		0.11	1.07
	3.2	0.81	0.04	0.15		0.15	1.00
	4.8	0.80	0.03	0.17		0.17	1.19
	5.1	0.79	0.02	0.19	0.00	0.19	1.20
	6.4	0.80	0.02	0.18		0.18	1.14
Toluene	1.5	0.77	0.12	0.11		0.11	1.18
	1.8	0.81	0.08	0.11		0.11	1.12
	3.2	0.83	0.03	0.15		0.15	1.17
	4.8	0.79	0.02	0.20		0.20	1.24
	5.1	0.79	0.00	0.21		0.21	1.12
	6.4	0.76	0.01	0.24		0.24	1.17
Dimethylformamide (DMF)	1.5	0.82	0.10	0.09		0.09	1.09
	1.8	0.83	0.08	0.09		0.09	1.22
	3.2	0.84	0.03	0.13		0.13	1.18
	4.8	0.79	0.02	0.19		0.19	1.11
	5.1	0.82	0.02	0.17		0.17	1.08
	6.4	0.78	0.01	0.21		0.21	1.08
Dioxane	1.5	0.74	0.17	0.08	0.02	0.09	1.17
	1.8	0.76	0.13	0.10		0.10	1.14
	3.2	0.82	0.05	0.13		0.13	1.16
	4.8	0.79	0.03	0.17		0.17	1.24
	5.1	0.80	0.02	0.17		0.17	1.19
	6.4	0.78	0.01	0.21		0.21	1.14

Table A3.4: Parameters retrieved from the global FBM analysis of the monomer decays of CoA-PS in various solvents with Equation 3.1.

Solvent	mol%	f_{Mdiff}	f_{Mfree}	k_{blob} (10^7 s^{-1})	$k_e[blob]$ (10^7 s^{-1})	<n>	χ^2
Methyl Acetate	1.1	0.82	0.18	0.9	0.5	1.16	1.09
	2.5	0.97	0.03	1.0	0.7	1.82	0.98
	3.7	0.99	0.01	1.1	0.9	2.31	1.08
	5.0	0.99	0.01	1.4	0.9	2.69	1.13
	5.2	0.99	0.01	1.4	1.1	2.85	1.10
	6.4	0.98	0.02	1.6	1.0	3.07	1.05
Methyl Ethyl Ketone (MEK)	1.1	0.73	0.27	1.1	0.9	0.87	1.16
	2.5	0.95	0.05	1.2	0.8	1.40	1.14
	3.7	0.98	0.02	1.2	0.9	1.96	1.06
	5.0	0.98	0.02	1.8	1.4	1.88	1.16
	5.2	0.99	0.01	1.4	1.1	2.43	1.09
	6.4	0.99	0.01	1.8	1.4	2.54	1.18
Dichloromethane (DCM)	1.1	0.63	0.37	1.3	0.7	0.91	1.02
	2.5	0.90	0.98	1.3	0.8	1.25	1.08
	3.7	0.97	0.03	1.2	0.8	1.79	1.13
	5.0	0.97	0.27	1.4	0.9	2.05	1.21
	5.2	0.97	0.03	1.6	1.3	1.98	1.11
	6.4	0.99	0.01	1.9	1.3	2.31	1.09
Tetrahydrofuran (THF)	1.1	0.74	0.26	0.9	0.4	0.78	1.16
	2.5	0.90	0.10	1.1	0.6	1.15	1.09
	3.7	0.96	0.04	1.0	0.7	1.50	1.07
	5.0	0.97	0.03	1.1	0.7	1.82	1.13
	5.2	0.98	0.02	1.2	0.8	2.00	1.15
	6.4	0.98	0.02	1.4	1.1	1.99	1.30
Toluene	1.1	0.76	0.24	1.1	0.6	0.78	1.24
	2.5	0.91	0.09	1.2	0.7	1.19	1.06
	3.7	0.97	0.03	1.2	0.8	1.64	1.07
	5.0	0.98	0.02	1.4	1.0	1.87	1.14
	5.2	0.98	0.02	1.5	1.0	1.83	1.05
	6.4	0.98	0.02	1.7	1.2	2.08	1.12
Dimethylformamide (DMF)	1.1	0.66	0.34	1.2	0.6	0.58	1.11
	2.5	0.89	0.11	1.7	0.8	0.84	1.09
	3.7	0.95	0.05	1.1	1.0	1.15	1.08
	5.0	0.96	0.04	1.2	1.0	1.35	1.02
	5.2	0.97	0.03	1.3	1.0	1.43	1.05
	6.4	0.98	0.02	1.7	1.3	1.38	1.16
Dioxane	1.1*	0.62	0.38	1.2	0.4	0.64	1.18
	2.5	0.87	0.13	1.2	0.6	0.78	1.16
	3.7	0.93	0.07	1.0	0.8	1.02	1.15
	5.0	0.95	0.05	1.2	1.1	1.08	1.25
	5.2	0.96	0.04	1.2	1.0	1.21	1.05
	6.4	0.97	0.03	1.1	1.0	1.49	1.16

* $f_{Mdiff} \approx 40\%$; The fraction of pyrene that did not form excimer within the time-scale of the experiment is too large to retrieve accurate FBM parameters, thus this sample is not used.

Table A3.5: Parameters retrieved from the global FBM analysis of the excimer decays of CoA-PS in various solvents with Equation 3.2.

Solvent	mol%	τ_{EE0} (ns)	τ_{ED} (ns)	f_{Ediff}	f_{EE0}	f_{ED}	χ^2
Methyl Acetate	1.1	63	180	0.90	0.06	0.03	1.09
	2.5	58	180	0.87	0.12	0.01	0.98
	3.7	55	180	0.86	0.13	0.01	1.08
	5.0	52	180	0.82	0.17	0.01	1.13
	5.2	53	180	0.80	0.19	0.01	1.10
	6.4	53	180	0.77	0.22	0.01	1.05
Methyl Ethyl Ketone (MEK)	1.1	55	180	0.92	0.07	0.02	1.16
	2.5	53	180	0.88	0.11	0.01	1.14
	3.7	50	180	0.87	0.13		1.06
	5.0	49	180	0.86	0.13	0.01	1.16
	5.2	51	180	0.82	0.18		1.09
	6.4	50	180	0.81	0.18	0.01	1.18
Dichloromethane (DCM)	1.1	60	180	0.89	0.09	0.02	1.02
	2.5	54	180	0.87	0.13		1.08
	3.7	51	180	0.86	0.13		1.13
	5.0	50	180	0.84	0.16		1.21
	5.2	48	180	0.82	0.17	0.01	1.11
	6.4	49	180	0.79	0.20	0.01	1.09
Tetrahydrofuran (THF)	1.1	62	180	0.89	0.07	0.04	1.16
	2.5	58	180	0.88	0.10	0.02	1.09
	3.7	56	180	0.87	0.12		1.07
	5.0	55	180	0.85	0.15		1.13
	5.2	55	180	0.83	0.16	0.01	1.15
	6.4	54	180	0.82	0.17	0.01	1.30
Toluene	1.1	59	180	0.88	0.10	0.02	1.24
	2.5	56	180	0.84	0.15	0.01	1.06
	3.7	51	180	0.83	0.16	0.01	1.07
	5.0	49	180	0.81	0.18	0.01	1.14
	5.2	50	180	0.80	0.19	0.01	1.05
	6.4	50	180	0.76	0.23	0.01	1.12
Dimethylformamide (DMF)	1.1	70	180	0.89	0.04	0.07	1.11
	2.5	62	180	0.89	0.08	0.03	1.09
	3.7	55	180	0.89	0.09	0.01	1.08
	5.0	56	180	0.87	0.11	0.02	1.02
	5.2	55	180	0.88	0.11	0.01	1.05
	6.4	54	180	0.88	0.11	0.01	1.16
Dioxane	1.1*	69	180	0.83	0.01	0.16	1.18
	2.5	69	180	0.85	0.10	0.04	1.16
	3.7	58	180	0.89	0.09	0.01	1.15
	5.0	54	180	0.89	0.10	0.02	1.25
	5.2	55	180	0.87	0.12	0.01	1.05
	6.4	54	180	0.85	0.13	0.02	1.16

* $f_{Mdiff} \approx 40\%$; The fraction of pyrene that did not form excimer within the time-scale of the experiment is too large to retrieve accurate FBM parameters, thus this sample is not used.

Table A3.6: Fractions of all pyrene species for CoA-PS, calculated from f_{Mdiff}, f_{Mfree}, f_{Ediff}, f_{EE0}, and f_{ED}.[26]

Solvent	mol%	f_{diff}	f_{free}	f_{E0}	f_{D}	f_{agg}	χ^2
Methyl Acetate	1.1	0.75	0.16	0.05	0.03	0.08	1.09
	2.5	0.84	0.03	0.12	0.01	0.13	0.98
	3.7	0.85	0.01	0.13	0.01	0.14	1.08
	5.0	0.81	0.01	0.17	0.01	0.18	1.13
	5.2	0.80	0.01	0.19	0.01	0.19	1.10
	6.4	0.76	0.01	0.22	0.01	0.23	1.05
Methyl Ethyl Ketone (MEK)	1.1	0.69	0.25	0.05	0.01	0.06	1.16
	2.5	0.84	0.05	0.10	0.01	0.11	1.14
	3.7	0.85	0.02	0.13		0.13	1.06
	5.0	0.85	0.02	0.13	0.01	0.14	1.16
	5.2	0.81	0.01	0.18		0.18	1.09
	6.4	0.80	0.01	0.18	0.01	0.19	1.18
Dichloromethane (DCM)	1.1	0.59	0.34	0.06	0.01	0.07	1.02
	2.5	0.45	0.49	0.06		0.06	1.08
	3.7	0.84	0.03	0.13		0.13	1.13
	5.0	0.68	0.19	0.13		0.13	1.21
	5.2	0.80	0.02	0.16	0.01	0.17	1.11
	6.4	0.79	0.01	0.20	0.01	0.21	1.09
Tetrahydrofuran (THF)	1.1	0.68	0.23	0.06	0.03	0.09	1.16
	2.5	0.80	0.09	0.09	0.02	0.11	1.09
	3.7	0.84	0.04	0.12		0.12	1.07
	5.0	0.83	0.02	0.15		0.15	1.13
	5.2	0.82	0.01	0.16	0.01	0.17	1.15
	6.4	0.80	0.02	0.17	0.01	0.18	1.30
Toluene	1.1	0.69	0.22	0.08	0.02	0.09	1.24
	2.5	0.78	0.07	0.13	0.01	0.14	1.06
	3.7	0.81	0.03	0.16	0.01	0.16	1.07
	5.0	0.80	0.02	0.18	0.01	0.19	1.14
	5.2	0.79	0.02	0.19	0.01	0.19	1.05
	6.4	0.75	0.02	0.22	0.01	0.23	1.12
Dimethylformamide (DMF)	1.1	0.61	0.31	0.03	0.05	0.08	1.11
	2.5	0.80	0.10	0.07	0.02	0.10	1.09
	3.7	0.79	0.12	0.08	0.01	0.09	1.08
	5.0	0.84	0.03	0.10	0.02	0.12	1.02
	5.2	0.86	0.02	0.11	0.01	0.12	1.05
	6.4	0.86	0.02	0.11	0.01	0.12	1.16
Dioxane	1.1*	0.55	0.34	0.01	0.10	0.11	1.18
	2.5	0.75	0.12	0.09	0.04	0.13	1.16
	3.7	0.84	0.06	0.09	0.02	0.10	1.15
	5.0	0.84	0.05	0.09	0.02	0.11	1.25
	5.2	0.84	0.03	0.11	0.01	0.12	1.05
	6.4	0.83	0.02	0.13	0.02	0.15	1.16

* $f_{Mdiff} \approx 40\%$; The fraction of pyrene that did not form excimer within the time-scale of the experiment is too large to retrieve accurate FBM parameters, thus this sample is not used.

Chapter 4:
An Analogy between Surfactant Micelles and Fluorescence Blobs to Study Polymer Chain Dynamics in Solution

4.1 Technical Note

Understanding the parameters that control long range polymer chain dynamics (LRPCD) in solution is useful to predict whether two monomers of the same polymer chain located at different positions in the polymer coil can encounter, react, or associate over a given time period. As was pointed out in a recent review,[1] the research topics most susceptible to benefit from this information include the study of the early stages of protein folding which are driven by encounters and associations between the amino acids,[2,3] or the investigation of the shear-thinning of an aqueous solution of associative polymers (AP) driven by a disruption of the equilibrium between the inter- and intramolecular associations of the AP's hydrophobic pendants.[4,5]

Over the past ten years, this laboratory has established a new analytical tool called the fluorescence blob model (FBM) designed to provide a measure of the sub-volume of a polymer coil probed by a chromophore covalently attached onto a polymer chain while the chromophore remains excited.[1,6] The sub-volume probed by the excited chromophore is referred to as a *blob* and is denoted as V_{blob}. Since the chromophore remains excited for a well-defined time window determined by its natural lifetime, τ_M, the FBM relates V_{blob} to τ_M. As τ_M increases, so does V_{blob}, and information about the LRPCD of the polymer can be retrieved from the relationship $V_{blob} = f(\tau_M)$.[7]

Except for two exceptions,[8,9] the overwhelming majority of FBM studies have been conducted in solution with polymers randomly labeled with the chromophore pyrene.[1] In these experiments, the polymer coil is compartmentalized into a cluster of *blobs* and the pyrenes distribute themselves randomly among the *blobs* according to a Poisson distribution. The kinetics of excimer formation between pyrenes located inside the *blobs* are handled in

the same manner as if the *blobs* were surfactant micelles. Consequently, the FBM equation (Equation 4.1) which is used to fit the pyrene monomer decays bears a strong resemblance with the equations used with surfactant micelles.[10,11]

$$[M^*]_{(t)} = f_{diff} \exp\left[-\left(A_2 + \frac{1}{\tau_M} \right) t - A_3 \left(1 - \exp\left(-A_4 t \right) \right) \right] + f_{free} \exp\left(-t / \tau_M \right) \qquad (4.1)$$

The expressions of the parameters A_2, A_3, and A_4 are given in Equation 4.2.

$$A_2 = < n > \frac{k_{blob} k_e [blob]}{k_{blob} + k_e [blob]} \qquad A_3 = < n > \frac{k_{blob}^2}{\left(k_{blob} + k_e [blob] \right)^2} \qquad A_4 = k_{blob} + k_e [blob] \qquad (4.2)$$

In Equation 4.1, f_{diff} represents the fraction of pyrene monomers that form excimer by diffusion whereas f_{free} represents the fraction of pyrene monomers that do not form excimer and emit with their natural lifetime, τ_M. In Equation 4.2, k_{blob} is the rate constant characterizing the diffusion-controlled encounters between one excited pyrene and one ground-state pyrene located inside the same *blob*, <*n*> is the average number of pyrenes per *blob*, and k_e[*blob*] describes the exchange of ground-state pyrenes from one *blob* to the next.

Although V_{blob} constitutes the fundamental structural unit on which the FBM is based, an interesting paradox is that V_{blob} can only be determined quantitatively when working in the semi-dilute concentration regime.[12] In the dilute regime, a measure of V_{blob} is obtained from the number of monomers, N_{blob}, encompassed inside V_{blob} since a larger *blob* yields a larger N_{blob}.[6] Consequently, N_{blob} turns out to be the most important parameter retrieved by the FBM to describe LRPCD in dilute solution. N_{blob} is calculated with Equation 4.3,[1] where

M_{Py}, M_u, and x represent the molar mass of a monomer labeled with pyrene, the molar mass of an unlabelled monomer, and the mole fraction of labeled monomers in the polymer, respectively. The pyrene content of the polymer (λ_{Py}) is expressed in moles of pyrene per gram of polymer.

$$N_{blob} = \frac{< n >}{\lambda_{Py} / f_{diff} \, [M_{Py} x + M_u (1 - x)]} \tag{4.3}$$

The inherent parallel existing between *blobs* and surfactant micelles implies that the parameter N_{blob} in the FBM is equivalent to the aggregation number of a surfactant micelle, N_{agg}. The pioneering work of Turro and Yekta (TY) demonstrated that N_{agg} for surfactant micelles can be obtained from the equivalence existing between $<n>$, the average number of quenchers per micelle, and $ln(I_o/I)$, where I and I_o represent the fluorescence intensity of a surfactant solution when a chromophore is introduced to the surfactant micelles in the presence or absence of a quencher, respectively.[13] The determination of N_{agg} proceeds by measuring the quantity $ln(I_o/I) = <n>$. $ln(I_o/I)$ increases linearly with quencher concentration and the slope of the straight line yields N_{agg}. Since then, numerous surfactant micelles have been characterized using the TY method.[14]

On the other hand, N_{blob} in the FBM is determined with Equation 4.3 for a series of pyrene-labeled polymers. N_{blob} is then plotted as a function of the corrected pyrene content (λ_{Py}/f_{diff}) (Figure 4.1).[1,6] In most cases, N_{blob} decreases with increasing λ_{Py} due to the decreased flexibility of the chain resulting from the increased number of pyrenes covalently attached to the chain.[1,6] The N_{blob} vs. λ_{Py}/f_{diff} trend is extrapolated to zero-pyrene content to yield the N_{blob} value of the *ideal* unlabeled polymer.[1,6,15] Although the procedures used to

determine N_{agg} and N_{blob} are different, they both revolve about the knowledge of $<n>$, be it the average number of quenchers per micelle given by $ln(I_o/I)$[13] or the average number of pyrenes per *blob* used in the numerator of Equation 4.3.[1,6]

The outstanding efficiency and simplicity of the TY method at determining N_{agg} for surfactant micelles draws its strength from the equality $<n> = ln(I_o/I)$. If a similar equality were to hold for pyrene-labeled polymers, it would drastically simplify the use of the FBM. Unfortunately whereas the I_o/I ratio can be easily obtained for surfactant systems, the same does not hold with a pyrene-labeled polymer. The pyrene labels can not jump from a *blob* to the next as easily as quenchers do from one micelle to the next, so that if a chain is richer in pyrene, those pyrenes can not distribute themselves among the *blobs* of another pyrene-poorer chain. Consequently, some residual excimer emission is always observed with pyrene-labeled polymers, making I_o difficult to obtain. Also, at low pyrene content, there always exists a substantial fraction ($f_{free} > 0.10$) of isolated pyrene monomers that do not form excimer, so that I does not reflect the emission of all quenched pyrenes. In other words, the I_o/I ratio can not be easily obtained for pyrene-labeled polymers.

To circumvent these complications, the number-average lifetime, $<\tau>$, and the natural lifetime, τ_M, of the pyrenyl pendants can be chosen in lieu of the fluorescence intensities I and I_o, respectively. Since $<\tau>$ is proportional to the quantum yield of the chromophore,[16] the ratio I_o/I used with the surfactant micelles is equivalent to the ratio $\tau_M /<\tau>$ for the pyrene-labeled polymers. τ_M can be determined by fitting the fluorescence decay of a pyrene-labeled polymer containing a very low pyrene content (< 0.2 mol%) and assigning the longest decay time to τ_M.[6] The fluorescence decays of the pyrene monomer obtained with the pyrene-labeled polymers having a larger pyrene content (> 1 mol%) can be fitted with a sum

of 3-4 exponentials (Equation 4.4) where the longest decay time is fixed to τ_M. The corresponding normalized pre-exponential factor $a_M / (\sum_{i=1}^{n} a_i + a_M)$ is taken as f_{free} so that f_{diff} in Equation 4.3 is given by $1 - a_M / (\sum_{i=1}^{n} a_i + a_M)$. The decay times shorter than τ_M are used with their corresponding pre-exponential factors to calculate $<\tau>$. This procedure ensures that only the excited pyrenes that generate excimer by diffusion are accounted for. The parameter $<n>$ in Equation 4.3 can be replaced by $Ln(\tau_M/<\tau>)$ and the resulting N_{blob} value is plotted as a function of λ_{Py}/f_{diff} in Figure 4.1.

$$[M^*]_{(t)} = \sum_{i=1}^{n} a_i \exp(-t/\tau_i) + a_M \exp(-t/\tau_M) \quad \text{where } n = 2\text{-}3 \qquad (4.4)$$

The procedure was applied to five different pyrene-labeled polymers, namely three polystyrene samples (CoA-PS, CoE-PS, and GrE-PS), poly(*N*,*N*-dimethylacrylamide) (Py-PDMA), and poly(*L*-glutamic acid) (Py-PGA) whose chemical structures are given in Table 4.1. The preparation of these polymers has been reported in earlier publications.[6,17-19] Details about the fits of the fluorescence decays with Equation 4.1 and 4.4 can be found in the Appendix.

For each polymer series and solvent, N_{blob} was calculated from $<n>$ obtained by either fitting the monomer fluorescence decays with Equation 4.1 or making the assumption that $<n> = Ln(\tau_M /<\tau>)$. With most polymer-solvent systems, the N_{blob} values obtained by fitting the fluorescence decays of the pyrene monomer by Equation 4.1 or 4.4 were surprisingly close for each data series. The trends shown in Figure 4.1 together with those of 14

additional polymer-solvent systems were extrapolated to zero-pyrene content to obtain the N_{blob} value of the *ideal* unlabeled polymer (Table 4.2).[1,6] The extrapolated N_{blob} values obtained by fitting the fluorescence decays with Equation 4.1 or 4.4 were plotted against each other in Figure 4.2.

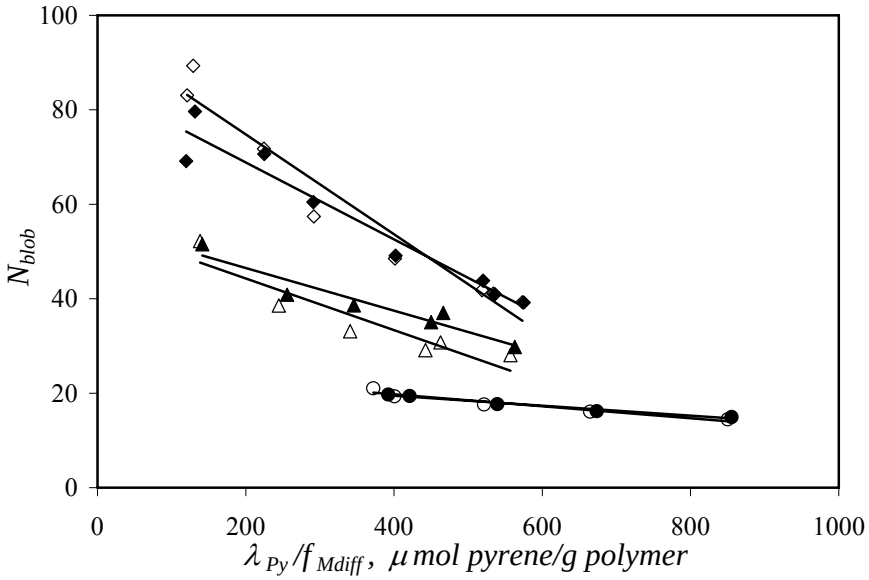

Figure 4.1: Plots of N_{blob} as a function of λ_{Py}/f_{Mdiff} obtained for the polymer series GrE-PS in THF (diamond), CoA-PS in THF (triangle), and PGA in DMF (circle). Closed and open symbols are used when the fluorescence decays of the pyrene monomer are fit with Equation 4.1 and 4.4, respectively.

A remarkably good agreement was observed between both types of N_{blob} values obtained with five polymers in seven different solvents. These data suggest that an equivalence exists between $<n>$ and $Ln(\tau_M/<\tau>)$ which in turn can be used to calculate N_{blob} (Equation 4.3). Fitting the fluorescence decays with a sum of exponentials instead of Equation 4.1 based on the FBM provides a "model independent" procedure that yields N_{blob}, an estimate of the volume probed by an excited pyrene. This procedure seems to be applicable to a wide variety of polymers ranging from polypeptides (Py-PGA) to vinyl

polymers (CoA-PS, CoE-PS, GrE-PS, and Py-PDMA) and should become a powerful tool to describe the encounters between two internal polymer segments of a chain.

Table 4.1: Chemical structures, pyrene contents and molecular weight information for each polymer. [a] Ref 19. [b] Ref 17. [c] Ref 18.

Structure

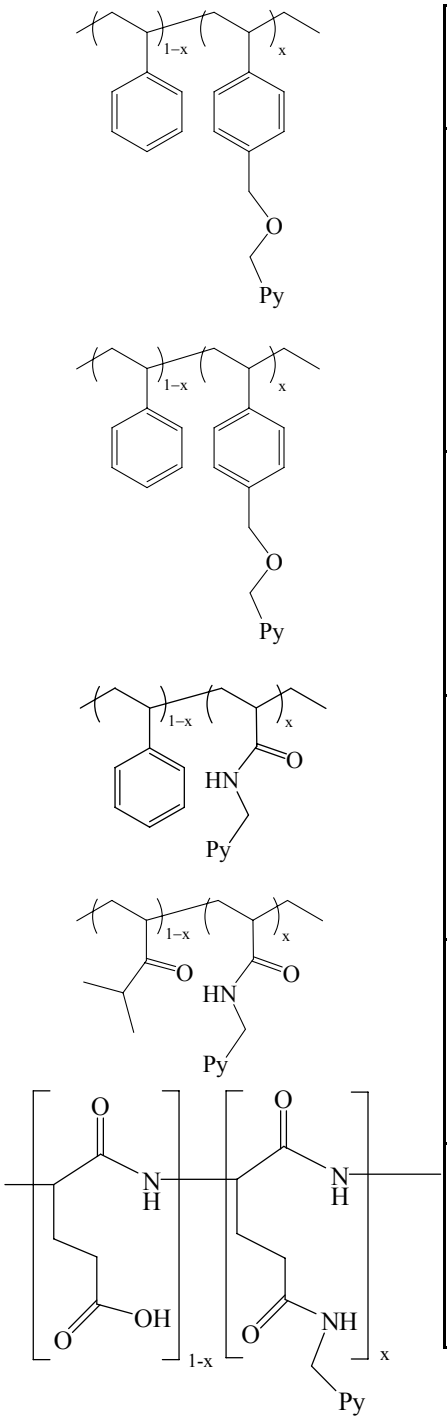

Sample	mol %	λ_{Py} μmol Py/ g polymer	M_n (kg/mol)	M_w (kg/mol)	PDI
GrE-PS[a]	1.1	101	113	116	1.03
	1.3	121	113	116	1.03
	2.4	218	110	163	1.48
	3.2	283	110	163	1.48
	4.6	398	113	116	1.03
	6.2	515	110	163	1.48
	6.3	525	110	163	1.48
	6.9	567	110	163	1.48
CoE-PS[a]	1.5	141	35	63	1.81
	1.8	169	45	84	1.87
	3.2	284	32	63	1.99
	4.8	412	16	30	1.85
	5.1	436	34	62	1.80
	6.4	533	46	75	1.65
CoA-PS[a]	1.1	105	43	80	1.88
	2.5	230	39	80	2.04
	3.7	331	55	102	1.90
	5.0	437	28	53	1.88
	6.4	459	39	74	1.91
	6.9	550	36	84	2.30
PDMA[b]	2.7	263		165	
	3.7	349		134	
	5.2	479		123	
	6.3	570		105	
	7.3	645		105	
PGA[c]	5.1	330		41	
	5.9	370		41	
	8.2	500		41	
	10.9	650		41	
	14.8	840		41	

Table 4.2: N_{blob} values determined for each polymer solvent system using the FBM or a sum of exponentials (SOE) to fit the monomer fluorescence decays.

Polymer	Solvent	N_{blob} SOE	±	N_{blob} FBM	±
CoA-PS	THF	55	7	56	6
	Toluene	57	4	58	2
	Dioxane	29	1	32	3
	DMF	35	1	39	2
	Methyl Acetate	81	3	94	6
	DCM	43	2	58	3
	MEK	59	3	65	5
CoE-PS	THF	81	4	75	2
	Toluene	81	3	72	2
	Dioxane	60	3	55	4
	DMF	72	4	68	2
	Methyl Acetate	130	10	115	7
	DCM	80	5	76	4
	MEK	97	5	98	4
GrE-PS	THF	96	4	85	3
Py-PGA	DMF	25	1	24	1
Py-PDMA	DMF	31	3	31	6

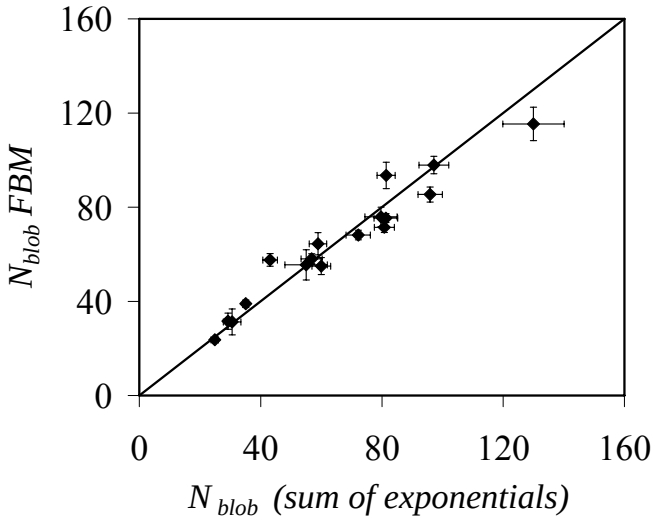

Figure 4.2: Plot of the N_{blob} values obtained by fitting the fluorescence decays with Equation 4.1 and extrapolated to zero-pyrene content and as a function of N_{blob} obtained by fitting the fluorescence decays with Equation 4.4 and extrapolated to zero-pyrene content.

4.2 References and Notes

1. Duhamel, J. *Acc. Chem. Res.* **2006**, *39*, 953-960.

2. Doucet, D.; Roitberg, A.; Hagen, S. J. *Biophys. J.* **2007**, *92*, 2281-2289.

3. Hagen, S. J.; Carswell, C. W.; Sjolander, E. M. *J. Mol. Biol.* **2001**, *305*, 1161-1171.

4. Annabale, T.; Buscall, R.; Ettelaie, R.; Whittlestone, D. *J. Rheol.* **1993**, *37*, 695-726.

5. English, R.; Gulati, H. S.; Jenkins, R. D.; Khan, S. A. *J. Rheol.* **1997**, *41*, 427-445.

6. Mathew, A. K.; Siu, H.; Duhamel, J. *Macromolecules* **1999**, *32*, 7100-7108.

7. Kanagalingam, S.; Spartalis, J.; Cao, T.-M.; Duhamel, J. *Macromolecules* **2002**, *35*, 8571-8577.

8. Duhamel, J.; Jones, A.; Dickson, T. J. *Macromolecules* **2000**, 33, 6344-6352.

9. Duhamel, J. *Macromolecules* **2004**, *37*, 1987-1989.

10. Tachyia, M. *Chem. Phys. Lett.* **1975**, *33*, 289-292.

11. Infelta, P. P.; Gratzel, M.; Thomas, J. K. *J. Phys. Chem.* **1974**, *78*, 190-195.

12. Irondi, K.; Zhang, M.; Duhamel, J. *J. Phys. Chem. B.* **2006**, *110*, 2628-2637.

13. Turro, N. J.; Yekta, A. *J. Am. Chem. Soc.* **1978**, *100*, 5951-5952.

14. Grieser, F.; Drummond, C. J *J. Phys. Chem.* **1988**, *92*, 5580-5593.

15. Figure 4.1 represents a sample of the N_{blob} vs. λ_{Py}/f_{diff} plots. Two of the three least similar N_{blob} vs. λ_{Py}/f_{diff} plots are shown in Figure A4.1 in the Appendix. Two of the most similar N_{blob} vs. λ_{Py}/f_{diff} plots are shown in Figure A4.2.

16. Lakowicz, J. R. *Principles of Fluorescence Spectroscopy* **1999**, Kluwer Academic, New York, p 14.

17. Kanagalingam, S.; Ngan, C. F.; Duhamel, J. *Macromolecules* **2002**, *35*, 8560-8570.

18. Duhamel, J.; Kanagalingam, S.; O'Brien, T.; Ingratta, M. *J. Am. Chem. Soc.* **2003**, *125*, 12810-12822.

19. Ingratta, M.; Duhamel, J. *Macromolecules* **2007**, *40*, 6647-6657.

4.3 Appendix

4.3.1 Experimental Section

Time-resolved fluorescence measurements: The fluorescence decays of all Py-PS (CoA-PS, CoE-PS, GrE-PS) and Py-PDMA solutions were obtained by exciting at 340 nm with an IBH 340 nm LED and collecting the emission at 375 nm and 510 nm for the monomer and excimer, respectively. Monomer fluorescence decays were acquired for Py-PGA solutions in DMF using an IBH 5000F coaxial nanosecond flash lamp filled with H_2 gas with an excitation of 346 nm and emission at 376 nm. All solutions had an optical density of 0.1 and were degassed for 30 minutes under a gentle flow of N_2 to remove oxygen.

All decays were acquired using 1024 channels to a peak maximum of 20,000 counts for the lamp and decay curves. The instrument response function was determined by applying the MIMIC method[A1] to the reference decays obtained with PPO [2,5-diphenyloxazole] in cyclohexanol (τ = 1.42 ns) and BBOT [2,5-bis(*tert*-butyl-2-benzoxazolyl)thiopene] in ethanol (τ =1.47 ns) for the monomer and excimer decays, respectively.

Analysis of the fluorescence decays: The monomer decays of all Py-PSs, Py-PDMAs and Py-PGAs were fit using a multi-exponential decay (Equation A4.1). The contribution of pyrene monomers able to form excimer are described by the decay times τ_i, and their pre-exponential factors, a_i, while isolated pyrene monomers unable to form excimer are described by the lifetime of the pyrene monomer, τ_M, and its pre-exponential factor, a_M. The lifetime of the unquenched pyrene monomer was estimated through the biexponential analysis of the fluorescence decays of a low pyrene content polymer (< 0.2 mol% pyrene) where the exponential with the longest decay time contributed more than 80% of the total pre-

exponential weight of the decay. The τ_M value for a particular polymer-solvent system ranges from 150 – 260 ns (Table A4.1–A4.3).

$$i(t) = \sum_{i=1}^{n_{\exp}} a_i \exp(-t/\tau_i) + a_M \exp(-t/\tau_M) \text{ with } n_{exp} = 2\text{-}4 \quad \text{(A4.1)}$$

The monomer and excimer decays of all Py-PS and Py-PDMA were analyzed using a global analysis whereby the monomer and excimer decays were simultaneously fitted with Equations A4.2 and A4.3, respectively.[A2] The monomer decays of Py-PGA were analyzed using Equation A4.2.

$$[Py^*]_{(t)} = [Py^*_{diff}]_{(t=0)} \exp\left[-\left(A_2 + \frac{1}{\tau_M}\right)t - A_3(1-\exp(-A_4 t))\right] + [Py^*_{free}]_{(t=0)} \exp(-t/\tau_M) \quad \text{(A4.2)}$$

$$[E^*] = -[Py^*_{diff}]_{(t=0)} e^{-A_3} \sum_{i=0}^{\infty} \frac{A_3{}^i}{i!} \frac{A_2 + i\,A_4}{\frac{1}{\tau_M} - \frac{1}{\tau_{E0}} + A_2 + i\,A_4} \exp\left(-\left(\frac{1}{\tau_M} + A_2 + i\,A_4\right)t\right)$$

$$+ \left([E0^*]_{(t=0)} + [Py^*_{diff}]_{(t=0)} e^{-A_3} \sum_{i=0}^{\infty} \frac{A_3{}^i}{i!} \frac{A_2 + i\,A_4}{\frac{1}{\tau_M} - \frac{1}{\tau_{E0}} + A_2 + i\,A_4} \right) e^{-t/\tau_{E0}} + [D^*]_0 e^{-t/\tau_D} \quad \text{(A4.3)}$$

The parameters A_2, A_3, and A_4 used in Equations A4.2 and A4.3 are described in Equation A4.4.

$$A_2 = \langle n \rangle \frac{k_{blob} k_e [blob]}{k_{blob} + k_e [blob]} \qquad A_3 = \langle n \rangle \frac{k_{blob}^2}{(k_{blob} + k_e [blob])^2} \qquad A_4 = k_{blob} + k_e [blob] \qquad \text{(A4.4)}$$

Equations A4.2-A4.4 assume that some of the excimer is formed through diffusive encounters between an excited pyrene, Py^*_{diff}, and a ground–state pyrene. In the monomer decay, the Py^*_{diff} monomers are described by the first exponential in Equation A4.2. The fraction of pyrene groups that are isolated and cannot form excimer, Py^*_{free}, are accounted for by the second exponential in Equation A4.2.

The FBM parameters retrieved from the analysis of the monomer decay and used in Equation A4.3 are defined as the rate constant of encounter between one excited pyrene and one ground–state pyrene located in the same *blob*, k_{blob}, the average number of ground–state pyrenes per *blob*, $\langle n \rangle$, and the rate constant describing the exchange of ground–state pyrenes between *blobs* times the *blob* concentration in the polymer coil, $k_e \times [blob]$.

Equation A4.3 fits the excimer decays assuming three pathways toward excimer formation. The excimers, $E0^*$, formed through the diffusive encounter of an excited pyrene, Py^*_{diff}, and a ground-state pyrene emit with a lifetime τ_{E0}. They can also be generated through direct excitation of a pre-associated dimer, *E0*. The long-lived pyrene dimers, D^*, fluoresce with a long lifetime τ_D resulting from improper stacking of the two pyrene moieties.

Optimization of the parameters used in Equations A4.1-A4.4 to fit globally the monomer and excimer fluorescence decays of Py-PS and Py-PDMA and the monomer

fluorescence decays of Py-PGA was performed with the Marquardt-Levenberg algorithm.[A3] The IBH 340 LED used to acquire the majority of the fluorescence decays generated a higher background noise level than the hydrogen lamp used for the Py-PGA samples. Therefore a background correction was applied to fit the fluorescence decays of the Py-PS and Py-PDMA samples.[A4] As done in earlier publications, a light scattering correction was also applied to account for those pyrene pairs which are in close contact and form excimer on a time-scale which is too fast to be detected accurately by our instrument.[A4] The fits of the monomer and excimer decays were considered good if the χ^2 was below 1.3 and the residuals were randomly distributed around zero.

4.3.2 References

A1. James, D. R.; Demmer, D. R.; Verall, R. E.; Steer, R. P. *Rev. Sci. Instrum.* **1983**, *54*, 1121-1130.

A2. Siu, H.; Duhamel, J. *Macromolecules* **2004**, *37*, 9287-9289.

A3. Press, W. H.; Flannery, B. P.; Teukolsky, S. A.; Vetterling, W. T. *Numerical Recipes. The Art of Scientific Computing (Fortran Version)*; Cambridge University Press: Cambridge, 1992, p 523 – 528.

A4. Demas, J. N. *Excited-State Lifetime Measurements*; Academic Press: New York, 1983, p 134, 147.

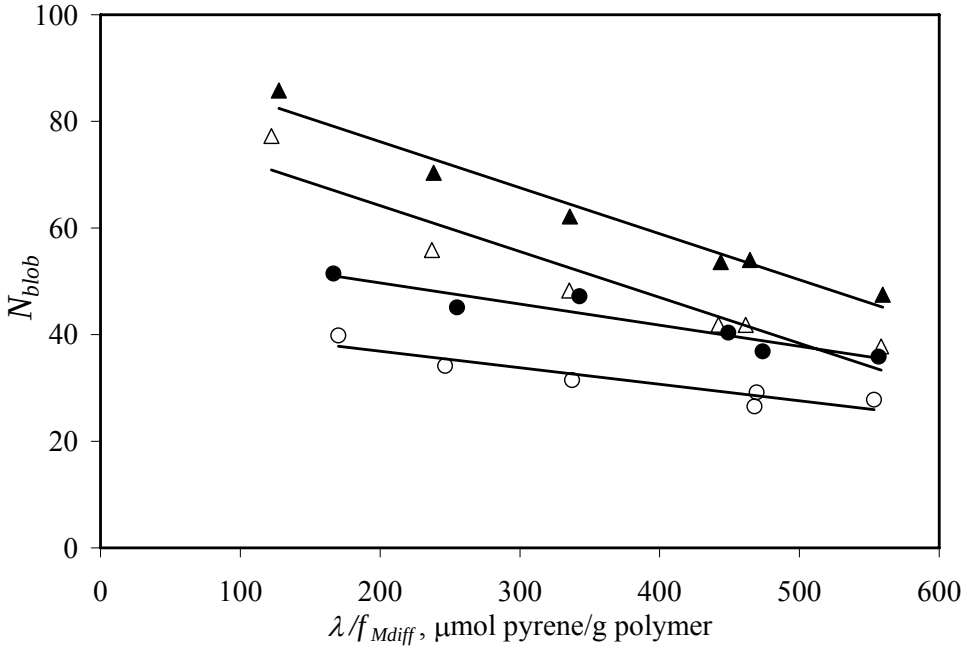

Figure A4.1: N_{blob} as a function of pyrene content. Two of the least similar N_{blob} values determined by the FBM and SOE methods. CoA-PS in methyl acetate, FBM (▲), SOE (△); CoA-PS in DCM, FBM (●), SOE (○).

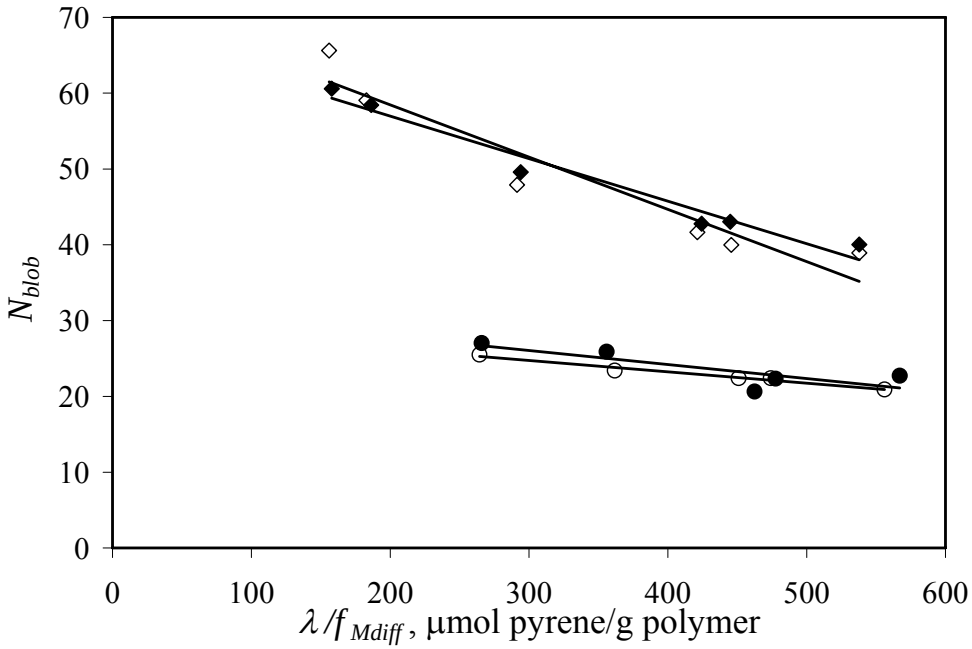

Figure A4.2: N_{blob} as a function of pyrene content. Two of the most similar N_{blob} values determined by the FBM and SOE methods. CoA-PS in dioxane, FBM (◆), SOE (◇); CoE-PS in DMF, FBM (●), SOE (○).

Table A4.1: Parameters retrieved from the global FBM analysis of the monomer decays of CoE-PS in various solvents with Equation A4.2.

Sample	mol%	f_{Mdiff}	f_{Mfree}	k_{blob} (10^7 s^{-1})	$k_e[blob]$ (10^7 s^{-1})	<n>	χ^2
CoE-PS	1.5	0.93	0.07	1.4	0.6	1.7	1.09
	1.8	0.96	0.04	1.5	0.6	1.9	1.18
Methyl Acetate	3.2	0.97	0.03	1.7	0.7	2.6	1.09
	4.8	0.99	0.01	2.1	0.5	3.3	1.13
	5.1	0.99	0.01	1.9	0.5	3.6	1.15
	6.4	0.99	0.01	2.0	0.5	4.4	1.08
CoE-PS	1.5	0.92	0.08	1.5	0.7	1.4	1.17
	1.8	0.95	0.05	1.5	0.7	1.5	1.08
Methyl Ethyl Ketone	3.2	0.98	0.02	1.7	0.8	2.2	1.07
(MEK)	4.8	0.99	0.01	2.0	0.6	2.7	1.21
	5.1	0.98	0.02	2.4	1.1	2.6	1.20
	6.4	0.99	0.01	2.8	1.3	3.2	1.18
CoE-PS	1.5	0.91	0.09	1.9	0.7	1.1	1.17
	1.8	0.93	0.07	1.9	0.7	1.2	1.13
Dichloromethane	3.2	0.95	0.05	2.2	1.0	1.7	1.21
(DCM)	4.8	0.96	0.04	2.8	1.2	2.1	1.23
	5.1	0.93	0.03	2.7	1.2	2.2	1.18
	6.4	0.99	0.01	2.9	1.2	2.7	1.18
CoE-PS	1.5	0.86	0.14	1.5	0.5	1.1	1.12
	1.8	0.90	0.10	1.5	0.5	1.2	1.07
Tetrahydrofuran	3.2	0.96	0.04	1.6	0.6	1.7	1.00
(THF)	4.8	0.96	0.04	2.1	0.7	2.1	1.19
	5.1	0.98	0.02	1.8	0.8	2.3	1.20
	6.4	0.98	0.02	2.3	0.8	2.6	1.14
CoE-PS	1.5	0.86	0.14	1.5	0.5	1.1	1.18
	1.8	0.91	0.09	1.6	0.5	1.2	1.12
Toluene	3.2	0.96	0.04	1.8	0.6	1.7	1.17
	4.8	0.98	0.02	2.0	0.5	2.3	1.24
	5.1	0.98	0.02	2.0	0.6	2.3	1.12
	6.4	0.99	0.01	2.3	0.9	2.8	1.17
CoE-PS	1.5	0.89	0.11	1.3	0.6	1.0	1.09
	1.8	0.91	0.09	1.2	0.7	1.2	1.22
Dimethylformamide	3.2	0.97	0.03	1.3	0.6	1.6	1.18
(DMF)	4.8	0.97	0.03	1.4	0.7	2.1	1.11
	5.1	0.98	0.02	1.3	0.8	2.2	1.08
	6.4	0.99	0.01	1.7	0.9	2.6	1.08
CoE-PS	1.5	0.82	0.18	1.2	0.5	0.9	1.17
	1.8	0.85	0.15	1.3	0.6	1.0	1.14
Dioxane	3.2	0.94	0.06	1.5	0.6	1.3	1.16
	4.8	0.96	0.04	1.8	0.7	1.6	1.24
	5.1	0.97	0.03	1.6	0.6	1.8	1.19
	6.4	0.99	0.01	1.7	0.7	2.2	1.14

Table A4.2: Parameters retrieved from the global FBM analysis of the monomer decays of CoA-PS in various solvents with Equation A4.2.

Sample	mol%	f_{Mdiff}	f_{Mfree}	k_{blob} (10^7 s^{-1})	$k_e[blob]$ (10^7 s^{-1})	<n>	χ^2
CoA-PS	1.1	0.82	0.18	0.9	0.5	1.16	1.09
	2.5	0.97	0.03	1.0	0.7	1.82	0.98
Methyl Acetate	3.7	0.99	0.01	1.1	0.9	2.31	1.08
	5.0	0.99	0.01	1.4	0.9	2.69	1.13
	5.2	0.99	0.01	1.4	1.1	2.85	1.10
	6.4	0.98	0.02	1.6	1.0	3.07	1.05
CoA-PS	1.1	0.73	0.27	1.1	0.9	0.87	1.16
	2.5	0.95	0.05	1.2	0.8	1.40	1.14
Methyl Ethyl Ketone	3.7	0.98	0.02	1.2	0.9	1.96	1.06
(MEK)	5.0	0.98	0.02	1.8	1.4	1.88	1.16
	5.2	0.99	0.01	1.4	1.1	2.43	1.09
	6.4	0.99	0.01	1.8	1.4	2.54	1.18
CoA-PS	1.1	0.63	0.37	1.3	0.7	0.91	1.02
	2.5	0.90	0.98	1.3	0.8	1.25	1.08
Dichloromethane	3.7	0.97	0.03	1.2	0.8	1.79	1.13
(DCM)	5.0	0.97	0.27	1.4	0.9	2.05	1.21
	5.2	0.97	0.03	1.6	1.3	1.98	1.11
	6.4	0.99	0.01	1.9	1.3	2.31	1.09
CoA-PS	1.1	0.74	0.26	0.9	0.4	0.78	1.16
	2.5	0.90	0.10	1.1	0.6	1.15	1.09
Tetrahydrofuran	3.7	0.96	0.04	1.0	0.7	1.50	1.07
(THF)	5.0	0.97	0.03	1.1	0.7	1.82	1.13
	5.2	0.98	0.02	1.2	0.8	2.00	1.15
	6.4	0.98	0.02	1.4	1.1	1.99	1.30
CoA-PS	1.1	0.76	0.24	1.1	0.6	0.78	1.24
	2.5	0.91	0.09	1.2	0.7	1.19	1.06
Toluene	3.7	0.97	0.03	1.2	0.8	1.64	1.07
	5.0	0.98	0.02	1.4	1.0	1.87	1.14
	5.2	0.98	0.02	1.5	1.0	1.83	1.05
	6.4	0.98	0.02	1.7	1.2	2.08	1.12
CoA-PS	1.1	0.66	0.34	1.2	0.6	0.58	1.11
	2.5	0.89	0.11	1.7	0.8	0.84	1.09
Dimethylformamide	3.7	0.95	0.05	1.1	1.0	1.15	1.08
(DMF)	5.0	0.96	0.04	1.2	1.0	1.35	1.02
	5.2	0.97	0.03	1.3	1.0	1.43	1.05
	6.4	0.98	0.02	1.7	1.3	1.38	1.16
CoA-PS	1.1	0.62	0.38	1.2	0.4	0.64	1.18
	2.5	0.87	0.13	1.2	0.6	0.78	1.16
Dioxane	3.7	0.93	0.07	1.0	0.8	1.02	1.15
	5.0	0.95	0.05	1.2	1.1	1.08	1.25
	5.2	0.96	0.04	1.2	1.0	1.21	1.05
	6.4	0.97	0.03	1.1	1.0	1.49	1.16

Table A4.3: Parameters retrieved from the global FBM analysis of the monomer decays of Py-PDMA and GrE-PS and the FBM analysis of the monomer decays of Py-PGA with Equation A4.2.

Sample	mol%	f_{Mdiff}	f_{Mfree}	k_{blob} (10^7 s^{-1})	$k_e[blob]$ (10^7 s^{-1})	<n>	χ^2
GrE-PS	1.1	0.82	0.18	1.6	0.5	0.9	1.15
	1.3	0.91	0.09	1.7	0.5	1.1	1.16
Tetrahydrofuran	2.4	0.97	0.03	1.8	0.4	1.7	1.27
(THF)	3.2	0.97	0.03	1.7	0.5	2.0	1.18
	4.6	0.99	0.01	2.1	0.8	2.3	1.21
	6.2	0.99	0.01	2.2	0.8	2.7	1.28
	6.3	0.98	0.02	2.3	1.0	2.6	1.23
	6.9	0.99	0.01	2.7	1.1	2.7	1.17
Py-PDMA	2.7	0.87	0.13	1.3	0.7	0.9	1.15
	3.7	0.88	0.12	1.3	0.8	1.0	1.07
Dimethylformamide	5.2	0.96	0.04	1.3	0.8	1.4	1.12
(DMF)	6.3	0.97	0.03	1.4	1.0	1.5	1.11
	7.3	0.98	0.02	1.6	0.9	1.8	1.18
Py-PGA	5.1	0.84	0.16	2.5	0.4	1.2	1.26
	5.9	0.88	0.12	1.9	0.3	1.3	1.1
Dimethylformamide	8.2	0.93	0.07	2.0	0.5	1.5	1.19
(DMF)	10.9	0.97	0.04	2.4	0.5	1.8	1.08
	14.8	0.98	0.02	2.3	0.5	2.3	1.13

Table A4.4: Parameters retrieved from the global FBM analysis of the excimer decays of CoE-PS in various solvents with Equation A4.3.

Solvent	mol%	τ_{EE0} (ns)	τ_{ED} (ns)	f_{Ediff}	f_{EE0}	f_{ED}	χ^2
CoE-PS	1.5	53	180	0.88	0.12	0.01	1.09
	1.8	54		0.87	0.13		1.18
Methyl Acetate	3.2	51		0.81	0.19		1.09
	4.8	51		0.75	0.26		1.13
	5.1	52		0.75	0.26		1.15
	6.4	50		0.69	0.30		1.08
CoE-PS	1.5	49		0.89	0.11		1.17
	1.8	49		0.88	0.12		1.08
Methyl Ethyl Ketone	3.2	48		0.84	0.16		1.07
(MEK)	4.8	47		0.79	0.21		1.21
	5.1	47		0.82	0.18		1.20
	6.4	46	180	0.77	0.22	0.01	1.18
CoE-PS	1.5	47		0.90	0.11		1.17
	1.8	47		0.89	0.11		1.13
Dichloromethane	3.2	46		0.87	0.13		1.21
(DCM)	4.8	47		0.81	0.19		1.23
	5.1	46		0.82	0.17		1.18
	6.4	46		0.79	0.21		1.18
CoE-PS	1.5	57		0.90	0.10		1.12
	1.8	56		0.89	0.12		1.07
Tetrahydrofuran	3.2	52		0.84	0.16		1.00
(THF)	4.8	53		0.82	0.18		1.19
	5.1	50	180	0.80	0.19	0.01	1.20
	6.4	50		0.81	0.19		1.14
CoE-PS	1.5	52		0.87	0.13		1.18
	1.8	53		0.88	0.12		1.12
Toluene	3.2	50		0.85	0.15		1.17
	4.8	50		0.80	0.20		1.24
	5.1	48		0.79	0.21		1.12
	6.4	48		0.73	0.23		1.17
CoE-PS	1.5	54		0.91	0.10		1.09
	1.8	51		0.90	0.09		1.22
Dimethylformamide	3.2	50		0.87	0.13		1.18
(DMF)	4.8	48		0.80	0.19		1.11
	5.1	47		0.83	0.17		1.08
	6.4	47		0.79	0.21		1.08
CoE-PS	1.5	61	180	0.89	0.09	0.02	1.17
	1.8	61		0.88	0.12		1.14
Dioxane	3.2	57		0.87	0.14		1.16
	4.8	55		0.82	0.18		1.24
	5.1	55		0.82	0.18		1.19
	6.4	53		0.79	0.21		1.14

Table A4.5: Parameters retrieved from the global FBM analysis of the excimer decays of CoA-PS in various solvents with Equation A4.3.

Solvent	mol%	τ_{EE0} (ns)	τ_{ED} (ns)	f_{Ediff}	f_{EE0}	f_{ED}	χ^2
CoA-PS	1.1	63	180	0.90	0.06	0.03	1.09
	2.5	58	180	0.87	0.12	0.01	0.98
Methyl Acetate	3.7	55	180	0.86	0.13	0.01	1.08
	5.0	52	180	0.82	0.17	0.01	1.13
	5.2	53	180	0.80	0.19	0.01	1.10
	6.4	53	180	0.77	0.22	0.01	1.05
CoA-PS	1.1	55	180	0.92	0.07	0.02	1.16
	2.5	53	180	0.88	0.11	0.01	1.14
Methyl Ethyl Ketone	3.7	50	180	0.87	0.13		1.06
(MEK)	5.0	49	180	0.86	0.13	0.01	1.16
	5.2	51	180	0.82	0.18		1.09
	6.4	50	180	0.81	0.18	0.01	1.18
CoA-PS	1.1	60	180	0.89	0.09	0.02	1.02
	2.5	54	180	0.87	0.13		1.08
Dichloromethane	3.7	51	180	0.86	0.13		1.13
(DCM)	5.0	50	180	0.84	0.16		1.21
	5.2	48	180	0.82	0.17	0.01	1.11
	6.4	49	180	0.79	0.20	0.01	1.09
CoA-PS	1.1	62	180	0.89	0.07	0.04	1.16
	2.5	58	180	0.88	0.10	0.02	1.09
Tetrahydrofuran	3.7	56	180	0.87	0.12		1.07
(THF)	5.0	55	180	0.85	0.15		1.13
	5.2	55	180	0.83	0.16	0.01	1.15
	6.4	54	180	0.82	0.17	0.01	1.30
CoA-PS	1.1	59	180	0.88	0.10	0.02	1.24
	2.5	56	180	0.84	0.15	0.01	1.06
Toluene	3.7	51	180	0.83	0.16	0.01	1.07
	5.0	49	180	0.81	0.18	0.01	1.14
	5.2	50	180	0.80	0.19	0.01	1.05
	6.4	50	180	0.76	0.23	0.01	1.12
CoA-PS	1.1	70	180	0.89	0.04	0.07	1.11
	2.5	62	180	0.89	0.08	0.03	1.09
Dimethylformamide	3.7	55	180	0.89	0.09	0.01	1.08
(DMF)	5.0	56	180	0.87	0.11	0.02	1.02
	5.2	55	180	0.88	0.11	0.01	1.05
	6.4	54	180	0.88	0.11	0.01	1.16
CoA-PS	1.1	69	180	0.83	0.01	0.16	1.18
	2.5	69	180	0.85	0.10	0.04	1.16
Dioxane	3.7	58	180	0.89	0.09	0.01	1.15
	5.0	54	180	0.89	0.10	0.02	1.25
	5.2	55	180	0.87	0.12	0.01	1.05
	6.4	54	180	0.85	0.13	0.02	1.16

Table A4.6: Parameters retrieved from the global FBM analysis of the excimer decays of GrE-PS and Py-PDMA with Equation A4.3.

Solvent	mol%	τ_{EE0} (ns)	τ_{ED} (ns)	f_{Ediff}	f_{EE0}	f_{ED}	χ^2
GrE-PS	1.1	62		0.88	0.12		1.15
	1.3	58		0.84	0.16		1.16
Tetrahydrofuran	2.4	58		0.79	0.21		1.27
(THF)	3.2	54		0.74	0.26		1.18
	4.6	50		0.76	0.24		1.21
	6.2	50		0.72	0.27		1.28
	6.3	50		0.67	0.33		1.23
	6.9	50		0.66	0.34		1.17
Py-PDMA	2.7	58	180	0.91	0.07	0.02	1.15
	3.7	59	180	0.90	0.08	0.02	1.07
Dimethylformamide	5.2	55	180	0.88	0.11	0.01	1.12
(DMF)	6.3	54	180	0.87	0.12	0.01	1.11
	7.3	52	180	0.83	0.16	0.01	1.18

Table A4.7: Fractions of all pyrene species for CoE-PS, calculated from f_{Mdiff}, f_{Mfree}, f_{Ediff}, f_{EE0}, and f_{ED}.

Solvent	mol%	f_{diff}	f_{free}	f_{E0}	f_D	f_{agg}	χ^2
CoE-PS	1.5	0.82	0.06	0.11	0.00	0.11	1.09
	1.8	0.84	0.03	0.13		0.13	1.18
Methyl Acetate	3.2	0.79	0.02	0.18		0.18	1.09
	4.8	0.74	0.01	0.26		0.26	1.13
	5.1	0.74	0.01	0.25		0.25	1.15
	6.4	0.69	0.00	0.30		0.30	1.08
CoE-PS	1.5	0.83	0.07	0.10		0.10	1.17
	1.8	0.84	0.04	0.11		0.11	1.08
Methyl Ethyl Ketone	3.2	0.82	0.02	0.16		0.16	1.07
(MEK)	4.8	0.78	0.01	0.21		0.21	1.21
	5.1	0.81	0.01	0.18		0.18	1.20
	6.4	0.77	0.01	0.22	0.00	0.22	1.18
CoE-PS	1.5	0.83	0.08	0.10		0.10	1.17
	1.8	0.84	0.06	0.11		0.11	1.13
Dichloromethane	3.2	0.83	0.04	0.12		0.12	1.21
(DCM)	4.8	0.79	0.03	0.18		0.18	1.23
	5.1	0.81	0.02	0.17		0.17	1.18
	6.4	0.78	0.01	0.21		0.21	1.18
CoE-PS	1.5	0.79	0.13	0.09		0.09	1.12
	1.8	0.81	0.09	0.11		0.11	1.07
Tetrahydrofuran	3.2	0.81	0.04	0.15		0.15	1.00
(THF)	4.8	0.80	0.03	0.17		0.17	1.19
	5.1	0.79	0.02	0.19	0.00	0.19	1.20
	6.4	0.80	0.02	0.18		0.18	1.14
CoE-PS	1.5	0.77	0.12	0.11		0.11	1.18
	1.8	0.81	0.08	0.11		0.11	1.12
Toluene	3.2	0.83	0.03	0.15		0.15	1.17
	4.8	0.79	0.02	0.20		0.20	1.24
	5.1	0.79	0.00	0.21		0.21	1.12
	6.4	0.76	0.01	0.24		0.24	1.17
CoE-PS	1.5	0.82	0.10	0.09		0.09	1.09
	1.8	0.83	0.08	0.09		0.09	1.22
Dimethylformamide	3.2	0.84	0.03	0.13		0.13	1.18
(DMF)	4.8	0.79	0.02	0.19		0.19	1.11
	5.1	0.82	0.02	0.17		0.17	1.08
	6.4	0.78	0.01	0.21		0.21	1.08
CoE-PS	1.5	0.74	0.17	0.08	0.02	0.09	1.17
	1.8	0.76	0.13	0.10		0.10	1.14
Dioxane	3.2	0.82	0.05	0.13		0.13	1.16
	4.8	0.79	0.03	0.17		0.17	1.24
	5.1	0.80	0.02	0.17		0.17	1.19
	6.4	0.78	0.01	0.21		0.21	1.14

Table A4.8: Fractions of all pyrene species for CoA-PS, calculated from f_{Mdiff}, f_{Mfree}, f_{Ediff}, f_{EE0}, and f_{ED}.

Solvent	mol%	f_{diff}	f_{free}	f_{E0}	f_{D}	f_{agg}	χ^2
CoA-PS	1.1	0.75	0.16	0.05	0.03	0.08	1.09
	2.5	0.84	0.03	0.12	0.01	0.13	0.98
Methyl Acetate	3.7	0.85	0.01	0.13	0.01	0.14	1.08
	5.0	0.81	0.01	0.17	0.01	0.18	1.13
	5.2	0.80	0.01	0.19	0.01	0.19	1.10
	6.4	0.76	0.01	0.22	0.01	0.23	1.05
CoA-PS	1.1	0.69	0.25	0.05	0.01	0.06	1.16
	2.5	0.84	0.05	0.10	0.01	0.11	1.14
Methyl Ethyl Ketone	3.7	0.85	0.02	0.13		0.13	1.06
(MEK)	5.0	0.85	0.02	0.13	0.01	0.14	1.16
	5.2	0.81	0.01	0.18		0.18	1.09
	6.4	0.80	0.01	0.18	0.01	0.19	1.18
CoA-PS	1.1	0.59	0.34	0.06	0.01	0.07	1.02
	2.5	0.45	0.49	0.06		0.06	1.08
Dichloromethane	3.7	0.84	0.03	0.13		0.13	1.13
(DCM)	5.0	0.68	0.19	0.13		0.13	1.21
	5.2	0.80	0.02	0.16	0.01	0.17	1.11
	6.4	0.79	0.01	0.20	0.01	0.21	1.09
CoA-PS	1.1	0.68	0.23	0.06	0.03	0.09	1.16
	2.5	0.80	0.09	0.09	0.02	0.11	1.09
Tetrahydrofuran	3.7	0.84	0.04	0.12		0.12	1.07
(THF)	5.0	0.83	0.02	0.15		0.15	1.13
	5.2	0.82	0.01	0.16	0.01	0.17	1.15
	6.4	0.80	0.02	0.17	0.01	0.18	1.30
CoA-PS	1.1	0.69	0.22	0.08	0.02	0.09	1.24
	2.5	0.78	0.07	0.13	0.01	0.14	1.06
Toluene	3.7	0.81	0.03	0.16	0.01	0.16	1.07
	5.0	0.80	0.02	0.18	0.01	0.19	1.14
	5.2	0.79	0.02	0.19	0.01	0.19	1.05
	6.4	0.75	0.02	0.22	0.01	0.23	1.12
CoA-PS	1.1	0.61	0.31	0.03	0.05	0.08	1.11
	2.5	0.80	0.10	0.07	0.02	0.10	1.09
Dimethylformamide	3.7	0.79	0.12	0.08	0.01	0.09	1.08
(DMF)	5.0	0.84	0.03	0.10	0.02	0.12	1.02
	5.2	0.86	0.02	0.11	0.01	0.12	1.05
	6.4	0.86	0.02	0.11	0.01	0.12	1.16
CoA-PS	1.1	0.55	0.34	0.01	0.10	0.11	1.18
	2.5	0.75	0.12	0.09	0.04	0.13	1.16
Dioxane	3.7	0.84	0.06	0.09	0.02	0.10	1.15
	5.0	0.84	0.05	0.09	0.02	0.11	1.25
	5.2	0.84	0.03	0.11	0.01	0.12	1.05
	6.4	0.83	0.02	0.13	0.02	0.15	1.16

Table A4.9: Fractions of all pyrene species for GrE-PS and Py-PDMA, calculated from f_{Mdiff}, f_{Mfree}, f_{Ediff}, f_{EE0}, and f_{ED}.

Solvent	mol%	f_{diff}	f_{free}	f_{E0}	f_{D}	f_{agg}	χ^2
GrE-PS	1.1	0.74	0.17	0.10		0.10	1.15
	1.3	0.78	0.07	0.14		0.15	1.16
Tetrahydrofuran	2.4	0.77	0.02	0.20		0.20	1.27
(THF)	3.2	0.73	0.02	0.25		0.25	1.18
	4.6	0.76	0.01	0.23		0.23	1.21
	6.2	0.72	0.01	0.27		0.27	1.28
	6.3	0.66	0.01	0.32		0.32	1.23
	6.9	0.66	0.01	0.33		0.33	1.17
Py-PDMA	2.7	0.80	0.12	0.06	0.01	0.08	1.15
	3.7	0.80	0.11	0.07	0.02	0.09	1.07
Dimethylformamide	5.2	0.85	0.04	0.10	0.01	0.11	1.12
(DMF)	6.3	0.84	0.03	0.12	0.01	0.13	1.11
	7.3	0.82	0.01	0.15	0.01	0.17	1.18

Table A4.10: Parameters retrieved from the exponential analysis of the monomer decays of CoE-PS with Equation A4.1.

Sample	mol %	τ_1	τ_2	τ_3	τ_M	a_1	a_2	a_3	a_M	χ^2
CoE-PS	1.5	10	38	89	250	0.32	0.41	0.27	0.01	1.12
	1.8	9	38	97	250	0.30	0.42	0.25	0.03	0.94
Methyl Acetate	3.2	7	27	69	250	0.40	0.42	0.16	0.01	1.07
	4.8	7	21	62	250	0.49	0.41	0.09	0.01	1.10
	5.1	6	19	53	250	0.44	0.45	0.10	0.01	1.16
	6.4	7	20	67	250	0.61	0.35	0.03	0.00	1.13
CoE-PS	1.5	5	30	84	170	0.23	0.34	0.36	0.06	1.07
	1.8	4	24	72	170	0.19	0.35	0.41	0.05	1.13
Methyl Ethyl Ketone	3.2	5	23	60	170	0.27	0.45	0.27	0.02	0.96
(MEK)	4.8	5	18	50	170	0.33	0.47	0.19	0.01	1.16
	5.1	3	17	40	170	0.31	0.46	0.21	0.01	1.13
	6.4	9	27		170	0.69	0.30		0.01	1.13
CoE-PS	1.1	7	34	88	150	0.24	0.33	0.38	0.05	0.99
	2.5	6	29	79	150	0.24	0.33	0.38	0.05	1.00
Dichloromethane	3.7	6	26	66	150	0.26	0.44	0.27	0.03	1.08
(DCM)	5.0	8	27	80	150	0.46	0.42	0.12	0.00	1.13
	5.2	3	14	40	150	0.32	0.41	0.26	0.02	1.01
	6.4	4	14	37	150	0.38	0.46	0.16	0.01	1.00
CoE-PS	1.5	10	52	147	260	0.22	0.34	0.35	0.09	1.11
	1.8	11	50	135	260	0.24	0.34	0.35	0.07	1.03
Tetrahydrofuran	3.2	9	37	100	260	0.28	0.41	0.29	0.03	1.03
(THF)	4.8	8	33	89	260	0.44	0.40	0.14	0.02	1.01
	5.1	7	28	76	260	0.36	0.45	0.19	0.01	1.07
	6.4	6	22	57	260	0.37	0.47	0.15	0.01	1.11
CoE-PS	1.5	10	54	145	230	0.22	0.37	0.33	0.08	1.05
	1.8	10	48	129	230	0.23	0.38	0.33	0.06	1.08
Toluene	3.2	9	37	101	230	0.27	0.46	0.24	0.02	0.93
	4.8	9	31	85	230	0.46	0.39	0.13	0.01	1.11
	5.1	6	22	62	230	0.31	0.44	0.24	0.01	1.07
	6.4	5	20	53	230	0.39	0.46	0.15	0.00	1.17
CoE-PS	1.5	8	44	116	220	0.15	0.27	0.49	0.09	0.98
	1.8	7	46	112	220	0.15	0.32	0.46	0.07	1.11
Dimethylformamide	3.2	9	41	96	220	0.21	0.43	0.34	0.02	1.10
(DMF)	4.8	7	32	80	220	0.26	0.47	0.25	0.02	1.04
	5.1	8	32	74	220	0.25	0.47	0.26	0.01	1.10
	6.4	9	26	56	220	0.32	0.45	0.22	0.01	1.11
CoE-PS	1.5	30	129		243	0.28	0.53		0.19	1.19
	1.8	23	122		243	0.36	0.51		0.13	1.24
Dioxane	3.2	12	58	135	243	0.29	0.40	0.28	0.03	1.10
	4.8	10	39	98	243	0.37	0.36	0.25	0.02	1.08
	5.1	12	46	107	243	0.38	0.40	0.20	0.01	1.05
	6.4	8	33	81	243	0.39	0.43	0.18	0.01	0.98

Table A4.11: Parameters retrieved from the exponential analysis of the monomer decays of CoA-PS with Equation A4.1.

Sample	mol %	τ_1	τ_2	τ_3	τ_M	a_1	a_2	a_3	a_M	χ^2
CoA-PS	1.1	5	55	141	250	0.11	0.32	0.43	0.14	1.04
	2.5	10	43	98	250	0.14	0.45	0.38	0.03	0.91
Methyl Acetate	3.7	8	34	73	250	0.16	0.52	0.30	0.01	1.07
	5.0	5	27	63	250	0.19	0.57	0.23	0.01	1.00
	5.2	5	25	57	250	0.21	0.57	0.22	0.00	0.99
	6.4	5	21	50	250	0.27	0.54	0.18	0.01	0.82
CoA-PS	1.1	5	46	109	170	0.11	0.20	0.47	0.21	1.13
	2.5	6	38	86	170	0.15	0.37	0.44	0.04	1.05
Methyl Ethyl Ketone	3.7	4	27	65	170	0.17	0.41	0.42	0.01	0.98
(MEK)	5.0	5	21	51	170	0.15	0.38	0.45	0.02	1.11
	5.2	3	22	50	170	0.23	0.43	0.33	0.01	1.04
	6.4	4	20	43	170	0.23	0.48	0.29	0.01	1.17
CoA-PS	1.1	34	91		150	0.19	0.43		0.38	0.97
	2.5	9	42	92	150	0.11	0.41	0.41	0.07	1.03
Dichloromethane	3.7	11	37	78	150	0.14	0.51	0.32	0.02	1.13
(DCM)	5.0	7	30	69	150	0.17	0.50	0.26	0.01	1.11
	5.2	5	23	52	150	0.16	0.42	0.40	0.02	1.11
	6.4	5	21	47	150	0.20	0.50	0.30	0.00	0.99
CoA-PS	1.1	7	61	167	260	0.09	0.20	0.47	0.24	1.07
	2.5	15	64	148	260	0.14	0.40	0.40	0.05	0.97
Tetrahydrofuran	3.7	12	52	117	260	0.14	0.43	0.40	0.03	1.01
(THF)	5.0	21	62	129	260	0.31	0.53	0.14	0.01	1.08
	5.2	13	43	94	260	0.22	0.51	0.26	0.01	1.06
	6.4	7	33	75	260	0.20	0.49	0.30	0.01	1.23
CoA-PS	1.1	8	63	160	241	0.08	0.25	0.48	0.19	1.12
	2.5	14	58	135	241	0.15	0.41	0.40	0.04	0.91
Toluene	3.7	17	55	120	241	0.22	0.54	0.24	0.00	0.93
	5.0	8	36	83	241	0.18	0.51	0.29	0.01	1.04
	5.2	10	38	84	241	0.21	0.50	0.28	0.01	0.94
	6.4	10	33	72	241	0.24	0.53	0.22	0.01	1.17
CoA-PS	1.1	25	91	183	220	0.08	0.24	0.54	0.14	1.01
	2.5	16	54	128	220	0.08	0.24	0.59	0.09	0.96
Dimethylformamide	3.7	20	68	115	220	0.14	0.43	0.40	0.03	1.06
(DMF)	5.0	4	38	92	220	0.20	0.30	0.48	0.02	0.98
	5.2	8	34	80	220	0.11	0.33	0.53	0.03	0.98
	6.4	6	31	73	220	0.11	0.35	0.52	0.02	1.06
CoA-PS	1.1	32	134		243	0.24	0.62		0.15	1.02
	2.5	27	143		243	0.43	0.44		0.13	1.01
Dioxane	3.7	35	114		243	0.23	0.68		0.08	1.13
	5.0	10	57	115	243	0.15	0.36	0.46	0.03	1.14
	5.2	8	40	100	243	0.10	0.29	0.57	0.03	1.00
	6.4	8	47	101	243	0.15	0.45	0.40	0.01	0.99

Table A4.12: Parameters retrieved from the exponential analysis of the monomer decays of GrE-PS and Py-PDMA with Equation A4.1.

Sample	mol %	τ_1	τ_2	τ_3	τ_M	a_1	a_2	a_3	a_M	χ^2
GrE-PS	1.1	13	57	150	260	0.20	0.25	0.39	0.16	1.09
	1.3	14	63	147	260	0.29	0.34	0.31	0.06	1.04
Tetrahydrofuran	2.4	11	40	109	260	0.40	0.34	0.23	0.03	1.04
(THF)	3.2	11	40	100	260	0.39	0.39	0.19	0.02	1.02
	4.6	6	25	67	260	0.29	0.50	0.20	0.01	1.19
	6.2	4	18	51	260	0.31	0.50	0.19	0.01	1.13
	6.3	4	16	46	260	0.28	0.49	0.22	0.02	1.37
	6.9	5	17	47	260	0.35	0.47	0.16	0.01	1.06
Py-PDMA	2.7	11	50	130	220	0.08	0.30	0.54	0.08	1.18
	3.7	11	49	122	220	0.09	0.33	0.49	0.09	1.04
Dimethylformamide	5.2	8	41	98	220	0.13	0.41	0.44	0.03	0.98
(DMF)	6.3	12	42	89	220	0.16	0.46	0.36	0.02	0.99
	7.3	5	26	68	220	0.12	0.45	0.42	0.01	1.15
Py-PGA	5.1	12	47	142	215	0.32	0.30	0.27	0.11	1.08
	5.9	12	48	141	215	0.32	0.33	0.28	0.08	1.03
Dimethylformamide	8.2	11	46	128	215	0.40	0.36	0.20	0.04	1.02
(DMF)	10.9	10	37	104	215	0.45	0.37	0.16	0.02	0.94
	14.8	7	27	83	215	0.44	0.42	0.14	0.02	0.92

Chapter 5:
Side-Chain Dynamics of a Pyrene Labeled α-Helical Polymer Studied with a Fluorescence Blob Model

5.1 Abstract

Two series of pyrene-labeled poly(glutamic acid) (Py-PGA) were synthesized utilizing two different linkers for pyrene attachment, namely 1-pyrenemethylamine (PMA) and 1-pyrenebutylamine (PBA). Several Py-PGAs were synthesized for each series with pyrene contents ranging from 4 to 15 mol%. Py-PGA forms a rigid α-helix in DMF that effectively locks the backbone in place, thus enabling only side-chain or linker motions to be monitored by time-resolved fluorescence. Time-resolved fluorescence decays were acquired for the pyrene monomer of the Py-PGA constructs and the fluorescence blob model (FBM) was used to quantify the dynamics of the different linkers connecting pyrene to the backbone. Nitromethane was used to shorten the lifetime of the pyrene monomer, in effect controlling the probing time of the pyrene group, from 50 to 155 ns for PGA-PBA and from 50 to 215 ns for PGA-PMA. The FBM analysis of the fluorescence decays led to the conclusion that excimer formation around the rigid α-helix backbone is severely hindered. The number of glutamic acid units within a *blob*, N_{blob}, decreased only slightly with decreasing probing time due to the compact geometry of the α-helical PGA. The PGA α-helix was modeled using *Hyperchem* software and the ability of two pyrene groups to encounter was evaluated as they were separated by increasing numbers of amino acids along the α-helix. The number of amino acids required for two pyrenes to lose their ability to overlap and form excimer matched closely the N_{blob} values retrieved using the FBM.

5.2 Introduction

Fluorescence dynamic quenching (FDQ) has been used for many years to study the end-to-end cyclization of polymers[1–3] as well as the intramolecular diffusional segmental encounters of a polymer chain.[4–7] The recent advent of the fluorescence blob model (FBM) has enabled the quantitative characterization of the long range polymer chain dynamics (LRPCD) of polymers randomly labeled with pyrene.[8] In these experiments, pyrene is excited by UV light and can fluoresce with its own natural lifetime (typically 200-300 ns) in the blue region of the spectrum (~380 nm), or it can diffusively encounter a ground-state pyrene and form an excimer species that fluoresces in the green region of the spectrum (~480 nm).[9] Analysis of the process of excimer formation provides information about LRPCD by treating an excimer formation event resulting from the encounter between an excited pyrene and a ground-state pyrene as being equivalent to the segmental encounter of those two monomer units of the polymer chain bearing the pyrene pendants.

The FBM characterizes the sub-volume inside a polymer coil probed by an excited pyrene attached onto the polymer while it remains excited. The sub-volume is referred to as V_{blob} and depends on the flexibility of the polymer chain and the lifetime of the pyrene monomer. Within the framework of the FBM, the lifetime of the pyrene monomer can be regarded as a given *probing time* for pyrene, with V_{blob} increasing or decreasing with a larger or smaller probing time, respectively.

The FBM has been applied to characterize the LRPCD of pyrene-labeled polystyrene (Py-PS)[10,11] and poly(*N*,*N*-dimethylacrylamide) (Py-PDMA) in dilute solution,[12,13] and Py-PDMA in semi-dilute PDMA solutions.[14] Use of an external quencher to reduce the natural lifetime of pyrene attached to PDMA was shown to yield a smaller V_{blob}, as expected from

the FBM fundamental assumption that a smaller probing time results in a smaller volume being probed.[13] More recently, the FBM was used to characterize how the length and rigidity of the linker used to attach the pyrene chromophore to the backbone affects the rate of excimer formation.[10] Assessing the magnitude of this effect is not trivial because it requires the ability to differentiate the contributions of the polymer backbone from those of the linker since both affect the dynamics of excimer formation. On the one hand, a very short linker enhances the contribution from the backbone motions, but decreases the pyrenes' ability to rearrange and form excimer. On the other hand, a long linker enables the pyrenes to rearrange more easily to form an excimer, but the motions of the longer linker might obscure the backbone dynamics.

These considerations illustrate some of the difficulties associated with the handling of the linker connecting the pyrene probe to the polymer backbone when trying to characterize the LRPCD of a pyrene-labeled polymer through the analysis of excimer formation events. Most importantly, they clearly highlight that the equivalence existing between pyrene encounters and segmental encounters between the monomers bearing those pyrenes holds only for one given type of linker and that fluorescence data obtained with a same polymer labeled with pyrene via two different linkers cannot be compared in a straightforward manner.[10] In view of the above, it would be valuable to fully characterize the effect that a type of linker has on the process of excimer formation between two pyrenes attached to a given polymer. To do so, conditions should be found that would enable the characterization of the motion of pyrene subject to the dynamics of the linker connecting it to the polymer without interference from the LRPCD of the polymer itself. Ideally this could be accomplished by finding a polymer system where LRPCD could be eliminated altogether.

To this end, poly(glutamic acid) (PGA) was chosen as the polymer backbone because it forms a rigid α-helix,[15] thus locking the backbone in place and eliminating the LRPCD over the time scale of the pyrene lifetime. Furthermore, PGA can be easily labeled with pyrene amino derivatives using linkers of different lengths.[16,17]

Two pyrene derivatives were chosen, 1-pyrenemethylamine (PMA) and 4-(1-pyrene)butylamine (PBA), whose primary amines can readily react with the carboxylic acids of PGA. The resulting pyrene-labeled polymers are referred to as PGA-PMA and PGA-PBA, respectively. Their structures are shown in Scheme 5.1 together with the structures of the Py-PS and Py-PDMA polymers previously studied. The fluorescence decays of these Py-PGA constructs were acquired and analyzed according to the FBM. The FBM analysis reflected the longer reach of the linker connecting pyrene to the α–helical backbone of the PGA-PBA construct by reporting a larger *blob* size characterized by the number of glutamic acids per *blob*, N_{blob}.

The experiments reported in this study demonstrate that the FBM is sensitive enough to accurately probe at the molecular level subtle changes induced by a mono-methylene and tetra-methylene linker used to connect pyrene to the PGA backbone. These experiments also provide quantitative information on the volume probed by an excited chromophore attached to a structured polypeptide. To the best of our knowledge, they represent the first attempt in the literature where fluorescence is used to characterize the dynamics of the side-chains of a polymer in the absence of LRPCD.

Py-PGA	Py-PDMA	Py-PS	
n=1, PGA-PMA n=4, PGA-PBA		CoA-PS	CoE-PS

Scheme 5.1: Structures of several pyrene-labeled polymers.

5.3 Experimental Section

Materials: Chemicals were purchased from Sigma-Aldrich (Milwaukee, WI) and used as received unless otherwise stated. Distilled in glass DMF was purchased from Caledon Laboratories (Georgetown, ON) and used as received. Two batches of PGA-sodium salt were purchased from Sigma-Aldrich with the following information: Batch 1: DP (viscosity) = 333, MW (viscosity) = 50.3 kg/mol, DP (MALLS) 141, MW (MALLS) 21.3 kg/mol. Batch 2: DP (viscosity) = 648, MW (viscosity) = 97.8 kg/mol, DP (MALLS) 274, MW (MALLS) 41.4 kg/mol. This range in molecular weights is not expected to affect the FBM parameters since the fluorescence experiments characterize the behavior of a pyrene inside a *blob* whose dimensions are usually much smaller than those of the polymer.[11] 4-(1-Pyrene)butylamine was purchased from Toronto Research Chemicals (Toronto, ON).

Synthesis of PGA-PMA and PGA-PBA: The synthesis and purification of pyrene-labeled PGA has been described elsewhere.[17] The only change made to the labeling procedure from Ref. 17 was the addition of two extra dialysis washes for the PGA-PBA samples to remove free PBA. The PGA-PBA solutions were first dialyzed twice against a 1:1 DMF:water mixture for 3 hours, followed by 4 days of dialysis against aqueous solutions following the same protocol as in Ref. 17.

Pyrene content determination: The pyrene content, λ_{Py}, expressed in μmol of pyrene per gram of polymer (μmol/g), was determined using Equation 5.1. The sodium salt of Py-PGA (PyPGNa) was dried using a Labconco Freezone 6 freeze drier prior to careful weighing of the polymer.[18] A mass, *m*, of freeze-dried PyPGNa was weighed and then dissolved in water where it was acidified using 1N HCl. The aqueous solution was then evaporated under a gentle flow of N_2 before the dry Py-PGA was subsequently dissolved in a known volume of DMF, *V*. The pyrene concentration [*Py*] was determined by UV-Vis absorption measurements using Beer-Lambert's Law applied to the pyrene absorption at 346 nm with an extinction coefficients of 40,000 $M^{-1}.cm^{-1}$ for PGA-PMA and 36,000 $M^{-1}.cm^{-1}$ for PGA-PBA, determined from the model compounds 1-pyrenemethanol and 1-pyrenebutanol, respectively. The absorption measurements needed to be conducted in DMF to prevent the distortion of the absorption spectra observed in aqueous solutions due to the formation of pyrene aggregates.[19]

$$\lambda_{Py} = \frac{[Py]}{m/V} \tag{5.1}$$

Steady-state fluorescence measurements: All fluorescence spectra were acquired on a PTI fluorometer using the usual right angle geometry with a 346 nm excitation wavelength. All PGA-PMA and PGA-PBA solutions were prepared in DMF with polymer concentrations below 2×10^{-6} M to avoid intermolecular excimer formation. Solutions were degassed for 20 minutes by bubbling a gentle flow of N_2 to remove oxygen. The monomer (I_M) and excimer (I_E) intensities were obtained by integrating the fluorescence spectra between 373 – 379 nm and 500 – 530 nm for the monomer and excimer, respectively.

Time-resolved fluorescence measurements: Monomer fluorescence decays were acquired for PGA-PMA and PGA-PBA solutions in DMF with various nitromethane concentrations (Table 5.1) using an IBH 5000F coaxial nanosecond flash lamp filled with H_2 gas with an excitation at 346 nm and emission at 376 nm. Excimer fluorescence decays were also acquired for PGA-PMA and PGA-PBA solutions in DMF with no quencher by exciting at 346 nm and collecting the emission at 510 nm. All decays were collected over 1024 channels with up to 20,000 counts at the peak maximum for the lamp and decay curves. The instrument response function was determined by applying the MIMIC method[20] to the lamp reference decays obtained with PPO [2,5-diphenyloxazole] in cyclohexanol (τ = 1.42 ns) and BBOT [2,5-bis(*tert*-butyl-2-benzoxazolyl)thiopene] in ethanol (τ =1.47 ns) for the monomer and excimer decays, respectively. The solutions were prepared in the same way as for steady-state fluorescence measurements.

Analysis of the fluorescence decays: The monomer and excimer fluorescence decays were fit with a sum of exponentials as shown in Equation 5.2. The monomer decays were also fit using Equation 5.3, which is based on the FBM analysis of the excimer kinetics.[8,11] Within the framework of the FBM, the polymer coil is compartmentalized into *blobs* among which

the pyrenes randomly attached to the polymer distribute themselves according to a Poisson distribution. The kinetics of excimer formation between pyrenes is handled in the same manner as if the *blobs* were surfactant micelles. Consequently, Equation 5.3 bears a strong resemblance with the equations that have been derived to describe the time-dependent concentration profile of chromophores located in a surfactant micelle loaded with quenchers.[21,22] Over the past ten years, the FBM has been used to study the dynamics of several polymers in dilute solution.[7,8,10–13]

$$i(t) = \sum_{i=1}^{n_{\exp}} a_i \exp(-t/\tau_i) \text{ with } n_{exp} = 3,4 \tag{5.2}$$

$$\left[Py^*\right]_{(t)} = \left[Py^*_{diff}\right]_{(t=0)} \exp\left[-\left(A_2 + \frac{1}{\tau_M}\right)t - A_3\left(1-\exp\left(-A_4 t\right)\right)\right] + \left[Py^*_{free}\right]_{(t=0)} \exp\left(-t/\tau_M\right) \tag{5.3}$$

The parameters A_2, A_3, and A_4 used in Equation 5.3 are expressed in Equation 5.4 as a function of the FBM parameters k_{blob}, $\langle n \rangle$, $k_e[blob]$.

$$A_2 = \langle n \rangle \frac{k_{blob} k_e[blob]}{k_{blob} + k_e[blob]} \quad A_3 = \langle n \rangle \frac{k^2_{blob}}{\left(k_{blob} + k_e[blob]\right)^2} \quad A_4 = k_{blob} + k_e[blob] \tag{5.4}$$

The first exponential in Equation 5.3 describes the behavior of the pyrene monomers that form excimer by the diffusive encounter of an excited pyrene and a ground-state pyrene. The unquenched lifetime of the pyrene monomer, τ_M, is determined from the monomer fluorescence decay of a polymer sparingly labeled with pyrene (pyrene content < 0.6 mol%) where more than 80% of the total pre-exponential weight is attributed to the long lifetime of

those isolated pyrenes which do not form excimer. τ_M was found to equal 215 and 155 ns for PGA-PMA and PGA-PBA in DMF, respectively. The parameters describing excimer formation are the rate constant for excimer formation between two pyrenes inside a *blob*, k_{blob}, the average number of pyrenes per *blob*, $<n>$, and the rate constant for ground-state pyrenes exchanging between *blobs* times the concentration of *blobs* inside the polymer coil, $k_e[blob]$. The second exponential in Equation 5.3 accounts for any unquenched pyrene monomer that is isolated and cannot form excimer within τ_M.

Optimization of the parameters used in Equations 5.2 and 5.4 to fit the fluorescence decays was performed using the Marquardt-Levenberg algorithm.[23] As done in previous publications a light scattering correction was applied to account for excimer formation that occurs on a time-scale too fast for our instrument to detect with accuracy.[24] The fits of the monomer decays were considered good if the χ^2 was less than 1.3 and the residuals were randomly distributed around zero.

Circular Dichroism: Circular dichroism (CD) experiments were carried out on a Jasco J-715 spectropolarimeter. A UV cell having a path length of 0.01 cm was used for PGA-PMA solutions in DMF with and without 8.64 mM of nitromethane. The pyrene concentrations of these solutions equaled ~2×10^{-3} M. Experiments were also carried out for PGA-PMA solutions in DMF containing 8.64 mM nitromethane and with a pyrene concentration of ~2×10^{-5} M. The CD spectra of these solutions were acquired with a UV cell having a path length of 1 cm. Ten scans were acquired from 250 to 400 nm and averaged. The integral of the molar ellipticity of the ^1B_b band of pyrene was integrated from 277 to 280.5 nm. Despite the weak signal due to the low labeling of the PGA-PMA samples, the PGA-PMA solutions in DMF with 8.64 mM nitromethane gave molar ellipticities that were identical, within

experimental error, to those of PGA-PMA in DMF alone and characteristic of oriented pyrenes attached onto an α-helix.[16,17] These experiments demonstrate that adding up to 8.64 mM nitromethane to PGA-PMA solutions in DMF does not alter the structure of the PGA α-helix (Figure A5.1 in the Appendix).

Efficiency of excimer formation: The bimolecular excimer formation rate constant, k_1, is the product of the collisional frequency, k_o, and the reaction probability per collision, p.[9] Given that the lifetime of an excited pyrene is affected by the type of linker used for attachment, it is possible that p for each pyrene derivative could be different as well. The probability p for PGA-PMA and PGA-PBA was evaluated using the model compounds 1-pyrenebutanol and 1-pyrenemethanol. Solutions of 1-pyrenemethanol and 1-pyrenebutanol in DMF with concentrations ranging from 1.3 mM to 11 mM were prepared. The monomer and excimer fluorescence decays of these solutions were acquired and fitted globally with a sum of two exponentials. The pre-exponential factors and decay times retrieved from the fits are listed in Table A5.1. The rate constant for excimer formation, k_1, and dissociation, k_{-1}, and the excimer lifetime τ_E were determined according to an analysis of the data listed in Table A5.1 based on the Birks scheme.[9] The parameters $k_1[M]$, k_{-1} and τ_E are also listed in Table A5.1. A plot of $k_1[M]$ versus $[M]$ is given in Figure A5.2. Two straight lines were obtained whose slopes yielded a k_1 value of $1.58\pm0.01 \times 10^9$ s^{-1} for 1-pyrenebutanol, while 1-pyrenemethanol took a 23% larger k_1 value of $1.96\pm0.01 \times 10^9$ s^{-1}. This difference is likely due to the smaller size of 1-pyrenemethanol. These experiments lead to the conclusion that 1-pyrenebutanol and 1-pyrenemethanol form excimer with a similar p values. Consequently, differences in the kinetic parameters obtained in the study of Py-PGA constructs cannot be attributed to differences in the p values of the two polymers.

Use of nitromethane as an external quencher: Several concentrations of nitromethane in DMF were used to shorten and control the long lifetime of the pyrene monomer for the PGA-PMA and PGA-PBA samples. The long lifetime was determined with PGA-PMA and PGA-PBA samples having a very low pyrene content (< 0.6 mol%). These samples yielded a biexponential decay where the pre-exponential weight of the longest decay time exceeded 80% of the total pre-exponential weight. The long decay time was attributed to the long lifetime of PMA or PBA for the nitromethane solution being used. The concentrations of nitromethane and monomer lifetimes for PGA-PMA and PGA-PBA are listed in Table 5.1. A Stern-Volmer plot[25] shown in Figure A5.3 gave quenching rate constants (k_q) of 1.81±0.05 × 10^9 s^{-1} and 2.10±0.05 × 10^9 s^{-1} for PGA-PMA and PGA-PBA, respectively. To determine whether the small difference in the quenching rate constant between the two different pyrene groups was due to the enhanced mobility experienced by pyrene connected to the PGA α-helix via a butyl linker, a Stern-Volmer plot was constructed with 1-pyrenemethanol and 1-pyrenebutanol using nitromethane as the quencher (Figure A5.3). k_q values of 2.97±0.05 × 10^9 s^{-1} and 3.22±0.05 × 10^9 s^{-1} were determined for 1-pyrenemethanol and 1-pyrenebutanol, respectively. Since k_q for 1-pyrenebutanol is 8% larger than for 1-pyrenemethanol, the 14% larger k_q value found for PGA-PBA is certainly due to an enhanced efficiency of nitromethane to quench a pyrene derivative having a butyl group vs. a methyl group in the 1-position.

Table 5.1: Concentrations of nitromethane in DMF and the corresponding long lifetimes of the PGA-PMA and PGA-PBA samples having a pyrene content of 0.5 mol% and 0.6 mol%, respectively.

PGA-PMA	
nitromethane (mM)	τ_M (ns)
0	215
0.26	192
0.59	175
1.01	154
1.71	131
3.01	100
4.88	75
8.64	49

PGA-PBA	
nitromethane (mM)	τ_M (ns)
0	155
0.53	130
1.73	96
3.23	75
6.42	50

5.4 Results

Steady-state fluorescence spectra were acquired for both PGA-PMA and PGA-PBA in DMF and are shown in Figure 5.1A and B. Since a longer-lived pyrene is expected to probe its surroundings for a longer time, it should form excimer more efficiently as it is likelier to encounter more ground-state pyrenes. To ensure that the long-lived 1-pyrenemethyl pendant of PGA-PMA would probe its surroundings for a similar time as the shorter-lived 1-pyrenebutyl pendant of PGA-PBA, the PGA-PMA solutions were spiked with 1.01 mM nitromethane to shorten the lifetime of PGA-PMA from 215 ns to 154 ns, the natural lifetime of PGA-PBA in DMF (Table 5.1). When studying pyrene labeled polymers, the I_E/I_M ratios are typically used as a first approximation of the rate of excimer formation.[1,8] The increase in I_E/I_M with increasing pyrene content observed for PGA-PMA and PGA-PBA in the insets

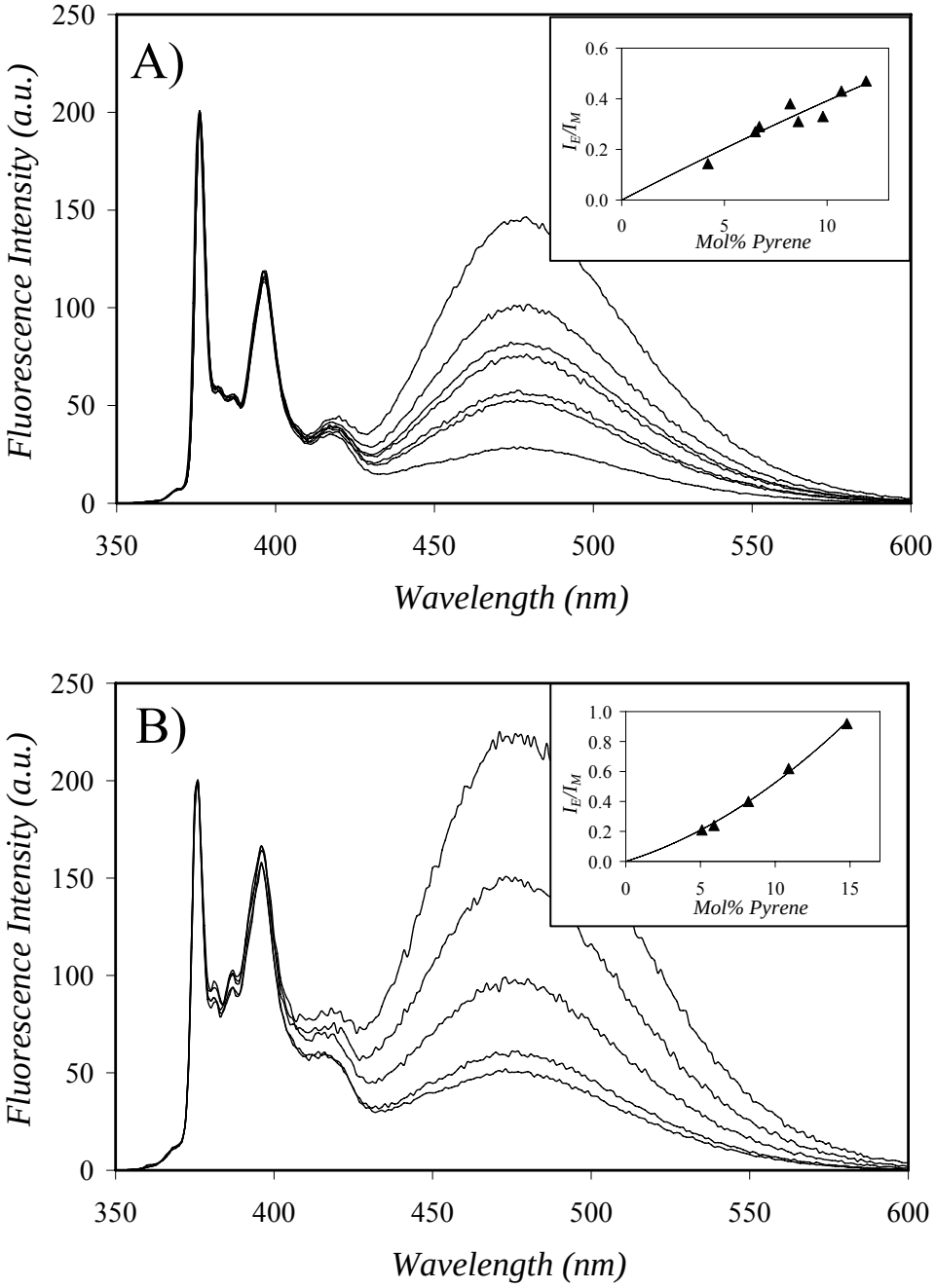

Figure 5.1: Steady-state fluorescence spectra of (A) PGA-PBA in DMF, (B) PGA-PMA in DMF with 1.01 mM nitromethane. The pyrene content increases from bottom to top. Inset: I_E/I_M ratios as a function of pyrene content, (A) PGA-PBA and (B) PGA-PMA. [Py] = 3×10^{-6} M, λ_{ex} = 344 nm.

of Figure 5.1 reflects the increase in the rate of excimer formation upon increasing the pyrene content of the polymer. Unfortunately, further comparison of the I_E/I_M ratios between PGA-PMA and PGA-PBA is hampered by the significant structural differences displayed by the monomer peaks of PMA and PBA in the fluorescence spectra (Figure 5.1). Indeed, the I_1/I_3 ratio of PGA-PMA and PGA-PBA equals 2.0 ± 0.1 and 3.7 ± 0.1, respectively. The first peak of PGA-PBA at 376 nm appears to be much larger than that of PGA-PMA. Since the first peak of the pyrene monomer is used to measure I_M for the ratio I_E/I_M, the difference in the spectral structures of PGA-PMA and PGA-PBA prevents the direct comparison of their I_E/I_M ratios.

Information on the dynamics of excimer formation can be retrieved from the analysis of the fluorescence decays acquired with the Py-PGA constructs. As for the steady-state fluorescence spectra, time-resolved monomer fluorescence decays were acquired using several concentrations of nitromethane to control the probing time of the pyrene group. The apparent rate constant for encounter, k_{exci}, is found by fitting the monomer decays with a sum of exponentials given in Equation 5.2 and calculating the number-average lifetime, $<\tau>$.[26] The parameters determined from the fits using Equations 5.2 are listed in Tables A5.2 and A5.3. k_{exci} is then calculated using Equation 5.5. A plot of k_{exci} as a function of pyrene content is shown in Figure 5.2 for Py-PGA with a τ_M adjusted to 154 ns for the PGA-PMA series by adding 1.01 mM nitromethane. The trends shown in Figure 5.2 indicate that PGA-PBA forms excimer at a faster rate than PGA-PMA. This is the first quantitative indication that the longer more flexible linker of PGA-PBA enables excimer formation at an increased rate compared to that of PGA-PMA.

$$k_{exci} = \frac{1}{<\tau>} - \frac{1}{\tau_M} \tag{5.5}$$

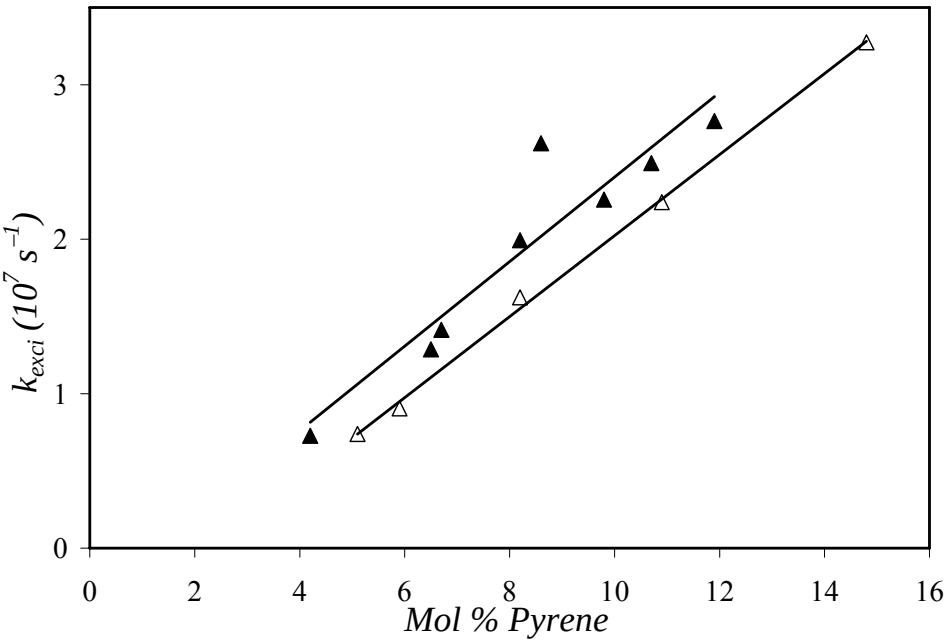

Figure 5.2: k_{exci} as a function of pyrene content. PGA-PBA in DMF (▲), PGA-PMA in DMF with 1.01 mM nitromethane (△). [Py] = 3×10^{-6} M.

The monomer decays were also fit according to Equation 5.3 to obtain the FBM parameters. Two examples of the quality of the fits using the FBM are shown in Figure A5.4. Within experimental error, k_{blob} and $k_e[blob]$ take a similar value for both PGA-PBA and PGA-PMA for the decays acquired with a probing time of ~155 ns, as shown in Figure 5.3 where they are plotted as a function of the corrected pyrene content. The corrected pyrene content in moles of pyrene per gram of polymer, λ_{Py}/f_{Mdiff}, is introduced in Figures 5.3 and 5.6 to account for those domains of the polymer that are pyrene poor and do not form any excimer. f_{Mdiff} represents the ratio $[Py^*_{diff}]_o / ([Py^*_{diff}]_o + [Py^*_{free}]_o)$, where a

measure of $[Py^*_{diff}]_o$ and $[Py^*_{free}]_o$ are obtained from fitting the monomer fluorescence decays with Equation 5.3. In most instances, f_{Mdiff} is close to 1.0 and represents a small correction. Since k_{blob} and $k_e[blob]$ take a constant value as a function of pyrene content, k^o_{blob} and $k_e[blob]^o$ are used to represent the average k_{blob} and $k_e[blob]$ values for a given probing time. k^o_{blob} and $k_e[blob]^o$ values for PGA-PMA and PGA-PBA are plotted as a function of probing time in Figure 5.4 by adjusting the lifetime of pyrene with known amounts of nitromethane (Table 5.1). Interestingly, the k^o_{blob} and $k_e[blob]^o$ values for the PGA-PMA series decrease with increasing lifetime from 50 to 155 ns, but changes little between 155 and 215 ns. The PGA-PBA series also shows a decrease in k^o_{blob} and $k_e[blob]^o$ with increasing lifetime from 50 to 155 ns, although this decrease is less pronounced than for the PGA-PMA series.

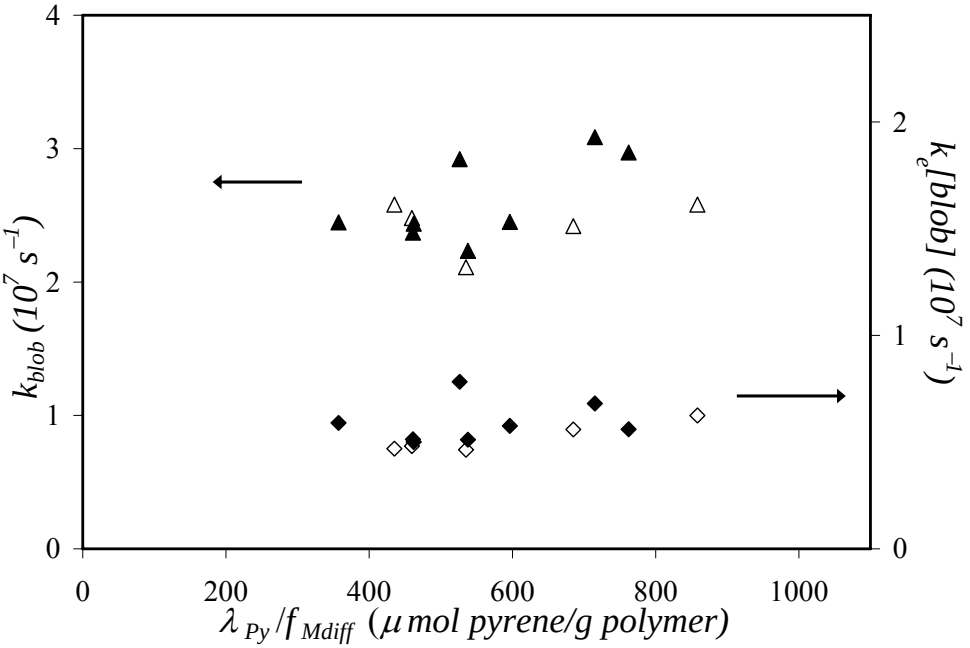

Figure 5.3: k_{blob} and $k_e[blob]$ as a function of the corrected pyrene content. PGA-PBA in DMF: k_{blob} (▲), $k_e[blob]$ (◆); PGA-PMA in DMF with 1.01 mM nitromethane: k_{blob} (△), $k_e[blob]$ (◇). [Py] = 3×10^{-6} M.

The change in the rate of excimer formation for PGA-PMA is also evident in a plot of k_{exci} determined with Equation 5.5 and shown in Figure 5.5 as a function of lifetime for two PGA-PBA and two PGA-PMA samples with pyrene contents of ~5 and ~11 mol%. k_{exci} decreases to a plateau value for the PGA-PMA series as the lifetime is increased from 50 to 150 ns, demonstrating that excimer formation occurs at a slower rate when a longer probing time is given. This conclusion is internally consistent with that drawn from the trends of k_{blob}^{o} and $k_e[blob]^o$ determined from the FBM analysis and shown in Figure 5.4.

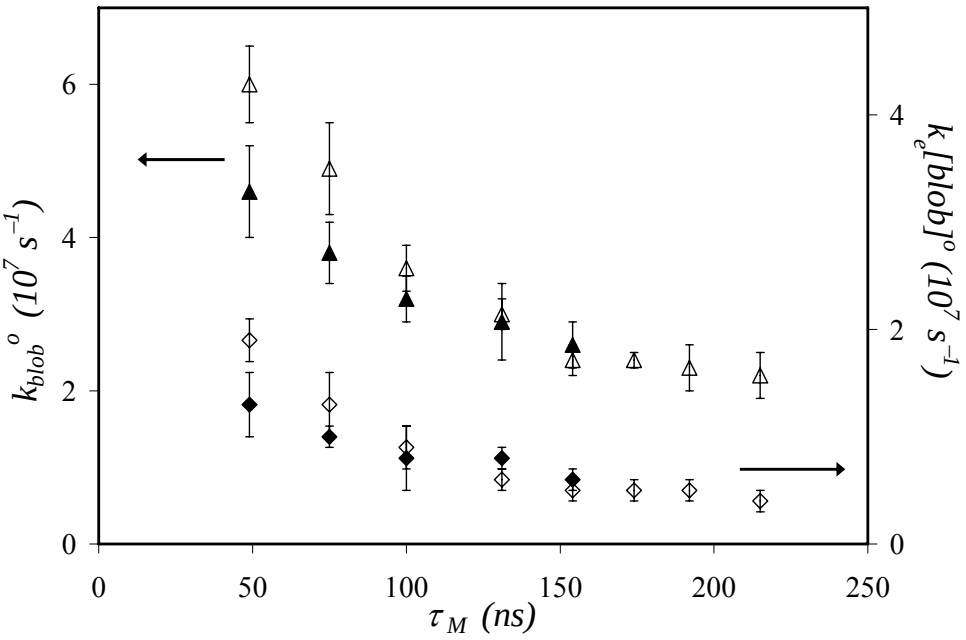

Figure 5.4: k_{blob}^{o} and $k_e[blob]^o$ as a function of pyrene lifetime. PGA-PBA: k_{blob}^{o} (▲) $k_e[blob]^o$ (◆); PGA-PMA: k_{blob}^{o} (△), $k_e[blob]^o$ (◇). [Py] = 3×10^{-6} M.

The average number of pyrenes per *blob*, <*n*>, retrieved from the analysis of the fluorescence decays are listed in Tables A5.5 and A5.6. For a given probing time, PGA-PBA has a higher average number of pyrenes per *blob* than PGA-PMA at all pyrene contents. This indicates that the *blob* size increases with the increased reach of the butyl spacer,

encompassing a larger number of pyrenes along the backbone. This longer reach is quantified by N_{blob}, which represents the number of monomers found in a *blob*. N_{blob} is calculated according to Equation 5.6, where M_{Py} is the molecular weight of the pyrene labeled monomer, 340 g/mol and 382 g/mol for the Glu-PMA and Glu-PBA units, respectively, M_{Glu} is the molecular weight of the glutamic acid monomer, 151 g/mol, x is the mole fraction of the pyrene labeled monomers in the polypeptide, λ_{Py} is the pyrene content of the Py-PGA sample in moles of pyrene per gram of polymer, and f_{Mdiff} is the fraction of pyrenes that form excimer by diffusion.

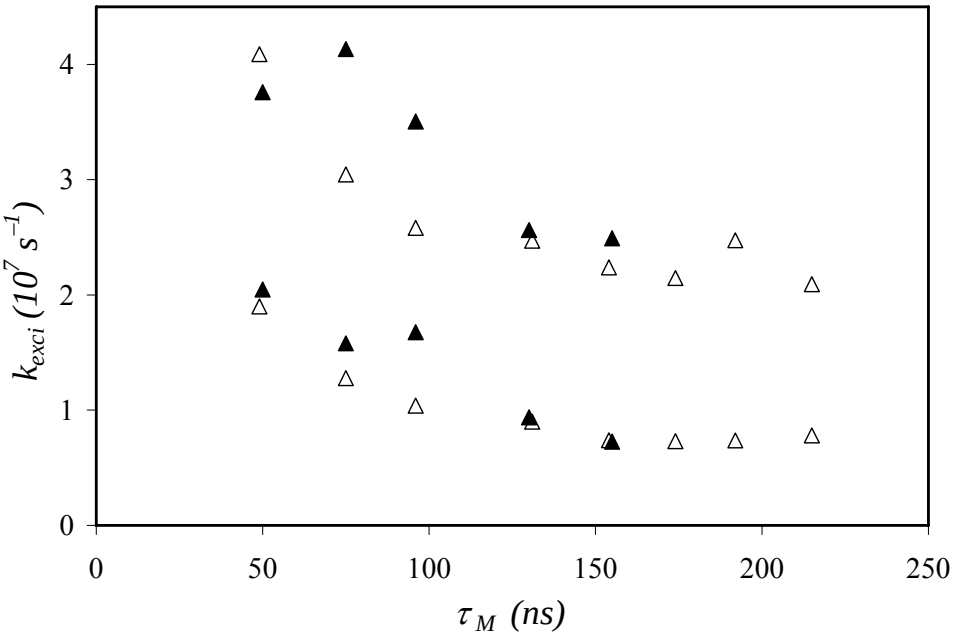

Figure 5.5: k_{exci} as a function of pyrene lifetime. The top samples contain ~ 11 mol % pyrene, the bottom samples contain ~6 mol% pyrene; PGA-PBA (▲), PGA-PMA (△). [Py] = 3×10^{-6} M.

$$N_{blob} = \frac{\langle n \rangle}{\lambda_{Py} / f_{Mdiff} \left[M_{Py}(x) + M_{Glu}(1-x) \right]} \tag{5.6}$$

The values of N_{blob} as a function of pyrene content are shown in Figures 5.6 A and B for PGA-PBA at 155, 96, and 50 ns and PGA-PMA at 215, 154, 100 and 50 ns, respectively. Slightly smaller N_{blob} values are obtained with increasing nitromethane concentration. This is expected since the addition of nitromethane shortens the lifetime of pyrene, and hence the probing time. Since N_{blob} decreases with increasing pyrene content, as has been observed for a variety of pyrene-labeled polymers,[10,11,17] the value of N_{blob}^{o} is found by extrapolating the N_{blob} trends shown in Figure 5.6 to zero pyrene content.[6,7] All N_{blob}^{o} values are shown in Figure 5.7 as a function of pyrene lifetime. The N_{blob}^{o} values are clearly larger for PGA-PBA compared to PGA-PMA at all probing times studied and they decrease slightly for both Py-PGA constructs with decreasing probing time.

5.5 Discussion

5.5.1 Effect of Linker length on N_{blob}

The data listed in Figure 5.7 indicate that a significant difference in N_{blob}^{o} exists between PGA-PMA and PGA-PBA at every probing time. However, N_{blob}^{o} changes little with probing time, increasing from 18.8 ± 0.6 to 21.8 ± 1.5 glutamic acid units for PGA-PMA and 25.7 ± 1.2 to 30.6 ± 1.5 glutamic acid units for PGA-PBA when the lifetime of pyrene increases from 50 to 155 ns. Typically, a change in N_{blob} reflects a change in V_{blob}, since a smaller V_{blob} will encompass a smaller number of monomers.[13] This relationship has been observed for two different Py-PSs in solvents having different viscosities,[27] as well as for Py-PDMA when the pyrene lifetime or the polymer concentration are changed.[13,14]

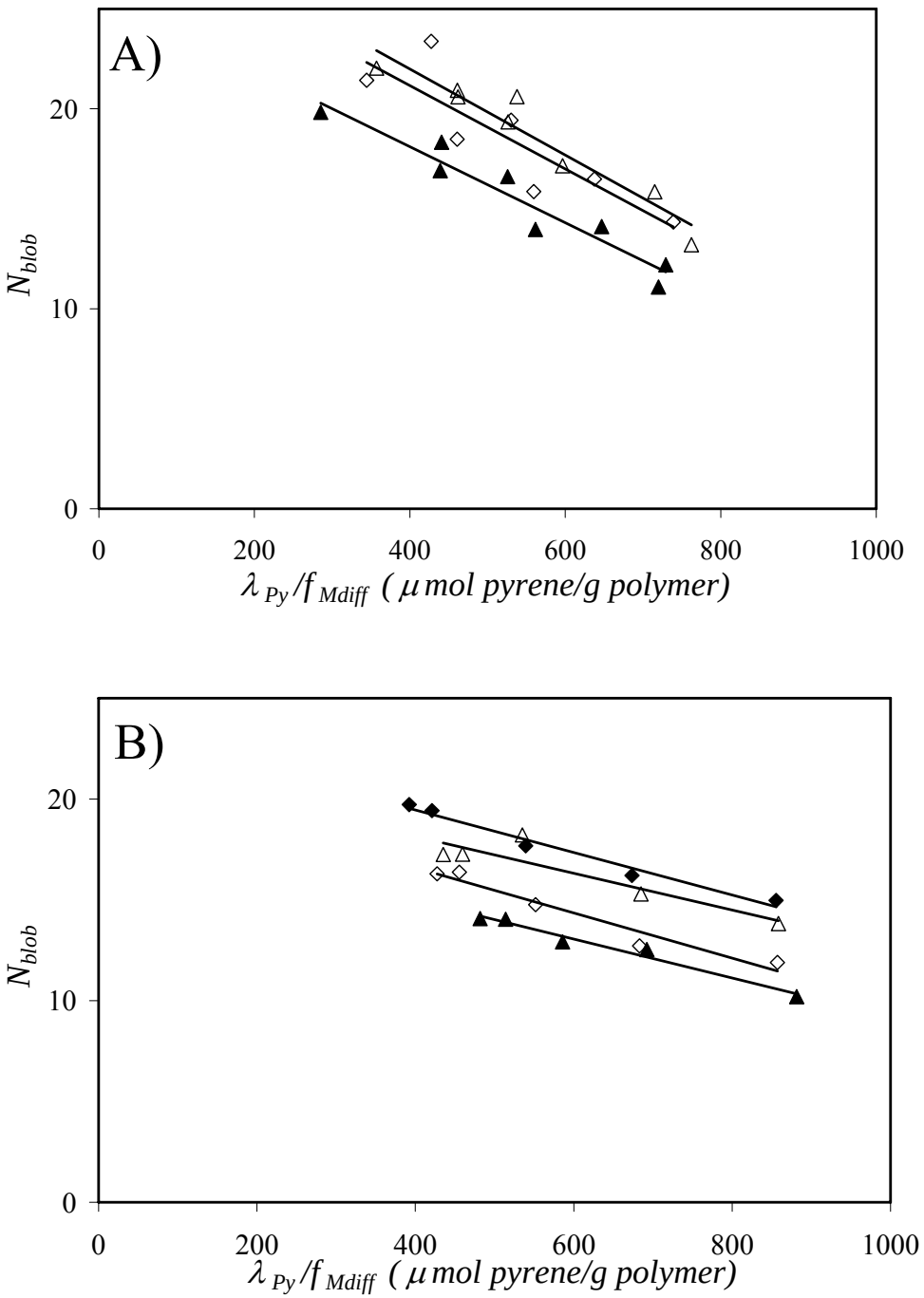

Figure 5.6: N_{blob} as a function of the corrected pyrene content. (A) PGA-PBA in DMF with nitromethane concentrations of 0, 1.73, and 6.42 mM, yielding probing times of 155 (△), 96 (◇), and 50 ns (▲); (B) PGA-PMA in DMF with nitromethane concentrations of 0, 1.01, 3.01, and 8.64 mM, yielding probing times of 215 (◆), 154 (△), 100 (◇), and 49 ns (▲).

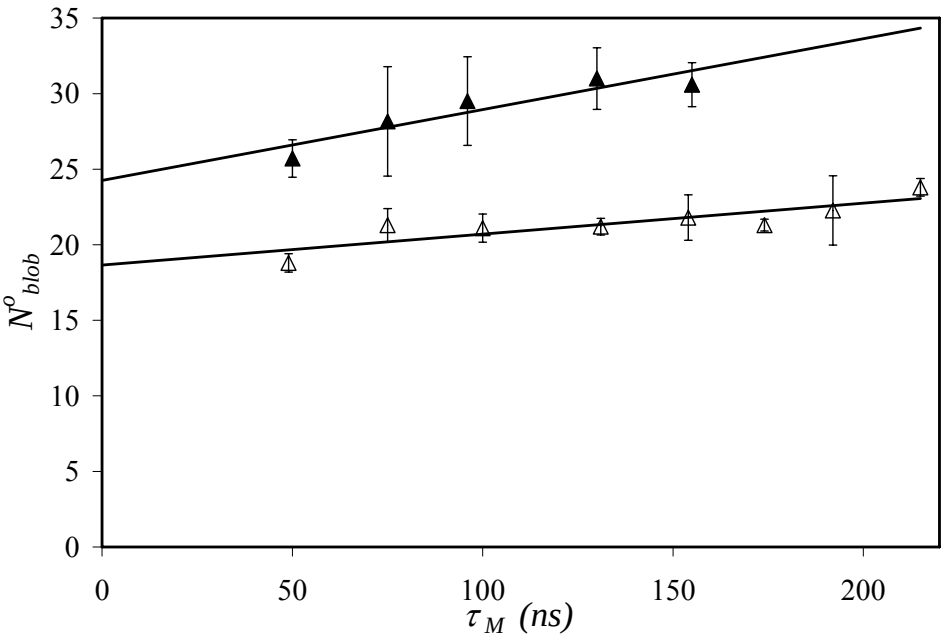

Figure 5.7: N^o_{blob} as a function of pyrene lifetime. PGA-PBA (▲), PGA-PMA (△). [Py] = 3 × 10^{-6} M.

Decreasing the lifetime of the chromophore,[13] increasing the solvent viscosity,[27] or the polymer solution concentration,[14] all decrease the volume probed by the chromophore while it remains excited, and this effect is detected by our fluorescence experiments. Unfortunately, V_{blob} can not be obtained directly by the FBM. A measure of V_{blob} is obtained with Equation 5.7. In Equation 5.7, the pseudo-unimolecular rate constant describing excimer formation from the diffusional encounter between one excited pyrene and one ground-state pyrene located inside the same *blob* is expressed as a product of a bimolecular rate constant for excimer formation by diffusion, k_{diff}, times the concentration equivalent to one ground-state pyrene in a *blob*, $1/V_{blob}$.

$$k_{blob} = k_{diff} \times \frac{1}{V_{blob}} \tag{5.7}$$

Thanks to Equation 5.7, a relationship was established for Py-PDMA in solution where V_{blob} was found to scale as N_{blob}^{α} where the exponent α equaled 3ν, ν being the Flory exponent equal to 0.5 in a θ solvent and 0.6 in a good solvent.[28] To obtain the scaling law $V_{blob} \propto N_{blob}^{\alpha}$, the FBM analysis was applied to the fluorescence decays of Py-PDMA in the presence of a quencher. For each quencher concentration, a pair of (k_{blob}, N_{blob}) values was obtained. Assuming that k_{diff} in Equation 5.7 is constant for a given type of pyrene labeled polymer, $-ln(k_{blob})$ was plotted as a function of $Ln(N_{blob})$ and the slope of the resulting straight line yielded the exponent α. The α-values retrieved for the $V_{blob} \propto N_{blob}^{\alpha}$ relationship with Py-PDMA agreed with the expected Flory exponents which reflect the low density of a polymer coil in solution.[13] A significant difference between Py-PDMA and the Py-PGA constructs is that Py-PGA is expected to adopt a much denser α–helical conformation in DMF resulting in a supposedly larger α-value for the $V_{blob} \propto N_{blob}^{\alpha}$ relationship.

To confirm this prediction, the k_{blob}^{o} values obtained in Figure 5.4 and the N_{blob}^{o} values obtained in Figure 5.7 were used to draw a plot of $-Ln(k_{blob})$ versus $Ln(N_{blob})$ in Figure 5.8. After approximating the trends in Figure 5.8 as straight lines, the slopes and corresponding α values were found to equal 4.6 ± 1.3 and 2.9 ± 0.5 for PGA-PMA and PGA-PBA, respectively. If V_{blob} were to scale as N_{blob}^{α}, the largest possible value that α could take equals 3 and it would be obtained for a highly compact polymer system. The exponent α found for PGA-PBA is close to 3.0, which suggests that the rigid PGA α–helix confines the pyrenes in a compact environment, much denser than the environment of a polymer coil for which α equals 1.5 or 1.8. On the other hand, the α value of 4.6 found for PGA-PMA is too large. It suggests that for the PGA-PMA constructs, k_{diff} does not remain constant with the

chromophore lifetime in Equation 5.7, but rather increases with decreasing lifetime. This is expected if the efficiency of excimer formation between two pyrenes increases with decreasing distance separating the two pyrenes, as is taking place upon shortening the pyrene lifetime. This effect appears to be pronounced for the PGA-PMA series where the shorter and more rigid linker connecting pyrene to the polypeptide backbone might favor excimer formation between two pyrenes attached onto nearby glutamic acids. This effect is not observed with PGA-PBA over the range of lifetimes studied, certainly thanks to the longer and more flexible PBA linker.

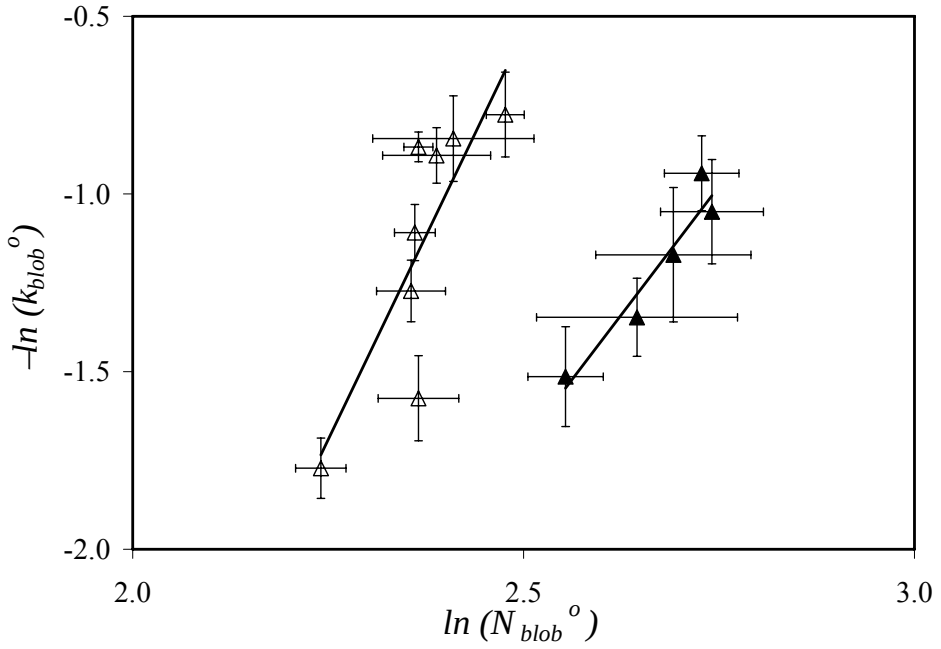

Figure 5.8: $-\ln(k_{blob}^{o})$ as a function of $\ln(N_{blob}^{o})$. PGA-PBA (▲), PGA-PMA (△).

5.5.2 Effect of Linker length and Probing Time on k_{blob}

Experimentally, both PGA-PMA and PGA-PBA exhibit very similar k_{blob} values when the lifetime of PGA-PMA (215 ns) is brought down via fluorescence quenching to the natural lifetime of PGA-PBA (Figure 5.3). If both PGA constructs were to form excimer with a similar k_{diff}, Equation 5.7 would imply that both constructs share a same V_{blob} as expected from the definition of a *blob*, a *blob* being the volume probed by a pyrene while it remains excited. However, the assumption that PGA-PMA and PGA-PBA could share the same k_{diff} seems highly unlikely based on the chemical structure of the linkers. The shorter PGA-PMA linker is expected to be much stiffer than the longer linker of PGA-PBA. Furthermore, the N_{blob} values obtained in Figure 5.6 indicate that V_{blob} for PGA-PBA is larger than for PGA-PMA, as expected from the longer reach enabled for pyrene by the longer and more flexible PGA-PBA linker. Thus a more plausible explanation of the results is that both k_{diff} and V_{blob} are larger for PGA-PBA than for PGA-PMA due to differences in linker length and flexibility. But since k_{blob} is the ratio of k_{diff} over V_{blob}, this effect is cancelled. This conclusion agrees with the one drawn from a study conducted on pyrene-labeled polystyrenes where the construct with the longer and more flexible linker connecting pyrene to the polystyrene backbone was also found to yield larger k_{diff} and V_{blob} values.[10]

The k^o_{blob} values recovered for both PGA-PBA and PGA-PMA are larger than those found for the vinyl polymers Py-PS and Py-PDMA studied previously. With only side-chain motions possible for Py-PGA in DMF and a same lifetime of 215 ns, k^o_{blob} for PGA-PMA averages 2.2±0.3 × 10^7 s^{-1}, compared to 1.0±0.1 × 10^7 s^{-1}, 0.9±0.2 × 10^7 s^{-1} and 1.1±0.1 × 10^7 s^{-1} for CoE-PS,[27] CoA-PS,[27] and Py-PDMA[12] in DMF, respectively. The structures of CoE-PS, CoA-PS and Py-PDMA are given in Scheme 5.1. The substantially larger k^o_{blob}

values obtained for the Py-PGA samples certainly reflects the smaller volume V_{blob} probed by an excited pyrene when it is attached to the Py-PGA backbone that does not undergo LRPCD.

Considering k^o_{blob} over the entire range of lifetimes as shown in Figure 5.4, k^o_{blob} for PGA-PMA exhibits an interesting trend. As the probing time is increased from 50 to 155 ns, k^o_{blob} decreases strongly before reaching a plateau between 155 and 215 ns. This decrease in k_{blob} with an increase in lifetime typically indicates an increase in V_{blob}.[13] However, based on the relationship $k_{blob} \sim N_{blob}^{4.6}$ for PGA-PMA in Figure 5.8, the decrease in k_{blob} is too steep to represent a change in V_{blob} only, and indicates that k_{diff} is also changing. For k_{diff} to be affected by the probing time, excimer formation around the α-helix must be severely hindered by the rigid molecular structure. This conclusion is supported by comparing the results obtained with the Py-PGA constructs and earlier cyclization experiments. End-to-end cyclization experiments were conducted as a function of chain length for pyrene labeled polystyrenes where pyrene had a lifetime of ~200 ns.[29] As the polymer chain length N was increased, the rate constant of excimer formation, k_{cyc}, was observed to decrease as N^{γ}, where $\gamma = 1.62$. If it were to take 150 ns for two pyrenes to probe their local surrounding as the data shown in Figures 5.4 and 5.5 suggest, it would be highly unlikely that any change in k_{cyc} with N would have been observed since k_{cyc} would depend only on the rate at which the pyrene end groups rearrange locally, regardless of N. Since a decrease in k_{cyc} is observed with increasing N, it implies that the pyrenes located at the ends of a flexible chain probe their local environment at a rate k_{loc} which is much larger than k_{cyc}, as illustrated in Scheme 5.2. The fact that $k_{loc} \sim k_{blob}$ for the Py-PGA constructs, since the LRPCD described by k_{cyc} in Scheme 5.2 are prevented by the rigid α-helix, and that k_{blob} for PGA-PMA plateaus at

150 ns suggests that in the absence of LRPCD in the α-helix, the rigid backbone hinders the motions of the side-chains quite significantly, resulting in less efficient excimer formation for the PGA-PMA series.

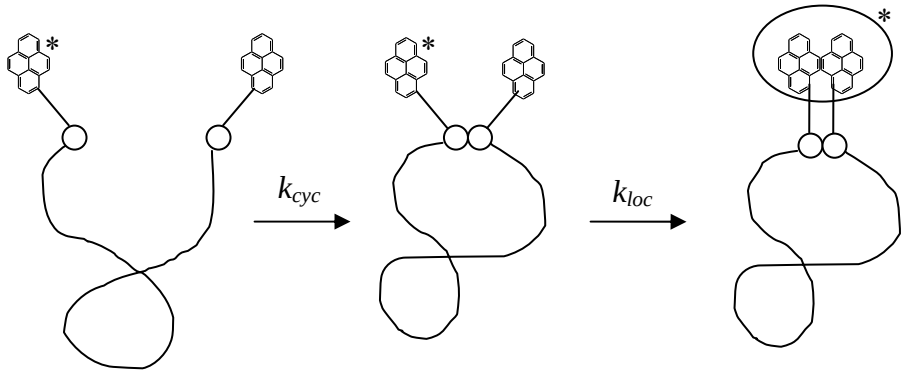

Scheme 5.2: Excimer formation involving polymers end-labeled with pyrene.

The timescale of side-chain motions has also been studied by other techniques such as NMR by using T1, T2, and NOE experiments carried out on peptides containing amino acids with methyl groups in their side-chain such as alanine and leucine.[30–32] Analysis of the T1, T2, and NOE data is based on a model originally developed by Lipari and Szabo[30] that has been used extensively to study the time-scale of side-chain motions in proteins typically found in the 20-100 picosecond range. More recently, the methyl groups of the leucine and isoleucine residues in some proteins have been found to undergo much slower dynamics with an associated correlation time around 2 ns.[31,32] Although these motions occur in the nanosecond timescale, the correlation times found by NMR describe dynamics which are still between one and two orders of magnitude faster than those found with k_{blob}^{o} (~2.2±0.3 10^7 s^{-1}) for τ_M > 150 ns. The discrepancy observed between the time scales described by the

correlation times τ_c obtained by NMR and k_{blob}^{o} obtained with the FBM are most certainly due to the amplitude of the motions probed by either technique. The distance, *d,* separating the methyl group of alanine or leucine from the peptide backbone equals 1.5 and 3.8 Å, respectively, whereas *d* equals 14 Å between the backbone and the center of the pyrenyl pendant for PGA-PMA. The motions probed by NMR and fluorescence are diffusion-controlled, which implies that τ_c^{-1} and k_{blob}^{o} are inversely proportional to the friction coefficient of the side-chain, itself proportional to the diameter of the bead used to approximate the side-chain. A measure of the bead diameter is given by *d*. Since *d* for the pyrene-labeled side-chains of PGA-PMA is respectively 9.3 and 3.7 times larger than *d* for alanine and leucine, the discrepancy found for τ_c^{-1} and k_{blob}^{o} is certainly a consequence of dealing with much bulkier probes when conducting fluorescence experiments.

5.5.3 Accuracy of the N_{blob} Parameter

A considerable benefit of the well-defined α-helical structure of Py-PGA is the ability to compare the experimental N_{blob}^{o} obtained using the FBM analysis to the known physical dimensions of a PGA α-helix. To this end, *Hyperchem* software (version 7.04) was used to create a 40 unit PGA α-helix labeled with two PMA or two PBA following a protocol which has been described in an earlier publication.[17] One pyrene group was first attached at the 8th glutamic acid, while the second pyrene was attached at the 9th glutamic acid. Molecular mechanics optimizations were performed on this construct with the Fletcher-Reeves algorithm in order to bring the plane of the two pyrenes within 3.4 Å from each other (Figure 5.9).[17] During optimization, only the pyrene groups and PGA side-chains were allowed to move while the backbone was held rigid. Keeping one pyrene attached on the 8th glutamic

acid, the second was then attached on a second glutamic acid located at position #9, 10, 11…33, and the optimization was conducted for each Py-PGA construct. The extent of pyrene-pyrene overlap was completed by counting the number of carbon atoms from the first pyrene that would be covered by the plane of the second pyrene. The number of overlapping carbons was determined for PGA-PMA and PGA-PBA and is shown as a function of the number of glutamic acids separating the two pyrenes in Figure 5.10. The overlap between two pyrenes worsens when the two pyrenes are separated by more than 11 and 17 Glu for PGA-PMA and PGA-PBA, respectively. The longer reach of the butyl linker of PGA-PBA enables a good overlap between the pyrene moieties over a longer stretch of α-helical PGA.

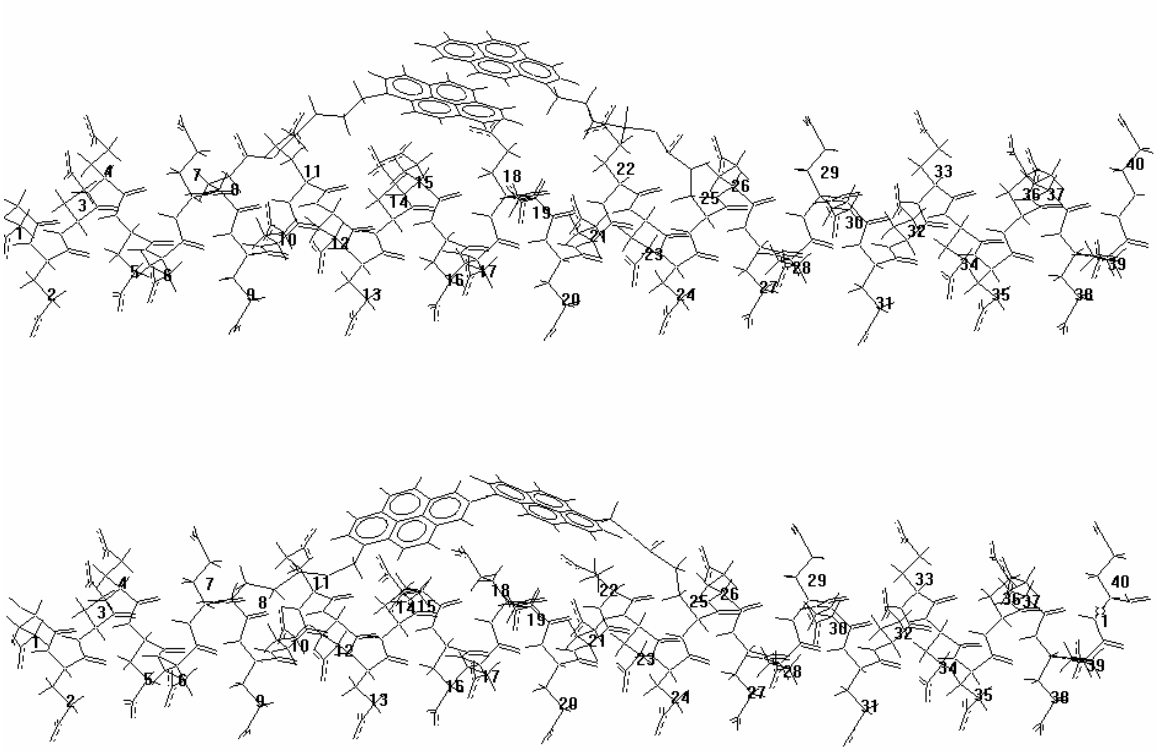

Figure 5.9: An illustration of the ability of two pyrene groups to overlap when separated by 17 Glu. Top: PGA-PBA; good overlap. Bottom: PGA-PMA; no overlap.

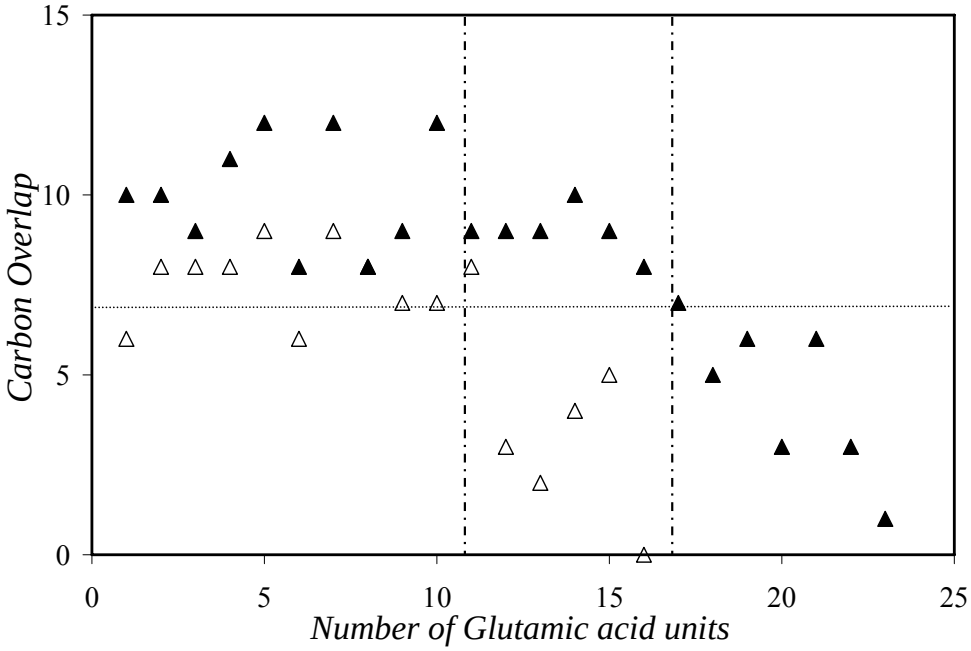

Figure 5.10: Pyrene carbon-overlap as a function of the number of glutamic acid units between pyrene groups. PGA-PBA (▲), PGA-PMA (△).

The number of overlapping carbons was much larger for PGA-PBA than for PGA-PMA and this with any number of Glu separating the two pyrene groups, even for those pyrenes that were only separated by a few amino acids (Figure 5.10). The increased capacity of the pyrene groups of PGA-PBA to overlap is due to the longer, more flexible butyl spacer that enables more rearrangements around the PGA α-helix than the shorter methylene linker of PGA-PMA can afford. N^{o}_{blob} values of 22 and 31 glutamic acids were obtained experimentally using the FBM for PGA-PMA and PGA-PBA with a probing time of 155 ns, respectively. Assuming that a PGA *blob* has an excited pyrene at its center, it would reach a ground-state pyrene located $N^{o}_{blob}/2$ amino acids upwards or downwards the α-helix. According to this statement, the maximum distance separating two pyrenes where they fail to overlap equals $N^{o}_{blob}/2 = 11$ for PGA-PMA or 15 for PGA-PBA. These conclusions obtained

from a FBM analysis of the fluorescence decays are in very good agreement with the predictions made based on the data shown in Figure 5.10 obtained via molecular mechanics optimizations.

5.6 Conclusions

Two Py-PGA constructs were prepared where the linker connecting pyrene to the polypeptide backbone was made of 5 (for PGA-PMA) or 8 (for PGA-PBA) atoms. The dynamics and amplitude of the motions of the pyrene pendants were characterized by studying their ability to form an excimer. To this end, the monomer fluorescence decays of the Py-PGA solutions were acquired and analyzed with the FBM. Information about the side-chain dynamics and amplitude was obtained with k^o_{blob} and N^o_{blob}, respectively. Interestingly, the rather minor change in the linker length from 5 to 8 atoms was clearly probed by the FBM, resulting in a concomitant increase of N^o_{blob} from 22 to 31 glutamic acids. The size of a PGA *blob* found by fluorescence was also determined from the cut-off distance estimated by molecular mechanics optimizations over which encounters between two pyrene moieties would be prevented by the spacing separating the two glutamic acids bearing the pyrenes. These optimizations resulted in N^o_{blob} values of 11×2+1 = 23 and 17×2+1 = 35, in excellent agreement with those of 22 and 31 obtained experimentally with the FBM.

The dynamics of the pyrenyl side-chains were described by the rate constant k_{blob} whose expression is given in Equation 7 as the ratio k_{diff}/V_{blob}. Comparison of the values of $ln(k^o_{blob})$ and $ln(N^o_{blob})$ in Figure 5.8 led to two important conclusions. First, a scaling relationship $k^o_{blob} \propto (N^o_{blob})^{\alpha}$ was found where α equaled 2.9 ± 0.5 and 4.6 ± 1.3 for PGA-PBA and PGA-

PMA, respectively. These α–values are much larger than those of 1.5 or 1.8 found for random polymer coils[28] and they reflect the more compact nature of the PGA α–helix. Second, the α–value of 4.6 found for PGA-PMA was larger than the maximum possible value of 3.0, which implies that k_{diff} increased as the pyrene lifetime decreased. This observation indicates that the shorter and more rigid linker of PGA-PMA induces some strain on the motion of the pyrenes. With longer lifetimes (τ_M > 150 ns), the linker is allowed enough time to probe those more strained conformations resulting in a small k^o_{blob} value. As the lifetime is shortened, the pyrenes can only probe those conformations which are less strained and k^o_{blob} takes a larger value.

Although the absence of LRPCD enabled the characterization of the side-chain dynamics of the Py-PGA constructs, it also introduced an unforeseen complication by straining and slowing down the motion of the side-chains. Thus the side-chain motions characterized in this study by their k^o_{blob} and N^o_{blob} values are certainly much slower for the structured α–helical PGA polypeptide than those found with the random coils of the Py-PS[10,11,27] and Py-PDMA[12-14] samples. Nevertheless, this study provides a novel procedure to investigate the side-chain dynamics of structured peptides and confirm the ability of the FBM to probe the motions of the pyrene label covalently attached to macromolecules at the molecular level.

5.7 References and Notes

1. Winnik, M. A. *Acc. Chem. Res.* **1985**, *18*, 73-79.

2. Cuniberti, C.; Perico, A. *Eur. Polym. J.* **1977**, *13*, 369-374.

3. Kane, M. A.; Panudey, S.; Baker, G. A.; Perez, S. A.; Bukowski, E. J.; Hoth, D. C.; Bright, F. V. *Macromolecules* **2001**, *34*, 6831-6838.

4. Cuniberti, C.; Perico, A. *Eur. Polym. J.* **1980**, *16*, 887-893.

5. Winnik, M. A.; Li, X.-B.; Guillet, J. E. *Macromolecules* **1984**, *17*, 699-702.

6. Lee, S.; Duhamel, J. *Macromolecules* **1998**, *31*, 9293-9200.

7. Picarra, S.; Relogio, P.; Alfonso, C. A. M.; Martinho, J. M. G.; Farinha, J. P. S. *Macromolecules* **2003**, *36*, 8119-8129.

8. Duhamel, J. *Acc. Chem. Res.* **2006**, 39, 953-960.

9. Birks, J. B. in *Photophysics of Aromatic Molecules*. Wiley: New York, 1970.

10. Ingratta, M.; Duhamel, J. *Macromolecules* **2007**, *40*, 6647-6657.

11. Mathew, H.; Siu, H.; Duhamel, J. *Macromolecules* **1999**, *32*, 7100-7108.

12. Kanagalingam, S.; Ngan, C. F.; Duhamel, J. *Macromolecules* **2002**, *35*, 8560-8570.

13. Kanagalingam, S.; Spartalis, J.; Cao, T.-M.; Duhamel, J. *Macromolecules* **2002**, *35*, 8571-8577.

14. Irondi, K.; Zhang, M.; Duhamel, J. *J. Phys. Chem. B* **2006**, *110*, 2628-2637.

15. Yamaoka, K.; Ueda, K. *J. Phys. Chem.* **1982**, *86*, 406-413.

16. Shoji, O.; Ohkawa, M.; Kuwata, H.; Sumida, T.; Kato, R.; Annaka, M.; Yoshikuni, M.; Nakahira, T. *Macromolecules* **2001**, *34*, 4270-4276.

17. Duhamel, J.; Kanagalingam, S.; O'Brien, T.; Ingratta, M. *J. Am. Chem. Soc.* **2003**, *125*, 12810-12822.

18. In previous work by Duhamel et al.,[17] the Py-PGA was purified using dialysis against aqueous solution. The aqueous solution was removed by rotary evaporation, and the polymer film was further dried under vacuum at 40 ^{o}C prior to pyrene content determination. In the current work, a Labconco freeze-drying system was used to recover the purified Py-PGA from aqueous solution. This difference has proven essential for accurate pyrene content determination, as it was determined that simple

vacuum drying did not remove all of the water from the polymer sample. Pyrene contents determined for the previous "wet" polymer samples were incorrect in some cases given that the mass of the polymer was actually lower than the amount weighed. This resulted in under-estimated pyrene content for some Py-PGAs. The pyrene content has the largest effect on the N_{blob} parameters reported in Ref. 17 as calculated by Equation 5.6. The N^{o}_{blob} value for Py-PGA reported in Ref. 17 dropped from 32 ± 1 to 27 ± 1 after the pyrene content of the Py-PGA samples had been re-determined after freeze-drying the samples and is very similar to the N^{o}_{blob} value of 24 ± 1 obtained in the current work.

19. Winnik, F. M. *Chem. Rev*. **1993**, *93*, 587-614.

20. James, D. R.; Demmer, D. R.; Verall, R. E.; Steer, R. P. *Rev. Sci. Instrum.* **1983**, *54*, 1121-1130.

21. Tachiya, M. *Chem. Phys. Lett.* **1975**, *33*, 289-292.

22. Infelta, P. P.; Graetzel, M.; Thomas, J. K. *J. Phys. Chem*. **1974**, *78*, 190-195.

23. Press, W. H.; Flannery, B. P.; Teukolsky, S. A.; Vetterling, W. T. *Numerical Recipes. The Art of Scientific Computing (Fortran Version)*; Cambridge University Press: Cambridge, 1992, p 523 – 528.

24. Demas, J. N. *Excited-State Lifetime Measurements*; Academic Press: New York, 1983, p 134, 147.

25. Lakowicz, *Principles of Fluorescence Spectroscopy*; Plenum Press: New York, 1983.

26. Winnik, M. A.; Egan, L. S.; Tencer, M.; Croucher, M. D. *Polymer* **1987**, *28*, 1553-1560.

27. See Chapter 3 in this thesis.

28. de Gennes, P.-G. *Scaling Concepts in Polymer Physics*; Cornell University Press: Ithaca, NY, 1979.

29. Redpath, A. E. C .; Winnik, M. A. *J. Am. Chem. Soc*. **1980**, *102*, 6869-6871.

30. Lipari, G; Szabo, A. *J. Am. Chem. Soc*. **1982**, *104*, 4559-45570.

31. Skrynnikov; N. R., Millet; O., Kay; L. E. *J. Am. Chem. Soc*. **2002**, *124*, 6449-6460.

32. Millet, O.; Mittermaier, A.; Baker, D.; Kay, L. E. *J. Mol. Biol*. **2003**, *329*, 551-563.

5.8 Appendix

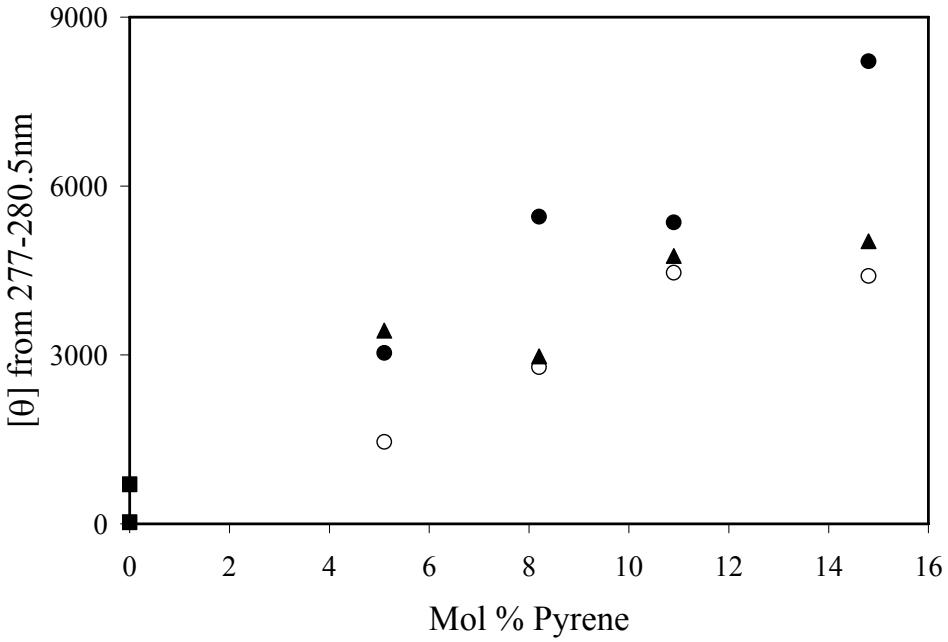

Figure A5.1: Average molar ellipticity values (277 – 280.5 nm) as a function of pyrene content. PGA-PMA in DMF, 0.01 cm cell (▲), PGA-PMA in 8.64 mM nitromethane in DMF, 0.01 cm cell (○), 1-pyrenylacrylamide in DMF, 0.01 cm cell (■); [Py] ~ 2×10^{-3} M. PGA-PMA in 8.64 mM nitromethane in DMF, 1.0 cm cell (●); [Py] ~ 2×10^{-5} M.

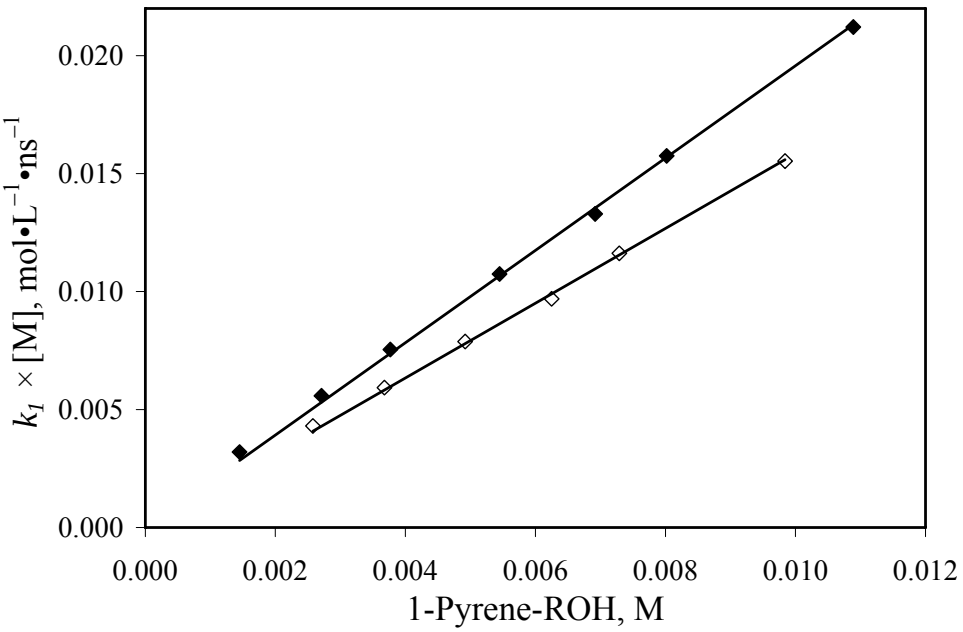

Figure A5.2: k_1[M] determined from the Birks' scheme as a function of pyrene content for 1-pyrenemethanol, (◆), and 1-pyrenebutanol, (◇).

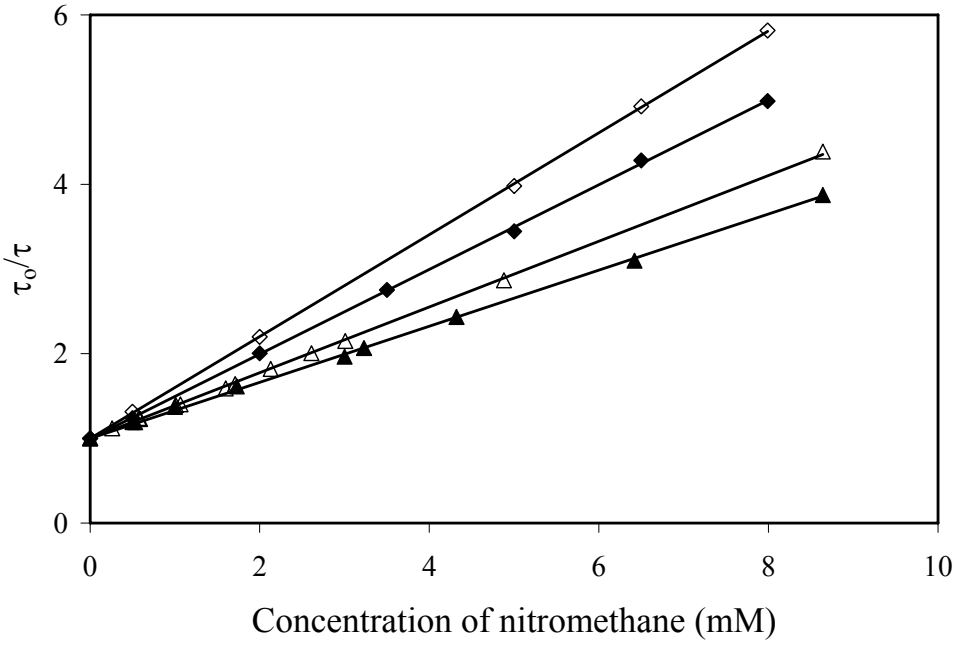

Figure A5.3: τ_o/τ as a function of nitromethane concentration in DMF. PGA-PBA (▲), PGA-PMA (△), 1-pyrenebutanol (◆), 1-pyrenemethanol (◇). [Py] = 3×10^{-6} M.

.

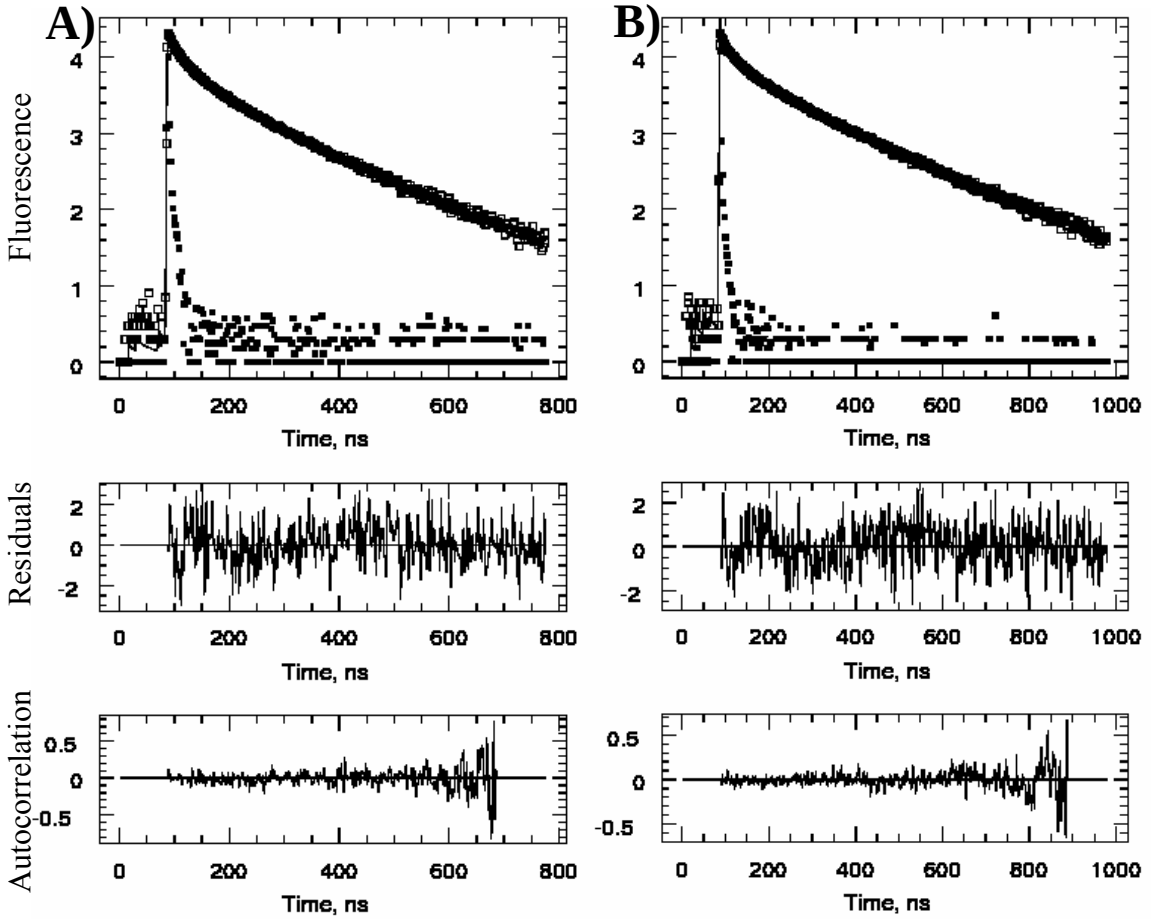

Figure A5.4: Monomer decays acquired in DMF for (A) a PGA-PBA sample labeled with 6.5 mol% pyrene, χ^2 =1.23, and (B) a PGA-PMA sample labeled with 5.9 mol% pyrene, χ^2 =1.10. λ_{ex} = 346 nm, λ_{em} = 376 nm, [Py] = 3×10^{-6} M.

Table A5.1: Parameters retrieved from the global analysis of the monomer and excimer fluorescence decays of 1-pyrenemethanol and 1-pyrenebutanol using several concentrations in DMF using Equation 5.2.

mol/L	χ^2	τ_1 (ns)	τ_2 (ns)	a_{M1}	a_{M2}	a_{E1}	a_{E2}	$k_1[M]$ (10^7 s^{-1}·mol·L^{-1})	k_{-1} (10^7 s^{-1})	τ_E (ns)
1-Pyrenemethanol										
0.00145	1.07	44	135	0.05	0.95	-0.72	0.74	0.32	0.33	54
0.00271	1.04	44	103	0.06	0.94	-0.90	0.92	0.56	0.17	49
0.00377	1.04	43	89	0.10	0.90	-1.07	1.10	0.75	0.17	49
0.00545	1.11	42	71	0.17	0.83	-1.44	1.46	1.07	0.13	47
0.00692	1.14	42	62	0.27	0.73	-1.97	1.99	1.33	0.09	48
0.00802	1.08	40	57	0.41	0.59	-2.05	2.07	1.57	0.09	47
0.01089	0.93	35	52	0.71	0.29	-1.97	1.99	2.12	0.09	47
1-Pyrenebutanol										
0.00134	1.06	44	128	0.07	0.93	-0.74	0.76	0.24	0.61	63
0.00258	1.00	42	108	0.10	0.90	-0.81	0.83	0.43	0.45	57
0.00368	1.11	42	96	0.15	0.85	-0.95	0.97	0.59	0.37	56
0.00492	1.03	41	84	0.19	0.81	-1.07	1.09	0.79	0.32	52
0.00625	1.06	40	76	0.25	0.75	-1.21	1.22	0.97	0.27	51
0.00729	1.07	38	71	0.33	0.67	-1.21	1.23	1.16	0.28	52
0.00984	1.08	35	63	0.49	0.51	-1.31	1.33	1.55	0.26	51

Table A5.2: Parameters retrieved from analysis of the monomer decays of PGA-PBA in nitromethane solution in DMF with Equation 5.2.

Sample	mol %	χ^2	τ_1	τ_2	τ_3	τ_4	a_1	a_2	a_3	a_4
0 mM	4.2	1.18	14	55	126	155	0.31	0.32	0.20	0.16
nitromethane	6.5	1.10	11	39	106	155	0.36	0.36	0.20	0.08
	6.7	1.03	8	31	93	155	0.31	0.40	0.25	0.07
τ_M=155ns	8.2	1.12	8	30	84	155	0.37	0.39	0.18	0.05
	8.6	0.93	9	28	71	155	0.37	0.40	0.23	0.00
	9.8	1.09	8	27	79	155	0.33	0.42	0.23	0.02
	10.7	1.25	8	28	84	155	0.45	0.37	0.14	0.04
	11.9	0.96	6	21	65	155	0.34	0.44	0.18	0.04
0.53 mM	4.2	1.13	8	37	99	130	0.27	0.33	0.26	0.15
nitromethane	6.5	1.11	6	23	71	130	0.25	0.38	0.26	0.10
	6.7	1.10	7	27	76	130	0.32	0.42	0.22	0.04
τ_M=130ns	8.2	1.10	5	20	60	130	0.32	0.42	0.23	0.04
	8.6	1.12	6	23	69	130	0.26	0.42	0.25	0.07
	9.8	1.09	3	13	41	130	0.19	0.40	0.31	0.10
	10.7	1.04	6	21	64	130	0.33	0.41	0.21	0.05
	11.9	1.04	5	18	54	130	0.33	0.45	0.18	0.04
1.73 mM	4.2	1.13	5	24	71	96	0.20	0.34	0.31	0.15
nitromethane	6.5	0.99	6	19	54	96	0.23	0.36	0.30	0.11
	6.7	1.03	4	18	52	96	0.24	0.45	0.29	0.02
τ_M=96ns	8.2	1.12	3	16	50	96	0.23	0.45	0.27	0.05
	8.6	1.11	8	18	53	96	0.24	0.40	0.27	0.10
	9.8	0.89	6	20	51	96	0.34	0.41	0.21	0.04
	10.7	1.11	6	19	55	96	0.34	0.42	0.20	0.04
3.23 mM	4.2	1.08	5	22	55	75	0.22	0.35	0.33	0.10
nitromethane	6.7	1.01	5	19	53	75	0.21	0.37	0.33	0.09
τ_M=75ns	8.2	1.05	4	15	40	75	0.26	0.43	0.27	0.03
	9.8	1.02	3	15	41	75	0.23	0.45	0.30	0.03
	10.7	1.16	5	18	50	75	0.41	0.42	0.17	0.00
6.42 mM	4.2	1.25	2	13	39	50	0.16	0.33	0.47	0.04
nitromethane	6.5	1.00	2	13	35	50	0.23	0.39	0.35	0.03
	6.7	1.06	2	11	30	50	0.19	0.41	0.36	0.04
τ_M=50ns	8.2	1.01	3	12	30	50	0.22	0.43	0.32	0.03
	8.6	1.02	4	13	34	50	0.20	0.41	0.36	0.05
	9.8	1.07	2	11	29	50	0.27	0.39	0.26	0.08
	10.7	1.03	3	12	32	50	0.22	0.44	0.30	0.04
	11.9	1.04	1	9	29	50	0.37	0.34	0.26	0.03

Table A5.3: Parameters retrieved from the FBM analysis of the monomer decays of PGA-PMA in nitromethane solution in DMF with Equation 5.2.

Sample	mol %	χ^2	τ_1	τ_2	τ_3	τ_4	a_1	a_2	a_3	a_4
0 mM	5.1	1.08	12	47	142	215	0.32	0.30	0.27	0.11
nitromethane	5.9	1.03	12	48	141	215	0.32	0.33	0.28	0.08
	8.2	1.02	11	46	128	215	0.40	0.36	0.20	0.04
τ_M=215ns	10.9	0.94	10	37	104	215	0.45	0.37	0.16	0.02
	14.8	0.92	7	27	83	215	0.44	0.42	0.14	0.02
0.26 mM	5.1	1.06	9	42	133	192	0.29	0.30	0.26	0.16
nitromethane	5.9	0.95	10	42	132	192	0.32	0.32	0.25	0.11
	8.2	1.02	1	40	113	192	0.41	0.37	0.19	0.03
τ_M=192ns	10.9	0.93	7	24	75	192	0.34	0.43	0.21	0.03
	14.8	1.16	8	25	71	192	0.43	0.41	0.15	0.01
0.59 mM	5.1	1.12	8	38	115	174	0.25	0.30	0.26	0.19
nitromethane	5.9	1.05	11	44	123	174	0.29	0.31	0.25	0.14
	8.2	1.05	13	49	123	174	0.42	0.36	0.19	0.02
τ_M=174ns	10.9	1.06	8	30	90	174	0.37	0.41	0.19	0.03
	14.8	1.70	5	22	67	174	0.38	0.43	0.17	0.02
1.01 mM	5.1	0.97	9	32	100	154	0.21	0.29	0.29	0.21
nitromethane	5.9	0.95	9	36	105	154	0.26	0.33	0.26	0.15
	8.2	1.16	9	33	91	154	0.34	0.38	0.24	0.05
τ_M=154ns	10.9	1.10	7	26	78	154	0.36	0.40	0.21	0.04
	14.8	1.10	7	25	73	154	0.43	0.41	0.15	0.01
1.71 mM	5.1	1.07	7	27	87	131	0.22	0.29	0.29	0.20
nitromethane	5.9	1.11	7	28	84	131	0.25	0.31	0.28	0.16
	8.2	1.05	8	30	82	131	0.34	0.36	0.24	0.05
τ_M=131ns	10.9	1.15	7	27	74	131	0.39	0.39	0.20	0.02
	14.8	1.03	7	24	62	131	0.45	0.38	0.16	0.01
3.01 mM	5.1	0.96	8	28	73	100	0.23	0.30	0.31	0.16
nitromethane	5.9	1.04	7	24	67	100	0.24	0.30	0.30	0.16
	8.2	1.01	7	22	60	100	0.29	0.34	0.30	0.07
τ_M=100ns	10.9	1.18	7	25	59	100	0.36	0.38	0.23	0.03
	14.8	1.14	3	14	41	100	0.33	0.44	0.22	0.01
4.88 mM	5.1	1.13	6	26	64	75	0.24	0.34	0.30	0.12
nitromethane	5.9	1.15	5	18	48	75	0.22	0.33	0.29	0.16
	8.2	1.12	4	16	40	75	0.35	0.38	0.23	0.03
τ_M=75ns	10.9	1.10	5	18	43	75	0.31	0.40	0.23	0.06
	14.8	1.30	3	14	37	75	0.34	0.45	0.20	0.01
8.64 mM	5.1	0.99	1	10	29	49	0.14	0.27	0.31	0.28
nitromethane	5.9	1.01	1	9	28	49	0.16	0.28	0.31	0.24
	8.2	1.11	2	10	29	49	0.15	0.36	0.35	0.13
τ_M=49ns	10.9	1.07	2	10	29	49	0.19	0.44	0.32	0.04
	14.8	0.93	2	9	24	49	0.24	0.41	0.31	0.04

Table A5.4: Parameters retrieved from analysis of the excimer decays of PGA-PBA and PGA-PMA in DMF with Equation 5.1.

Sample	mol %	χ^2	τ_1	τ_2	τ_3	a_1	a_2	a_3	a_{E-}/a_{E+}
PGA-PBA	4.2	1.12	16	63	97	-5.03	5.13	0.89	0.84
0 mM	6.5	1.14	15	60	87	-5.51	5.54	0.97	0.85
nitromethane	6.7	1.24	16	61	84	-3.90	4.14	0.84	0.78
	8.2	1.19	14	55	72	-4.22	3.50	1.72	0.81
τ_M=155ns	8.6	1.15	14	51	60	-2.79	2.88	0.91	0.74
	9.8	1.27	14	54	63	-3.97	3.73	1.23	0.80
	10.7	1.30	14	58	58	-3.01	3.48	0.54	0.75
	11.9	1.29	13	57	65	-3.39	3.27	1.12	0.77
PGA-PMA	5.1	1.17	13	66	169	-2.72	3.60	0.12	0.73
0 mM	5.9	1.20	13	67	171	-2.75	3.63	0.12	0.73
nitromethane	8.2	1.27	13	63	132	-2.63	3.49	0.13	0.72
	10.9	1.28	14	57	88	-1.95	2.55	0.40	0.66
τ_M=215ns	14.8	1.15	12	44	64	-1.55	0.82	1.73	0.61

Table A5.5: Parameters retrieved from the FBM analysis of the monomer decays of PGA-PBA in nitromethane solution in DMF with Equation 5.3.

Sample	mol%	f_{Mdiff}	f_{Mfree}	k_{blob} (10^7 s^{-1})	$k_e[blob]$ (10^7 s^{-1})	<n>	χ^2
0 mM	4.2	0.76	0.24	2.4	0.6	1.2	1.24
nitromethane	6.5	0.87	0.13	2.4	0.5	1.5	1.22
	6.7	0.90	0.09	2.4	0.5	1.6	1.24
τ_M=155ns	8.2	0.93	0.07	2.2	0.5	1.8	1.25
	8.6	0.99	0.01	2.9	0.8	1.7	1.19
	9.8	0.97	0.03	2.5	0.6	1.7	1.24
	10.7	0.92	0.08	3.0	0.6	1.7	1.15
	11.9	0.95	0.05	3.1	0.7	2.0	1.23
0.53 mM	4.2	0.77	0.23	2.3	0.5	1.2	1.27
nitromethane	6.5	0.89	0.11	3.0	0.6	1.5	1.28
	6.7	0.93	0.07	2.5	0.6	1.7	1.27
τ_M=130ns	8.2	0.96	0.04	2.9	0.8	1.8	1.23
	8.6	0.92	0.08	2.5	0.6	1.7	1.25
	9.8	0.89	0.11	3.5	1.4	1.7	1.08
	10.7	0.94	0.06	3.4	0.7	1.8	1.23
	11.9	0.95	0.05	3.2	0.8	2.1	1.22
1.73 mM	4.2	0.78	0.22	2.8	0.6	1.2	1.24
nitromethane	6.5	0.88	0.12	3.5	0.9	1.4	1.08
	6.7	0.97	0.03	2.7	0.7	1.6	1.21
τ_M=96ns	8.2	0.94	0.06	2.9	0.8	1.7	1.17
	8.6	0.91	0.09	3.4	0.8	1.5	1.25
	9.8	0.95	0.05	3.6	1.0	1.7	1.10
	10.7	0.95	0.05	3.2	0.7	1.8	1.24
3.23 mM	4.2	0.83	0.17	3.7	1.1	1.1	1.15
nitromethane	6.7	0.86	0.14	3.8	0.9	1.2	1.09
τ_M=75ns	8.2	0.96	0.04	3.7	1.1	1.7	1.16
	9.8	0.96	0.04	3.3	0.9	1.6	1.08
	10.7	0.94	0.06	4.5	1.2	1.6	1.21
6.42 mM	4.2	0.95	0.05	3.5	0.8	0.9	1.25
nitromethane	6.5	0.92	0.08	4.3	1.2	1.2	1.17
	6.7	0.94	0.06	4.9	1.7	1.3	1.26
τ_M=50ns	8.2	0.95	0.05	4.8	1.6	1.4	1.13
	8.6	0.93	0.07	4.3	1.3	1.3	1.07
	9.8	0.90	0.10	5.1	1.5	1.6	1.20
	10.7	0.96	0.04	4.2	1.0	1.5	1.12
	11.9	0.94	0.06	5.6	1.4	1.4	1.20

Table A5.6: Parameters retrieved from the FBM analysis of the monomer decays of PGA-PMA in nitromethane solution in DMF with Equation 5.3.

Sample	mol%	f_{Mdiff}	f_{Mfree}	k_{blob} (10^7 s^{-1})	$k_e[blob]$ (10^7 s^{-1})	<n>	χ^2
0 mM	5.1	0.84	0.16	2.5	0.4	1.2	1.26
nitromethane	5.9	0.88	0.12	1.9	0.3	1.3	1.1
	8.2	0.93	0.07	2.0	0.5	1.5	1.19
τ_M=215ns	10.9	0.97	0.04	2.4	0.5	1.8	1.08
	14.8	0.98	0.02	2.3	0.5	2.3	1.13
0.26 mM	5.1	0.79	0.21	2.5	0.4	1.2	1.29
nitromethane	5.9	0.84	0.16	2.4	0.4	1.3	1.20
	8.2	0.95	0.05	1.9	0.4	1.7	1.21
τ_M=192ns	10.9	0.97	0.03	2.6	0.6	1.9	1.17
	14.8	0.98	0.02	2.2	0.5	2.4	1.26
0.59 mM	5.1	0.76	0.24	2.5	0.5	1.2	1.27
nitromethane	5.9	0.80	0.20	2.3	0.4	1.3	1.17
	8.2	0.93	0.07	2.5	0.5	1.5	1.23
τ_M=174ns	10.9	0.96	0.04	2.3	0.5	1.8	1.22
	14.8	0.98	0.02	2.4	0.6	2.1	1.23
1.01 mM	5.1	0.76	0.24	2.6	0.5	1.2	1.03
nitromethane	5.9	0.81	0.19	2.5	0.5	1.3	1.10
	8.2	0.93	0.07	2.1	0.5	1.6	1.26
τ_M=154ns	10.9	0.95	0.05	2.4	0.6	1.8	1.24
	14.8	0.98	0.02	2.6	0.6	2.1	1.25
1.71 mM	5.1	0.77	0.23	3.3	0.6	1.1	1.20
nitromethane	5.9	0.81	0.19	3.0	0.6	1.2	1.27
	8.2	0.92	0.08	2.9	0.6	1.4	1.03
τ_M=131ns	10.9	0.96	0.04	2.7	0.6	1.7	1.31
	14.8	0.98	0.02	3.2	0.8	1.9	1.25
3.01 mM	5.1	0.77	0.23	3.5	0.8	1.1	1.05
nitromethane	5.9	0.81	0.19	3.6	0.7	1.2	1.12
	8.2	0.91	0.09	3.8	0.9	1.3	1.13
τ_M=100ns	10.9	0.95	0.05	3.9	1.1	1.5	1.29
	14.8	0.98	0.02	3.1	1.0	1.8	1.07
4.88 mM	5.1	0.72	0.28	5.0	1.3	1.1	1.27
nitromethane	5.9	0.80	0.20	4.5	1.1	1.2	1.23
	8.2	0.94	0.06	5.9	1.8	1.4	1.25
τ_M=75ns	10.9	0.92	0.08	4.4	1.5	1.5	1.25
	14.8	0.96	0.04	4.7	1.1	1.8	1.24
8.64 mM	5.1	0.68	0.31	6.6	2.0	1.1	1.05
nitromethane	5.9	0.72	0.28	6.2	2.0	1.1	1.10
	8.2	0.85	0.15	5.7	1.7	1.2	1.18
τ_M=49ns	10.9	0.94	0.06	5.3	1.6	1.5	1.22
	14.8	0.95	0.05	6.2	2.0	1.6	1.18

Chapter 6:
Study of the Chain Dynamics of Pyrene-Labeled Poly(Aspartic Acid)

6.1 Abstract

A series of pyrene-labeled poly(aspartic acid) (Py-PAA) was prepared by randomly labeling the carboxylic acid side-chains with 1-pyrenemethylamine. Steady-state fluorescence measurements using pyrene excimer formation and fluorescence resonance energy transfer, and size exclusion chromatography experiments were completed at low polypeptide concentration in *N*,*N*-dimethylformamide (DMF) and *N*,*N*-dimethylacetamide (DMA), with and without lithium chloride (LiCl). These experiments established that Py-PAA exhibits ionomer-like behavior in these solvents. The time-resolved monomer and excimer fluorescence decays were acquired and analyzed using a multi-exponential fit as well as a global analysis using the fluorescence blob model (FBM). Both analyses indicated that many pyrene groups were clustered along the backbone, resulting in a large fraction of the pyrene groups forming excimer at a very fast rate. To accommodate this fast excimer formation, the decay analysis required an extra rate constant, k_2, which was found to equal $13\pm1 \times 10^7$ s^{-1} and $12\pm1 \times 10^7$ s^{-1} in DMF and DMA, respectively, over 10 times larger than the rate constant for diffusion controlled excimer formation inside a blob, k_{blob}, determined to equal $\sim 0.80\pm0.15 \times 10^7$ s^{-1} in DMF and DMA. N_{blob}, the number of aspartic acid units constituting the coil sub-volume probed by an excited pyrene, was determined to remain constant in DMF and DMA with values of 114±12 and 99±8, respectively. The addition of LiCl did not significantly affect k_2, k_{blob}, or N_{blob}. This study led to three major conclusions. Firstly, Py-PAA behaves as a polyelectrolyte in polar organic solvents, secondly, the pyrene groups are clustered along the backbone which greatly complicates the analysis of the time-resolved fluorescence decays, and thirdly, excimer formation is not controlled by the solvent viscosity, a clear contrast to other pyrene labeled polymers that have been studied previously.

6.2 Introduction

The determination of the time scale over which proteins and peptides fold into their native structure is the focus of intense research. This is due to the complex nature of the folding process, with countless combinations of amino acid sequences that can interact to form distinct secondary, tertiary, and quaternary structures, all specific for the function of the protein. Much of the experimental work in recent years has utilized time-resolved techniques such as temperature[1] and pressure[2] jumps, photochemical initiation,[3] and pH jumps[4] to induce the folding of a disordered protein. The folding process can be monitored with circular dichroism (CD)[3b] and infrared spectroscopy (FT-IR)[5] to assess the secondary structure content, NMR spectroscopy[6] to monitor the time-scale of the motions of the backbone[6c] and side-chains[6d], or small angle x-ray scattering (SAXS)[7] to monitor the change in the dimensions of the protein as it collapses from a random coil to a compact globule.

To complement these methods, time-resolved fluorescence dynamic quenching (FDQ) or triplet-triplet energy transfer (TTET) can be utilized to monitor chain dynamics. Fluorescence is ideal because its high sensitivity enables the use of very dilute solutions that avoid intermolecular interactions. End-to-end cyclization experiments are one application of fluorescence that has been used for many years to study polymer chain dynamics.[8] More recently, cyclization experiments have been conducted on short polypeptides, generating a large body of results towards the "speed-limit" of protein folding.[9–14] Kiefaber et al. have used TTET to monitor the chain dynamics of polypeptides as a function of chain length and peptide composition.[9–11] In addition, Nau et al. used peptides end-labeled with a chromophore and its quencher to describe chain dynamics as a function of chain length and temperature.[11–13] However, characterizing the mobility of the chain ends may not be

representative of the dynamics experienced by those monomer units in the middle of the chain, and constitutes the first of three important drawbacks associated with the study of end-to-end cyclization to characterize chain dynamics.[15] The second drawback is that only short chains can be used in order to generate enough cyclization events to be monitored. The longest peptide studied thus far was made of 57 peptide bonds and cyclization was monitored using triplet-triplet energy transfer.[9–11] The third drawback is that only the chain ends are monitored during the experiment, leaving the middle of the chain invisible.

Interestingly, these limitations can be avoided by labeling the entire chain of a higher molecular weight polypeptide with the appropriate set of chromophores. Pyrene is often preferred to study polymer chain dynamics because of its high quantum yield, its long lifetime, and its ability to act both as a chromophore and its own quencher, thus simplifying the labeling procedure.[16] The fluorescence decays generated by polymers randomly labeled with pyrene are analyzed with the fluorescence blob model (FBM).[17] The FBM is crucial to handle the multi-exponential decays that can be produced by the infinite number of rate constants for excimer formation resulting from the distribution of chain lengths separating every two pyrene groups randomly attached along the polymer. However, a major restriction in using pyrene is that it is extremely hydrophobic and will associate in aqueous solutions. Thus, organic solvents must be used to study the chain dynamics of polymers labeled with pyrene.

The goal of this work is an exploratory study of the chain dynamics of polypeptides randomly labeled with pyrene groups in organic solvents. Polypeptides are generally more complicated than vinyl polymers due to their complex composition based on 20 amino acids displaying different functionalities and hydrophobicities. Poly(aspartic acid) (PAA) was

selected as a model polypeptide for this study due to its ease of labeling the carboxylic acid groups with pyrene, and its potential importance to industry as a mass produced biocompatible polymer.[18–22] Many studies have been completed in recent years to examine the biodegradability of PAA under various environmental conditions,[18,19] and its potential as a biodegradable polymer for use in drug delivery applications.[20–22] For large scale manufacture, PAA is typically synthesized by acid catalyzed thermal condensation of L-aspartic acid to form poly(succinimide) followed by hydrolysis to yield PAA with a mixed microstructure of α– and β–aspartic acid units as shown in Scheme 6.1.[23] The mixed microstructure of PAA makes it more difficult for this polyelectrolyte to adopt a stable, well-defined secondary structure as the α-helical poly(glutamic acid) does. For this reason, PAA with a mixed microstructure appears to be ideal to study the chain dynamics of a polypeptide adopting a random conformation in solution.

The experiments reported in this study illustrate the similarities and differences between the chain dynamics exhibited by a series of pyrene-labeled PAA (Py-PAA) samples in a variety of solvents, namely *N*,*N*-dimethylformamide (DMF), *N*,*N*-dimethylacetamide (DMA), DMF with 1 g/L lithium chloride (LiCl), and DMA with 1 g/L LiCl. DMF and DMA are very similar solvents in terms of polarity and hydrogen-bonding capabilities,[24] but the viscosity of DMA is nearly 2.5 times greater than that of DMF. LiCl is used to shield any charges generated by the carboxylic acids along the backbone or the amine end group. The results of the fluorescence experiments obtained with Py-PAA will also be compared with those obtained with three pyrene-labeled vinyl polymers, namely polystyrene (Py-PS),[25] poly(*N*,*N*-dimethylacrylamide) (Py-PDMA), and poly(acrylic acid) (Py-PAcrylA), and a

polypeptide, namely poly(glutamic acid) (Py-PGA). Drawing from these comparisons, conclusions are made about the behavior and chain dynamics of Py-PAA in solution.

6.3 Experimental Section

Materials: Chemicals were purchased from Sigma-Aldrich (Milwaukee, WI) and used as received unless otherwise stated. HPLC grade *N*,*N*-dimethylacetamide (DMA) was purchased from Aldrich and used as received. ACS grade ethyl ether was purchased from EMD Chemicals Inc. and used as received. Distilled in glass *N*,*N*-dimethylformamide (DMF) was purchased from Caledon Laboratories (Georgetown, ON) and used as received. Poly(aspartic acid) (PAA) sodium salt was purchased from Sigma-Aldrich which provided the following product information: DP viscosity = 235, MW (viscosity) = 32.2 kg/mol, DP (MALLS) 172, MW (MALLS) 23.6 kg/mol.

Structural determination of PAA: PAA is known to form succinimide rings during synthesis.[26] Opening of the succinimide rings yields α– or β–linkages as shown in Scheme 6.1. For this reason, the ratio of α– or β–aspartic acid linkages present in the commercially available PAA sample was determined by ^{1}H NMR. The ^{1}H NMR spectra of PAA in D_2O is shown in Figure A6.1 in the Appendix. A proton with a chemical shift of 4.3 or 4.5 ppm represents a CH proton being part of a β– or α–linkage, respectively.[27] The ratio of the peak intensities at 4.3 and 4.5 ppm gives a ratio of α/β linkages of 30/70. To account for the irregular composition of the PAA backbone, the pyrene content is referred to in terms of the number of *pyrene per backbone atom* (p.p.b.a), with one aspartic acid residue represented by 3.7 backbone atoms. For example, a Py-PAA sample with 10 mol% of the aspartic acid

residues labeled with a pyrene group bears 0.10 ÷ 3.7 = 0.027 p.p.b.a.; also note that using this labeling method, the maximum number of p.p.b.a. is 1 ÷ 3.7 = 0.27.

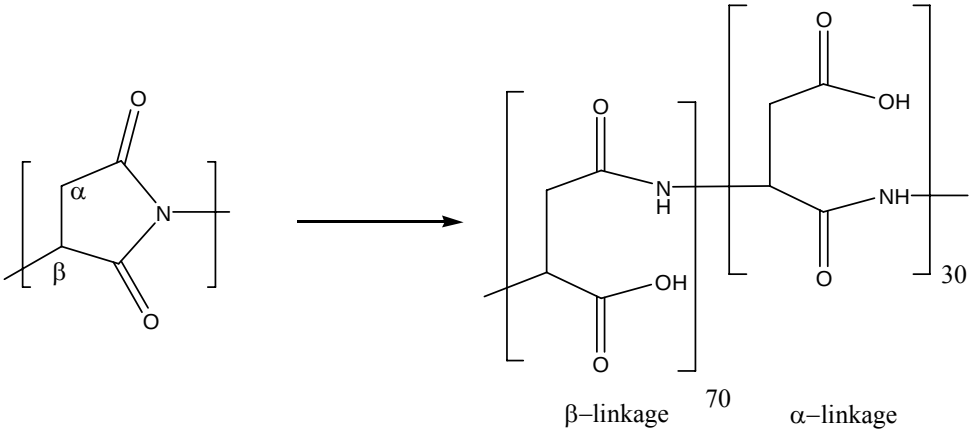

Scheme 6.1: Succinimide ring opening into an α– or β–linkage.

Synthesis of pyrene labeled poly(aspartic acid) (Py-PAA), naphthalene-labeled poly(aspartic acid) (Np-PAA), and pyrene-labeled poly(acrylic acid) (Py-PAcrylA): These syntheses were conducted in the same manner as that of pyrene-labeled poly(glutamic acid) (Py-PGA).[28] The purification procedure for Py-PGA relies on dialysis of the reaction mixture against acidic, basic, and neutral aqueous solutions to remove any unreacted starting materials and solvent. For the samples prepared here, an additional purification step was required to remove free pyrene. A basic aqueous solution containing Py-PAA was extracted at least 5 times using ethyl ether. The extractions were repeated until UV absorption measurements of the ether solution showed no sign of pyrene at 346 nm. Dialysis against basic and neutral solutions were completed a second time before removing the water using a freeze drier. This procedure results in the polypeptide being recovered in its sodium salt form. Similar steps were applied to the purification of Np-PAA and Py-PAcrylA.

Size Exclusion Chromatography (SEC): SEC was performed using a Waters system with DMF, DMF with 1g/L LiCl, or DMA with 1 g/L LiCl as the eluent and a Jordi linear DVB mixed-bed column. The instrument was coupled with a fluorescence detector with excitation and emission wavelengths set at 346 and 375 nm, respectively. Sample concentrations were 3 to 50 mg/L (0.1 to 1.5 optical density (OD) for pyrene absorption at 346 nm). The average level of unlabeled free pyrene still present after purification was determined by integrating the peak corresponding to the fluorescence signal of the polymer and comparing it to the fluorescence signal of any free pyrene monomer eluting with the solvent peak. The level of free pyrene was determined to be < 2 % in all cases.

Pyrene content determination: The pyrene content, λ_{Py}, is expressed in μmol of pyrene per gram of polymer and was determined according to Equation 6.1. The sodium salt of Py-PAA was freeze-dried. A mass *m* of the dry polymer was weighed and dissolved in water to yield a typical concentration of ~ 1 mg/mL. Upon acidification with a few drops of 1N HCl, the solution turned cloudy. The cloudy solution was dried under a gentle stream of N_2 and dissolved in a known volume of DMF, *V*. The pyrene concentration [*Py*] was determined by UV-Vis absorption measurements. The Beer-Lambert Law was applied to the absorption at 346 nm using the extinction coefficient of a model compound, namely 1-pyrenemethylacrylamide, equal to 40,000 $M^{-1}.cm^{-1}$ in DMF.

$$\lambda_{Py} = \frac{[Py]}{m/V} \tag{6.1}$$

Circular Dichroism: Circular dichroism (CD) experiments were carried out on a Jasco J-715 spectropolarimeter with UV cells having a path length of 1 cm with Py-PAA solutions having

concentrations of 1–2 × 10^{-5} M (~1.5 OD). This concentration and path length were chosen to remain as close as possible to the conditions used for the fluorescence experiments while still obtaining a reasonable signal-to-noise ratio from the CD instrument. Ten scans were acquired from 260 to 390 nm and averaged. The integral of the molar ellipticity of the ^1B_b band of pyrene was integrated from 277 to 282 nm as has been done previously for (Py-PGA).[28]

Steady-state fluorescence measurements: All fluorescence spectra were acquired on a PTI fluorometer using the usual right angle geometry. Solutions were degassed for 30 minutes by bubbling N_2 to remove oxygen. The monomer (I_M) and excimer (I_E) intensities were obtained by integrating between 373 – 379 nm and 500 – 530 nm for the monomer and excimer, respectively.

Fluorescence resonance energy transfer (FRET) experiments: FRET experiments were conducted with a Np-PAA and Py-PAA sample bearing 0.01 naphthalenes per backbone atom and 0.008 p.p.b.a., respectively. The overall PAA concentration was kept at ~ 50 mg/L. Three solutions were prepared for each experiment, one with Py-PAA, one with Np-PAA, and a final solution containing both Py-PAA and Np-PAA. The solutions were excited at 290 nm, where naphthalene absorbs strongly and pyrene absorbs very little. The fluorescence emission was collected from 300 nm to 550 nm. The total OD at 290 nm was kept below 0.05 to avoid the inner filter effect and the absorption across the entire spectrum never exceeded 0.1 OD to avoid direct energy transfer.

Time-resolved fluorescence measurements: Monomer and excimer fluorescence decays were acquired for Py-PAA solutions using an IBH 340 nm nano-LED with an excitation of 340 nm and emission at 376 and 510 nm, respectively. All decays were collected over 1024 channels

with up to 20,000 counts at the peak maximum for the lamp and decay curves. The instrument response function was determined by applying the MIMIC method[29] to the lamp reference decays obtained with PPO [2,5-diphenyloxazole] in cyclohexanol (τ = 1.42 ns) and BBOT [2,5-bis(*tert*-butyl-2-benzoxazolyl)thiopene] in ethanol (τ =1.47 ns) for the monomer and excimer decays, respectively. The solutions were prepared in the same way as for the steady-state fluorescence experiments.

Analysis of the fluorescence decays: The monomer and excimer fluorescence decays were fit with the sum of exponentials given in Equation 6.2. The monomer and excimer fluorescence decays were also fit globally using Equations 6.3 and 6.4, respectively. Equations 6.3 and 6.4 are derived by using the FBM. The FBM has been used to study the encounters of pyrenes randomly attached along a polymer backbone in previous studies.[17,30–32]

The first exponential in Equation 6.3 describes the formation of excimer by the diffusive encounter of an excited pyrene and a ground-state pyrene. τ_M is the unquenched lifetime of the pyrene monomer and is determined from the monomer fluorescence decay of a polymer having a small pyrene content (5×10^{-4} p.p.b.a.) so that the decay is predominantly mono-exponential with $\geq$ 80% contribution from the long lifetime. τ_M was found to equal 215 ns, 205 ns, 215 ns, and 210 ns for Py-PAA in DMF, DMF with 1 g/L LiCl, DMA, and DMA with 1 g/L LiCl, respectively. The parameters describing excimer formation by diffusive encounters are the rate constant for excimer formation, k_{blob}, the average number of pyrenes per *blob*, $\langle n \rangle$, and the rate constant for pyrene exchange between blobs times the concentration of *blobs*, $k_e[blob]$. An additional rate constant, k_2, is used to describe excimer formation between two pyrenes located in close proximity on a time scale much faster than that for diffusive encounters described by k_{blob}. Such pyrenes are encountered when they are

incorporated in the polymer in a clustered manner. The third exponential in Equation 6.2 accounts for any unquenched free pyrene monomer that is isolated and cannot form excimer within τ_M.

$$i(t) = \sum_{i=1}^{n_{\exp}} a_i \exp(-t/\tau_i) \text{ with } n_{exp} = 3,4 \tag{6.2}$$

$$[Py^*]_{(t)} = [Py^*_{diff}]_o \exp\left(-\left(A_2 + \frac{1}{\tau_M}\right)t - A_3\left(1 - \exp(-A_4 t)\right)\right) +$$

$$[Py^*_{k2}]_o \exp\left(-\left(k_2 + \frac{1}{\tau_M}\right)t\right) + [Py^*_{free}]_o \exp\left(-\frac{t}{\tau_M}\right) \tag{6.3}$$

$$[E^*]_{(t)} = [Py^*_{diff}]_o \exp(-A_3)\sum_{i=0}^{\infty}\frac{A_3^i}{i!}\frac{A_2 + iA_4}{A_2 + iA_4 + \frac{1}{\tau_M} - \frac{1}{\tau_{E0}}} \times \left(\exp\left(-\frac{t}{\tau_{E0}}\right) - \exp\left(-\left(A_2 + iA_4 + \frac{1}{\tau_M}\right)t\right)\right)$$

$$+ k_2[Py^*_{k2}]_o \frac{\exp\left(-\frac{t}{\tau_{E0}}\right) - \exp\left(-\left(k_2 + \frac{1}{\tau_M}\right)t\right)}{k_2 + \frac{1}{\tau_M} - \frac{1}{\tau_{E0}}} + [E0^*]_o \exp\left(-\frac{t}{\tau_{E0}}\right) + [D^*]_o \exp\left(-\frac{t}{\tau_D}\right) \tag{6.4}$$

The parameters A_2, A_3, and A_4 used in Equations 6.3 and 6.4 are described in Equation 6.5.

$$A_2 = \langle n \rangle \frac{k_{blob} k_e [blob]}{k_{blob} + k_e [blob]} \quad A_3 = \langle n \rangle \frac{k^2_{blob}}{(k_{blob} + k_e [blob])^2} \quad A_4 = k_{blob} + k_e [blob] \tag{6.5}$$

The excimer decays were fit using Equation 6.4, where τ_{E0} is the excimer lifetime. Equation 6.4 assumes that the excimer is formed and emits as one of four species in solution. These species result from the diffusional encounter of an excited pyrene monomer and a ground-state pyrene (Py^*_{diff}), fast excimer formation from pyrenes located very close to one another (Py^*_{k2}), the direct excitation of ground-state dimers ($E0^*$), and long-lived ground-state dimers (D^*). The fits of the monomer and excimer decays with Equations 6.3 and 6.4 enables one to determine the fractions of all pyrene species, Py_{diff}, Py_{k2}, Py_{free}, $E0$, and D, present in solution. The fraction of aggregated pyrenes, f_{agg}, is the sum of $f_{E0} + f_D + f_{k2}$. A more detailed explanation on the determination of the fractions is found in previous works.[31,32]

Optimization of the parameters used in Equations 6.2 to 6.4 to fit the fluorescence decays was performed with the Marquardt-Levenberg algorithm.[33] The IBH 340 LED used to acquire the fluorescence decays was found to generate a higher noise level than the IBH hydrogen lamp used previously.[32] Consequently, a background correction was applied to fit the fluorescence decays.[33] As done in previous publications a light scattering correction was applied to account for excimer formation that occurs on a time-scale too fast for our instrument to detect with accuracy.[34] The fits were considered good if the χ^2 was less than 1.3 and the residuals were randomly distributed around zero.

6.4 Results

Eight Py-PAA samples were synthesized and studied under very dilute solution conditions (~3 to 50 mg/L) in DMF, DMA, DMF with 1 g/L LiCl, and DMA with 1 g/L

LiCl. Only six of the eight Py-PAA samples, those with the highest pyrene contents, were used for the majority of the experiments due to the rather small amount of excimer generated by the Py-PAA samples having low pyrene contents. The pyrene contents of each Py-PAA sample are expressed in μmol of pyrene per gram of polymer or pyrene per backbone atom (p.p.b.a.). The units p.p.b.a. are used to provide a more representative comparison of the number of pyrenes along the polymer chain since a monomer unit in PAA yields more atoms in the main chain that the monomer of a vinyl polymer does.

Polypeptides consisting entirely of β-polypeptide linkages are known to form various helicies similar to that of α-polypeptides.[35] However, PAA is known to have little secondary structure when its backbone is composed of both α– and β–linkages.[36] CD experiments were carried out to establish the presence or absence of secondary structure for the Py-PAA samples in each solvent. Secondary structure determination is difficult in the present study using typical methods such as CD or FT-IR since DMF absorbs very strongly where the peptide bonds of the backbone do, making it impossible to assess whether they adopt the regular orientation found in α-helices and β-sheets. Therefore an indirect method for structure determination is needed. Earlier studies have shown that the orientation of the pyrene groups attached to the side-chains of a structured polypeptide is preserved over a few amino acids so that CD can be used to infer the structural features of a polypeptide, as has been done for pyrene-labeled poly(glutamic acid) in DMA[37] and DMF.[28] When polypeptides such as Py-PGA adopt an α-helical secondary structure, the pyrene groups attached at the side-chains exhibit a common orientation which yields a positive CD band centered at ~278 nm.

Figure 6.1 shows the molar ellipticities of a series of Py-PGA and Py-PAA samples in DMF. The solid line in the figure represents the absorbance of the solvent over the wavelength range considered. The much smaller molar ellipticities found for Py-PAA at ~278 nm demonstrate that Py-PAA has little helical structure in DMF compared to Py-PGA. The molar ellipticity values for Py-PAA are shown as a function of pyrene content in DMF, DMA, DMF with 1 g/L LiCl, and DMA with 1 g/L LiCl in Figure 6.2. The Py-PAA ellipticities are only slightly larger than those of a model compound, *N*-(1-pyrenylmethyl)acrylamide (PyAAm) in DMF and DMA. Also, their value remains small, regardless of solvent used or pyrene content. Together, these results indicate that Py-PAA has much less, if any, structure than Py-PGA.

To determine if any intermolecular interactions were present at the low polypeptide concentrations used for the fluorescence studies, steady-state fluorescence spectra were acquired for two Py-PAA samples with 0.020 and 0.039 p.p.b.a. in the four solvents at polymer concentrations ranging from 0.3 to ~50 mg/L (0.01 to ~1.5 OD). The ratio of the excimer fluorescence intensity (I_E) averaged over 500 – 530 nm to that of the monomer fluorescence intensity (I_M) averaged over 373 – 379 nm is shown as a function of polymer concentration for the two samples in DMF and DMF with 1 g/L LiCl in Figure 6.3A. The I_E/I_M ratio is constant from 0.3 to 5 mg/L for all solvents, with a steep increase in DMF and DMA for concentrations greater than 5 mg/L. The addition of LiCl to the solution delays the increase in excimer formation but does not eliminate it entirely. The arrows in Figure 6.3A indicate the concentration corresponding to a pyrene absorption at 346 nm equal to 0.1 and 1.5 OD.

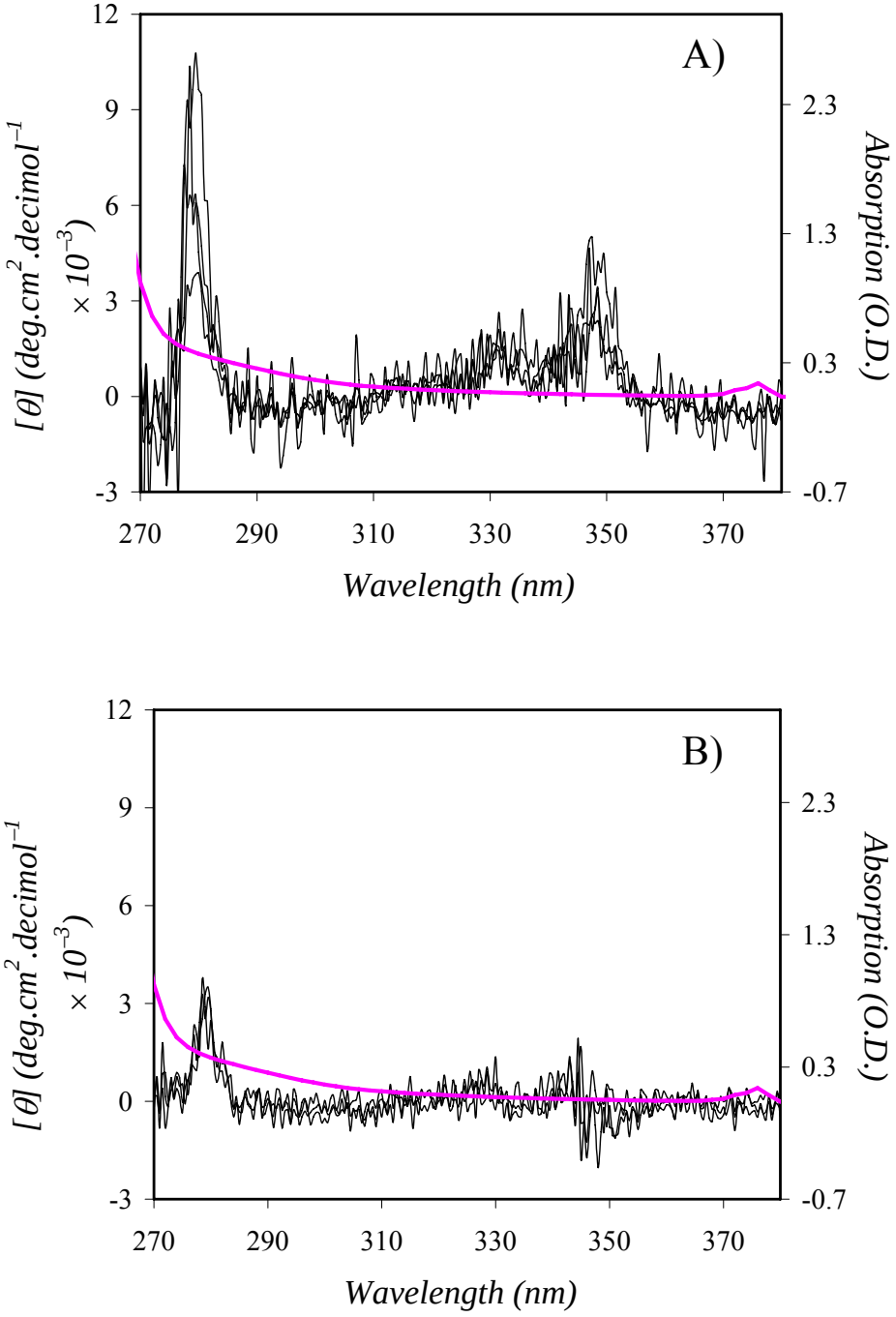

Figure 6.1: Circular Dichroism spectra of (A) Py-PGA in DMF with decreasing pyrene contents. From top to bottom the pyrene content equals 0.040, 0.029, 0.022 and 0.014 p.p.b.a. and (B) Py-PAA in DMF 0.039, 0.033, 0.020 p.p.b.a. The solid line gives the absorption of DMF as a function of wavelength measured with a 1 cm path length UV cell.

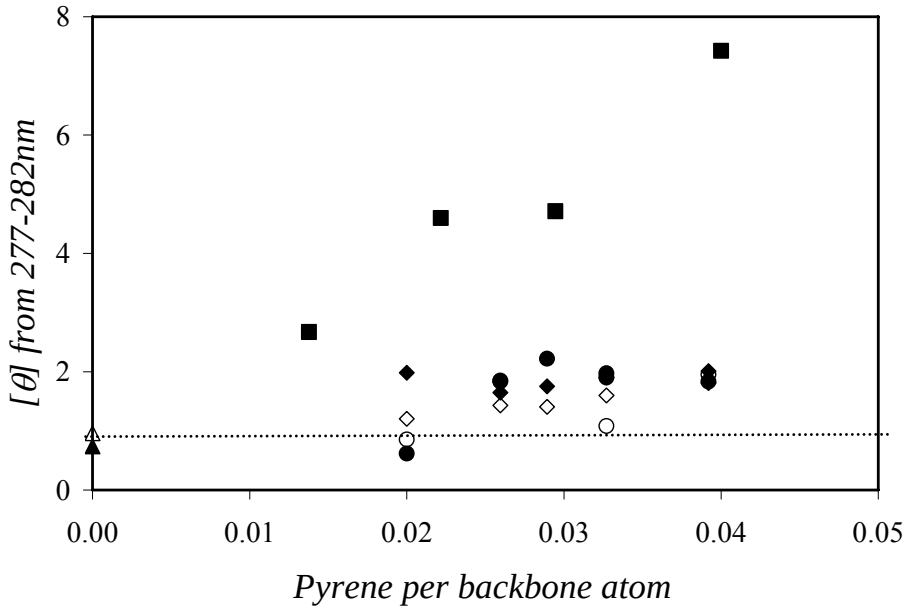

Figure 6.2: Molar ellipticity as a function of pyrene content; Py-PAA in DMF (◆), DMA (●), DMF with 1 g/L LiCl (◇), and DMA with 1 g/L LiCl (○); Py-PGA in DMF (■); 1-pyrenylacrylamide in DMF (△) and DMA (▲).

The fluorescence spectra of Py-PS with 0.025 p.p.b.a. in DMF, DMA with 1 g/L LiCl, and methyl acetate were acquired to compare the behavior obtained with Py-PAA in Figure 6.3A with that of a randomly coiled polymer in solution where the solvent quality decreases in the order DMA with 1 g/L LiCl > DMF > methyl acetate, where methyl acetate is considered a theta solvent, as determined from the intrinsic viscosities measured for a 40K PS sample (Figure A6.2 in the Appendix). In addition, the I_E/I_M trends were obtained for Py-PGA with 0.050 p.p.b.a., Py-PDMA with 0.0125 p.p.b.a., and pyrene-labeled poly(acrylic acid) (Py-PAcrylA) with 0.025 p.p.b.a., each in DMF. Py-PGA was chosen because it is both a polyacid and a polypeptide with a chemical structure that resembles that of Py-PAA and because it forms a structured α–helix in organic solvents,[28,37] contrary to Py-PAA. Py-PAcrylA and Py-PDMA were chosen because they are water-soluble, randomly coiled

polymers with and without carboxylic acid groups in their side-chains, respectively. By using these numerous comparisons, the basis for the change in I_E/I_M with polymer concentration can be resolved into the effect of *solvent quality* towards a polymer (Py-PS), *secondary structure* of a polypeptide (Py-PGA), *amphiphilicity* of a water-soluble polymer bearing hydrophobes without (Py-PDMA), or with (Py-PAcrylA) *carboxylic acid groups*.

Figure 6.3B shows the I_E/I_M ratios obtained as a function of polymer concentration for Py-PS, Py-PGA, Py-PDMA and Py-PAcrylA. The I_E/I_M ratios remain constant with increasing polymer concentration for an α-helical polypeptide, Py-PGA, a water-soluble pyrene-labeled random coil polymer, Py-PDMA, and a hydrophobic pyrene-labeled random coil polymer, Py-PS in a good solvent (DMA), a mediocre solvent (DMF), and a θ-solvent (methyl acetate). However, Py-PAcrylA, which is a coiled polyacid similar to Py-PAA, shows a similar increase in I_E/I_M with increasing concentration. Thus, the increase in I_E/I_M with polymer concentration occurs for unstructured, randomly coiled polyacids such as Py-PAA and Py-PAcrylA, but is seen neither for polyacids with secondary structure, such as Py-PGA, nor for random coil polymers bearing no acid side-chains such as Py-PS and Py-PDMA.

To determine whether the increase in I_E/I_M with polymer concentration was an indication of aggregation of the Py-PAA coils or an electrostatic effect resulting from the carboxylic acid groups present along the backbone, fluorescence resonance energy transfer (FRET) experiments were conducted. FRET experiments are an invaluable tool to report on the aggregation of polymers in solution.[38] They rely on the non-radiative transfer of energy from an excited donor chromophore whose emission spectrum overlaps the absorption spectrum of an acceptor chromophore. When the distance between a donor and acceptor

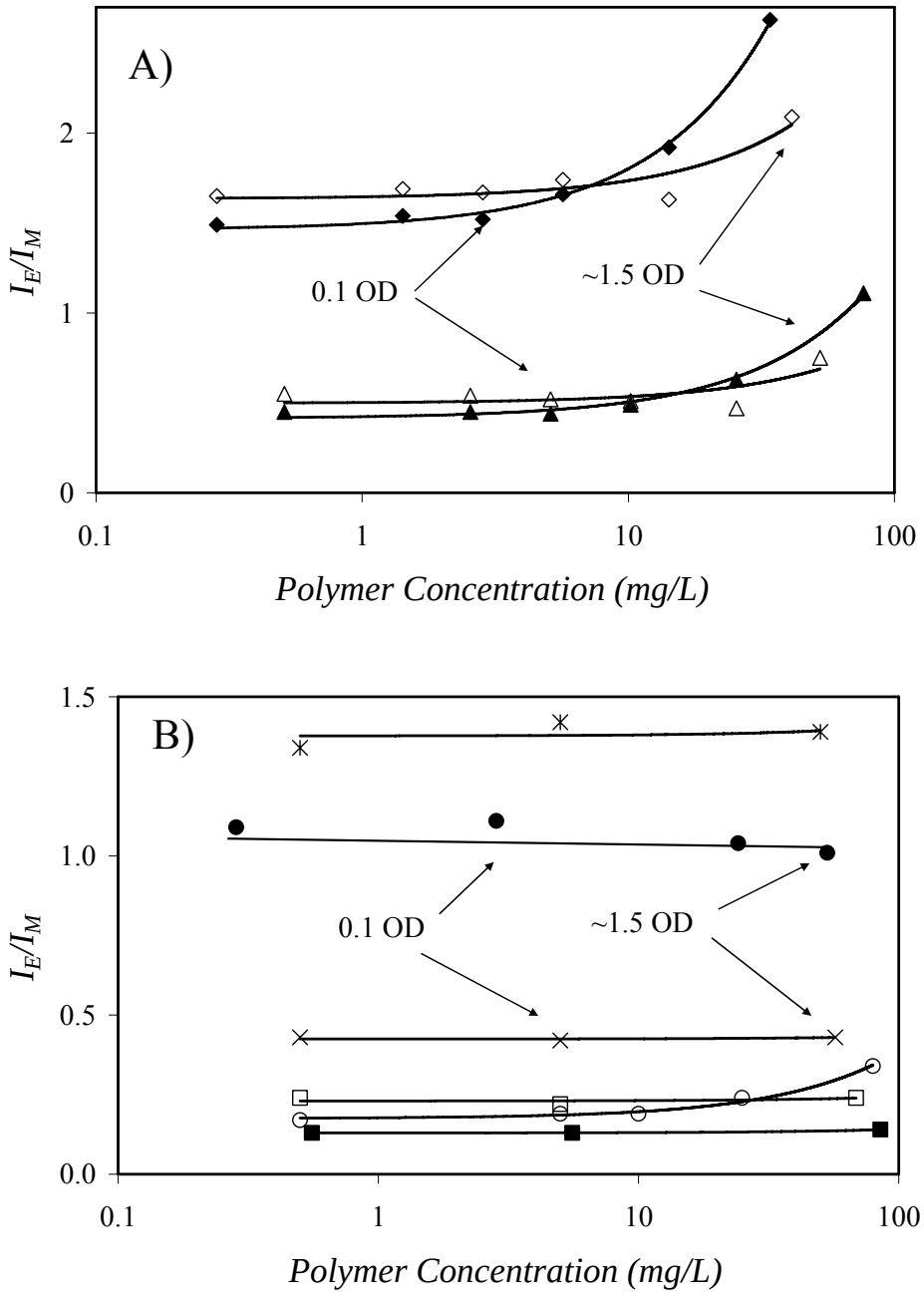

Figure 6.3: (A) I_E/I_M ratios for Py-PAA as a function of polymer concentration; 0.020 p.p.b.a. (diamonds), 0.039 p.p.b.a. (triangles) in DMF (◆, ▲) and DMF with 1 g/L LiCl (◇, △). (B) I_E/I_M ratios as a function of polymer concentration for Py-PGA in DMF (●), Py-PDMA in DMF (■), Py-PS in DMF, (×), Py-PS in DMA with 1 g/L LiCl (□), Py-PS in methyl acetate (∗), Py-PAcrylA in DMF (○).

pair is smaller than the Förster radius, the fluorescence of the donor is effectively quenched and the emission of the acceptor is observed, whereas when the distance between donor and acceptor is larger than twice the Förster radius, essentially no energy transfer is observed.[38] The Förster radius is dependent on the extent of overlap between the donor emission spectrum and the acceptor absorption spectrum, and the relative orientation of the donor and acceptor emission dipoles. In the current work, naphthalene and pyrene were chosen as the donor and acceptor. They are known to have a Förster radius of 29 Å.[39,40]

A naphthalene labeled PAA (Np-PAA) was synthesized with 0.01 naphthalenes per backbone atom and was used with a Py-PAA sample containing 0.008 p.p.b.a. Total polymer concentrations of 46.3 mg/L made of 40 mg/L Np-PAA and 6.3 mg/L Py-PAA were used in each solvent to mimic the concentration of the Py-PAA solutions where an increase in the I_E/I_M ratio occurs in Figure 6.3A. The solutions were excited at 290 nm, where pyrene has little absorption, and the emission was collected between 300 and 550 nm. Figure 6.4 shows the steady-state fluorescence spectra of the solutions of Py-PAA, Np-PAA, and the mixture of Np-PAA and Py-PAA in DMA with 1 g/L LiCl. Addition of the Np-PAA and Py-PAA spectra results in a spectrum that overlaps rather well with the spectrum obtained with the Np-PAA and Py-PAA mixture, above all for the naphthalene emission, while the pyrene monomer emission is slightly lower for the mixture of Py-PAA and Np-PAA as compared to the sum of the two solutions. This illustrates that no energy transfer occurs between the naphthalene and pyrene groups and that the PAA coils are not aggregated in DMF, DMA, or DMF and DMA with 1 g/L LiCl. Interestingly, in addition to the slight decrease in the intensity of the monomer peak for the mixture compared to the sum of the two solutions acquired separately, the intensity of the pyrene excimer peak in DMF is higher for the

mixture than the sum of the two solutions acquired separately (Inset of Figure 6.4). The polymer concentration for the Py-PAA solution is 6.3 mg/L, below the point where the I_E/I_M ratio begins to increase with concentration (Figure 6.3A), while the Py-PAA and Np-PAA mixture has a polymer concentration of 46.3 mg/L, far into the region where I_E/I_M is expected to increase with polypeptide concentration. This result confirms that the increase in I_E/I_M occurs due to the PAA concentration and is not specific to Py-PAA or Np-PAA (Figure 6.3A).

In addition to the fluorescence experiments used to extract information on the Py-PAA coils in solution, SEC was employed as a complementary technique to study their behavior in organic solvents. The Py-PAA samples with 0.020 and 0.039 p.p.b.a. were analyzed using SEC with an online fluorescence detector using polymer concentrations of ~5 and ~50 mg/L in DMF, DMF with 1 g/L LiCl, and DMA with 1 g/L LiCl as the eluent. The corresponding chromatograms for the 0.039 p.p.b.a. samples with concentrations of 50 mg/L are shown in Figure 6.5. In DMF, Py-PAA elutes at early times indicating that it adopts a large hydrodynamic volume. Adding salt to DMF or DMA induces the polypeptide to elute at later times, suggesting a decrease in hydrodynamic volume. These results are similar to those obtained for a polystyrene based ionomer, where the peak obtained when using DMF as the eluent appeared much sooner than when salt was added to the solution.[41]

It is important to note that two different analytical columns were used to obtain the SEC traces in Figure 6.5, one using DMF or DMF with 1 g/L LiCl as the eluent, and the other using DMA with 1 g/L LiCl. Therefore, the shift of the polymer peak for DMF with 1 g/L LiCl relative to DMA with 1 g/L LiCl may not be indicative of a change in hydrodynamic volume and is only used to demonstrate the large difference between eluents with and

without 1 g/L LiCl. The tailing in the SEC trace for Py-PAA in DMF with 1 g/L LiCl is possibly due to non-ideal separation of the polypeptide whereby some polypeptide adsorbs on to the column. Thus, the "free pyrene" shown at the 30 mL elution volume is considered to be the small peak, not the entire tail from the polypeptide peak.

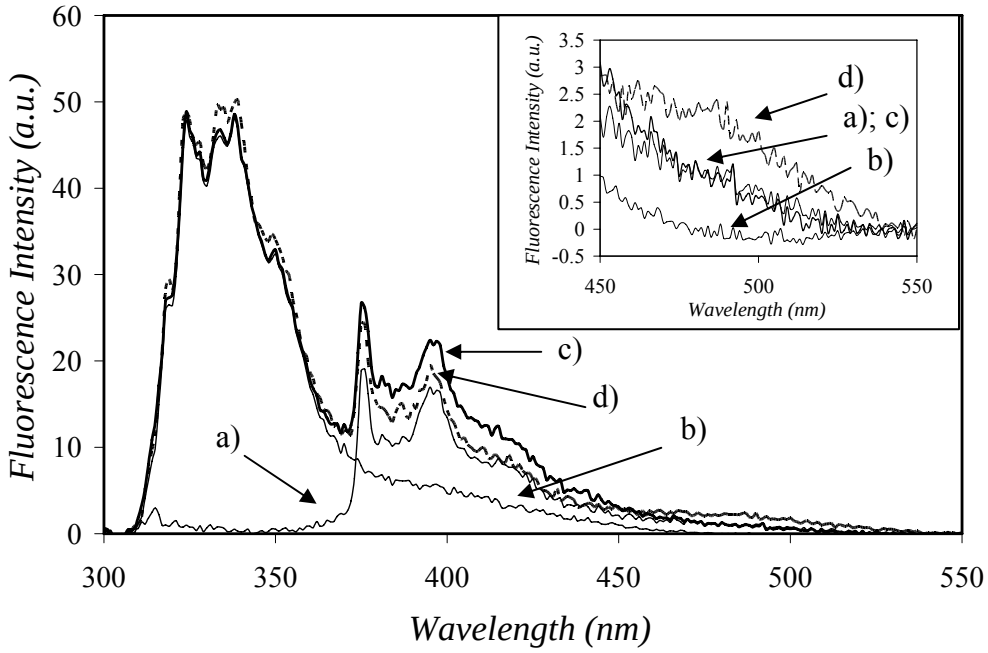

Figure 6.4: Fluorescence emission spectra of solution of Py-PAA and Np-PAA in DMF: a) Py-PAA concentration = 6.3 mg/L, b) Np-PAA concentration = 40 mg/L, c) sum of the two preceding spectra, d) Py-PAA and Np-PAA with concentrations of 6.3 and 40 mg/L, respectively. Insets: Section of spectra illustrating the changes in pyrene excimer formation. λ_{ex} = 290 nm.

At this point, it is important to summarize the results obtained for Py-PAA thus far. The I_E/I_M ratios show that a change in excimer formation occurs as a function of polymer concentration. Comparison of this behavior with that of other randomly coiled or structured polymers led to the conclusion that the carboxylic acid side-chains of Py-PAA induced the change in I_E/I_M. Typically, an increase in I_E/I_M with polymer concentration is an indication of aggregation or a change in the conformation of the coil.

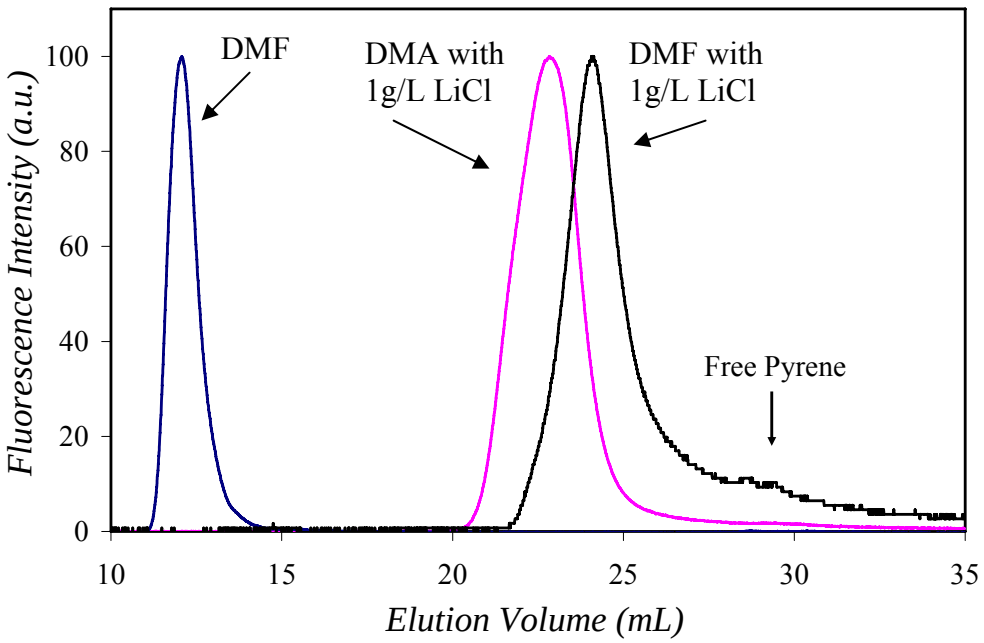

Figure 6.5: SEC traces obtained using an online fluorescence detector. The fluorescence intensity is plotted as a function of elution volume for Py-PAA samples with 0.039 p.p.b.a. in DMF, DMF with 1 g/L LiCl, and DMA with 1 g/L LiCl. λ_{ex} = 346 nm, λ_{em} = 376 nm, flow rate = 1mL/min.

Since the carboxylic acid side-chains of Py-PAA could induce electrostatic interactions between coils leading to aggregation as is known for polyelectrolytes and ionomers,[42] FRET measurements were performed. They showed unequivocally that no aggregation was occurring, indicating that the change in I_E/I_M is due to a change in coil conformation. An increase in I_E/I_M with polymer concentration was seen in these measurements, even with > 80% (40 out of the 46 mg/L) of the PAA coils containing the much less hydrophobic naphthalene instead of pyrene. It indicates that the increase in I_E/I_M is an intrinsic property of the PAA coils themselves that is not induced by the hydrophobic pyrene groups. Finally, SEC measurements show that Py-PAA behaves in a manner similar to PS based ionomers in DMF and DMA with added salt, further confirming that PAA behaves like a partially charged random coil polymer. This topic is discussed in greater detail later in the Chapter.

Due to the dependence of the I_E/I_M ratio on polymer concentration, information on the chain dynamics of Py-PAA in DMF and DMA with or without added salt was obtained by using steady-state and time-resolved fluorescence in the plateau region of Figure 6.3A for solutions having an absorbance below 0.1 OD. Steady-state fluorescence spectra were acquired and those obtained with the Py-PAA solutions in DMF are shown in Figure A6.3 in the Appendix. The spectra are normalized at 376 nm and demonstrate that the amount of excimer increases with increasing pyrene content. The ratio of the intensity of the first and third peaks of the monomer, I_1/I_3, reflects the local polarity of the medium surrounding the pyrene group.[16] This ratio is virtually identical for Py-PAA in all four solvents, as shown in Table 6.1.

Figure 6.6 illustrates that the I_E/I_M ratios of Py-PAA in DMF and DMF with 1 g/L LiCl are very similar. A comparable result is observed for DMA and DMA with 1 g/L LiCl. The I_E/I_M ratios of Py-PS and Py-PAA in DMF and DMA with 1 g/L LiCl are compared in the inset of Figure 6.6 as a function of pyrene content. Both polymers exhibit stronger excimer formation in DMF than in DMA with 1 g/L LiCl due to the viscosity of DMF (0.79 mPas) being much lower than that of DMA (1.92 mPas). At low pyrene contents of 0.01 p.p.b.a., very little excimer is formed by Py-PS or Py-PAA, while at pyrene contents larger than 0.02 p.p.b.a., Py-PAA forms much more excimer than Py-PS in either solvent. This increase in excimer formation indicates one of three possibilities. Firstly, either the backbone of Py-PAA is much more flexible than that of Py-PS, secondly, the pyrene groups are distributed in a more clustered manner in Py-PAA than in Py-PS, or thirdly, that the very polar microenvironment of the Py-PAA backbone and carboxylic acid groups causes the pyrene groups to aggregate together.

Table 6.1: Absorption and fluorescence indicators determined for Py-PS in DMF and DMA with 1 g/L LiCl, Py-PDMA in DMF, and Py-PAA in DMF, DMA, DMF with 1 g/L LiCl, and DMA with 1 g/L LiCl.

	PyAAm in DMF	Py-PDMA in DMF	Py-PS in DMF	Py-PS in DMA 1 g/L LiCl
P_A *value*	2.9	2.9 ± 0.1	2.8 ± 0.1	2.7 ± 0.1
a_{E-}/a_{E+}	-	–0.81 ± 0.01	–0.79 ± 0.05	–0.82 ± 0.09
I_1/I_3	1.95	1.91 ± 0.06	1.85 ± 0.02	2.09 ± 0.04
N_{blob} (p.p.b.a.)	-	56 ± 5	78 ± 3	48 ± 2
k_{blob} ($10^7 s^{-1}$)	-	1.04 ± 0.11	0.94 ± 0.2	1.37 ± 0.3

	Py-PAA in DMF	Py-PAA in DMF 1 g/L LiCl	Py-PAA in DMA	Py-PAA in DMA 1 g/L LiCl
P_A *value*	2.5 ± 0.1	2.5 ± 0.1	2.6 ± 0.1	2.5 ± 0.1
a_{E-}/a_{E+}	–0.60 ± 0.07	–0.66 ± 0.05	–0.72 ± 0.02	–0.71 ± 0.02
I_1/I_3	2.13 ± 0.08	2.09 ± 0.05	2.15 ± 0.04	2.16 ± 0.03
N_{blob} (p.p.b.a.)	114 ± 12	141 ± 10	99 ± 8	95 ± 7
k_{blob} ($10^7 s^{-1}$)	0.79 ± 0.15	0.62 ± 0.19	0.84 ± 0.13	0.63 ± 0.10

The first possibility appears to be unlikely, as is illustrated in Figure 6.7 where the I_E/I_M ratio is multiplied by the solvent viscosity and shown as a function of pyrene content. Several studies of pyrene labeled polymers, including the one on Py-PS in Chapter 3, have all illustrated that excimer formation is viscosity controlled.[43] If excimer formation were viscosity controlled for Py-PAA, the $I_E/I_M \times \eta$ trends in Figure 6.7 should overlap. The large difference in excimer formation between Py-PAA in DMF and DMA after adjusting for viscosity implies that excimer formation is not controlled by the solvent viscosity, but rather the intrinsic inflexibility of the polypeptide backbone.

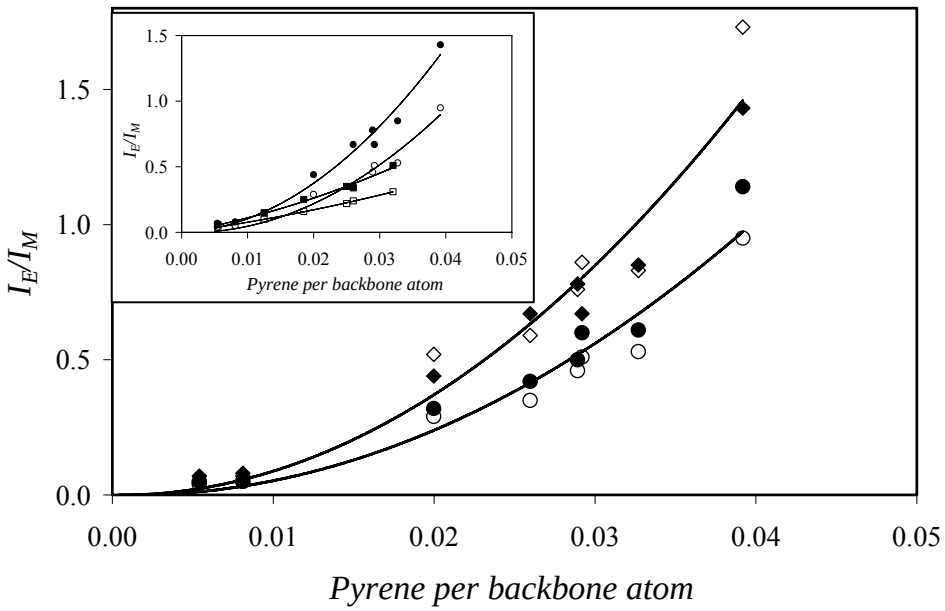

Figure 6.6: I_E/I_M ratios as a function of pyrene content; Py-PAA in DMF (◆), DMA (●), DMF with 1 g/L LiCl (◇), DMA with 1 g/L LiCl (○). Inset: I_E/I_M ratios as a function of pyrene content for Py-PAA in DMF (◆), DMA with 1 g/L LiCl (○), Py-PS in DMF (■), Py-PS in DMA with 1 g/L LiCl (□). [Py] = 2.5×10^{-6} M, λ_{ex} = 346 nm.

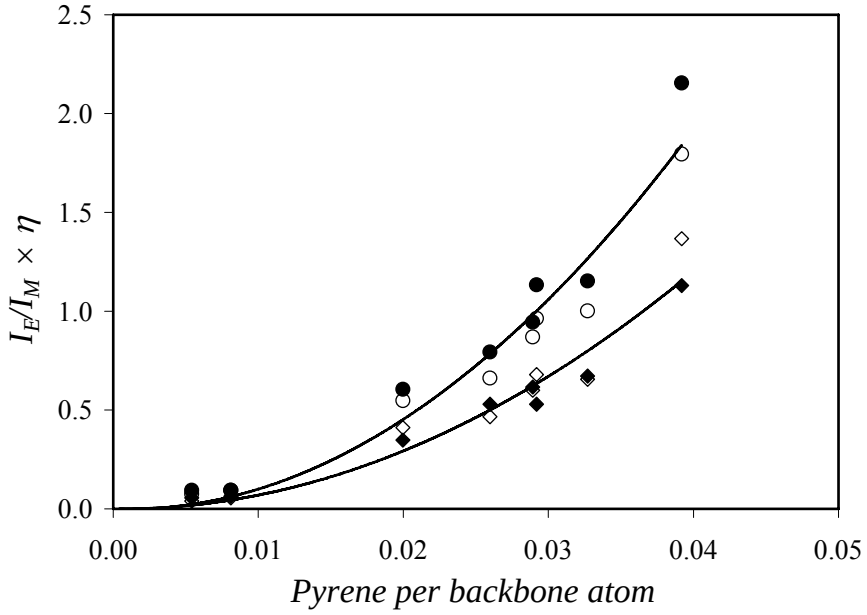

Figure 6.7: $I_E/I_M \times \eta$ ratios as a function of pyrene content; Py-PAA in DMF (◆), DMA (●), DMF with 1 g/L LiCl (◇), DMA with 1 g/L LiCl (○). [Py] = 2.5×10^{-6} M, λ_{ex} = 346 nm.

Time-resolved monomer and excimer fluorescence decays were acquired for Py-PAA at 0.1 OD. The apparent rate constant for excimer formation, k_{exci}, is determined through the analysis of time-resolved monomer fluorescence decays.[44] k_{exci} is calculated using Equation 6.6, where $<\tau>$ represents the number-average decay time of the pyrene monomer determined using a multi-exponential fit given in Equation 6.2, while τ_M represents the unquenched lifetime of the monomer. The parameters retrieved using Equation 6.2 are found in Tables A6.1 and A6.2 in the Appendix. Figure 6.8 is a plot of k_{exci} as a function of pyrene content in different solvents and the trends are similar to those obtained with the I_E/I_M ratios presented in Figure 6.6, as well as in the inset where the plot of $k_{exci} \times \eta$ as a function of pyrene content mirrors that of $I_E/I_M \times \eta$ in Figure 6.7. A minor difference can be noted between the DMF and DMF with 1 g/L LiCl solutions, where excimer formation appears to be slightly enhanced when LiCl is added.

$$k_{exci} = \frac{1}{<\tau>} - \frac{1}{\tau_M} \tag{6.6}$$

Analysis of the excimer decays using Equation 6.2 provides a measure of the level of clustering of the pyrene pendants along the backbone. If the ratio of the sum of the negative pre-exponential factors over the sum of the positive pre-exponential factors (a_{E-}/a_{E+}) is close to −1.0, all excimer formation is considered to proceed via diffusion; a more positive a_{E-}/a_{E+} value reflects some clustering of the pyrene groups. As shown in Table 6.1, the a_{E-}/a_{E+} ratio is much smaller in absolute value for Py-PAA than Py-PS or Py-PDMA. The a_{E-}/a_{E+} ratio

indicates that the pyrenyl pendants in the Py-PAA series are much more aggregated than in the Py-PS or Py-PDMA series.

The UV-Vis absorption spectra also provide a qualitative measure of the level of pyrene aggregation for the Py-PAA samples. The ratio between the highest absorption peak at ~346 nm and the absorption trough at ~336 nm is known as the peak-to-valley ratio (P_A value).[16] Pyrene-labeled polymers free of aggregated pyrene groups typically have P_A values close to 3.0.[16] The P_A values for Py-PAA are very similar at 2.5±0.1 in all four solvents, as shown in Table 6.1. The P_A values for Py-PS and Py-PDMA in DMF are 2.8±0.1 and 2.9±0.1, respectively, indicating that the pyrene pendants of Py-PAA are more aggregated.

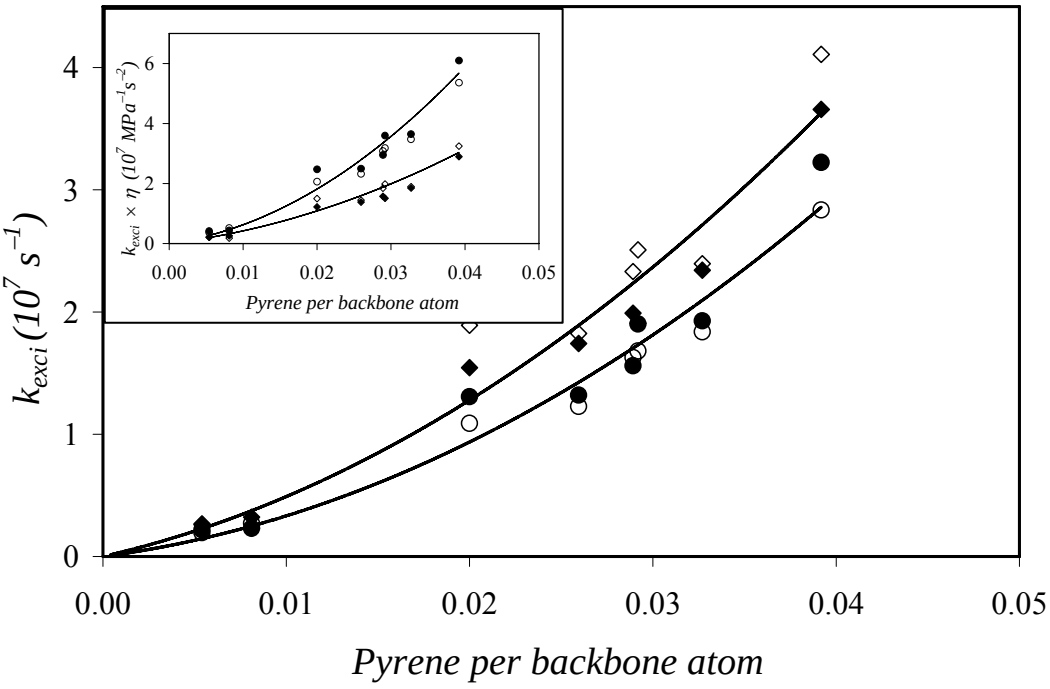

Figure 6.8: k_{exci} as a function of pyrene content; Py-PAA in DMF (◆), DMA (●), DMF with 1 g/L LiCl (◇), DMA with 1 g/L LiCl (○). Inset; $k_{exci} \times \eta$ as a function of pyrene content in DMF (◆), DMA (●) DMF with 1 g/L LiCl (◇), DMA with 1 g/L LiCl (○). [Py] = 2.5×10^{-6} M, λ_{ex} = 346 nm.

6.4.1 FBM Results:

Figure 6.9 shows the monomer and excimer decays of a Py-PAA and a Py-PS sample with 0.03 and 0.035 p.p.b.a., respectively, in DMF with a pyrene concentration of 2.5×10^{-6} M. The Py-PS sample yields a typical set of monomer and excimer decays, where the decaytimes found in the pyrene monomer decay are reflected in that of the excimer. Indeed the two traces are almost parallel at the longer times. This is a consequence of the kinetics of excimer formation yielding coupled differential equations for the pyrene monomer and excimer.[45] In contrast, the monomer and excimer decays of Py-PAA are quite different since they intersect within the time window of the experiment, with a strong long-lived contribution in the Py-PAA monomer which does not appear in the excimer decay.

This effect is unlikely due to free pyrene monomer since the SEC measurements in Figure 6.5 confirm the presence of minute amounts of free pyrene, and the exponential analysis and FBM analysis of the monomer decays shows very limited contribution from a lifetime at 215 ns. This observation signals that to some extent, the kinetics of excimer formation between the pyrene monomer and excimer are uncoupled for Py-PAA. The short rise time in the excimer decay is matched by a short decay time in the monomer decay. It suggests that excimer formation occurs rapidly, as if from pyrene clusters. The few pyrenes that are not clustered form excimer on a longer time scale, either due to the stiffer polypeptide backbone or the depletion of pyrene pendants inside the polypeptide coil outside the pyrene clusters. Thus, the excimer appears to be formed very quickly, as seen from the sharp curvature in the monomer decay, and very slowly as shown by the longer-lived contribution that is still shorter than that of unquenched monomer (215 ns).

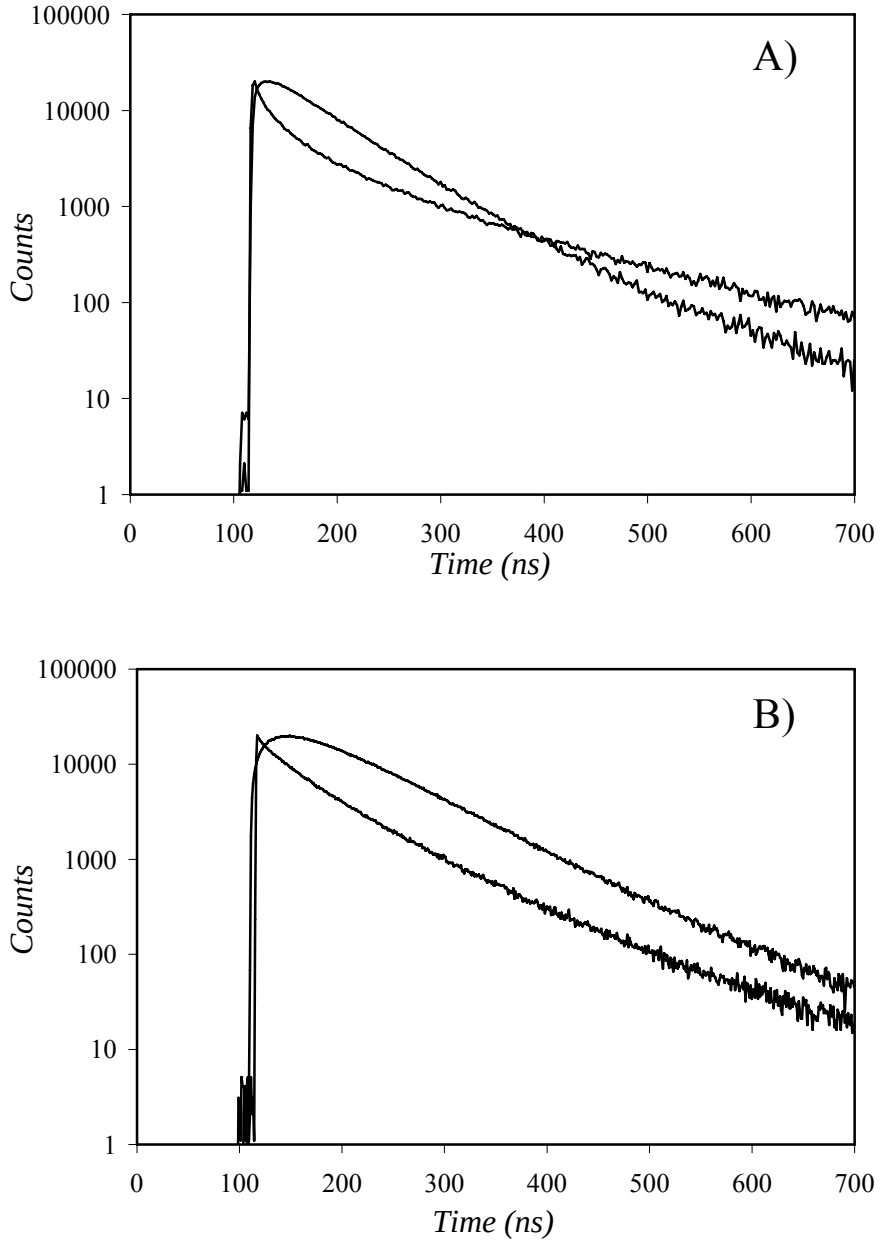

Figure 6.9: (A) Monomer and excimer fluorescence decays of Py-PAA labeled with 0.030 p.p.b.a. in DMF. (B) Monomer and excimer fluorescence decays of Py-PS labeled with 0.035 p.p.b.a. in DMF. [Py] = 2.5×10^{-6} M, λ_{ex} = 340 nm, λ_{em} = 375 nm.

To obtain information from this extreme case, where some excimer is formed very rapidly due to the "closeness" of pyrene groups along the backbone and some more slowly due to large gaps between non-aggregated groups, Scheme 6.2 is proposed. Scheme 6.2

depicts three distinct regions that are encountered inside a Py-PAA coil. The region to the right represents those pyrene groups that are isolated and cannot form excimer within the lifetime of the pyrene monomer. In the center region, excimer is formed through the diffusive encounter between an excited pyrene monomer and a ground-state pyrene. Finally, in the third region on the left, the pyrene groups are clustered and form excimer with a rate constant k_2 that is much faster than k_{blob}. Examples of the fits obtained using the FBM equation to analyze the monomer alone or the monomer and excimer decays simultaneously with and without a contribution from excimers formed with a rate constant k_2 are shown in Figures A6.2 to A6.4 in the Appendix. Without accounting for excimers formed via a k_2 route, the fits are very poor, resulting in χ^2 >1.5, whereas the FBM analysis including a k_2 rate constant for excimer formation fits the decays very well with χ^2 values typically in the 1.0-1.1 range. Thus, the modified FBM resulting in Equations 6.3 to 6.5 was used.

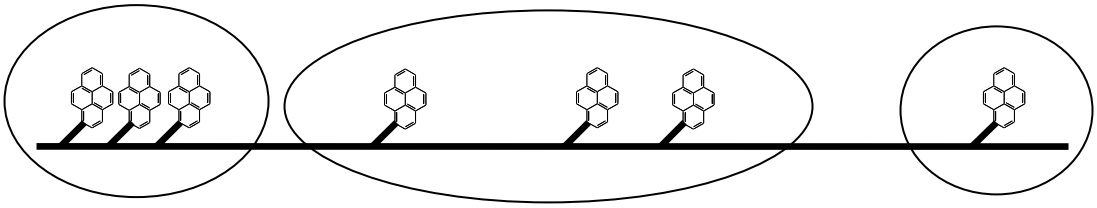

Clustered Pyrenes (f_{Mk2}) that form excimer with a rate constant k_2

Pyrenes that form excimer through diffusion (f_{Mdiff})

Isolated pyrenes (f_{Mfree}) that cannot form excimer

Scheme 6.2: Illustration of the different environments experienced by pyrene along the Py-PAA backbone.

The modified FBM analysis was used to fit globally the monomer and excimer fluorescence decays for Py-PAA in DMF, DMA, DMF with 1 g/L LiCl, and DMA with 1 g/L

LiCl for pyrene contents above 0.02 p.p.b.a. The two lower pyrene content samples with 0.005 and 0.008 p.p.b.a. do not form very much excimer, resulting in unreliable FBM parameters. The time-resolved fluorescence decays of Py-PAA were analyzed with Equations 6.3 and 6.4 and the parameters retrieved from the analysis are listed in Tables A6.3 to A6.5 in the Appendix.

The k_2 value determined for Py-PAA remained constant with pyrene content and took a value of 13±1 × 10^7 s^{-1} in DMF and DMF with 1g/L LiCl and 12±1 × 10^7 s^{-1} in DMA and DMA with 1 g/L LiCl. The k_2 value is more than 10 times larger than the k_{blob} values obtained for Py-PAA. The contribution of excimer formed at a rate k_2 is larger in DMF than DMA, and increases linearly with pyrene content. The fraction of monomers forming excimer with the rate constant k_2 increases from ~ 0.30 up to 0.55 as the pyrene content increases from 0.020 to 0.039 p.p.b.a.. This greatly reduces the fraction of pyrenes that form excimer by diffusion in the monomer decay (f_{Mdiff}), as is seen in Figure 6.10. At the highest pyrene content of 0.039 p.p.b.a., f_{Mdiff} is even lower than 0.50.

In contrast to the fast excimer formation between clustered pyrenes described by k_2, the FBM describes the diffusive encounters between pyrenes randomly distributed along the backbone. Hence these kinetics occur on a much slower time scale. Figure 6.11 shows k_{blob} as a function of the corrected pyrene content. The corrected pyrene content, $\lambda_{Py}/(1-f_{Mfree})$, is used to account for domains of the polymer that are pyrene-poor and do not form excimer. The fraction f_{Mfree} is equal to $[Py^*_{free}]_{(t=0)}$ / ($[Py^*_{diff}]_{(t=0)}$ + $[Py^*_{free}]_{(t=0)}$ + $[Py^*_{k2}]_{(t=0)}$) and is obtained from fitting the monomer decays with Equation 6.3. k^o_{blob} is determined by extrapolating the k_{blob} values shown in Figure 6.11 to zero pyrene content. The values of k^o_{blob} are 0.79±0.15 × 10^{-7}, 0.62±0.19 × 10^{-7}, 0.84±0.13 × 10^{-7} and 0.63±0.10 × 10^{-7} in

DMF, DMF with 1 g/L LiCl, DMA, and DMA with 1 g/L LiCl, respectively. As found in Chapter 3 and previous work,[46,47] the pseudo unimolecular rate constant k^{o}_{blob} is not affected much by the viscosity of the solvent.

N_{blob} is plotted as a function of the corrected pyrene content in Figure 6.12. The N_{blob} values are determined for each sample using Equation 6.7, where λ_{Py} is the pyrene content in moles per gram polymer, x is the mole percent pyrene labeling, and M_{Py} and $M_{a.a.}$ are the molecular weights of a pyrene labeled aspartic acid and aspartic acid monomer, respectively.

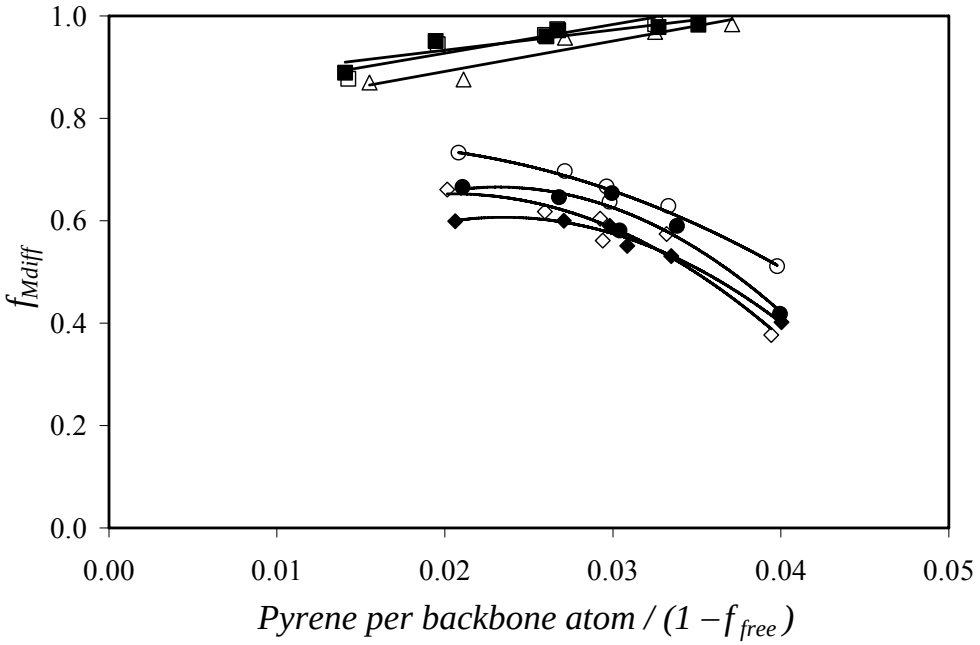

Figure 6.10: f_{Mdiff} as a function of pyrene content; Py-PAA in DMF (◆), DMA (●), DMF with 1 g/L LiCl (◇), DMA with 1 g/L LiCl (○), Py-PS in DMF (■), and DMA with 1 g/L LiCl (□), and Py-PDMA in DMF (△).

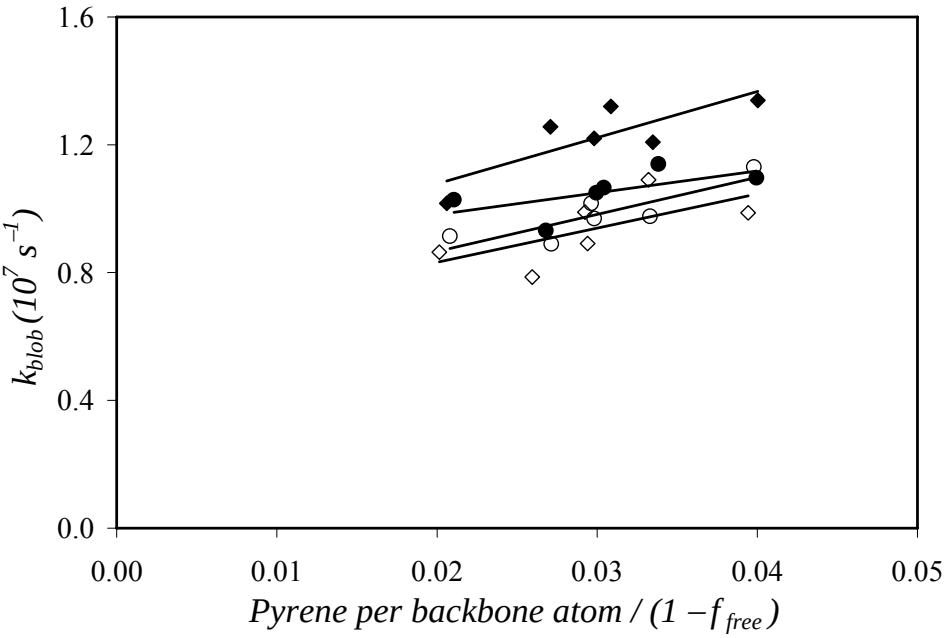

Figure 6.11: k_{blob} as a function of pyrene content; Py-PAA in DMF (◆), DMA (●), DMF with 1 g/L LiCl (◇), DMA with 1 g/L LiCl (○). [Py] = 2.5×10^{-6} M.

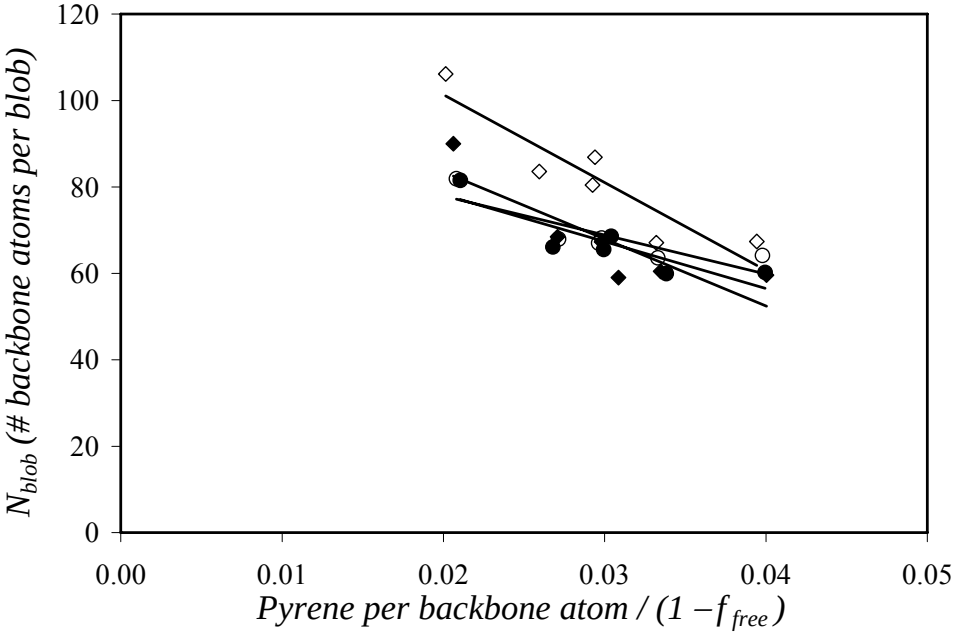

Figure 6.12: N_{blob} as a function of pyrene content; Py-PAA in DMF (◆), DMA (●), DMF with 1 g/L LiCl (◇), DMA with 1 g/L LiCl (○). [Py] = 2.5×10^{-6} M.

The overall N_{blob}^{o} values for Py-PAA in a particular solvent are determined by extrapolating N_{blob} to zero pyrene content. Extrapolation gives N_{blob}^{o} values of 114±12, 141±10, 99±8 and 95±7 backbone atoms for Py-PAA in DMF, DMF with 1 g/L LiCl, DMA, and DMA with 1 g/L LiCl, respectively. In DMF, the N_{blob}^{o} value increases slightly upon the addition of salt and implies that the coil is more condensed. In DMA, N_{blob}^{o} remains the same after salt addition. It is possible that the viscosity of the solution is high enough that a small change in coil conformation does not result in an enhancement of excimer formation. More certainly, the small effect exerted by the viscosity of the solvent on N_{blob}^{o} confirms that the encounters between pyrene pendants are controlled by the slow polymer chain dynamics rather than the solvent viscosity.

$$N_{blob} = \frac{\langle n \rangle}{\left(\lambda_{Py}/\left(1-f_{free}\right)\right)\left[M_{Py}(x)+M_{a.a.}(1-x)\right]} \tag{6.7}$$

The fraction of aggregated pyrene groups, f_{agg} (= f_{k2}+f_{E0}+f_{D}), is very similar for all solvents, with f_{agg} in DMF being slightly higher than in DMF with 1 g/L LiCl, which is in turn slightly larger than f_{agg} in DMA and DMA with 1 g/L LiCl. Overall, the level of aggregation is extremely high compared to other randomly coiled pyrene-labeled polymers, as is shown in Figure 6.13 where Py-PS in DMF and DMA with 1 g/L LiCl have f_{agg} values ~0.10 at all pyrene contents. Due to the extremely large f_{agg} values obtained for the Py-PAA samples (Figure 6.13), excimers formed via diffusion are the product of a very small fraction of pyrene monomers, namely $f_{diff} = 1-f_{agg}-f_{free}$.

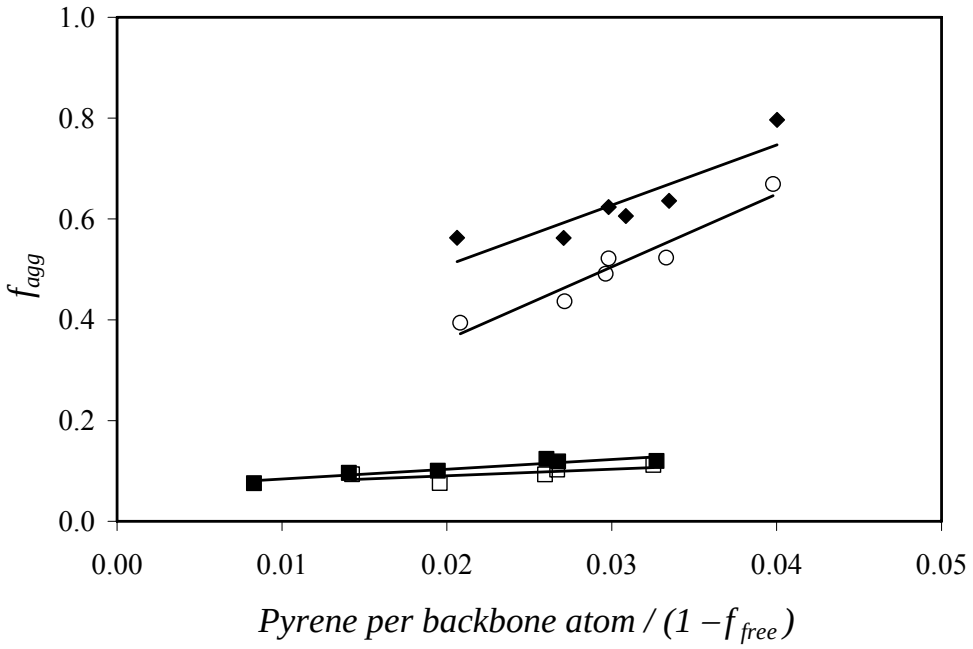

Figure 6.13: f_{agg} as a function of pyrene content; Py-PAA in DMF (◆), Py-PAA in DMA with 1 g/L LiCl (○), Py-PS in DMF (■), Py-PS in DMA with 1 g/L LiCl (□). [Py] = 2.5×10^{-6} M.

6.5 Discussion

6.5.1 Explaining the Behavior of Py-PAA in Organic Solvents

Py-PAA displays a rather interesting behavior as the polymer concentration is increased and when 1 g/L LiCl is added to the solution. When increasing amounts of Py-PAA are added to the solution, the I_E/I_M ratio increases substantially (Figure 6.3A). This increase is moderated when salt is added. The FRET experiments in Figure 6.4 show that no interpolymeric aggregation is taking place, and that the I_E/I_M ratio for the Py-PAA increases when Np-PAA is added, illustrating that the increase in I_E/I_M is not related only to Py-PAA, but PAA itself. The similar increase in the I_E/I_M ratios with polymer concentration observed in Figure 6.3 for Py-PAA and Py-PAcrylA demonstrates that these polymers are rather unique with respect to their properties in polar organic solvents compared to those displayed

by randomly coiled Py-PDMA and Py-PS and α-helical Py-PGA. The common attribute between Py-PAA and Py-PAcrylA is the carboxylic acid side-chain in their repeat unit and their random coil conformation as established with the CD experiments for Py-PAA (Figure 6.2).

The behavior of these polymers in DMF and DMA can be rationalized by assuming that Py-PAA behaves as an ionomer in organic solvent. Ionomers can have broad definitions, but generally refer to polymers containing less than 15% ionic groups where "the bulk properties are governed by ionic interactions in discrete regions of the material (the ionic aggregates)".[48] Largely, ionomers are defined as much by their properties as their composition. In low polarity solvents such as THF and toluene, ionomers aggregate to form large networks, while in polar solvents such as DMF and DMA, an ionomer will behave as a polyelectrolyte, as is the case here.[42]

Py-PAA and Py-PAcrylA are polyelectrolytes because they contain carboxylic acid groups where the protonated form is always in equilibrium with the ionized form in solution. Thus, charges are likely present along the backbone of Py-PAA. The pK_a of acetic acid has been found to be ~13.5 in DMF.[49] However, the pK_a of carboxylic acid groups within a polymer coil where the local concentration of acid groups is very high is likely to be different. Also, if the sample preparation method does not produce a fully protonated Py-PAA, carboxylate anions will be present along the backbone, and even if present in minute amounts, they are bound to affect the conformation of the polymer. A telechelic polymer with a single charge located at one chain end has been found to behave like an ionomer in organic solvents.[50]

Extensive viscosity and scattering studies of ionomers in polar organic solvents and polyelectrolytes in aqueous solution have shown that as the polymer concentration is decreased, chain expansion occurs due to a reduction in long range electrostatic repulsion.[42] This behavior explains why the I_E/I_M ratio decreases with a decrease in polymer concentration. In this case, the I_E/I_M ratio can be considered as being the coiling index of the polymer.[51] Expansion of the polymer coil upon decreasing the polymer concentration results in the dilution of the pyrene pendants in the coil and a lower I_E/I_M ratio.

Few techniques are sensitive enough to monitor the differences between inter- and intramolecular electrostatic interactions at very low polymer concentrations as is done in Figure 6.3 with polymers at concentrations smaller than 1 mg/L. Several studies of the solution properties of ionomers have been completed under very dilute conditions using pyrene-labeled polymers[52,53] and fluorescent probes.[54] In one of these studies, a polystyrene was functionalized at both ends with quaternary amines. In addition, a portion of the polystyrene was functionalized with quaternary amines *and* pyrene groups at both chain ends. The work aimed at determining the polymer concentration at which intramolecular interactions between the ionic chain ends decreased and intermolecular interactions became dominant. In THF, a low polarity solvent, the ionic groups aggregate, bringing the pyrene groups close enough to form excimer. I_E/I_M ratios were used to monitor changes in polymer interactions. By keeping the concentration of the pyrene labeled polymer constant and gradually increasing the concentration of the unlabeled polystyrene ionomer, a decrease in the I_E/I_M ratios was observed. A critical concentration of ~17 mg/mL was determined where intramolecular ionic aggregates of the chain ends, which give rise to excimer formation, gave way to intermolecular aggregates where the pyrene groups were separated and monomer

fluorescence was predominant.[53] Coincidentally, 17 mg/L coincides with an OD of 0.3 to 0.5 for the Py-PAA samples, very close to the polypeptide concentration where the I_E/I_M ratio increases for Py-PAA in DMF and DMA. Although ionomers behave very differently in THF and DMF as stated previously, the changes in I_E/I_M illustrate that long range electrostatic interactions are felt even at the very low polymer concentrations used to study Py-PAA in this work.

Besides the small number of studies that use fluorescence to characterize ionomer properties, intrinsic viscosity measurements are used extensively. It has been noted for several decades that the reduced viscosity of polyelectrolytes increases with decreasing polymer concentration before passing through a maximum value, after which the reduced viscosity decreases with decreasing polymer concentration. It has been argued that this decrease is the result of residual ions present in solution that screen the long range electrostatic repulsions felt by the polyelectolytes. Examples of polyelectrolytes exhibiting this behavior are sulfonated polystyrene[55] and star-shaped dendrimers[56] studied in aqueous solution. The polymer concentration at the point where the reduced viscosity stops increasing and begins to decrease is approximately 10 mg/L for these two ionomers. The plateau region in the I_E/I_M ratio for Py-PAA (Figure 6.3A) also begins as the concentration reaches approximately 10 mg/L. A constant I_E/I_M ratio implies a maximum expansion of the Py-PAA coil, as would be expected with no residual ions present in the solvent to screen the electrostatic interactions. The difference between the results obtained with Py-PAA by fluorescence and other polyelectrolytes by viscosity at polymer concentrations below 10 mg/L may be a result of the different levels of residual salt in the solvent used, or possibly

even the difference in the backbone structure of Py-PAA (a polyamide) compared to the sulfonated polystyrenes previously studied.

Recently, the solution properties of a PS based ionomer resulting from salt addition were examined with a SEC instrument coupled with a differential refractive index and multi-angle light scattering detectors.[41] It was found that in DMF the polymer eluted beyond the high molecular weight limit at very low elution volumes. The radius of gyration appeared to remain constant throughout the elution peak, an abnormal result, since the radius of gyration should scale with the molecular weight of a polymer. The addition of 0.2 M LiCl resulted in a large shift of the peak towards larger elution volumes and radii of gyration typically found for unfunctionalized polymers. The non-size exclusion behaviour in DMF compared to DMF with 1 g/L LiCl is very similar to the results presented for Py-PAA in Figure 6.5.

Although no previous study has to the best of our knowledge ever examined polyelectrolyte-like behavior of polypeptides in organic solvents, comparison of the results obtained for PAA from the I_E/I_M ratios, FRET, and SEC techniques with those obtained for ionomers in polar solvents strongly suggests that the unique properties displayed by Py-PAA in DMF and DMA are those of ionomers.

6.5.2 Chain Dynamics of Py-PAA

Several different pyrene-labeled polymers have been studied using the FBM, including Py-PS,[25,57] Py-PDMA,[46,47] Py-PGA,[28] and Py-polyisoprene.[58] Of all these polymers, Py-PAA is unique in that it behaves as a random coil ionomer, and thus behaves like a polyelectrolyte in aqueous solution when dissolved in polar solvents like DMF.

Table 6.2 compares some of the results obtained with two vinyl polymers, namely Py-PS and Py-PDMA, and Py-PAA in DMF and DMA with 1 g/L LiCl. The a_{E^-}/a_{E^+} ratios show

that the pyrene groups attached to the vinyl polymers are much less aggregated than those of Py-PAA. The I_1/I_3 ratios obtained from steady-state fluorescence measurements indicate similar local polarities experienced by the pyrene monomers of each polymer. The N^o_{blob} values for Py-PS and Py-PDMA reflect the solvent quality of DMF towards each polymer, a good solvent for Py-PDMA, and a poor solvent for Py-PS. The coil of Py-PDMA is more expanded (a smaller number of *N*,*N*-dimethylacrylamide units probed) than the coil of Py-PS which is more contracted (a larger number of styrene units probed). Py-PAA on the other hand, is expected to be expanded in DMF due to its polyelectrolyte character in polar solvents. Instead, the N^o_{blob} value is much larger than for Py-PS or Py-PDMA, indicating a collapsed coil or a more flexible backbone. This result seems very unlikely and highlights the probability that the FBM parameters are not equivalent when the FBM equation is modified as in Equation 6.3 to include a rate constant for pyrene groups attached in close proximity to one another. Certainly, the introduction of the contribution of excimers formed with a very fast rate constant (k_2) affects the FBM parameters. Another major complication is that the pyrene $\leftrightarrow$ quencher equivalence may not apply here, since clusters of pyrene groups could act as a single quencher.[47] This observation is bound to affect <*n*>, the average number of pyrenes per blob, and as such N_{blob} in Equation 6.7.

The existence of a rapid process for excimer formation might also affect the k^o_{blob} values, since k^o_{blob} for Py-PAA is lower than for Py-PS and Py-PDMA in DMF. Because the rate of excimer formation is described by k_2 and k_{blob} for Py-PAA and only k_{blob} for the vinyl polymers, comparisons between the kinetic parameters retrieved through the FBM analysis

are difficult to draw. The k_2 and k_{blob}^{o} values are however internally consistent for Py-PAA in the different solvents.

Regardless of the difficulties in comparing the FBM parameters retrieved for Py-PAA to the vinyl polymers previously studied, it remains clear from both the exponential analysis and the more sophisticated FBM analysis that the Py-PAA chains are much stiffer than Py-PS or Py-PAA. This is evident using the exponential analysis from the fact that a nearly 2.5 times increase in viscosity from DMF to DMA only resulted in a 25% reduction in the I_E/I_M ratios (Figure 6.6) and k_{exci} (Figure 6.8). Using the FBM analysis, both k_{blob} and N_{blob} remain constant for Py-PAA despite the large change in viscosity. Excimer formation is also unaffected by a change in coil conformation. From the SEC measurements it is clear that the size of the coil is strongly affected by the addition of LiCl. This is not reflected in the k_{exci} value retrieved from the exponential analysis or the FBM analysis. If excimer formation was due to long range diffusive encounters, a much closer relationship between coil conformation, solvent viscosity, and excimer formation would be expected. A very stiff backbone enables excimer formation only through the relatively rapid diffusive encounters between clustered pyrene groups. This conclusion is similar to those drawn with end-labeled polypeptides, where the stiffness of the polypeptide backbone imposes that only short chains be used so that sufficient end-to-end cyclization events can be generated.[9–14]

This exploratory study on the chain dynamics of polypeptides randomly labeled with pyrene has revealed two important aspects that must be taken into account for future studies. Firstly, a labeling method must be devised to reduce the number of pyrene groups that are aggregated together and form excimer at a very fast rate k_2. This would hopefully allow for the typical FBM analysis that would yield results which could be better compared to those

obtained with Py-PS and Py-PDMA. Previous work with Py-PS (Chapter 2) has shown that incorporating pyrene through co-polymerization reactions results in polymers with fewer aggregated pyrenes. This is a synthetic route that could be considered to produce Py-PAA samples where the labels are not clustered. Secondly, a polypeptide should be chosen that is free of ionic groups. The chain expansion associated with polyelectrolytes is an enormous topic of study and could be investigated separately using typical ionomers such as functionalized polystyrene.

6.6 Conclusions

The characteristics of the Py-PAA coil were analyzed in DMF, DMA, DMF with 1 g/L LiCl, and DMA with 1 g/L LiCl using CD, SEC, and fluorescence techniques. CD experiments indicated that Py-PAA had little to no secondary structure in any of the solvents used compared to Py-PGA (Figures 6.1 and 6.2). Steady-state measurements were conducted as a function of Py-PAA concentration and showed that excimer formation increased with an increase in concentration (Figure 6.3A). For comparison, the I_E/I_M ratios of several other pyrene labeled polymers were also acquired as a function of polymer concentration. The I_E/I_M ratios remained constant with polymer concentration for a randomly coiled polymer in a good and a theta-solvent (Py-PS in DMA with 1 g/L LiCl and methyl acetate), a water soluble polymer (Py-PDMA), and an α-helical polypeptide containing a carboxylic acid side-chain (Py-PGA). However, a randomly coiled polyelectrolyte, Py-PArcylA, had a behavior similar to that of Py-PAA. This illustrated that the change in the I_E/I_M ratios is due to the carboxylic acid side-chain of Py-PAA, and that it behaves as a randomly coiled polyelectrolyte. To confirm that the increase in excimer formation was due to a change in coil conformation and not aggregation of the PAA coils, FRET experiments were conducted

using Np-PAA and Py-PAA. The FRET experiments showed that no aggregation was occurring between the PAA coils, and that pyrene excimer formation increased with PAA concentration whether Py-PAA was used alone (Figure 6.3A) or when Np-PAA was added to the solution (Figure 6.4). SEC measurements also confirmed that Py-PAA exhibited a polyelectrolyte-like behavior through its non-size exclusion behavior when DMF was used as the eluent (Figure 6.5). Time-resolved fluorescence experiments conducted in the plateau region of the I_E/I_M ratios (Figure 6.3A) showed an extremely high level of clustering between pyrene groups. This complicated the analysis of excimer formation which is used to determine the chain dynamics of Py-PAA. The aggregation was large enough to require the addition of a large rate constant (k_2) in order to fit the decays. Using the modified FBM equation, the values obtained for N_{blob}^{o} and k_{blob}^{o} were larger and smaller, respectively, than what would be expected from the extended coil conformation of a polyelectrolyte and compared to the FBM parameters obtained for Py-PS and Py-PDMA. This is likely due to the addition of the rate constant k_2 to the analysis which isolates the fast excimer forming contribution from the model. The most important result obtained was that excimer formation was not controlled by the solvent viscosity. This was determined based on the observation that regardless of the treatment of the time-resolved decays, excimer formation was relatively constant when the solution viscosity was increased by almost 2.5 times, in stark contrast to previous work[43] as well as the study on Py-PS conducted in Chapter 3 which showed that excimer formation is viscosity controlled.

In summary, this examination of a randomly coiled polypeptide randomly labeled with pyrene demonstrated polyelectrolyte character in polar organic solvents and illustrated the

stiffness of the PAA backbone which hindered excimer formation to such an extent that excimer formation was not controlled by the solvent viscosity.

6.7 References

1. a) Williams, S.; Causgrove, T. P.; Gilmanshin, R.; Fang, K. S.; Callender, R. H.; Woodruff, W. H.; Dyer, R. B. *Biochemistry* **1996**, *35*, 691-697. b) Lednev, I. K., Karnoup, A. S., Sparrow, M. C., Asher, S. A. *J. Am. Chem. Soc*. **1999**, *121*, 8074-8086. c) Thompson, P. A.; Munoz, V.; Jas, G. S.; Henry, E. R.; Eaton, W. A.; Hofrichter, J. *J. Phys. Chem. B* **2000**, *104*, 378-389.

2. Zscherp, C.; Barth, A. *Biochemistry* **2001**, *40*, 1875-1883.

3. a) Hagen, S. J.; Hofrichter, J.; Szabo, A.; Eaton, W. A. *Proc. Natl. Acad. Sci. USA* **1996**, *93*, 11615-11617. b) Abel, C. J.; Goldbeck R. A.; Latypov, R. F.; Roder, H.; Kliger, D. S. *Biochemistry* **2007**, *46*, 4090-4099.

4. a) Huang, G. S.; Oas, T. G. *Proc. Natl. Acad. Sci. USA* **1995**, *92*, 6878-6882. b) Wang, M.; Tang, Y.; Sato, S.; Vugmeyster, L.; McKnight, C. J., Raleigh D. P. *J. Am. Chem. Soc*. **2003**, *125*, 6032-6033. c) Jarymowycz, V. A.; Stone, M. J. *Chem. Rev*. **2006**, *106*, 1624-1671. d) Igumenova, T. I.; Frederick, K. K.; Wand, A. J. *Chem. Rev*. **2006**, *106*, 1672-1699.

5. Decatur, S. *Acc. Chem. Res*. **2006**, *39*, 169-175.

6. Nabuchi, Y.; Murao, N.; Asoh, Y.; Takayama, M. *Anal. Chem.* **2007**, *79*, 8342-8349.

7. Uzawa, T.; Kimura, T.; Ishimori, K.; Morishima, I.; Matsui, T.; Ikeda-Saito, M.; Takahashi, S.; Akiyama, S.; Fujisawa, T. *J. Mol. Biol*. **2006**, *357*, 997-1008.

8. a) Cuniberti, C.; Perico, A. *Prog. Polym. Sci*. **1984**, *10*, 271-316. b) Winnik, M. A. *Acc. Chem. Res.* **1985**, *18*, 73-79.

9. Bieri, O.; Wirz, J.; Hellrung, B.; Schutkowski, M.; Drewello, M.; Kiefhaber, T. *Proc. Natl. Acad. Sci. USA* **1999**, *96*, 9597-9601.

10. Krieger, F.; Fierz, B.; Bieri, O.; Drewello, M.; Kiefhaber, T. *J. Mol. Biol*. **2003**, *332*, 265-274.

11. Moglich, A.; Krieger, F.; Kiefhaber, T. *J. Mol. Biol*. **2005**, *345*, 153-162.

12. Lapidus, L. J.; Eaton, W. A.; Hofrichter, J. *Proc. Natl. Acad. Sci*. **2000**, *97*, 7220-7225.

13. Hudgins, R. R.; Huang, F.; Gramlich, G.; Nau, W. M. *J. Am. Chem. Soc*. **2002**, *124*, 556-564.

14. Huang, F.; Hudgins, R. R.; Nau, W. M. *J. Am. Chem. Soc*. **2004**, *126*, 16665-16675.

15. a) Hyeon, C.; Thirumalai, D. *J. Chem. Phys*. **2006**, *124*, 104905-104919. b) Doucet, D.; Roitberg, A.; Hagen, S. J. *Biophys. J*. **2007**, *92*, 2281-2289.

16. Winnik, F. M. *Chem. Rev*. **1993**, *93*, 587-614.

17. Duhamel, J. *Acc. Chem. Res.* **2006**, 39, 953-960.

18. a) Tabata, K.; Kasuya, K-I.; Abe, H.; Masuda, K.; Doi, Y. *Appl. Environ. Microbiol*. **1999**, *65*, 4268-4270. b) Tabata, K.; Abe, H.; Doi Y. *Biomacromolecules* **2000**, *1*, 157-161.

19. Nakato, T.; Yoshitake, M.; Matsubara, K.; Tomida, M. *Macromolecules* **1998**, *31*, 2107-2113.

20. Caldwell, G.; Neuse, N. W.; Perlwitz, A. G. *J. Appl. Polym. Sci*. **1997**, *66*, 911-919.

21. Shinoda, H.; Asou, Y.; Suetsugu, A.; Tanaka, K. *Macromol. Biosci*. **2003**, *3*, 34-43.

22. Kang, H. S.; Yang, R. R.; Kim, J.-D.; Han, S.-H.; Chang, I.-S. *Langmuir* **2001**, *17*, 7501-7506.

23. Tomida, M.; Nakato, T.; Kuramochi, M.; Shibata, M.; Matsunami, S.; Kakuchi, T. *Polymer* **1997**, *38*, 4733-4736.

24. Marcus, Y. *Chem. Soc. Rev*. **1993**, *22*, 409-416.

25. Py-PS was the CoA-PS used in Chapters 2 and 3.

26. a) Picova, H.; Saudek, V.; Drobnik, J.; Vlasak, J. *Biopolymers* **1981**, *20*, 1605-1614. b)Saudek, V.; Picova, H.; Drobnik, J. *Biopolymers* **1981**, *20*, 1615-1623.

27. a) Tomida, M.; Nakato, T.; Matsunami, S.; Kakuchi, T. *Polymer* **1997**, *38*, 4733-4736. b) Nakato, T.; Tomida, M.; Suwa, M.; Morishima, Y.; Kusuno, A.; Kakuchi, T. *Polymer Bull.* **2000**, *44*, 385-391. c) Kang, H. S.; Shin, M.-S.; Yang, J.-W. *Polymer Bull*. **2000**, *45*, 39-43.

28. Duhamel, J.; Kanagalingam, S.; O'Brien, T.; Ingratta, M. *J. Am. Chem. Soc.* **2003**, *125*, 12810-12822.

29. James, D. R.; Demmer, D. R.; Verall, R. E.; Steer, R. P. *Rev. Sci. Instrum.* **1983**, *54*, 1121-1130.

30. Mathew, H.; Siu, H.; Duhamel, J. *Macromolecules* **1999**, *32*, 7100-7108.

31. Prazeres, T. J. V.; Beingessner, R.; Duhamel, J.; Olesen, K.; Shay, G.; Bassett, D. R. *Macromolecules* **2001**, *34*, 7876-7884.

32. Siu, H.; Duhamel, J. *Macromolecules* **2006**, *39,* 1144-1155.

33. Press, W. H.; Flannery, B. P.; Teukolsky, S. A.; Vetterling, W. T. in *Numerical Recipes. The Art of Scientific Computing (Fortran Version)*; Cambridge University Press: Cambridge, 1992, p 523 – 528.

34. Demas, J. N. *Excited-State Lifetime Measurements*; Academic Press: New York, 1983, p 134, 147.

35. a) Cheng, R. P.; Gellman, S. H.; DeGrado, W. F. *Chem. Rev*. **2001**, *101*, 3219-3232. b) Ahmed, S.; Beleid, R.; Sprules, T.; Kaur, K. *Org. Lett*. **2007**, *9*, 25-28.

36. a) Saudek, V.; Strokrova, S.; Schmidt, P. *Biopolymers* **1982**, *21*, 1011-1020. b) Saudek, V.; Strokrova, S.; Schmidt, P. *Biopolymers* **1982**, *21*, 2195-2203.

37. Shoji, O.; Ohkawa, M.; Kuwata, H.; Sumida, T.; Kato, R.; Annaka, M.; Yoshikuni, M.; Nakahira, T. *Macromolecules* **2001**, *34*, 4270-4276.

38. Lakowicz, J. R. *Principles of Fluorescence Spectroscopy, 2nd Ed*. Kluwer Academic/Plenum Publishers: New York, 1999.

39. Berlman, I. B. *Energy Transfer Parameters of Aromatic Compounds*, Academic Press: New York, 1973.

40. Winnik, F. M. *Polymer* **1990**, *31*, 2125-2134.

41. Marcelo, G.; Mendicuti, F.; Saiz, E.; Tarazona, M. P. *Macromolecules* **2007**, *40*, 1311-1320.

42. a) Eisenberg, A.; Kim, J.-S. in *Introduction to Ionomers*, John Wiley and Sons Inc.: New York, 1998. b) Tant, M. R.; Mauritz, K. A.; Wilkes, G. L. in *Ionomers: Synthesis, Structure, Properties and Applications,* Blackie Academic and Professional: London, 1997.

43. a) Cuniberti, C.; Perico, A. *Eur. Polym. J.* **1980**, *16*, 887-893. b) Cheung, S.-T.; Winnik, M. A.; Redpath, A. E. C. *Makromol. Chem.* **1982**, *183*, 1815-1824.

44. Winnik, M. A.; Egan, L. S.; Tencer, M.; Croucher, M. D. *Polymer* **1987**, *28*, 1553-1560.

45. Kanagalingam, S.; Spartalis, J.; Cao, T.-M.; Duhamel, J. *Macromolecules* **2002**, *35*, 8571-8577.

46. Kanagalingam, S.; Ngan, C. F.; Duhamel, J. *Macromolecules* **2002**, *35*, 8560-8570.

47. Birks, J. B. in *Photophysics of Aromatic Molecules*. Wiley: New York, 1970; p 301.

48. Eisenberg, A.; Rinaudo, M. *Polymer Bull*. **1990**, *24*, 671.

49. Maran, F. Celadon, D.; Severin, M.; Vianello, E. *J. Am. Chem. Soc*. **1991**, *113*, 9320-9329.

50. a) Hara, M.; Wu, J.-L.; Jerome, R. J.; Granville, M. *Macromolecules* **1988**, *21*, 3330-3331. b) Wu, J.-L.; Wang, Y.-M.; Hara, M.; Granville, M.; Jerome, R. J. *Macromolecules* **1994**, *27*, 1195-1200.

51. Kramer, G.; Somasundaran, P. *Langmuir* **2002**, *18*, 9357-9361.

52. Hermans, B.; De Schryver, F. C.; van Stam, J.; Boens, N.; Jerome, R.; Teyssie, P.; Trossaert, G.; Goethals, E.; Schacht, E. *Macromolecules* **1995**, *28*, 3380-3386.

53. Granville, M.; Jerome, R. J.; Teyssie, P.; De Schryver, F. C. *Macromolecules* **1988**, *21*, 2894-2896.

54. a) Dowling, K. C.; Thomas, J. K. *Macromolecules* **1991**, *24*, 4213-4130. b) Bakeev, K. N.; MacKnight, W. J. *Macromolecules* **1991**, *24*, 4578-4582.

55. Cohen, J. Priel, Z.; Rabin, Y. *J. Chem. Phys*. **1998**, *88*, 7111-7116.

56. Moinard, D; Borsali, R.; Taton, D.; Gnanou, Y. *Macromolecules* **2005**, *38*, 7105-7120.

57. Mathew, A. K.; Siu, H.; Duhamel, J. *Macromolecules* **1999**, *32*, 7100-7108.

58. Teertstra, S. PhD. Dissertation, **2006**, University of Waterloo, Ontario, Canada.

6.8 Appendix

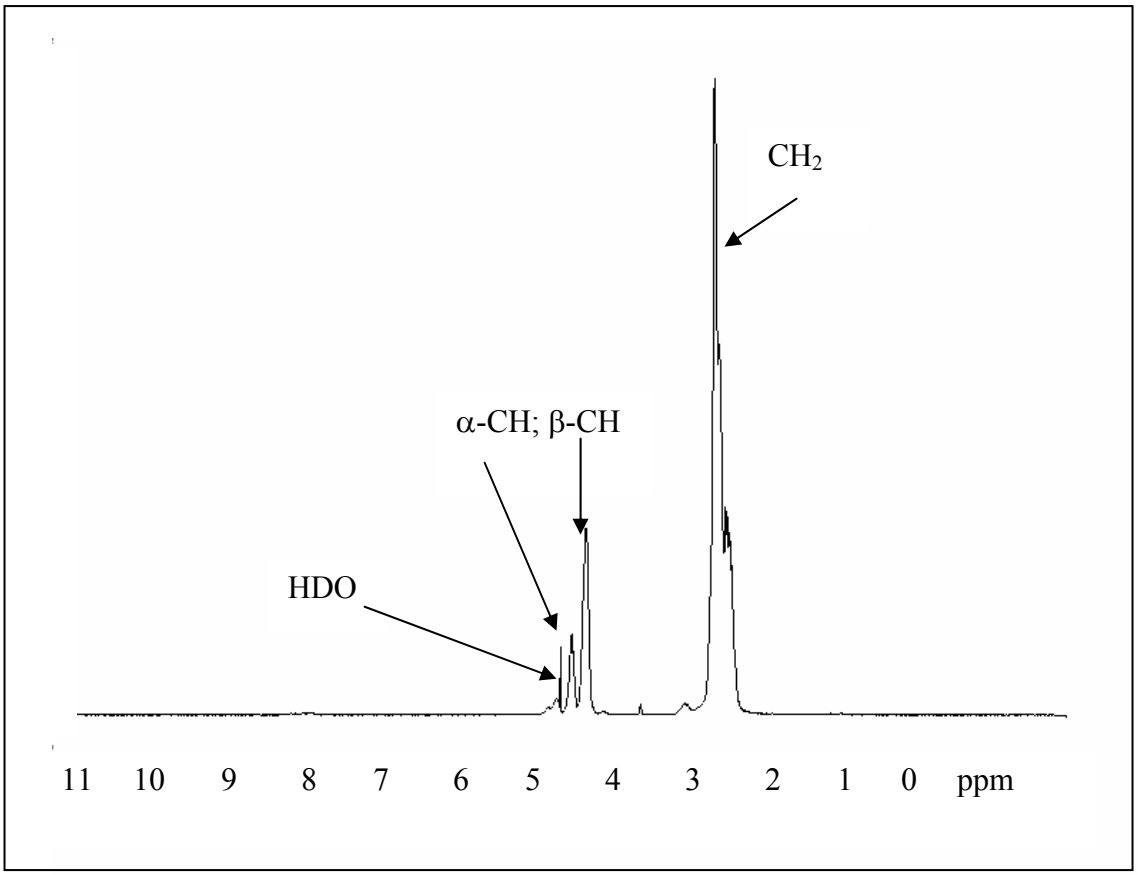

Figure A6.1: 300 MHz ^{1}H NMR (D_2O): Poly(aspartic acid) (Sigma Aldrich): δ 2.5 (CH_2), δ 4.3 (β-CH), δ 4.5 (α-CH).

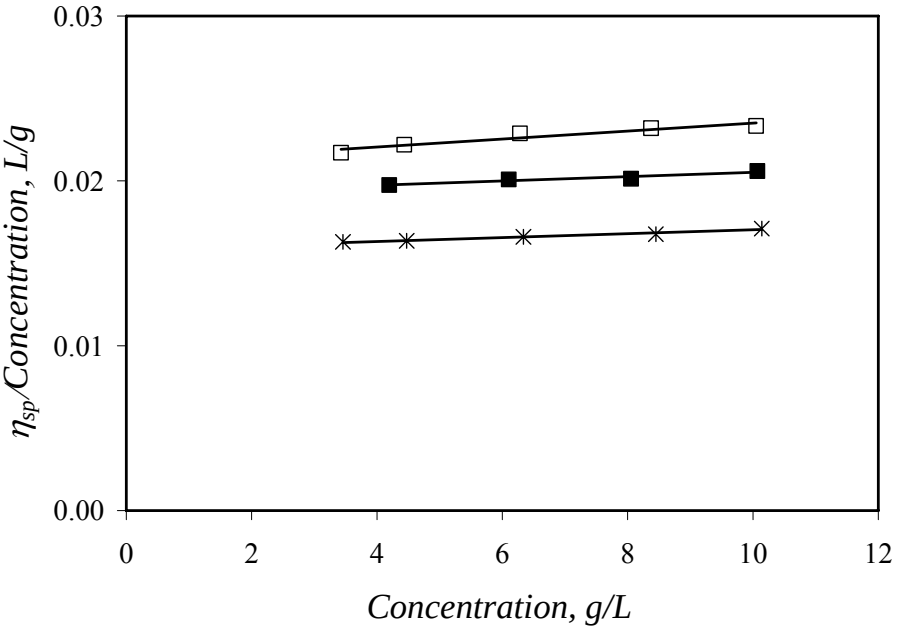

Figure A6.2: Reduced viscosity of PS-40K at T = 25 °C in DMA with 1 g/L LiCl (□), $[\eta]_{40K\ PS}$ = 0.023±0.002, DMF (■), $[\eta]_{40K\ PS}$ = 0.0192±0.0003, methyl acetate (∗), $[\eta]_{40K\ PS}$ = 0.0159±0.0001.

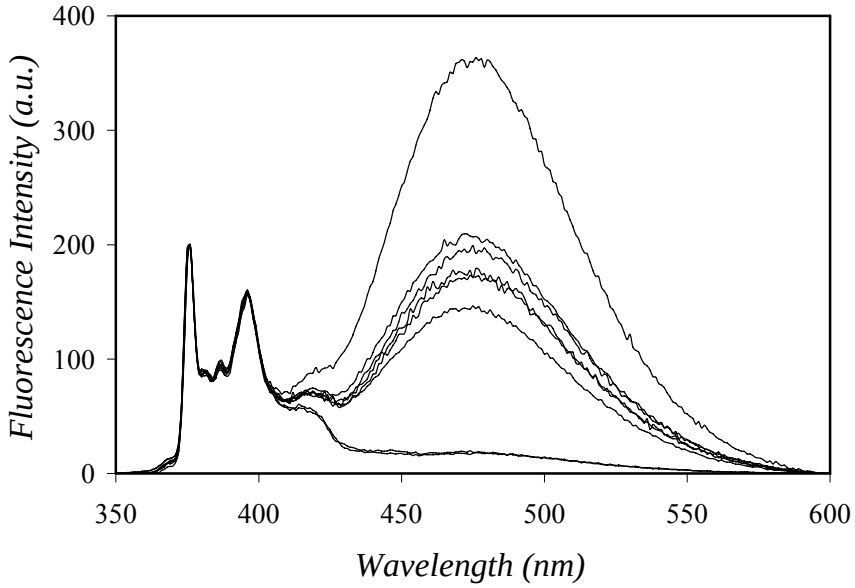

Figure A6.3: Steady-state fluorescence spectra of Py-PAA in DMF. The pyrene content increases from bottom to top and equals 0.005, 0.008, 0.020, 0.026, 0.026, 0.029, 0.033, and 0.039 p.p.b.a. [Py] = 2.5×10^{-6} M, λ_{ex} = 346 nm.

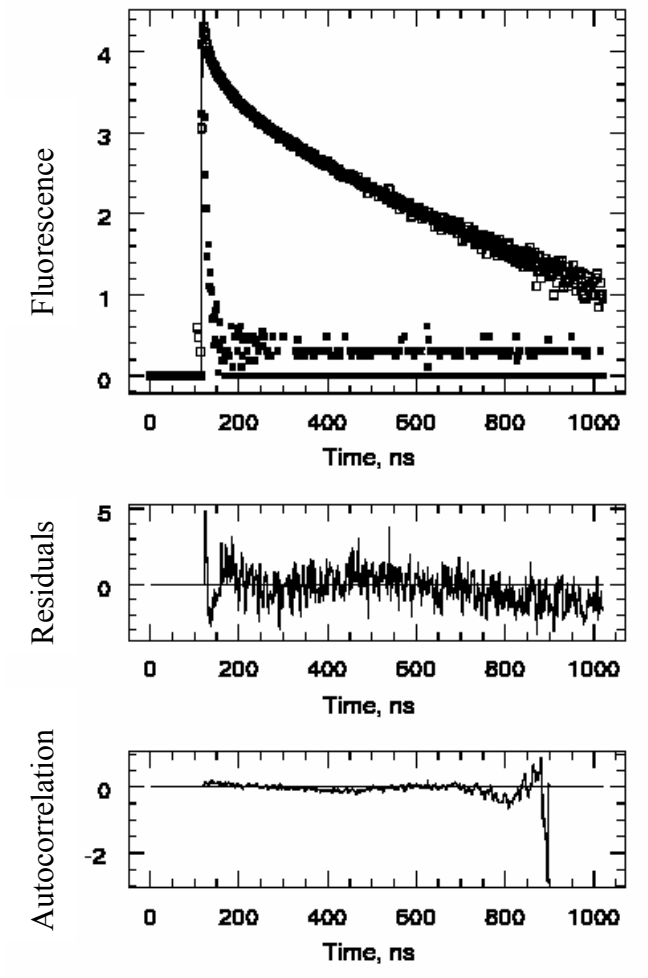

Figure A6.3: Monomer fluorescence decay of Py-PAA with 0.033 pyrenes per backbone atom in DMF. The decay is analyzed with Equations 6.3 without the parameters describing excimer formation with a rate constant k_2. [Py] = 2.5×10^{-6} M, λ_{ex} = 340 nm, λ_{em} = 376 nm; χ^2 = 1.86.

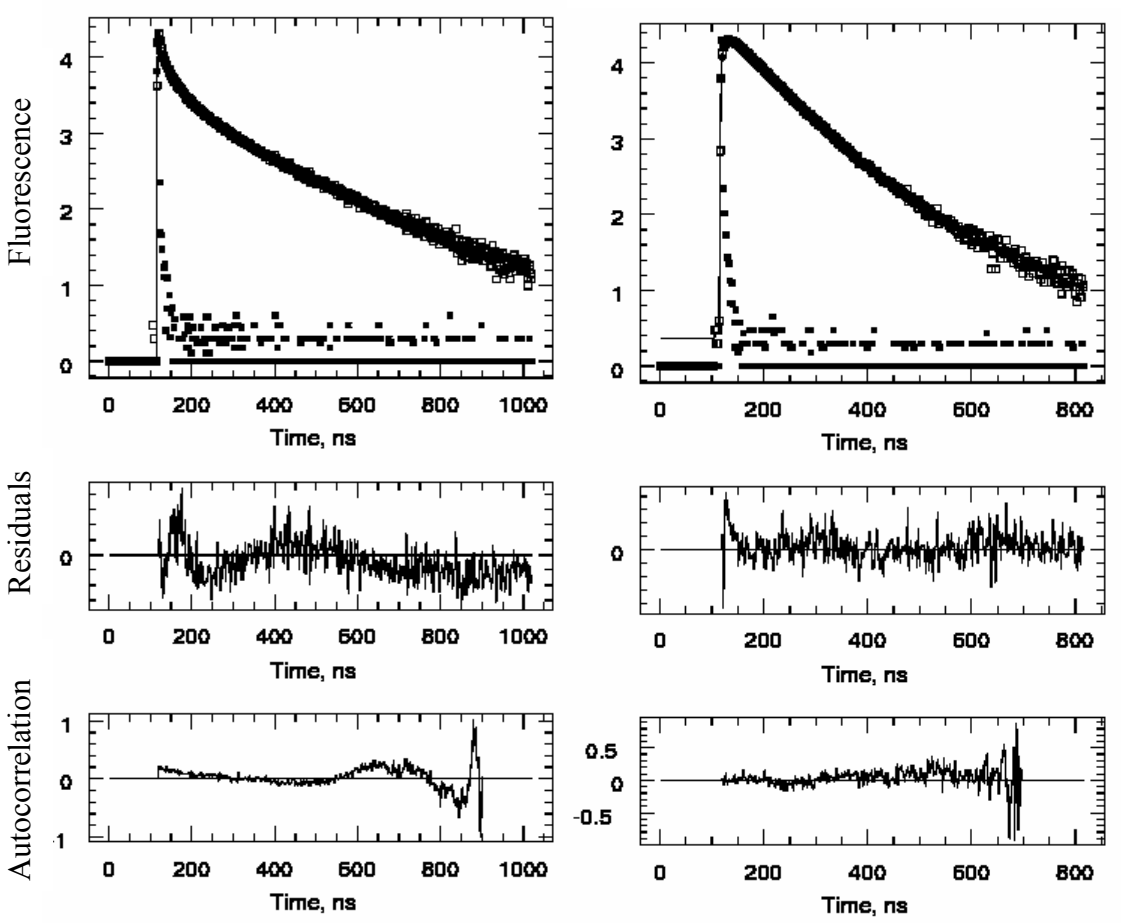

Figure A6.4: Monomer (left) and excimer (right) fluorescence decays of Py-PAA with 0.033 pyrenes per backbone atom in DMF. The monomer and excimer decays are analyzed simultaneously with Equations 6.3 and 6.5, respectively, without the parameters describing excimer formation with a rate constant k_2. [Py] = 2.5×10^{-6} M, λ_{ex} = 340 nm, λ_{em}(mono) = 376 nm, λ_{em}(exci)= 510 nm; $\chi^2 = 1.77$.

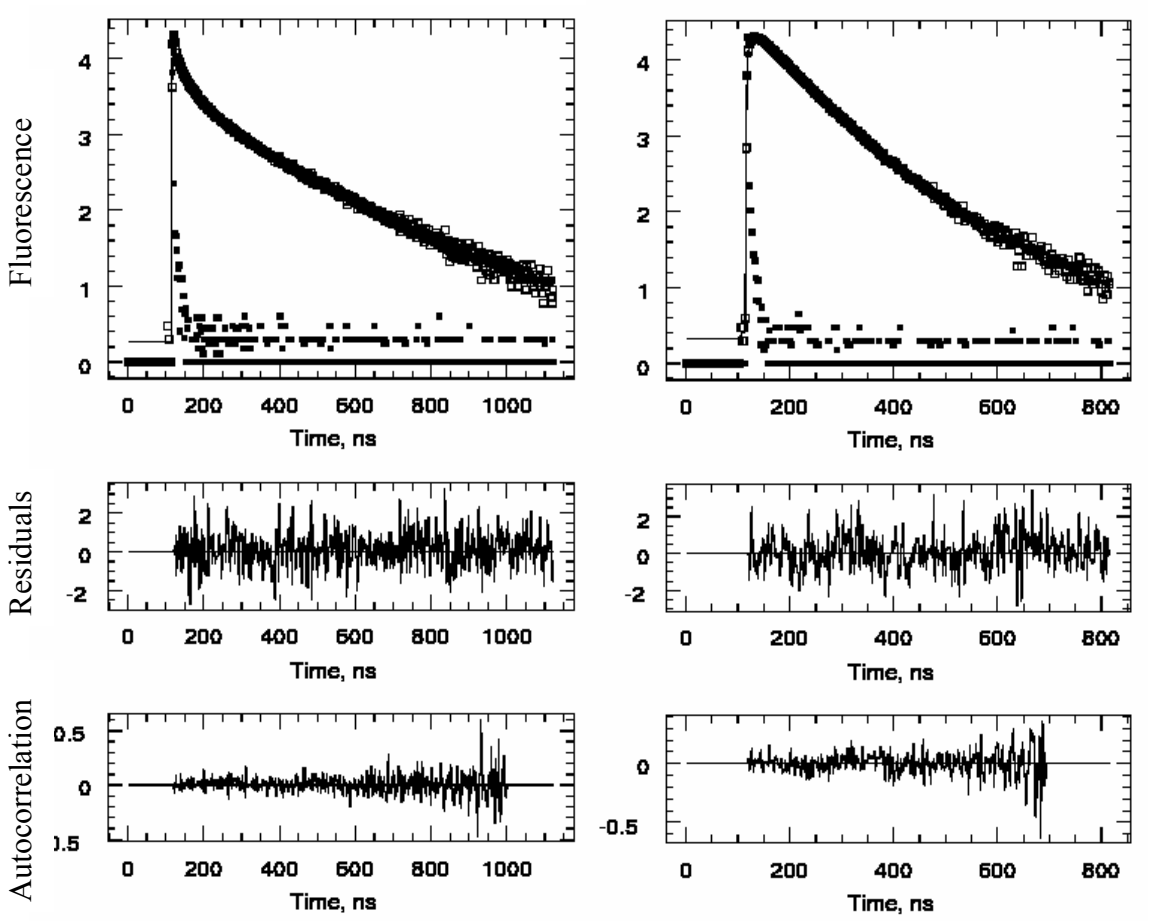

Figure A6.5: Monomer (left) and excimer (right) fluorescence decays of Py-PAA with 0.033 pyrenes per backbone atom in DMF. The monomer and excimer decays are analyzed simultaneously with Equations 6.3 and 6.5, respectively. [Py] = 2.5×10^{-6} M, λ_{ex} = 340 nm, λ_{em}(mono) = 376 nm, λ_{em}(exci)= 510 nm; $\chi^2 = 0.99$.

Table A6.1: Parameters retrieved from the multi-exponential fits of the monomer decays of Py-PAA, Py–PS and Py-PDMA in various solvents with Equation 6.2.

Sample	Pyrene per atom	τ_1 (ns)	τ_2 (ns)	τ_3 (ns)	τ_4 (ns)	a_1	a_2	a_3	a_4	χ^2
Py-PAA	0.005		26	119	215		0.24	0.33	0.43	1.07
	0.008		33	142	215		0.33	0.37	0.29	1.19
DMF	0.020	10	45	142	215	0.45	0.36	0.16	0.03	1.07
	0.026	7	34	116	215	0.42	0.36	0.17	0.05	1.15
	0.029	9	35	110	215	0.46	0.35	0.16	0.03	1.12
	0.029	7	32	109	215	0.45	0.34	0.16	0.05	1.15
	0.033	7	31	105	215	0.48	0.34	0.14	0.03	1.09
	0.039	6	23	88	215	0.57	0.32	0.09	0.03	1.19
	0.005		23	123	215		0.21	0.31	0.48	1.13
	0.008		26	116	215		0.25	0.25	0.50	1.20
Py-PAA	0.020	6	31	110	215	0.28	0.42	0.23	0.08	1.16
	0.026	10	47	138	215	0.39	0.38	0.18	0.04	1.05
DMA	0.029	9	37	117	215	0.36	0.40	0.19	0.04	1.14
	0.029	7	32	102	215	0.40	0.38	0.18	0.04	1.10
	0.033	7	28	98	215	0.36	0.41	0.18	0.05	1.15
	0.039	6	21	79	215	0.47	0.37	0.13	0.03	1.28
	0.005		20	84	205		0.24	0.23	0.53	1.08
	0.008		20	104	205		0.20	0.28	0.52	1.05
Py-PAA	0.020	6	29	93	205	0.27	0.43	0.24	0.03	1.07
	0.026	9	38	104	205	0.40	0.38	0.20	0.02	1.06
DMF	0.029	7	30	92	205	0.40	0.40	0.19	0.02	1.22
1 g/L LiCl	0.029	7	31	90	205	0.43	0.38	0.17	0.02	1.12
	0.033	7	29	93	205	0.42	0.39	0.17	0.02	1.07
	0.039	6	23	80	205	0.56	0.32	0.11	0.01	1.16
	0.005		19	118	210		0.20	0.25	0.55	1.10
	0.008		21	96	210		0.26	0.24	0.50	1.18
Py-PAA	0.020	13	51	139	210	0.33	0.40	0.25	0.03	1.04
	0.026	10	41	119	210	0.30	0.39	0.26	0.05	1.02
DMA	0.029	8	33	101	210	0.30	0.41	0.26	0.03	1.29
1 g/L LiCl	0.029	10	40	121	210	0.41	0.39	0.18	0.02	1.23
	0.033	9	35	109	210	0.39	0.40	0.19	0.03	1.10
	0.039	9	34	113	210	0.56	0.33	0.09	0.02	1.10
	0.006	25	91	183	220	0.08	0.24	0.54	0.14	1.01
Py-PS	0.013	16	54	128	220	0.08	0.24	0.59	0.09	0.96
DMF	0.019	20	68	115	220	0.14	0.43	0.40	0.03	1.06
	0.025	4	38	92	220	0.20	0.30	0.48	0.02	0.98
	0.026	8	34	80	220	0.11	0.33	0.53	0.03	0.98
	0.032	6	31	73	220	0.11	0.35	0.52	0.02	1.06
	0.006	30	141	210		0.13	0.44	0.43		1.11
Py-PS	0.013	41	137	210		0.25	0.65	0.10		1.13
DMA	0.019	41	120	210		0.30	0.66	0.04		1.25
1 g/L LiCl	0.025	35	103	210		0.33	0.63	0.03		1.21
	0.026	31	99	210		0.33	0.64	0.02		1.17
	0.032	31	86	210		0.38	0.60	0.01		1.27
	0.014	11	50	130	220	0.08	0.30	0.54	0.08	1.18
Py-PDMA	0.019	11	49	122	220	0.09	0.33	0.49	0.09	1.04
DMF	0.026	8	41	98	220	0.13	0.41	0.44	0.03	0.98
	0.032	12	42	89	220	0.16	0.46	0.36	0.02	0.99
	0.037	5	26	68	220	0.12	0.45	0.42	0.01	1.15

Table A6.1: Parameters retrieved from the multi-exponential fits of the excimer decays of Py-PAA, Py–PS and Py-PDMA in various solvents with Equation 6.2.

Sample	Pyrene per atom	τ_1 (ns)	τ_2 (ns)	τ_3 (ns)	τ_4 (ns)	a_1	a_2	a_3	a_4	χ^2
	0.005		22	81	149		-1.00	1.72	0.28	1.18
	0.008		18	69	152		-0.82	1.62	0.19	1.02
Py-PAA	0.020	4	12	62	122	-0.21	-1.33	2.37	0.17	1.02
	0.026	7	19	56	103	-0.80	-0.66	2.14	0.32	1.09
DMF	0.029	8	20	52	90	-0.68	-0.53	1.78	0.42	1.11
	0.029	5	15	55	110	-0.61	-0.99	2.35	0.26	1.09
	0.033	3	13	56	115	-0.97	-1.67	3.34	0.31	1.12
	0.039	5	15	45	74	-0.54	-0.52	1.37	0.69	1.09
	0.005		30	82	159		-0.91	1.42	0.49	0.92
	0.008		22	71	142		-0.86	1.47	0.38	1.13
Py-PAA	0.020	5	18	55	94	-0.48	-1.81	2.40	0.90	1.16
	0.026	6	20	59	118	-1.00	-1.87	3.43	0.45	1.10
DMA	0.029	3	15	58	107	-0.67	-1.89	3.05	0.51	0.91
	0.029	7	26	46	90	-1.19	-1.80	3.08	0.92	1.20
	0.033	4	15	59	116	-0.74	-1.87	3.31	0.31	1.03
	0.039	4	15	51	90	-0.99	-1.33	2.76	0.57	1.07
	0.005		30	77	152		-0.82	1.43	0.38	1.00
	0.008		19	71	148		-0.81	1.57	0.23	1.07
Py-PAA	0.020	5	17	60	120	-0.90	-1.57	3.13	0.35	1.08
	0.026	7	21	59	123	-1.20	-1.07	2.99	0.28	1.17
DMF	0.029	7	24	55	110	-1.07	-0.90	2.65	0.32	1.42
1 g/L LiCl	0.029	4	13	58	116	-0.58	-1.22	2.58	0.22	0.99
	0.033	3	13	57	114	-0.60	-1.48	2.82	0.26	1.24
	0.039	5	15	51	95	-0.77	-0.53	2.01	0.29	1.09
	0.005		39	68	152		-1.28	1.65	0.63	0.94
	0.008		23	75	159		-0.84	1.57	0.27	1.19
Py-PAA	0.020	6	18	64	117	-0.55	-1.82	2.90	0.47	1.13
	0.026	7	20	61	114	-0.82	-1.49	2.85	0.45	1.17
DMA	0.029	6	20	55	97	-0.90	-1.54	2.65	0.80	1.02
1 g/L LiCl	0.029	3	16	60	113	-0.80	-1.95	3.34	0.41	1.12
	0.033	6	19	59	115	-0.88	-1.44	3.01	0.32	1.09
	0.039	8	32	45	86	-1.17	-1.63	3.17	0.62	1.04
	0.006		32	129	225		-2.43	3.02	0.40	1.11
Py-PS	0.013		30	111	232		-3.24	4.09	0.17	1.13
DMF	0.019		29	94	145		-4.11	4.82	0.30	1.13
	0.025		27	99	84		-4.16	1.98	3.18	1.10
	0.026	7	28	83		-0.84	-6.20	8.05		1.02
	0.032	6	27	79		-0.59	-5.37	6.97		1.07
	0.006		32	108	169		-1.94	1.59	1.34	0.98
Py-PS	0.013		29	113	170		-2.93	3.34	0.59	1.00
DMA	0.019		27	102	124		-4.88	3.86	2.02	1.15
1 g/L LiCl	0.025	11	36	80	120	-1.80	-7.35	7.43	2.71	1.06
	0.026	7	30	87	126	-0.82	-6.34	6.87	1.29	1.04
	0.032	9	28	87		-0.96	-5.90	7.85		1.14
	0.014		27	96	160		-4.41	4.60	0.81	1.02
Py-PDMA	0.019		26	96	163		-4.209	4.71	0.50	1.00
DMF	0.026		26	80	116		-4.56	4.73	0.83	1.22
	0.032		23	75	92		-4.33	4.18	1.14	1.13
	0.037		21	68	78		-3.77	3.04	1.72	1.15

Table A6.3: Parameters retrieved from the global analysis of the monomer decays of Py-PAA, Py-PS and Py-PDMA in various solvents with Equation 6.3.

Polymer	Pyrene per atom	f_{Mdiff}	f_{Mfree}	f_{Mk2}	k_2 (10^7 s^{-1})	k_{blob} (10^7 s^{-1})	k_e [blob] (10^7 s^{-1})	<n>	χ^2
Py-PAA	0.020	0.60	0.03	0.37	12	1.0	0.2	1.8	1.03
	0.026	0.60	0.04	0.36	15	1.3	0.2	1.8	1.07
DMF	0.029	0.59	0.03	0.38	13	1.2	0.3	2.0	1.1
	0.029	0.55	0.05	0.39	14	1.3	0.2	1.8	1.09
	0.033	0.53	0.02	0.44	14	1.2	0.2	2.0	0.99
	0.039*	0.40	0.02	0.58	13	1.3	0.2	2.4	1.12
Py-PAA	0.020	0.67	0.05	0.28	11	1.0	0.2	1.7	1.05
	0.026	0.65	0.03	0.32	11	0.9	0.1	1.7	1.04
DMA	0.029	0.65	0.03	0.31	13	1.1	0.2	1.9	1.02
	0.029	0.58	0.04	0.38	12	1.1	0.3	2.1	1.16
	0.033	0.59	0.03	0.37	12	1.1	0.2	2.0	1.08
	0.039*	0.42	0.02	0.56	12	1.1	0.1	2.4	1.17
Py-PAA	0.020	0.66	0.01	0.33	12	0.9	0.2	2.1	1.07
	0.026	0.62	0.00	0.38	12	0.8	0.1	2.1	1.01
DMF	0.029	0.60	0.01	0.38	15	1.0	0.2	2.3	1.23
1 g/L LiCl	0.029	0.56	0.01	0.43	13	0.9	0.1	2.5	1.07
	0.033	0.57	0.02	0.41	14	1.1	0.2	2.2	1.20
	0.039*	0.38	0.01	0.62	13	1.0	0.1	2.6	1.19
Py-PAA	0.020	0.73	0.04	0.23	11	0.9	0.2	1.7	1.15
	0.026	0.70	0.04	0.27	10	0.9	0.2	1.8	1.09
DMA	0.029	0.67	0.02	0.31	13	1.0	0.3	1.9	1.11
1 g/L LiCl	0.029	0.64	0.02	0.34	12	1.0	0.2	2.0	1.20
	0.033	0.63	0.02	0.35	12	1.0	0.2	2.1	1.13
	0.039	0.51	0.02	0.47	13	1.1	0.1	2.5	1.08
	0.006	0.66	0.34			1.2	0.6	0.6	1.11
Py-PS	0.013	0.89	0.11			1.2	0.8	0.8	1.09
DMF	0.019	0.95	0.15			1.1	1.0	1.2	1.08
	0.025	0.96	0.04			1.2	1.0	1.4	1.02
	0.026	0.97	0.03			1.3	1.0	1.4	1.05
	0.032	0.98	0.02			1.7	1.3	1.4	1.16
	0.006	* f_{Mdiff} > 40%							
Py-PS	0.013	0.88	0.12			1.4	0.7	0.6	1.09
DMA	0.019	0.95	0.05			1.3	0.8	0.8	1.15
1 g/L LiCl	0.025	0.96	0.04			1.2	0.8	1.1	1.18
	0.026	0.97	0.03			1.3	0.8	1.1	1.08
	0.032	0.98	0.02			1.3	0.9	1.3	1.24
Py-PDMA	0.014	0.87	0.13			1.3	0.7	0.9	1.15
	0.019	0.88	0.12			1.3	0.8	1.0	1.07
	0.026	0.96	0.04			1.3	0.8	1.4	1.12
	0.032	0.97	0.03			1.4	1.0	1.5	1.11
	0.037	0.98	0.02			1.6	0.9	1.8	1.18

* k_2 was found to be variable when left floating. In this case, it was fixed in the analysis to the average of the other five Py-PAA samples.

* f_{Mdiff} > 40%; The amount of pyrene tht did not form excimer within the time-scale of the experiment was greater than 40%, thus the parameters retrieved are considered unreliable.

Table A6.4: Parameters retrieved from the global analysis of the excimer decays of Py-PAA, Py-PS and Py-PDMA in various solvents with Equation 6.5.

Polymer	Pyrene per atom	τ_{EE0} (ns)	τ_{ED} (ns)	f_{Ek2}	f_{Ediff}	f_{EE0}	f_{ED}	χ^2
Py-PAA	0.020	40	78	0.43	0.26	0.00	0.31	1.03
	0.026	39	78	0.42	0.25	0.00	0.33	1.07
DMF	0.029	38	74	0.37	0.23	0.03	0.37	1.1
	0.029	45	87	0.37	0.27	0.20	0.16	1.09
	0.033	44	88	0.35	0.30	0.17	0.18	0.99
	0.039*	39	70	0.20	0.28	0.11	0.42	1.12
Py-PAA	0.020	43	91	0.55	0.23	0.04	0.18	1.05
	0.026	45	95	0.52	0.26	0.08	0.15	1.04
DMA	0.029	40	86	0.50	0.24	0.02	0.25	1.02
	0.029	43	86	0.43	0.28	0.07	0.22	1.16
	0.033	45	90	0.46	0.28	0.10	0.18	1.08
	0.039*	45	82	0.26	0.35	0.17	0.22	1.17
Py-PAA	0.020	44	101	0.50	0.25	0.13	0.12	1.07
	0.026	45	104	0.46	0.28	0.16	0.10	1.01
DMF	0.029	45	97	0.43	0.27	0.17	0.13	1.23
1 g/L LiCl	0.029	44	91	0.37	0.28	0.18	0.17	1.07
	0.033	45	93	0.39	0.28	0.19	0.14	1.20
	0.039*	45	83	0.20	0.32	0.27	0.21	1.19
Py-PAA	0.020	40	90	0.59	0.18	0.00	0.22	1.15
	0.026	43	90	0.55	0.21	0.04	0.20	1.09
DMA	0.029	41	86	0.50	0.23	0.02	0.25	1.11
1 g/L LiCl	0.029	44	91	0.47	0.25	0.10	0.18	1.20
	0.033	45	93	0.47	0.26	0.12	0.15	1.13
	0.039	43	81	0.32	0.30	0.13	0.24	1.08
	0.006	70	180		0.89	0.04	0.07	1.11
Py-PS	0.013	62	180		0.89	0.08	0.03	1.09
DMF	0.019	55	180		0.89	0.09	0.01	1.08
	0.025	56	180		0.87	0.11	0.02	1.02
	0.026	55	180		0.88	0.11	0.01	1.05
	0.032	54	180		0.88	0.11	0.01	1.16
	0.006	* f_{Mdiff} > 40%						
Py-PS	0.013	69	180		0.89	0.09	0.01	1.09
DMA	0.019	61	180		0.92	0.08	0.00	1.15
1 g/L LiCl	0.025	59	180		0.90	0.09	0.01	1.18
	0.026	60	180		0.89	0.10	0.00	1.08
	0.032	57	180		0.89	0.11	0.01	1.24
Py-PDMA	0.014	58	180		0.91	0.07	0.02	1.15
	0.019	59	180		0.90	0.08	0.02	1.07
	0.026	55	180		0.88	0.11	0.01	1.12
	0.032	54	180		0.87	0.12	0.01	1.11
	0.037	52	180		0.83	0.16	0.01	1.18

* k_2 was found to be variable when left floating. In this case, it was fixed in the analysis to the average of the other five Py-PAA samples.

* f_{Mdiff} > 40%; The amount of pyrene tht did not form excimer within the time-scale of the experiment was greater than 40%, thus the parameters retrieved are considered unreliable.

Table A6.5: Fractions of all pyrene species for Py-PAA, Py-PS, and Py-PDMA, calculated from f_{Mdiff}, f_{Mfree}, f_{Mk2}, f_{Ediff}, f_{EE0}, f_{Ek2} and f_{ED}.

Polymer	Pyrene per atom	f_{diff}	f_{k2}	f_{free}	f_{E0}	f_D	f_{agg}	χ^2
Py-PAA	0.020	0.42	0.26	0.02	0.00	0.30	0.56	1.03
	0.026	0.41	0.24	0.03	0.00	0.32	0.56	1.07
DMF	0.029	0.36	0.23	0.02	0.03	0.36	0.62	1.1
	0.029	0.36	0.26	0.04	0.19	0.16	0.61	1.09
	0.033	0.35	0.29	0.02	0.16	0.18	0.64	0.99
	0.039*	0.19	0.28	0.01	0.11	0.41	0.80	1.12
Py-PAA	0.020	0.53	0.22	0.04	0.04	0.17	0.43	1.05
	0.026	0.50	0.25	0.02	0.08	0.14	0.47	1.04
DMA	0.029	0.49	0.23	0.03	0.02	0.24	0.49	1.02
	0.029	0.42	0.27	0.03	0.07	0.21	0.55	1.16
	0.033	0.43	0.27	0.02	0.10	0.17	0.54	1.08
	0.039*	0.26	0.34	0.01	0.17	0.22	0.73	1.17
Py-PAA	0.020	0.49	0.25	0.01	0.13	0.12	0.50	1.07
	0.026	0.46	0.28	0.00	0.16	0.10	0.54	1.01
DMF	0.029	0.42	0.27	0.01	0.17	0.13	0.57	1.23
1 g/L LiCl	0.029	0.37	0.28	0.00	0.18	0.17	0.63	1.07
	0.033	0.39	0.28	0.01	0.18	0.14	0.60	1.20
	0.039*	0.20	0.32	0.00	0.27	0.21	0.80	1.19
Py-PAA	0.020	0.58	0.18	0.03	0.00	0.22	0.39	1.15
	0.026	0.53	0.20	0.03	0.04	0.19	0.44	1.09
DMA	0.029	0.49	0.23	0.02	0.02	0.25	0.49	1.11
1 g/L LiCl	0.029	0.46	0.25	0.02	0.09	0.18	0.52	1.20
	0.033	0.46	0.26	0.01	0.12	0.15	0.52	1.13
	0.039	0.32	0.30	0.01	0.13	0.25	0.67	1.08
	0.006	0.61		0.31	0.03	0.05	0.08	1.11
Py-PS	0.013	0.80		0.10	0.07	0.02	0.10	1.09
DMF	0.019	0.79		0.12	0.08	0.01	0.09	1.08
	0.025	0.84		0.03	0.10	0.02	0.12	1.02
	0.026	0.86		0.02	0.11	0.01	0.12	1.05
	0.032	0.86		0.02	0.11	0.01	0.12	1.16
	0.006	* f_{Mdiff} > 40%						
Py-PS	0.013	0.80		0.11	0.08	0.01	0.09	1.09
DMA	0.019	0.87		0.05	0.07	0.00	0.08	1.15
1 g/L LiCl	0.025	0.87		0.03	0.09	0.01	0.09	1.18
	0.026	0.87		0.02	0.10	0.00	0.10	1.08
	0.032	0.87		0.01	0.11	0.01	0.11	1.24
Py-PDMA	0.014	0.80		0.12	0.06	0.01	0.08	1.15
	0.019	0.80		0.11	0.07	0.02	0.09	1.07
	0.026	0.85		0.04	0.10	0.01	0.11	1.12
	0.032	0.84		0.03	0.12	0.01	0.13	1.11
	0.037	0.82		0.01	0.15	0.01	0.17	1.18

* k_2 was found to be variable when left floating. In this case, it was fixed in the analysis to the average of the other five Py-PAA samples.

* f_{Mdiff} > 40%; The amount of pyrene tht did not form excimer within the time-scale of the experiment was greater than 40%, thus the parameters retrieved are considered unreliable.

Chapter 7:
Concluding Remarks and Future Work

7.1 Summary of Accomplished Work

Pyrene labeled polymers have been and remain an important tool in the study of polymer chain dynamics.[1] They have been used to study the chain dynamics of linear[2] and branched chains[3] in dilute solution, polymer thin films,[4] and biological systems.[5] The information derived can range from qualitative, such as following the change in the I_E/I_M ratio as the number of cross-links in a polymer gel are increased,[6] to quantitative, such as determining the time scale of the end-to-end cyclization of a polymer.[2] More recently, quantitative experiments have been conducted where the kinetics of excimer formation of polymers randomly labeled with pyrene groups are characterized utilizing the fluorescence blob model (FBM) analysis.[1] As more studies are completed, it becomes increasingly important to develop a thorough understanding of what each parameter retrieved through the FBM analysis of the fluorescence decays means and what aspects of the polymer backbone and side-chains affect them.

This thesis has investigated the effect that several parameters have on the excimer formation of polymers randomly labeled with pyrene. The first study completed established the effect of the method used for pyrene attachment on excimer formation. To accomplish this, four series of Py-PS were synthesized with pyrene contents ranging from 1 to 7 mol%, and their monomer and excimer time-resolved fluorescence decays were compared. Two copolymers were prepared through radical copolymerization (CoA-PS and CoE-PS). The difference between the two polymers was the nature of the linker connecting the pyrene group to the backbone, with one being longer and more flexible (CoE-PS) than the other (CoA-PS). To ensure the "randomness" of pyrene incorporation, experiments with ^{1}H NMR and SEC utilizing a fluorescence detector were conducted throughout the reaction. ^{1}H NMR

was used to determine the conversion from monomer to polymer, while SEC equipped with a fluorescence detector was used to determine the I_E/I_M ratio of the polymer formed at that level of conversion. A constant I_E/I_M ratio up to 0.4 conversion indicated that little drift in polymer composition had occurred up to that point. Thus, a comparison of the effect of *linker length* on excimer formation could be completed.

A copolymer with pyrene groups randomly grafted onto the backbone was synthesized (GrE-PS) previously in this laboratory using chloromethylation of the styrene ring followed by reaction with sodium 1-pyrenemethoxide. The chemical structure was exactly the same as the one of CoE-PS synthesized through radical copolymerization. Thus, a comparison of the *method* of pyrene incorporation was achieved.

Finally, a Py-PS was synthesized with pyrene groups evenly spaced throughout the backbone (ES-PS) through condensation polymerization of monodisperse blocks of PS end-capped with carboxylic acid groups and a pyrene compound containing two amine groups. The linker connecting pyrene to the backbone was similar to one of the random copolymers (CoA-PS). Thus, the effect of the *distribution* of pyrene on excimer formation was determined.

Using the FBM analysis it was shown that the longer linker of CoE-PS and GrE-PS does indeed increase the rate of excimer formation within a *blob* (k_{blob}) as well as increase the volume probed by the excited pyrene during its lifetime as represented by the number of styrene units per *blob*, N_{blob}. The GrE-PS series had significantly higher aggregation of pyrene groups than the chemically similar CoE-PS, indicating that the *grafting-onto* reaction leads to clustering of pyrene along the backbone. This result has particularly strong implication for the synthesis of branched polymers and hydrophobically modified polymers.

Finally, distributing pyrene groups evenly along the backbone led to an even distribution of pyrene groups in the polymer coil, very different from the other three randomly labeled polymers.

The second study utilized CoA-PS and CoE-PS to determine how the FBM parameters describe the change in excimer formation with a change in solvent viscosity. Seven solvents were used, including methyl acetate, MEK, dichloromethane, THF, toluene, DMF, and dioxane, ranging in viscosities from 0.36 mPa·s to 1.19 mPa·s. k_{blob} was found to remain constant with a change in viscosity, as expected from previous work with Py-PDMA,[7] while N_{blob} was found to increase substantially with a decrease in solvent viscosity. Comparisons made strictly on solvent viscosity were complicated however, due to the fact that a change in solvent not only affects the viscosity, but also the lifetime of the excited pyrene monomer and the solvent quality towards the polymer. To circumvent this complication, the product $k_{blob} \times N_{blob}$ was used to account for changes in solvent quality and viscosity and was found to increase linearly with the product $\eta^{-1} \times [\eta]^{-1}$. This study illustrated that the FBM analysis can be used to determine quantitative information on the changes in excimer formation brought about by changes in solvent viscosity and solvent quality.

A technical note was compiled using the time-resolved monomer fluorescence decays from GrE-PS (Chapter 2), CoA-PS (Chapters 2 and 3), CoE-PS (Chapters 2 and 3), PGA-PMA (Chapter 5), and Py-PDMA (Chapter 6) in several solvents to illustrate the remarkable agreement between the N_{agg} value obtained using an analysis developed initially by Turro and Yekta (TY) to quantify the aggregation of surfactant micelles, and the N_{blob} value determined by the FBM analysis. The procedure worked as follows: 1) The time-resolved fluorescence decays of several pyrene labeled polymers with increasing pyrene contents are

acquired; 2) They are analyzed using a sum of exponentials (SOE) or the FBM analysis; 3) N_{blob} is calculated for each sample; 4) the N_{blob} trend is extrapolated to zero pyrene content to obtain N_{blob}^{o}. The N_{blob}^{o} values obtained for 5 different polymers in seven different solvents using this method were within ±10% of each other for each polymer-solvent combination. This note should make it much easier to other researchers to determine the N_{blob} value of their pyrene-labeled polymer even though they do not have access to the more complex FBM analysis.

In the fourth study, an α-helical polypeptide was randomly labeled with two different pyrene derivatives, namely 1-pyrenemethylamine (PMA) and 4-(1-pyrene)butylamine (PBA), allowing for two important elements of excimer formation to be investigated. The first element was the ability to describe the motions of the linker connecting the pyrene pendant to the helical backbone using the FBM. Because PGA forms a well-defined α-helix, molecular modeling was employed to determine an estimate of the N_{blob} parameter that was physically possible for an excited pyrene to probe. It was shown that a small increase in the linker length resulted in a measurable, fairly accurate increase in the N_{blob} value obtained as the pyrene groups' reach was increased. The second element investigated was the effect of the timescale of the linker motions on the volume probed by an excited pyrene. Nitromethane was added to DMF as a quencher for the excited pyrene monomer. The range of lifetimes used for PGA-PMA ranged from a low of 50 ns to a high of 215 ns when no quencher was added. N_{blob} was found to remain relatively constant with the decrease in lifetime, while k_{blob} remained constant as the lifetime was decreased from 215 to 150 ns, followed by a steep increase between 150 and 50 ns. Since k_{blob} is an indicator of the volume probed by an excited pyrene,[7] this result is quite surprising, as it indicates that the pyrene

attached via a short linker required ~ 150 ns to probe the volume around the α-helix to form excimer. A similar conclusion for the longer butyl linker could not be made due to the shorter maximum lifetime of 155 ns of the PBA monomer. It is suggested that this seemingly long time-scale is likely the result of the side-chain motions being restricted by the rigid PGA backbone.

In the final study, the chain dynamics of Py-PAA were studied in DMF and DMA with and without 1 g/L LiCl. Two major conclusions were reached from this work. Firstly, an increase in the I_E/I_M ratio as a function of polypeptide concentration was observed, which was unique compared to other pyrene-labeled polymers, such as Py-PS, Py-PDMA, and Py-PGA in good and poor solvents. This behavior did however resemble that of a pyrene-labeled poly(acrylic acid), a randomly coiled polyelectrolyte, suggesting that Py-PAA behaved as a randomly coiled polyelectrolyte. FRET experiments using a mixture of Np-PAA and Py-PAA revealed that no aggregation was taking place between PAA coils, illustrating that the changes in I_E/I_M were due to changes in the polymer conformation. SEC measurements were completed with and without added LiCl, with the results further supporting that PAA behaved in a manner resembling an ionomer in DMF and DMA.

After establishing that PAA behaved as an ionomer, time-resolved monomer and excimer fluorescence decays were acquired at a concentration where the I_E/I_M ratio remained constant with a change in polypeptide concentration (≤ 0.1 OD for pyrene absorption). Analysis of the fluorescence decays using the FBM showed that a large fraction of the pyrenes were clustered along the PAA backbone. This is likely due to the *grafting-onto* labeling method used to attach pyrene, which was shown in Chapter 2 to result in pyrene groups that are clustered along the backbone. An extra rate constant to describe the fast

excimer formation (k_2) was required to analyze the decays, making comparisons of the FBM parameters obtained with other polymers such as Py-PS and Py-PDMA difficult. However, the analysis is internally consistent, making the comparison of the FBM parameters obtained with Py-PAA in DMA and DMF relevant. It was shown that excimer formation remained relatively unchanged when Py-PAA was studied in DMF or DMA, which is extraordinary considering that the viscosity increases by nearly 2.5 times when changing the solvent from DMF to DMA. This illustrates that the PAA backbone is so stiff that excimer formation is no longer controlled by the solvent viscosity, as was found for Py-PS in Chapter 3.

This thesis has shown the considerable sensitivity of pyrene excimer formation to changes in polymer side-chain and backbone structure. More importantly, quantitative analysis based on the FBM was used to quantify these changes and the results obtained from these studies are expected to become a benchmark against which future studies of pyrene-labeled polymers can be compared.

7.2 Future Work

One of the more unexpected results of Chapter 2 is that the method of pyrene incorporation, *grafting-onto* vs. copolymerization, made a large impact on the distribution of pyrene groups in terms of clustering. This result has far reaching implications for the synthesis of functionalized polymers and should be explored further to determine whether it is a universal phenomenon or simply a product of the chloromethylation method used in this study. Two avenues in which this could be explored are investigating a new polymer entirely, or continuing to study Py-PSs using different pyrene incorporations. For example, Py-PS could also be synthesized by randomly acetylating the polystyrene ring to add

functional groups for a *grafting-onto* reaction.[8] This second grafting-onto method could reinforce the results found for the GrE-PS series, or add an entirely new result to the study.

In addition to a second *grafting-onto* series, a third copolymerization could be used to further explore the effect of linker length and flexibility through the use of a butyl group in place of the methyl group used in the pyrenyl monomer for the CoA-PS series. The butyl linker is a pyrene derivative commonly used by polymer chemists and its effect on excimer formation would be an important addition to the Py-PS data set.

The second opportunity to study the effect of pyrene incorporation through copolymerization or grafting-onto is to study pyrene-labeled poly(acrylic acid) (Py-PAcrylA). Py-PAcrylA is a strong candidate because it is easily labeled using the carboxylic acid side-chains with a pyrene derivative such as 1-pyrenemethylamine and could also be labeled in a copolymerization reaction similar to that used to prepare the CoA-PS samples in Chapter 2.

The CoA-PS and CoE-PS series used in Chapters 2 and 3 could also be used in a study similar to Chapter 5 and previous work with Py-PDMA[7] where nitromethane was used to control the lifetime of the excited pyrene. The scaling relationship between k_{blob} and N_{blob} in good and poor solvents would strengthen the contention that the FBM parameters describe the motions of polymer chains within a *blob* according to the relationships expected from polymer scaling laws.

The second accomplishment of this thesis, the study of pyrene-labeled polypeptides, should be expanded to include a water-soluble chromophore in order to access chain dynamics in the aqueous solutions typically used to study biological systems. Although pyrene has been used extensively to study polymers, pyrene is very hydrophobic and requires

that studies of pyrene-labeled polypeptides be conducted in organic solvents where pyrene associations are reduced. Now that these studies have been conducted on two different pyrene-labeled polypeptides and have shown that the FBM is applicable, a water-soluble chromophore should be used. A chromophore such as 2,3-diazabicyclo[2.2.2]oct-2-ene (DBO) would be an ideal candidate for use with the FBM. DBO has several favorable characteristics that include high solubility in water, a long lifetime, 420 to 730 ns in deaerated H_2O and D_2O, respectively, its relatively small size, and finally that its fluorescence is quenched by a natural amino acid, tryptophan.[9]

The study of Py-PGA could also be expanded through the use of a denaturant such as guanidinium hydrochloride (Gdm). Preliminary studies indicated that a 6 to 8 M Gdm solution in DMF denatured the PGA α-helix. This was established from the disappearance of the pyrene peak at 278 nm in the CD spectra (not presented in this thesis). Studies conducted as a function of Gdm concentration could give information on the polypeptide chain dynamics as it is unraveled.

7.3 References

1. Duhamel, J. *Acc. Chem. Res.* **2006**, *39*, 953-960.

2. Winnik, M. A. *Acc. Chem. Res.* **1985**, *18*, 73-79.

3. Frank, R. S.; Merkle, G.; Gauthier, M. *Macromolecules* **1997**, *30*, 5397-5402.

4. Ellison, C. J.; Torkelson, J. M. *Nat. Mater*. **2003**, *2*, 695-700.

5. Hossain, M. A.; Hamasaki, K.; Mihara, H.; Ueno, A. *Chem. Lett*. **2000**, *3*, 252-253.

6. Kong H. J.; Lee, K. Y.; Mooney, D. J. *Macromolecules* **2003**, *36*, 7887-7890.

7. Kanagalingam, S.; Spartalis, J.; Cao, T.-M.; Duhamel, J. *Macromolecules* **2002**, *35*, 8571-8577. b) Kanagalingam, S.; Ngan, C. F.; Duhamel, J. *Macromolecules* **2002**, *35*, 8560-8570

8. Li, J.; Gauthier, M. *Macromolecules* **2001**, *34*, 8918-8924.

9. Hudgins, R. R.; Huang, F.; Gramlich, G.; Nau, W. M. *J. Am. Chem. Soc*. **2002**, *124*, 556-564. b) Huang, F.; Hudgins, R. R.; Nau, W. M. *J. Am. Chem. Soc*. **2004**, *126*, 16665-16675. c) Roccatano, D.; Sahoo, H.; Zacharias, M.; Nau, W. M. *J. Phys. Chem. B* **2007**, *111*, 2639-2646.